



**UNIVERSIDAD NACIONAL AUTÓNOMA DE MÉXICO**  
**PROGRAMA DE MAESTRÍA Y DOCTORADO EN INGENIERÍA**  
**ENERGÍA – FUENTES RENOVABLES**

**EFFECT OF NANOPARTICLES ON MICROALGAE CULTURE AND BIOGAS UPGRADING**

**TESIS**  
**QUE PARA OPTAR POR EL GRADO DE:**  
**DOCTOR EN INGENIERÍA**

**PRESENTA:**  
**M.I. LAURA GABRIELA VARGAS ESTRADA**

**TUTOR PRINCIPAL**  
**Dr. JOSEPH SEBASTIAN PATHIYAMATTOM, INSTITUTO DE ENERGÍAS RENOVABLES**

**COMITÉ TUTOR**  
**Dra. ADRIANA MARGARITA LONGORIA HERNÁNDEZ, IPN**  
**Dr. ALBERTO ÁLVAREZ GALLEGOS, CIICA<sub>p</sub>-UAEM**  
**Dr. JOEL MOREIRA ACOSTA, UVM, TUXTLA**  
**Dr. SERGIO ALBERTO GAMBOA SÁNCHEZ, IER-UNAM**

TEMIXCO, MORELOS

ENERO, 2023



Universidad Nacional  
Autónoma de México

Dirección General de Bibliotecas de la UNAM

**Biblioteca Central**



**UNAM – Dirección General de Bibliotecas**  
**Tesis Digitales**  
**Restricciones de uso**

**DERECHOS RESERVADOS ©**  
**PROHIBIDA SU REPRODUCCIÓN TOTAL O PARCIAL**

Todo el material contenido en esta tesis esta protegido por la Ley Federal del Derecho de Autor (LFDA) de los Estados Unidos Mexicanos (México).

El uso de imágenes, fragmentos de videos, y demás material que sea objeto de protección de los derechos de autor, será exclusivamente para fines educativos e informativos y deberá citar la fuente donde la obtuvo mencionando el autor o autores. Cualquier uso distinto como el lucro, reproducción, edición o modificación, será perseguido y sancionado por el respectivo titular de los Derechos de Autor.



**JURADO ASIGNADO:**

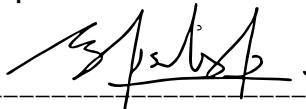
Presidente: Dr. Armando González Sánchez  
Secretario: Dra. Dulce María Arias Lizárraga  
1 er. Vocal: Dr. Joseph Sebastian Pathiyamattom  
2 do. Vocal: Dr. Sergio Alberto Gamboa Sánchez  
3 er. Vocal: Dr. Raúl Muñoz Torre

Lugar o lugares donde se realizó la tesis:  
Instituto de Energías Renovables, Universidad Nacional Autónoma de México, Temixco,  
México

Instituto de Procesos Sostenibles, Universidad de Valladolid, Valladolid, España.

**TUTOR DE TESIS:**

Dr. Joseph Sebastian Pathiyamattom



---

**FIRMA**



# Acknowledgments

---

I would like to gratefully acknowledge:

The National Council of Science and Technology (CONACYT) of Mexico for the PhD grant No. 736224.

To the General Directorate of Academic Personnel Affairs (DGAPA) of the National Autonomous University of Mexico (UNAM) for the financial support for materials and equipment. Project number: IN108922.

To the National Autonomous University of Mexico (UNAM) and the Institute of Renewable Energies (IER) for being my home for the last six years.

To the Institute of Sustainable Processes (ISP) and the University of Valladolid (UVa).

To the Institute of Engineering (II), UNAM.

To CALPECH and SMALLOPS for kindly providing the nanoparticles.

To my supervisor, Dr. Joseph Sebastian Pathiyamattom, for always supporting my projects and ideas.

To Dr. Raúl Muñoz, thank you for receiving me in your laboratory and in your research group, I will be forever grateful.

To Dr. Armando González Sánchez, for receiving me at the II-UNAM.

To José Campos and Jaime Villalobos for the technical support at the IER.

## *Acknowledgments*

---

To Enrique Marcos and Araceli Crespon for the technical support at the ISP, UVa.

To Diana Aguirre, for the technical support at the II.

To my lab mates and students under my supervision for the experimental support at the IER: Armando Vargas, Alma Cienfuegos, Valentina Rojas, Fernanda Linarte, Alexis Bahena.

To my lab mates for the experimental support at the ISP, UVa: Edwin Hoyos, Cristian Sepulveda, Leonardo Martínez-Mendoza, Fanny Rivera, Lara Méndez.

To Dr. Patrick U. Okoye, thank you for the academic and personal support, I enjoy how the ideas for new projects flow when we talk.

To all the researchers, technicians and colleagues at IER, II and Sciences Faculty of UNAM, who were willing to collaborate in the development of my project and in the construction of my system at the IER.

To all the people at IER who always supported me whether carrying the wastewater gallons or with the paperwork.

Thank you!

# Dedications

---

To my parents. Thank you mum and dad for always supporting my career no matter how far it takes me from you. I will always do my best to make you feel proud of me. Thank you mum for giving me the tools to become the woman I am.

To my sister, thank you for always believing in me even when I did not, your tough words gave me the strength to continue.

Finally, to him. All that love did not die, it only changed its way to science and made me the researcher I am today. There would be no L. Vargas-Estrada without you. Thank you. Miss you JJ.





# Summary

---

Photosynthetic biogas upgrading is based on the CO<sub>2</sub> capture by microalgae and has become an attractive, cost-effective, and environmentally friendly technology to increase biogas calorific power. Microalgae are microorganisms that consume CO<sub>2</sub> through the photosynthesis process and even if theoretically 1 ton of microalgae can consume 1.8 ton of CO<sub>2</sub>, the reality is that the photosynthesis process is limited by the low diffusion rate of CO<sub>2</sub> to the culture media. Recently, the use of nanoporous materials has recently attracted a renewed attention in the field of CO<sub>2</sub> capture because they exhibit key advantages such as a large surface area to volume ratio, high reactivity, abundant active sites and high adsorption capacity. Metal oxide nanoparticles (NPs) and nanoporous carbons rank among the most popular nanomaterials for CO<sub>2</sub> capture and could represent an innovative tool to enhance CO<sub>2</sub> fixation during photosynthetic biogas upgrading. Therefore, the aim of this PhD thesis was to assess the effect of the addition of mesoporous NPs to microalgae cultures devoted to biogas upgrading to improve the CO<sub>2</sub> consumption by microalgae. Thus, this thesis was divided in three parts.

Firstly, the effect of Fe<sub>2</sub>O<sub>3</sub> NPs on microalgae cultivated at laboratory scale was assessed. Two different types of Fe<sub>2</sub>O<sub>3</sub> were synthesized to obtain different crystal phases ( $\gamma$ - and  $\alpha$ - phase), subsequently, they were added to *Chlorella* spp. cultures at concentrations < 20 mg L<sup>-1</sup> in controlled culture medium. The results showed that the NPs containing a higher content of the  $\gamma$ - phase were not toxic for microalgae and the carbohydrate content was increased by 121% and 184% when 10

and 20 mg L<sup>-1</sup> were added, respectively. Subsequently, to make the process more cost-effective, *Chlorella* sp. was cultivated in wastewater at different concentrations. To confirm if the wastewater dilution affected the biomass production, nutrient and energy recovery, biochemical methane potential (BMP) assays were carried out. Although no significant difference was observed between the BMP tests, the biomass cultivated in pristine wastewater presented a higher biogas production potential of 204.47 mL. The latter suggested that pristine wastewater can be used as a culture media to make the process more cost-effective. Thereafter, the effect of long-term exposure to Fe<sub>2</sub>O<sub>3</sub> NPs of a microalgae-cyanobacteria consortium cultivated in pristine wastewater was elucidated. The results showed that concentrations between 20 and 30 mg L<sup>-1</sup> of Fe<sub>2</sub>O<sub>3</sub> NPs reduced microalgae growth (on a VSS basis), however there was not significant difference in the nutrient uptake (NH<sub>4</sub><sup>+</sup>, PO<sub>4</sub><sup>3-</sup>, NO<sub>3</sub><sup>-</sup>, NO<sub>2</sub><sup>-</sup>). Additionally, the carbohydrate content was also increased when 30 mg L<sup>-1</sup> of Fe<sub>2</sub>O<sub>3</sub> NPs were added to the culture.

In the second part of the thesis, the effect of mesoporous Fe<sub>2</sub>O<sub>3</sub> and carbon coated zero-valent iron NPs was assessed in a pure microalgae strain of *Chlorella sorokiniana*, cultivated in a mineral medium rich in carbonates and under a synthetic biogas atmosphere. The assays were carried out in batch conditions, and different NPs concentrations were assessed (10, 20, 30 and 70 mg L<sup>-1</sup>) under different light sources (visible and visible + UV light). The results showed that the mesoporous surface of the NPs induced the CO<sub>2</sub> availability to *C. sorokiniana* regardless of the concentration and type of nanoparticles tested. However, the iron source influenced differently the metabolism of *C. sorokiniana* and was the

responsible for the carbohydrates/lipids accumulation. Finally, the results demonstrated that the carbon coated zero-valent iron NPs (CALPECH) stimulated significantly the CO<sub>2</sub> consumption and biomass production of *C. sorokiniana* when 70 mg L<sup>-1</sup> were added. Furthermore, the effect of mesoporous NPs (SiO<sub>2</sub>, Fe<sub>2</sub>O<sub>3</sub> and CALPECH) was assessed in a mixed microalgae-bacteria culture under the same conditions described above. The results obtained confirmed the fact that CALPECH NPs induced an enhanced CO<sub>2</sub> consumption, growth and biomass production of microalgae when 70 mg L<sup>-1</sup> were added to the culture. In this context, the latter NPs were selected as the optimal NPs to improve the photosynthetic biogas upgrading process.

Finally, in the third part of the thesis, the effect of CALPECH NPs on photosynthetic biogas upgrading was assessed in an indoor pilot scale high rate algal pond interconnected to an absorption column. The addition of 70 mg L<sup>-1</sup> of NPs stimulated the photosynthetic activity, resulting in an enhanced concentration of biomass from 1.56 to 3.26 g VSS L<sup>-1</sup>. Additionally, the presence of the NPs in the culture broth increased CO<sub>2</sub> removal from 86% to 92% at low IC concentrations ( $\leq$  600 mg L<sup>-1</sup>) and decreased the content of O<sub>2</sub> and N<sub>2</sub> in the upgraded biomethane.

In conclusion, the results obtained in this thesis suggest that the addition of CALPECH NPs can be used as a viable strategy to improve biogas upgrading coupled to microalgae production.



# Content

---

<i>Acknowledgments</i> .....	5
<i>Dedications</i> .....	7
<i>Summary</i> .....	9
<i>Content</i> .....	13
<i>List of Tables</i> .....	19
<i>List of Figures</i> .....	21
<i>Introduction</i> .....	27
<i>Objectives and Thesis Outline</i> .....	31
2.1 Objectives .....	31
2.2 Thesis outline .....	32
<i>Chapter 1</i> .....	35
State of the art .....	35
1. Introduction .....	37
2. Nanoparticles overview .....	41
3. Effects of nanoparticles addition on microalgal growth .....	44
3.1 Lipid production .....	47
3.2 CO <sub>2</sub> absorption and sequestration .....	49
3.3 Light conversion .....	57
3.4 Toxicity .....	58
3.5 Generation of reactive oxygen species (ROS) .....	60
3.6 Ultrastructural alterations in algal cells .....	61
3.6.1 Internalization of nanoparticles in cells .....	63
3.6.2 Damages in the cell membrane and cell wall .....	64
3.7 Shading effect .....	66
4. Prospects and recommendations .....	67
<i>Chapter 2</i> .....	69

Influence of the crystal phase of Fe <sub>2</sub> O <sub>3</sub> nanoparticles on <i>Chlorella</i> cultures and biomass production.....	69
1. Introduction.....	71
2. Methods.....	73
2.1 Fe <sub>2</sub> O <sub>3</sub> nanoparticle synthesis.....	73
2.2 Nanoparticle stock solution.....	74
2.3 Microalgae strain and culture.....	74
2.4 Experimental set-up.....	75
2.5 Analytical determinations.....	76
2.6 Statistical analysis.....	79
3. Results and discussion.....	79
3.1 Characterization of the Fe <sub>2</sub> O <sub>3</sub> nanoparticles.....	79
3.2 Effect of Fe <sub>2</sub> O <sub>3</sub> nanoparticles on <i>Chlorella vulgaris</i> .....	82
3.3 Effect of Fe <sub>2</sub> O <sub>3</sub> nanoparticles on <i>Chlorella</i> sp.....	90
4. Conclusions.....	95
<i>Chapter 3</i> .....	97
Effect of wastewater composition on microalgae growth, nutrient uptake, biomass composition and energy recovery.....	97
1. Introduction.....	99
2. Methods.....	102
2.1 Description of the Wastewater.....	102
2.2 Microalgae culture.....	103
2.3 Experimental set-up.....	103
2.4 Biochemical methane potential test.....	104
2.5 Analytical procedures.....	106
3. Results and discussion.....	108
3.1 Microalgae and nitrifying bacteria growth.....	108
3.2 Nutrient removal.....	112
3.3 Biomass composition.....	116
3.4 Biogas production.....	118

---

4. Conclusions.....	121
<i>Chapter 4</i> .....	<i>123</i>
Effect of long-term exposure to Fe <sub>2</sub> O <sub>3</sub> nanoparticles on microalgae growth, nutrient uptake and biomass composition .....	123
1. Introduction.....	125
2. Materials and methods .....	126
2.1 Nanoparticles.....	126
2.2 Microalgae and culture media.....	127
2.3 Experimental set-up .....	127
2.4 Sampling procedures and operational conditions .....	128
2.5 Analytical procedures .....	129
2.6 Statistical analysis .....	130
3. Results and discussions .....	130
3.1 Nanoparticles characterization .....	130
3.2 Microalgae growth .....	131
3.3 Nutrient uptake and PBRs performance.....	134
3.4 Biomass composition.....	138
4. Conclusions.....	140
<i>Chapter 5</i> .....	<i>141</i>
Effect of iron based nanoparticles on <i>Chlorella sorokiniana</i> metabolism and biogas upgrading .....	141
1. Introduction.....	143
2. Materials and methods .....	145
2.1 Nanoparticles and stock solutions .....	145
2.2 Microalgae culture and biogas .....	145
2.3 Experimental set-up .....	146
2.4 Analytical procedures .....	148
2.5 Statistical analysis .....	149
3. Results and discussion.....	149



3.1	Characterization of nanoparticles .....	149
3.2	Influence of biogas composition on <i>C. sorokiniana</i> growth and CO <sub>2</sub> removal 151	
3.3	Influence of nanoparticle concentration on <i>C. sorokiniana</i> growth and CO <sub>2</sub> removal under visible light .....	155
3.4	Influence of nanoparticle concentration on <i>C. sorokiniana</i> growth and CO <sub>2</sub> removal under visible + UV light.....	161
4.	Conclusions .....	167
<i>Chapter 6</i> .....		169
Effect of nanoparticles on a mixed microalgae-bacteria consortium's metabolism and biogas upgrading.....		169
1.	Introduction .....	171
2.	Materials and methods .....	176
2.1	Nanoparticles and stock solutions .....	176
2.2	Microalgae culture and biogas .....	176
2.3	Experimental set-up .....	177
2.4	Analytical procedures .....	178
2.5	Statistical analysis .....	179
3.	Results and discussion.....	179
3.1	Nanoparticle characterization .....	179
3.2	Influence of type of biogas and nanoparticle addition on microalgae growth	182
3.3	Influence of nanoparticle concentration under visible light .....	188
3.4	Influence of nanoparticle concentration under UV-visible light.....	194
4.	Conclusions and future prospective .....	199
<i>Chapter 7</i> .....		201
Effect of carbon coated zero-valent iron nanoparticles on photosynthetic biogas upgrading at pilot-scale.....		201
1.	Introduction .....	203
2.	Materials and methods .....	206

---

2.1	Nanoparticles.....	206
2.2	Gas-liquid mass transfer rate calculation .....	207
2.3	Experimental set-up .....	207
2.4	Sampling procedures and operational conditions .....	209
2.5	Analytical procedures .....	210
2.6	Statistical analysis .....	211
3.	Results and discussion.....	211
3.1	Nanoparticles characterization .....	211
3.2	Effect of nanoparticles on the gas-liquid mass transfer rate.....	212
3.3	Effect of nanoparticles on algal open pond performance.....	213
4.	Conclusions.....	226
<i>Chapter 8</i> .....		<i>227</i>
Discussion .....		227
1.	Effect of nanoparticles on microalgae metabolism.....	229
2.	Effect of nanoparticles on CO <sub>2</sub> availability .....	235
3.	Effect of nanoparticles on photosynthetic biogas upgrading at pilot scale.....	238
<i>Chapter 9</i> .....		<i>241</i>
Conclusions and Future Prospects .....		241
1.	Conclusions.....	243
1.1	Effect of nanoparticles on microalgae metabolism.....	243
1.2	Effect of nanoparticles on CO <sub>2</sub> availability .....	244
1.3	Effect of nanoparticles on photosynthetic biogas upgrading at pilot scale....	245
2.	Future prospects .....	246
<i>References</i> .....		<i>249</i>
<i>Appendix</i> .....		<i>279</i>



# List of Tables

---

<b>Table 1.</b> <i>Effect of nanoparticle addition to microalgae growth</i> .....	54
<b>Table 2.</b> <i>Chemical compositions of the Fe<sub>2</sub>O<sub>3</sub> nanoparticles.</i> .....	80
<b>Table 3.</b> <i>Kinetic growth parameters of Chlorella sp. and C. vulgaris with 10 mg L<sup>-1</sup> of Fe<sub>2</sub>O<sub>3</sub>.</i> .....	85
<b>Table 4.</b> <i>Kinetic growth parameters of C. vulgaris and Chlorella sp. with 5 mg L<sup>-1</sup> and 20 mg L<sup>-1</sup> of Fe<sub>2</sub>O<sub>3</sub>-450.</i> .....	86
<b>Table 5.</b> <i>Chemical composition of each PBR at the beginning of the experiment</i> .....	109
<b>Table 6.</b> <i>Microalgae biomass productivity (P) and specific growth rate (μ) .....</i>	112
<b>Table 7.</b> <i>Total solids (TS), volatile solids (VS) and VS/TS ratio of the microalgae biomass.</i> .....	118
<b>Table 8.</b> <i>Kinetic parameters and anaerobic digestion efficiency of the different microalgae biomass. B<sub>0</sub> methane yield potential; R<sub>m</sub> maximum methane yield rate; λ is the lag time; VS volatile solids.</i> .....	121
<b>Table 9.</b> <i>Environmental parameters of the PBRs during the experiment</i> .....	135
<b>Table 10.</b> <i>Biomass productivity and initial and final IC concentration in the Chlorella sorokiniana assays supplemented with 10 mg L<sup>-1</sup> of the different NPs.</i>	155
<b>Table 11.</b> <i>Influence of the type and concentration of nanoparticles on biomass productivity as a function of the type of light source: visible light (white background) and visible light + UV light (grey background).</i> .....	159
<b>Table 12.</b> <i>Effect of nanoparticles on microalgae growth. PAN: polyacrylonitrile; DMF: dimethylformamide (DMF); NFs: nanofibers.</i> .....	174
<b>Table 13.</b> <i>Chemical composition of the different nanoparticles used. The values represent the atomic percentage. CACOI: carbon coated zero valent iron.</i> .....	180

**Table 14.** BET surface area, pore volume and average pore diameter of the nanoparticles used in this study. BET: Brunauer-Emmett-Teller; CACOI: carbon coated iron .....182

**Table 15.** Biomass productivity (Px) and pH of the algal consortium broth supplemented with 10 mg L<sup>-1</sup> of the different nanoparticles. CACOI: carbon coated zero valent iron.....187

**Table 16.** Biomass productivity (Px) as a function of the type of nanoparticles and light source, at different concentrations. CACOI: carbon coated zero valent iron. ....189

**Table 17.** Environmental and operational parameters of algal open pond during the experiment .....219

**Table 18.** TN, TOC and P-PO<sub>4</sub><sup>3-</sup> concentrations in the centrate and cultivation broth of the algal open pond during the experiment .....221

**Table 19.** Effect of the nanoparticles on microalgae metabolism. Note +refers to the control, ..... 234

**Table 20.** Effect of nanoparticles on cumulative CO<sub>2</sub> and produced O<sub>2</sub>. ..... 238

**Table A1.** Influence of the type and concentration of nanoparticles on the initial and final IC concentrations of the batch assays as a function of the light source: visible light (white background) and visible light + UV light (grey background) ..... 283

**Table A2.** Influence of the type and concentration of nanoparticles on the initial and final pH of the batch assays as a function of light source: visible light (white background) and visible light + UV light (grey background) ..... 284

# List of Figures

---

<b>Fig. 1.</b> Classification of nanoparticles. ....	43
<b>Fig. 2.</b> Effects of nano-particles addition to microalgae culture. ....	47
<b>Fig. 3.</b> Schematic of the plasmonic miniphotobioreactor enhanced with Ag nanoparticles (Torkamani et al., 2010b). ....	58
<b>Fig. 4.</b> Diagram of the shading effect of 500 mg L <sup>-1</sup> TiO <sub>2</sub> nanoparticles on microalgae (Hu et al., 2018b). ....	67
<b>Fig. 5.</b> SEM images of a) Fe <sub>2</sub> O <sub>3</sub> -450, b) Fe <sub>2</sub> O <sub>3</sub> -1000 and TEM images of c) Fe <sub>2</sub> O <sub>3</sub> -450, d) Fe <sub>2</sub> O <sub>3</sub> -1000 .....	80
<b>Fig. 6.</b> XRD analysis results of a) Fe <sub>2</sub> O <sub>3</sub> -450; and b) Fe <sub>2</sub> O <sub>3</sub> -1000.....	82
<b>Fig. 7.</b> Time course of the cell density a) and b); and chlorophyll content c) and d) of <i>Chlorella vulgaris</i> cultivated in BG-11 medium under different conditions assessed: control (green circles), 10 mg L <sup>-1</sup> Fe <sub>2</sub> O <sub>3</sub> -450 (blue triangles), 10 mg L <sup>-1</sup> Fe <sub>2</sub> O <sub>3</sub> -100 (yellow cruces); 5 mg L <sup>-1</sup> Fe <sub>2</sub> O <sub>3</sub> -450 (red squares); 20 mg L <sup>-1</sup> Fe <sub>2</sub> O <sub>3</sub> -450 (navy blue diamonds). ....	84
<b>Fig. 8.</b> TEM micrographs of <i>Chlorella vulgaris</i> . a) Control; b) Fe <sub>2</sub> O <sub>3</sub> -450; c) Fe <sub>2</sub> O <sub>3</sub> -1000; and <i>Chlorella sp.</i> d) Control; e) Fe <sub>2</sub> O <sub>3</sub> -450; f) Fe <sub>2</sub> O <sub>3</sub> -1000. Red arrows indicate deformed cells, red circles indicate the presence of nanoparticles .....	87
<b>Fig. 9.</b> Carbohydrate (black) and lipid (light grey) content of <i>Chlorella vulgaris</i> cultivated with and 10 mg L <sup>-1</sup> of the corresponding Fe <sub>2</sub> O <sub>3</sub> NPs; b) <i>C. vulgaris</i> cultivated with 5 mg L <sup>-1</sup> and 20 mg L <sup>-1</sup> of Fe <sub>2</sub> O <sub>3</sub> -450; c) <i>Chlorella sp.</i> cultivated with and 10 mg L <sup>-1</sup> of the corresponding Fe <sub>2</sub> O <sub>3</sub> NPs; d) <i>Chlorella sp.</i> cultivated with 5 mg L <sup>-1</sup> and 20 mg L <sup>-1</sup> of Fe <sub>2</sub> O <sub>3</sub> -450.....	90
<b>Fig. 10.</b> Time course of the cell density a) and b); and chlorophyll content c) and d) of <i>Chlorella sp.</i> cultivated in Bayfolan forte medium under different conditions assessed: control (green circles), 10 mg L <sup>-1</sup> Fe <sub>2</sub> O <sub>3</sub> -450 (light blue triangles), 10 mg L <sup>-1</sup> Fe <sub>2</sub> O <sub>3</sub> -100 (yellow cruces); 5 mg L <sup>-1</sup> Fe <sub>2</sub> O <sub>3</sub> -450 (red squares); 20 mg L <sup>-1</sup> Fe <sub>2</sub> O <sub>3</sub> -450 (navy blue diamonds). ....	92

**Fig. 11.** Microalgae growth. a) cell density (cell mL<sup>-1</sup>); b) dry weight (TSS L<sup>-1</sup>). 110

**Fig. 12.** Nutrient content at the beginning and at the end of the study a) COD; b) TP; c) NH<sub>4</sub><sup>+</sup>; d) NO<sub>2</sub><sup>-</sup> and e) NO<sub>3</sub><sup>-</sup>; f) TIN. .... 115

**Fig. 13.** Microalgae biomass composition at the end of the study. .... 117

**Fig. 14.** a) Accumulated biogas and b) accumulated methane production after 33 days of incubation under mesophilic conditions. .... 119

**Fig. 15.** Schematic diagram of the experimental set up. Dotted lines represent air flow, continuous lines represent liquid flow. ....128

**Fig. 16.** SEM micrograph of the Fe<sub>2</sub>O<sub>3</sub> nanoparticles ..... 131

**Fig. 17.** Fe<sub>2</sub>O<sub>3</sub> nanoparticles deposited in the filamentous species contained in PBR-NPs. The circles and arrows indicate the presence of Fe<sub>2</sub>O<sub>3</sub> nanoparticles. ....132

**Fig. 18.** Time course of biomass production in PBR-Control (empty triangles) and PBR-NPs (dark diamonds).....134

**Fig. 19.** Time course of a) P-PO<sub>4</sub><sup>3-</sup>; b) N-NH<sub>4</sub><sup>+</sup>; N-NO<sub>3</sub><sup>-</sup>; N-NO<sub>2</sub><sup>-</sup> concentrations in the PBR-Control (empty triangles), PBR-NPs (dark diamonds) and wastewater (dark squares) ..... 137

**Fig. 20.** Time course of the a) Lipids and b) carbohydrates content of PBR-Control (empty triangles) and PBR-NPs (dark diamonds). ....140

**Fig. 21.** SEM micrographs of a) Fe<sub>2</sub>O<sub>3</sub>, b) CALPECH and c) SMALLOPS nanoparticles. ....150

**Fig. 22.** Time course of the cumulative CO<sub>2</sub> consumption in the assays with 10 mg L<sup>-1</sup> of a) Fe<sub>2</sub>O<sub>3</sub> NPs, b) CALPECH NPs, c) SMALLOPS NPs; of the cumulative O<sub>2</sub> production in the assays with 10 mg L<sup>-1</sup> of d) Fe<sub>2</sub>O<sub>3</sub> NPs, e) CALPECH NPs, f) SMALLOPS NPs; and of culture absorbance (OD<sub>750</sub>) in the assays with 10 mg L<sup>-1</sup> of g) Fe<sub>2</sub>O<sub>3</sub> NPs, h) CALPECH NPs, i) SMALLOPS NPs. NPs refers to the addition of nanoparticles; BA (squares) refers to the assays with biogas A; BAN (diamonds) refers to assays with biogas A and NPs; BB refers (circles) to the assays with biogas B; and BBN (triangles) refers to the assays with biogas B and NPs. .... 154

- Fig. 23.** Time course of the cumulative CO<sub>2</sub> consumptions in assays supplied with a) Fe<sub>2</sub>O<sub>3</sub>, b) CALPECH, c) SMALLOPS; of the cumulative O<sub>2</sub> production in the assays supplied with d) Fe<sub>2</sub>O<sub>3</sub>, e) CALPECH, e) SMALLOPS; and of the cumulative OD<sub>750</sub> in the assays supplied with d) Fe<sub>2</sub>O<sub>3</sub>, e) CALPECH, e) SMALLOPS. The assays were carried out under visible light. ....160
- Fig. 24.** Influence of the concentration of a) Fe<sub>2</sub>O<sub>3</sub> NPs; b) CALPECH NPs; c) SMALLOPS NPs on the carbohydrate (black) and lipid (grey) content of microalgae biomass at the end of the assays under visible light..... 161
- Fig. 25.** Time course of the cumulative CO<sub>2</sub> consumptions in assays with a) Fe<sub>2</sub>O<sub>3</sub>, b) CALPECH, c) SMALLOPS; cumulative O<sub>2</sub> production in assays with d) Fe<sub>2</sub>O<sub>3</sub>, e) CALPECH, e) SMALLOPS; and cumulative OD<sub>750</sub> in assays with d) Fe<sub>2</sub>O<sub>3</sub>, e) CALPECH, e) SMALLOPS. The assays were carried out under visible light + UV light .....166
- Fig. 26.** Influence of the concentration of a) Fe<sub>2</sub>O<sub>3</sub> NPs; b) CALPECH NPs; c) SMALLOPS NPs on the carbohydrate (black) and lipid (grey) content of microalgae biomass at the end of the assays under visible light + UV light..... 167
- Fig. 27.** Scanning Electron Microscope micrographs of a) Fe<sub>2</sub>O<sub>3</sub>, b) CACOI; carbon coated zero valent iron, and c) SiO<sub>2</sub> nanoparticles. .... 180
- Fig. 28.** Time course of the cumulative CO<sub>2</sub> consumption in the assays supplied with a) Fe<sub>2</sub>O<sub>3</sub> NPs, b) CACOI NPs, c) SiO<sub>2</sub> NPs; cumulative O<sub>2</sub> production in the assays supplemented with d) Fe<sub>2</sub>O<sub>3</sub> NPs, e) CACOI NPs, f) SiO<sub>2</sub> NPs; and culture absorbance of the algal consortium supplied with g) Fe<sub>2</sub>O<sub>3</sub> NPs, h) CACOI NPs, 1) SiO<sub>2</sub> NPs. NPs: nanoparticles; BA (triangles): assays with biogas A; BAN (circles): assays with biogas A and NPs; BB (diamonds): assays with biogas B; BBN (cross): assays with biogas B and NPs; CACOI: carbon coated zero valent iron. ....185
- Fig. 29.** Time course of the cumulative CO<sub>2</sub> consumption in the assays supplied with different concentrations of a) Fe<sub>2</sub>O<sub>3</sub> NPs, b) CACOI NPs, c) SiO<sub>2</sub> NPs; of the cumulative O<sub>2</sub> production in the tests supplemented with different concentrations of d) Fe<sub>2</sub>O<sub>3</sub> NPs, e) CACOI NPs, f) SiO<sub>2</sub> NPs; and culture absorbance of the algal consortium supplied with different concentrations of g) Fe<sub>2</sub>O<sub>3</sub> NPs, h) CACOI NPs,



1) SiO<sub>2</sub> NPs. The assays were run under visible light. CACOI: carbon coated zero valent iron; NPs: nanoparticles. ....190

**Fig. 30.** Influence of the concentration of a) Fe<sub>2</sub>O<sub>3</sub> NPs; b) CACOI NPs; c) SiO<sub>2</sub> NPs on the carbohydrate (green) and lipid (blue) content of microalgae biomass at the end of the assays under visible light. CACOI: carbon coated zero valent iron; NPs: nanoparticles. ....192

**Fig. 31.** Time course of the cumulative CO<sub>2</sub> consumption in the assays supplied with different concentrations of a) Fe<sub>2</sub>O<sub>3</sub> NPs, b) CACOI NPs, c) SiO<sub>2</sub> NPs; of the cumulative O<sub>2</sub> production in the tests supplemented with different concentrations of d) Fe<sub>2</sub>O<sub>3</sub> NPs, e) CACOI NPs, f) SiO<sub>2</sub> NPs; and culture absorbance of the algal consortium supplied with different concentrations of g) Fe<sub>2</sub>O<sub>3</sub> NPs, h) CACOI NPs, 1) SiO<sub>2</sub> NPs. The assays were run under UV+visible light. CACOI: carbon coated zero valent iron; NPs: nanoparticles. ....196

**Fig. 32.** Influence of the concentration of a) Fe<sub>2</sub>O<sub>3</sub> NPs; b) CACOI NPs; c) SiO<sub>2</sub> NPs on the carbohydrate (green) and lipid (blue) content of microalgae biomass at the end of the assays under UV+visible light. CACOI: carbon coated zero valent iron; NPs: nanoparticles. ....197

**Fig. 33.** Schematic diagram of the experimental set-up. Continuous and dotted lines represent liquid and gas flow, respectively. .... 209

**Fig. 34.** Time course of CO<sub>2</sub> concentration without CALPECH NPs (dark circles) and with CALPECH NPs (empty circles)..... 213

**Fig. 35.** Time course of biomass concentration (VSS g L<sup>-1</sup>) in the algal open pond. .... 214

**Fig. 36.** Time course of a) pH and b) inorganic carbon concentration in the cultivation broth of the algal open pond (empty diamonds), purification column (empty squares) and centrate (solid triangles). .... 216

**Fig. 37.** Time course of a) dissolved oxygen, b) N-NH<sub>4</sub><sup>+</sup>, c) N-NO<sub>2</sub><sup>-</sup>, d) N-NO<sub>3</sub><sup>-</sup> and e) S-SO<sub>4</sub><sup>-</sup> concentrations in the cultivation broth of the algal open pond (empty diamonds) and centrate (solid triangles)..... 218

---

<b>Fig. 38.</b> Time course of the concentration of a) CH <sub>4</sub> , b) CO <sub>2</sub> , c) O <sub>2</sub> , d) N <sub>2</sub> in the synthetic biogas (solid circles) and in biomethane (empty circles). Note: the dotted lines denote the limits of the European regulations .....	225
<b>Fig.39.</b> Flow inside the HRAP a) before and b) after the addition of the CALPECH nanoparticles. ....	240
<b>Fig. 40.</b> Photosynthetic biogas upgrading system under environmental conditions at the Institute of Renewable Energies, Temixco, Mexico .....	247
<b>Fig. A1.</b> Elemental analysis of Fe <sub>2</sub> O <sub>3</sub> NPs. ....	279
<b>Fig. A2.</b> Elemental analysis of CALPECH NPs. ....	280
<b>Fig. A3.</b> Elemental analysis of SMALLOPS NPs .....	281
<b>Fig. A4.</b> SEM micrographs of CALPECH nanoparticles .....	282



# Introduction

---

Biogas produced *via* anaerobic digestion of biodegradable organic matter has emerged as a renewable and sustainable energy source that can be used to generate heat, power, or as a substitute of natural gas for injection into natural gas grids or use as vehicle fuel (Ángeles et al., 2021; Ferreira et al., 2019; Mulu, M'Arimi, et al., 2021). The composition of biogas depends on the oxidation-reduction state and biodegradability of the organic carbon present in the substrate and the type of the anaerobic digester (Das et al., 2022a; Rodero et al., 2018). The typical composition of biogas is 50-75% methane (CH<sub>4</sub>), 25-50% carbon dioxide (CO<sub>2</sub>), 0-3% hydrogen sulfide (H<sub>2</sub>S), 0-10% nitrogen (N<sub>2</sub>) (0-1%) hydrogen, 0-1% ammonia, and trace levels of halogenated compounds and volatile organic compounds (Aghel et al., 2022). The presence of these contaminants limits the use and energetic value of raw biogas and their removal is mandatory before injection to the natural gas grid or as a vehicle fuel (Rodero et al., 2018).

Several technologies for biogas upgrading are available at commercial level *i.e.* water scrubbing, chemical scrubbing, cryogenic partition, pressure swing adsorption, membrane separation and organic solvent scrubbing. However they are highly energy demand and have environmental impacts. Thus, the implementation of biological methods has attracted an increasing attention. Photosynthetic biogas upgrading using microalgae stands as a promising technology due to its economic and environmental advantages.

Photosynthetic biogas upgrading based on a symbiosis of microalgae-bacteria has emerged as an attractive, cost-effective and environmental option for CO<sub>2</sub> and H<sub>2</sub>S removal from biogas (Rodero, Carvajal, et al., 2020; Rodero et al., 2019), since the produced O<sub>2</sub> by microalgae is consumed by sulfur-oxidizing bacteria to oxidized H<sub>2</sub>S to SO<sub>4</sub><sup>-</sup> (Ángeles et al., 2021). This technology has proved to reach CO<sub>2</sub> removals up to 98.6% at pilot and demo scale (Rodero, Carvajal, et al., 2020; Rodero, Severi, et al., 2020). Additionally, this technology has been feasible when microalgae is grown in anaerobic effluents, which are rich in nutrients. In this way, photosynthetic biogas upgrading can promote a process where nutrients and energy is recovered to produce biomass (Rodero et al., 2018). Nevertheless, there are some challenges and limitations that need to be addressed such as: i) low CO<sub>2</sub> mass transfer to the culture medium, ii) high sensitivity of biomethane quality to variations in the liquid and gas flow rates, pH and alkalinity, and iii) diurnal and seasonal variability of environmental parameters influencing photosynthetic activity (Bose et al., 2019).

The weak diffusion and dissolution of CO<sub>2</sub> in water leads to inefficient use of the CO<sub>2</sub> molecule by algae to synthesize organic macromolecules (Cheng et al., 2020). Therefore, increasing the concentration of the dissolved CO<sub>2</sub> in the culture media is essential for CO<sub>2</sub> fixation by photosynthesis (Cheng et al., 2020). Hence, the CO<sub>2</sub> residence time during the cultivation of the microalgae must be sufficient for it to be retained (Vaz, Mastrantonio, et al., 2019) to achieve efficient transfer into the culture medium and prevent any photosynthetic cell starvation (Kacheff et al., 2014) and CO<sub>2</sub> losses (Vaz, Costa, et al., 2019). The increase in CO<sub>2</sub> fixation leads to rich nutrition to the microalgae resulting in an increase in biomass productivity

during logarithmic growth and the accumulation of value-added products (Ling et al., 2015; Vaz, Mastrantonio, et al., 2019; Zeng et al., 2012).

Recently, the use of adsorbent materials has become popular in the CO<sub>2</sub> capture industry, especially the use of nanoporous materials such as metal nanoparticles (NPs) or mesoporous carbon NPs. In this regard, NPs can be added to microalgae cultures to create a microorganism-particle assembly, which can be used for CO<sub>2</sub> fixation and *in-situ* conversion to biomass (Li et al., 2016a). Thus, gas remains adsorbed on the nanoparticles to be gradually desorbed into the culture medium, and rapidly consumed by the microalgae.

Even if the addition of mesoporous NPs could represent an innovative strategy for improving CO<sub>2</sub> mass transfer to microalgae culture, the addition of metal oxide NPs to microalgae culture is a controversial topic and the majority of the studies are focused on their toxic effect (Liang et al., 2020). In this way, the number of studies assessing the benefits of NPs addition on microalgae metabolism (He et al., 2017) and literature on the effect of NPs on photosynthetic biogas upgrading is scarce.



# Objectives and Thesis Outline

---

## 2.1 Objectives

The main objective of this PhD thesis was to assess the effect of nanoparticles on microalgae cultures devoted to biogas upgrading.

To fulfil the main objective, this thesis was divided as follows:

1. In the first part different  $\text{Fe}_2\text{O}_3$  nanoparticles were synthesized to find the optimal nanoparticles and concentration for microalgae growth and macromolecule accumulation. The specific objectives of this section were:
  - To assess the influence of crystal phase of  $\text{Fe}_2\text{O}_3$  nanoparticles on *Chlorella* sp. cultures.
  - To assess the effect of wastewater composition on *Chlorella* sp. biomass production and nutrient and energy recovery.
  - To assess the effect long term exposure to  $\text{Fe}_2\text{O}_3$  nanoparticles in a mixed microalgae-cyanobacteria consortium grown in wastewater.
2. In the second part, the effect of metal oxide and mesoporous carbon nanoparticles on *Chlorella sorokiniana* cultures and in a mixed microalgae-bacteria consortium was assessed under a synthetic biogas atmosphere. The specific objectives of this section were:



- To assess the influence of nanoparticles on H<sub>2</sub>S (contained in biogas) removal.
  - To assess the effect of different concentrations (10, 20, 40 and 70 mg L<sup>-1</sup>) of different nanoparticles (SiO<sub>2</sub>, Fe<sub>2</sub>O<sub>3</sub>, and two different carbon coated zero-valent iron) on microalgae growth, CO<sub>2</sub> consumption, and microalgae metabolism.
  - To assess the effect of light source (visible and visible + UV) on nanoparticles-microalgae assembly.
3. In the third part, the effect of carbon coated zero-valent nanoparticles in an indoor pilot plant high rate algal pond (HRAP) interconnected to an absorption column devoted to biogas upgrading was assessed. The specific objectives of this section were:
- To assess the influence of the nanoparticles on microalgae growth.
  - To assess the influence of the nanoparticles on nutrient uptake by microalgae.
  - To assess the influence of the nanoparticles on the composition of the upgraded biomethane.

## **2.2 Thesis outline**

This PhD thesis is based in scientific articles sequentially ordered according the specific objectives.

In **Chapter 1**, a detailed review of the state of the art, current trends and perspectives of nanoparticles applied to microalgae is presented. The effects of nanoparticles in tailoring the microalgae metabolic pathways and their morphologic toxicity were investigated as well. This chapter also highlights the current limitations of the photosynthetic biogas upgrading process and proposes the use of nanoparticles as a technology that can be implemented to overcome some limitations.

In **Chapter 2**, batch assays at laboratory scale were carried out to assess the influence of the crystal phase on *Chlorella* sp. cultures growth and macromolecule accumulation. Low concentrations of the Fe<sub>2</sub>O<sub>3</sub> nanoparticles were added to the cultures, ranging from 5 to 20 mg L<sup>-1</sup> to prevent growth inhibition.

In **Chapter 3**, the viability of microalgae cultivation in wastewater was evaluated under environmental conditions. Different wastewater dilutions were assessed to compare their influence in biomass productivity, biomass composition, and nutrient and energy recovery. Since no significant difference was observed in energy recovery from microalgae biomass, pristine wastewater was used to assess the long-term exposure of a mixed microalgae-cyanobacteria consortium to Fe<sub>2</sub>O<sub>3</sub> nanoparticles (**Chapter 4**). During the later experiments, Fe<sub>2</sub>O<sub>3</sub> nanoparticles concentration were gradually increased and the effect on biomass production (gVSS L<sup>-1</sup>), nutrient uptake and carbohydrates and lipids production were evaluated.

Afterwards, the effect of mesoporous nanoparticles of Fe<sub>2</sub>O<sub>3</sub>, SiO<sub>2</sub>, and two different carbon coated zero-valent iron on *Chlorella sorokiniana* cultures (**Chapter 5**) and a mixed microalgae-bacteria consortium (**Chapter 6**) was

elucidated at laboratory scale. The assays were conducted in batch mode, under a synthetic biogas atmosphere and under visible and visible + UV light. The effect of different concentrations of the different nanoparticles on biomass productivity, CO<sub>2</sub> consumption and carbohydrates and lipid production was evaluated.

In **Chapter 7**, the effect of zero valent iron nanoparticles on photosynthetic biogas upgrading was elucidated. The system consisted of a 180 L high rate algal pond (HRAP) interconnected to an absorption column where the upgrading process is carried out. The nanoparticles were added to the HRAP at a concentration of 70 mg L<sup>-1</sup>, and then the nanoparticles were daily added at the same concentration. The performance of the system in terms of biomass production, nutrient uptake and the composition of the upgraded biomethane were compared before and after the addition of the nanoparticles.

The discussion of the obtained results is presented in **Chapter 8**. Finally, the conclusions and future prospects are presented in **Chapter 9**.

# Chapter 1

---

## State of the art

This chapter is adapted from the publication:

- Vargas-Estrada, L., Torres-Arellano, S., Longoria, A., Arias, D. M., Okoye, P. U., & Sebastian, P. J. (2020). Role of nanoparticles on microalgal cultivation: A review. *Fuel*, 280 doi:10.1016/j.fuel.2020.118598
- Vargas-Estrada, L., Longoria, A., Arenas, E., Moreira, J., Okoye, P. U., Bustos-Terrones, Y., & Sebastian, P. J. (2022). A review on current trends in biogas production from microalgae biomass and microalgae waste by



## 1. Introduction

Biogas produced via anaerobic digestion of biodegradable organic matter has emerged as a renewable and sustainable energy source that can be used to generate heat, power, or as a substitute of natural gas for injection into natural gas grids or use as vehicle fuel (Ángeles et al., 2021; Ferreira et al., 2019; Mulu, M'Arimi, et al., 2021; Vargas-Estrada, Longoria, Arenas, et al., 2021). Biogas composition strongly depends on the substrate and type of anaerobic digester (Das et al., 2022b), but is typically mainly composed of 50-75% CH<sub>4</sub> and 25-50% carbon dioxide (CO<sub>2</sub>), and other minor contaminants such as 0-3% hydrogen sulfide (H<sub>2</sub>S), 0-10% nitrogen (N<sub>2</sub>) (0-1%) hydrogen, 0-1% ammonia, and trace levels of halogenated compounds and volatile organic compounds (Aghel et al., 2022; Mulu, M'Arimi, et al., 2021). The presence of these contaminants limits the use of raw biogas, and their removal is mandatory prior use as a vehicle fuel or injection into the natural gas grid (Marín et al., 2021; Rodero, Carvajal, et al., 2020). To date, several physical and chemical technologies for biogas upgrading are available at commercial level such as water scrubbing, chemical scrubbing, cryogenic partition, pressure swing adsorption, membrane separation and organic solvent scrubbing (Aghel et al., 2022; Mulu, M'Arimi, et al., 2021). However, these technologies require a high energy demand and exhibit large environmental impacts (Rodero et al., 2018). In this context, the implementation of biological methods such as photosynthetic biogas upgrading using microalgae has attracted an increasing attention based on its economic and environmental advantages.

Photosynthetic biogas upgrading is based on a solar-driven CO<sub>2</sub> fixation by microalgae that has emerged as an attractive, cost-effective and environment friendly option for CO<sub>2</sub> and H<sub>2</sub>S removal from biogas (Ángeles et al., 2021; M. del R. Rodero, Carvajal, et al., 2020; Rodero et al., 2019). Photosynthetic biogas upgrading in algal-bacterial photobioreactors interconnected to an absorption column has demonstrated to be a feasible technology (Franco-Morgado et al., 2018; Marín et al., 2020; Meier et al., 2015; Posadas et al., 2015; Rodero, Carvajal, et al., 2020; Toledo-Cervantes et al., 2016; Xu et al., 2015), reaching CO<sub>2</sub> removals up to 98.6% at pilot and demo scale (Rodero, Severi, et al., 2020) (Rodero, Carvajal, et al., 2020). Conducted studies by Posadas et al. (Posadas et al., 2016), Lu et al. (2018) and Zhao et al. (2019) demonstrated that the CO<sub>2</sub> of about 99%, 94.8%, and 74.2% respectively could be removed from biogas using microalgae under indoor conditions. Moreover, Posadas et al. (2017) assessed the biogas upgrading via microalgae photosynthetic CO<sub>2</sub> capture under outdoor conditions and observed a CO<sub>2</sub> removal ranging from 50 to 92%. Similarly, Marín et al. (2018) assessed the seasonal variation of biogas upgrading under outdoor conditions and observed a CO<sub>2</sub> concentration of 0.7% in biogas during August and 11.9% during December.

Even if photosynthetic biogas upgrading stands as a cost-effective and sustainable technology, still presents some challenges and limitations that need to be addressed:

- Low CO<sub>2</sub> mass transfer to the culture medium
- High sensitivity of biomethane quality to variations in the liquid and gas flow rates, pH and alkalinity

- Diurnal and seasonal variability of environmental parameters influencing photosynthetic activity (Bose et al., 2019).

In this context, innovative operational strategies are required to enhance CO<sub>2</sub> biofixation during photosynthetic biogas upgrading.

Recently, the use of nanoporous materials has recently attracted a renewed attention in the field of CO<sub>2</sub> capture because they exhibit key advantages such as a large surface area to volume ratio, high reactivity, abundant active sites and high adsorption capacity (Kumar et al., 2020). Metal oxide nanoparticles (NPs) and nanoporous carbons rank among the most popular nanomaterials for CO<sub>2</sub> capture (Kumar et al., 2020). Three potential mechanisms have been hypothesized to explain the CO<sub>2</sub> capture enhancement by the addition of NPs :

- 1) Bubble braking effect, where NPs induce a small sized bubble and hence the diffusion area increases.
- 2) Shuttle effect, where the gas is adsorbed to the NPs surface and then is released into the liquid.
- 3) Hydrodynamic effect, where the NPs collide, inducing turbulence and refreshing the liquid-gas boundary layer (Choi et al., 2015).

The mechanism of interaction will depend on operational factors, such as the type of reactor, agitation and the liquid phase (Kluytmans et al., 2003). The shuttle and the hydrodynamic effect have been previously observed in stirred tanks (Alper & Öztürk, 1986; Kluytmans et al., 2003), although the results reported are contradictory, in both cases the mass transfer was increased. Thus, mesoporous NPs



of metal oxides and carbon could represent an innovative tool to enhance CO<sub>2</sub> fixation during photosynthetic biogas upgrading.

The addition of metal oxide NPs to microalgae culture is a controversial topic and the majority of the studies are focused on their toxic effect (Liang et al., 2020), and the number of studies assessing the benefits of NPs addition on microalgae metabolism is scarce (He et al., 2017), however the addition of nanoparticles during microalgae cultivation and harvesting presents attractive prospects (Hossain et al., 2019). Nanoparticle addition in the microalgal cultivation stage can improve the yield of CO<sub>2</sub> absorption from the atmosphere and can even enhance an efficient light conversion in the photobioreactor, boosting the microalgae growth. Although the addition of nanoadditives to microalgae cultures presents some advantages, several aspects related to the characteristics and the concentration of the nanoparticles must be considered. The most important aspect that relates to the toxic effects of nanoparticles on different microalgae species, specifically from compounds, such as zinc oxide (ZnO) (Zhou et al., 2014a), chromium oxide III (Cr<sub>2</sub>O<sub>3</sub>) (Henning et al., 2016a), zero-valent iron (ZVI) (Lei et al., 2016a), cerium dioxide (CeO<sub>2</sub>) (Hoecke et al., 2011; Manier et al., 2013a), graphene oxide (GO) (Nogueira et al., 2015) and titanium dioxide (TiO<sub>2</sub>) (Wang et al., 2011) requires detailed investigation.

Nanoparticle toxicity depends on their characteristics (particle size, oxidation state, crystal structure), concentration, cultivation media, and microalgae species. Most of the reported studies about the addition of nanoparticles to microalgal culture are focused on assessing the toxicity of nanoparticles and how they impact the marine environment (Chen et al., 2018a; Lei et al., 2016b; Manier et al., 2013b;

Navarro et al., 2008a; Sadiq et al., 2011a; Zhou et al., 2014b). This chapter aims to present recent trends and perspectives on nanoparticles applied to microalgae cultivation. The effect of different nanoparticles in metabolic pathways of microalgae, light conversion, toxicity, cellular damage, and accumulation of intracellular compounds are reviewed in detail. Outlook on process optimization for improved microalgae growth was recommended. It is hoped that this chapter would intensify research on the efficient application of nanoparticles to microalgae culture to propagate energy-effective commercialization of microalgae for vast application channels.

## **2. Nanoparticles overview**

Nanotechnology is a technology for invention, synthesis, and application of materials at the nanoscale. Nanotechnology produces materials with specific properties and functions, different than their counterparts. Nanomaterials can be classified according to their size ranges in different dimensions (Rai et al., 2018; Yu et al., 2015):

- 0-dimension, this category considers spherical shaped particles with a diameter ranging between 1- 100 nm, such as nanoparticles, fullerenes, and quantum dots.
- 1-dimension, this category considers nanomaterials with two dimensions in the nano range, such as nanotubes, nanofibers, nanoribbons, nanowires, and nanobelts.

- 2-dimension, this category considers nanomaterials with one dimension in the nano range and two larger than 100 nm, such as graphene, nanosheets/nanolayers.
- 3-dimension, in this category nanomaterials, have all the three dimensions larger than 100 nm and exhibited nano-sized effects, such as porous nanostructures.

Nanoparticles feature several advantages over their bulk particles/particulate matter, such as a high surface area to volume ratio, which leads to increased heat treatment, improved mass transport channels, dissolution rate, and catalytic activity. Also, nanoparticles have diverse functionalities, easy to functionalize, abundant surface active sites with improved electrical and optical properties, and high adsorption capacity (Anwar et al., 2018; Khezerlou et al., 2018; Klaine et al., 2008; Mora-Godínez et al., 2020; Nguyen et al., 2019a; Panahi et al., 2018; Rai et al., 2018). The classification of nanoparticles is vast and varies depending on their chemical composition, origin, size, and morphology (Capaldi Arruda et al., 2015; Tighe-Neira et al., 2018). **Fig. 1.** summarizes the classification of nanoparticles based on the type of material, origin, size, composition, and morphology.

Nanotechnology has gained popularity and a large variety of nanomaterials have been developed, and used in different fields of research. Besides, the use of nanotechnology has significantly advanced technological activities in many industrial applications (Rai et al., 2018). Nanoparticles are widely used in commercial products, from plastics, cosmetics, ultra-high-definition screens,

medical applications, pharmaceuticals, environmental field, among others (Besha et al., 2020; Panahi et al., 2018; Tighe-Neira et al., 2018). The application of nanotechnology and nanoparticle engineering has a significant influence on the economic viability of microalgae-based products, such as oils, lipids, bioactive compounds, and biofuels (Duman et al., 2019; Javed et al., 2019; Lau et al., 2020a).

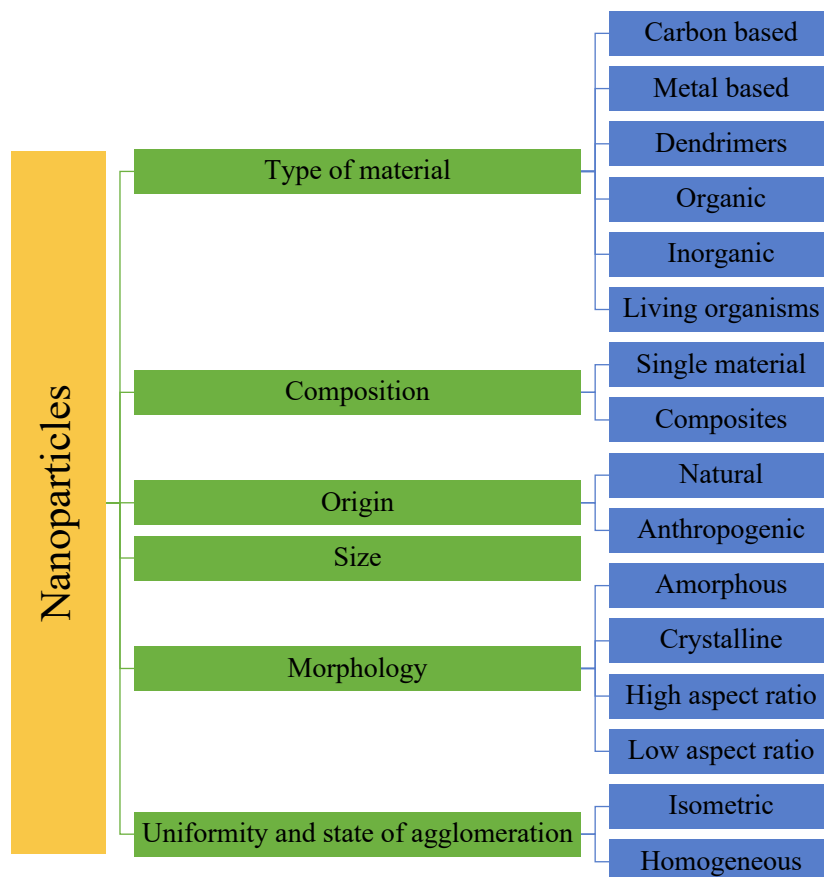


**Fig. 1.** Classification of nanoparticles.

### **3. Effects of nanoparticles addition on microalgal growth**

Metal nanoparticles have been integrated into microalgae culture at different concentrations to test their effects on the growth rate, biomass production, and accumulation of intracellular compounds. These materials have been used as nutritional supplements for photosynthetic microalgae cells to improve their growth and lipid production (Sarma et al., 2014). Also, nanoparticles in culture media can be considered as competitors of nutrient absorption, stimulating microalgae's rapid absorption of nutrients and, sometimes, lipid accumulation. For instance, TiO<sub>2</sub> nanoparticles may adsorb nutrients such as Zn and P, limiting their availability to algae (Ji et al., 2011a). Another benefit of using nanoparticles is that they have bactericidal properties, inhibiting the growth of microbial and fungi populations that might coexist in the media, which are nutritional competitors of microalgae.

Notwithstanding the notable advantages of adding nanoparticles to microalgae culture, it is essential to mention that most of the benefits were obtained when a low concentration of nanoparticles was added to the culture. Many chemicals at low concentrations, such as heavy metal, cyanide, polycyclic aromatic hydrocarbons, polychlorinated biphenyls, pesticides, and organic arsenic compounds, showed the hormesis effect on different biological systems (Chen et al., 2018b).

Chen et al. (2018b), studied the addition of cobalt (Co) nanoparticles to three different species of microalgae, *Platymonas subcordiformis*, *Chaetoceros curvisetus*,

and *Skeletonema costatum*, at different concentrations. They observed no inhibition in *P. subcordiforus* after 24 h of exposure. Consequently, they reported that  $1 \text{ mg L}^{-1}$  Co nanoparticles promoted the microalgae growth, confirming a hormesis effect. Also, as the Co nanoparticles concentration increased, the inhibition effect increased simultaneously. Furthermore, the microalgae presented different sensitivity to Co nanoparticles, with *P. subcordiforus* and *S. costatum* being the least and highest sensitive microalgae.

Similarly, Ji et al. (2011a), reported that  $\text{Al}_2\text{O}_3$  nanoparticles enhanced the *Chlorella* sp. microalgae growth by 18.9% after 4 days of exposure to a concentration of  $1000 \text{ mg L}^{-1}$   $\text{Al}_2\text{O}_3$ . Pedroso and co-workers (2013a), studied the toxicity of CuO nanoparticles in *Chlamydomonas reinhardtii*. Different concentrations of CuO nanoparticles were assessed, ranging from 0.1, 1, 10, 100, and  $1000 \text{ mg L}^{-1}$ . They observed a viability stimulation at the lower concentrations tested and a gradual decrease as the concentration of CuO increased. Moreover, they revealed that after 72 h of exposure, the cell density was significantly lower than the control, with the addition of  $1000 \text{ mg L}^{-1}$  CuO. Henning et al. (2016a), studied the effect of  $\text{Cr}_2\text{O}_3$  nanoparticles on *C. reinhardtii* at different concentrations 0.01, 0.1, 1.0, and  $10 \text{ g L}^{-1}$ . Observing higher cell densities when exposed to  $\text{Cr}_2\text{O}_3$  of 0.1 and  $1.0 \text{ g L}^{-1}$  concentrations after 72 h of exposure, however, a significantly lower cell density was observed at  $10 \text{ g L}^{-1}$   $\text{Cr}_2\text{O}_3$ .

Hence, based on the mentioned studies, lower concentrations of nanoparticles favored some microalgae species, whereas higher concentrations negatively impacted the microalgae cell density and growth and vice versa. However,

the limit of “low” or “high” concentrations cannot be established since the sensitivity of microalgae to nanoparticles strongly depend on the type of the nanoparticle and the specie of microalgae, and other parameters such as culture media, pH, shape, and size of the nanoparticles.

In terms of toxicity, conducted studies have shown that Ag nanoparticles are one of the most toxic nanoparticles for microalgae due to its high reactivity, fast adsorption, and its antimicrobial properties (Johari et al., 2018; Khezerlou et al., 2018; Klaine et al., 2008; Moreno-Garrido et al., 2015a; Oukarroum & Popovic, 2012a; Sendra et al., 2017a). Thus, research effort has been directed towards finding nanoparticles that can act as nutritional supplements to increase microalgae growth and enhance the accumulation of high-value products. **Fig. 2** summarizes the effects of using nanoparticles on microalgae culture at “low” and “high” concentrations. The following sections include a description of the effects of the addition of nanoparticles to microalgae culture.

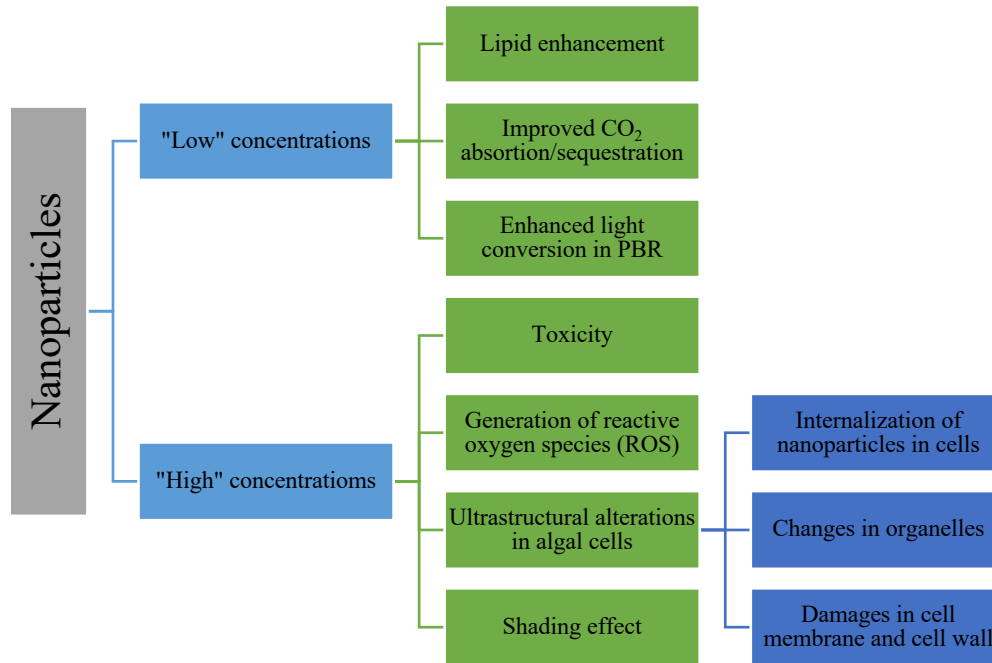


**Fig. 2.** Effects of nano-particles addition to microalgae culture.

### 3.1 Lipid production

The typical stress response in microalgae, is mainly caused by nutrient limitation, and it is performed to accumulate a huge amount of carbon sources in the shape of pigments, starch, lipids, or moieties for self-protection from damage (Kaliyamurthi et al., 2019a). When lipid body reserves are produced, usually the levels of saturated and monounsaturated fatty acids are increased, and long-chain polyunsaturated fatty acids, associated with polar membrane lipids, are decreased, resulting in a decreased cellular growth (Kadar et al., 2012b). Nanoparticles have been added to microalgal culture media as nutritional supplements to enhance their growth and lipid accumulation. Pádřova et al. (2015), observed a lipid increment from 26.20% to 35% in the specie of *Trachydiscus minutus* when 5.1 mg L<sup>-1</sup> zero-valent iron



nanoparticles (nZVI ) were added. A similar performance was observed with *Desmodesmus subspicatus* specie, resulting in about 38% lipid accumulation when the same concentration of nZVI was added.

Furthermore, Ren et al. (2020), revealed that the lipid content of *Scenedesmus* sp. was enhanced when SiC nanoparticles were added. In their study, they use a concentration of 150 mg L<sup>-1</sup> of SiC nanoparticles under xenon light and observed a biomass production of 3.18 g L<sup>-1</sup> and lipid content of up to 40.26%. The increase in the lipid content was attributed to the acetyl-coenzyme A carboxylase (ACCase) activity. ACCase is a key rate-limiting enzyme that catalyzes the first step in the biosynthesis of fatty acids. Thus, they demonstrated that SiC nanoparticles stimulate the activity of ACCase under xenon light, which resulted in increased lipids synthesis.

Kadar et al. (2012a), studied the effect of nZVI on different microalgae species and reported a lipid enhancement of 41.90% in *Tetraselmis suecica* when exposed to uncoated nZVI. They also observed a lipid increment of 46.34% in *Pavlova lutheri* when inorganically coated nZVI powder was added. Notwithstanding, the authors could not determine whether the lipid increment was attributed to the increased bioavailability of Fe and/or a stress response that resulted from an increased carbon fixation to lipid storage reserves. The addition of nZVI showed a positive response in *P. lutheri* since no decrease in the cellular growth was observed. With these findings, it is possible to consider the addition of nZVI to the culture media of *P. lutheri* to produce high-value products or biofuels, such as biodiesel. Vaz et al. (2020), reported an increment of 10.9 and 16.7% in the lipid content of *Chlorella fusca* LEB

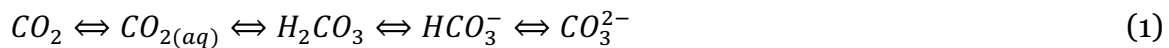
111 when cultivated with 0.3 and 0.5 g L<sup>-1</sup> of nanofibers, under outdoor conditions, respectively. The nanofibers consist contained 4% (w v<sup>-1</sup>) Fe<sub>2</sub>O<sub>3</sub> nanoparticles. Since the composition of microalgae is directly related to the parameters of cultivation such as luminosity, temperature, pH, and CO<sub>2</sub> concentration (Zhao & Su, 2014), they attributed the lipid enhancement to the high luminous intensities reached under outdoor conditions and stress limitations.

Hence, conducted studies demonstrate that the lipid enhancement in microalgae strongly depends on the type and concentration of nanoparticles used on the microalgae species. Noteworthy is that the lipid increment was achieved by the use of nanoparticles, which have a positive effect on cellular activity. For instance, Fe is an essential micronutrient for phytoplankton, as is required to perform fundamental cellular functions like photosynthesis and respiration, and its availability controls phytoplankton productivity, community structure and ecosystem functioning (Kadar et al., 2012c). Thus, iron oxides are promising alternatives due to their low toxicity and strong magnetism and have been broadly used for the treatment of contaminated water and soils (Rocha et al., 2017). Moreover, the activity of Crd1, an enzyme that contains Fe and functions in the Benson and Calvin cycle for chlorophyll biosynthesis and biomass growth, is promoted by Fe<sup>3+</sup> (Cheng et al., 2020).

### **3.2 CO<sub>2</sub> absorption and sequestration**

Photosynthesis is considered the main pathway to utilize the captured CO<sub>2</sub>. Microalgae are considered the prime candidates for biological fixation of CO<sub>2</sub> (Li et

al., 2016b) since it is estimated that 1 ton of microalgae can fix 1.8 tons of CO<sub>2</sub> (Huang & Tan, 2014). Hence a carbon source must be supplied sufficiently to avoid impaired growth (Vaz, Costa, et al., 2019). Although the theoretical calculations indicate that microalgae have a great potential for CO<sub>2</sub> fixation, the weak diffusion and dissolution of CO<sub>2</sub> in water leads to inefficient use of the CO<sub>2</sub> molecule by algae to synthesize organic macromolecules (Cheng et al., 2020). The CO<sub>2</sub> dissolution during microalgae cultivation is represented by the following equilibrium equation (Eq 1) (Rosa et al., 2015):



HCO<sub>3</sub><sup>-</sup> and CO<sub>2</sub> is the carbon source species that are preferentially absorbed by microalgal and cyanobacteria metabolism (Cheng et al., 2020). The increased HCO<sub>3</sub><sup>-</sup> concentration facilitates the carboxysome accumulation, which activates the photosynthetic Calvin cycle. The increase in HCO<sub>3</sub><sup>-</sup> concentration not only serves as a carbon source that can be directly used by microalgae but also reduces the damage caused by reactive oxygen species (ROS) in PSII (Cheng et al., 2020). The formation of these carbon species is related to the pH in the medium. When pH is alkaline, and there is a sufficient CO<sub>2</sub> supply the RuBisCO enzyme is activated, which is responsible for catalyzing CO<sub>2</sub> fixation and is considered the rate-limiting enzyme in the Calvin cycle (Cheng et al., 2020; Vaz et al., 2020). The RuBisCO enzyme activation results in increased photosynthetic efficiency and CO<sub>2</sub> fixation (Vaz, Mastrantonio, et al., 2019). On the other hand, low pH improves the formation of H<sub>2</sub>CO<sub>3</sub> that reduces the activity of the RuBisCO enzyme. Therefore, increasing the concentration of the dissolved CO<sub>2</sub> in the culture media is essential for CO<sub>2</sub> fixation

by photosynthesis (Cheng et al., 2020). Hence, the CO<sub>2</sub> residence time during the cultivation of the microalgae must be sufficient for it to be retained (Vaz, Mastrantonio, et al., 2019) to achieve efficient transfer of into the culture medium to prevent any cell starvation (Kacheff et al., 2014) and CO<sub>2</sub> losses (Vaz, Costa, et al., 2019).

The increase in CO<sub>2</sub> fixation leads to rich nutrition to the microalgae resulting in an increase in biomass productivity during logarithmic growth and the accumulation of value-added products (Ling et al., 2015; Vaz, Mastrantonio, et al., 2019; Zeng et al., 2012). Choi et al. (2012), revealed that the CO<sub>2</sub> fixation by microalgae could be improved if the amount of dissolved gas in the liquid was increased beyond the natural balance of the algal culture. Many methods have been proposed for CO<sub>2</sub> fixation (Anwar et al., 2018; Huang & Tan, 2014), but the main factors that need to be considered are that the adsorption of CO<sub>2</sub> should be energy and cost-effective (Vaz, Mastrantonio, et al., 2019). Recently, the use of adsorbent materials has become popular, especially the use of nanoporous materials such as polymeric nanofibers (Vaz, Costa, et al., 2019). The addition of polymeric nanofibers as CO<sub>2</sub> absorbent in microalgae cultivation is an alternative to increase the permittivity of the gas in the medium, the contact time between the microalgae and the CO<sub>2</sub> and the mass transfer of CO<sub>2</sub> to the cells (Vaz et al., 2020; Vaz, Mastrantonio, et al., 2019). Besides, the use of nanofibers has the advantage of being easily separated from the microalgal biomass (Vaz, Costa, et al., 2019).

Studies have demonstrated that metal nanoparticles or metal oxides can be incorporated into nanofibers to form functional composite nanostructures, which

increase the adsorption efficiencies, resulting in improved diffusion and interactions of molecules (Vaz, Costa, et al., 2019; Vaz et al., 2020; Vaz, Mastrantonio, et al., 2019). The aim of adding nanoparticles to microalgal culture media is to create a microorganisms-particle assembly, which can be used for CO<sub>2</sub> fixation and *in-situ* conversion (Li et al., 2016b). Thus, gas remains adsorbed on the nanofibers to be gradually desorbed into the culture medium, and the desorbing process depends on the pH of the medium (Vaz, Mastrantonio, et al., 2019).

Vaz et al. (2020) studied the CO<sub>2</sub> fixation of *C. fusca* LEB 111 with polymeric nanofibers with 4% Fe<sub>2</sub>O<sub>3</sub> nanoparticles under outdoor and indoor conditions. They observed a higher CO<sub>2</sub> fixation in outdoor assays, attributed to the increase in biomass concentration because of the nanofibers-maintained CO<sub>2</sub> for an extended time. Furthermore, they observed that the assays with higher biomass yielded higher gas fixation. Moreover, the increment in the biomass concentration under outdoor conditions was also attributed to the temperature and luminosity, which are parameters that affect the biomass productivity and CO<sub>2</sub> fixation. High temperatures can reduce the solubility of CO<sub>2</sub> and in consequence, the metabolic activity of microalgae is reduced. Moreover, low luminosity reduces the biomass concentration, but high light intensity can lead to photoinhibition; thus, the wide luminosity spectrum from outdoor conditions promoted the CO<sub>2</sub> fixation. Finally, they concluded that the cultivation of *C. fusca* LEB 111 with nanofibers under outdoor conditions was more cost-effective than indoor cultivation.

Similar studies have reported the use of nanoparticles in their free form to enhance biomass production. **Table 1** summarizes the effect of nanoparticles

addition to microalgae in terms of biomass growth. Jeon et al. (2017), studied the addition of SiO<sub>2</sub> nanoparticles in *Chlorella vulgaris* and observed an enhancement of 177% in biomass production (dry weight). Also, Rudic et al. (2011), reported that CdSe nanoparticles increased the biomass production of *Porphyridium cruentum* by 34-47.5% when the concentration of CdSe ranged between 4.0 – 6.0 mg L<sup>-1</sup>. Pedroso et al. (2013a), observed stimulation of *C. reinhardtii* viability at 0.1 mg L<sup>-1</sup> of CuO nanoparticles, (the lowest concentration tested). Gunawan et al. (2013a), studied the exposure of *C. reinhardtii* to 1,10, 100 mg L<sup>-1</sup> concentrations of TiO<sub>2</sub> nanoparticles and revealed that the proliferation characteristics were not altered despite the observed cellular internalization of TiO<sub>2</sub> on the algal cells.

Kacheff et al. (2014), studied the adaptation of a commercial tubular hydrophilic ceramic membrane into an efficient hydrophobic gas/liquid contactor. The addition of TiO<sub>2</sub> nanoparticles provided a fully controlled delivery of CO<sub>2</sub> into the water at a remarkable efficiency. Also, the addition of a nanoporous layer enhances the gas-to-liquid transfer by more than a factor of 10, although microalgae cultivation was not tested in their study, this adaptation to the tubular hydrophilic ceramic membrane presents a promising alternative to enhance CO<sub>2</sub> capture, which could lead to an increase in microalgae biomass production.

**Table 1.** Effect of nanoparticle addition to microalgae growth

Microalgae strain	Nanoparticle		Time (h)	Biomass growth*, **	Reference
	Type	Concentration (mg L <sup>-1</sup> )			
<i>Chlamydomonas reinhardtii</i>	Cr <sub>2</sub> O <sub>3</sub>	10	72	=	(Henning et al., 2016a)
		100	72	+	
		1000	72	-	
		10000	72	-	
<i>Chlorella pyrenoidosa</i>	α- Fe <sub>2</sub> O <sub>3</sub> γ-Fe <sub>2</sub> O <sub>3</sub> Fe <sub>3</sub> O <sub>4</sub> nZVI - 20 nm nZVI - 50 nm nZVI - 80 nm nZVI - 100 nm	400	96	-	(Lei et al., 2016a)
		400	96	-	
		200	96	-	
		200	96	-	
		200	96	-	
		200	96	-	
		200	96	-	
<i>Chlamydomonas reinhardtii</i>	AgNP <2nm	0.01	72	-	(Sendra et al., 2017a)
		0.04	72	-	
		0.075	72	-	
		0.15	72	-	
		0.3	72	-	
	AgNP <15nm	0.01	72	-	
		0.04	72	-	
		0.075	72	-	
		0.15	72	-	
		0.3	72	-	
	AgNP 30-50 nm	0.01	72	+	
		0.04	72	+	
		0.075	72	+	
		0.15	72	+	
		0.3	72	-	
<i>Phaeodactylum tricornutum</i>	AgNP <2nm     AgNP <15nm	0.01	72	-	
		0.04	72	-	
		0.075	72	-	
		0.15	72	-	
		0.3	72	-	
		0.01	72	-	
		0.04	72	-	
		0.075	72	-	
		0.15	72	-	

		0.3	72	-	
	AgNP 30-50 nm	0.01	72	-	
		0.04	72	-	
		0.075	72	-	
		0.15	72	-	
		0.3	72	-	
<i>Chlorella vulgaris</i> LEB-104	MgSO <sub>4</sub>	1000	144	+	(Sarma et al., 2014)
	TiO <sub>2</sub>	3	72	-	(Sadiq et al., 2011a)
		6	72	-	
<i>Chlorella</i> sp.		12	72	-	
		24	72	-	
		48	72	-	
		96	72	-	
		192	72	-	
	TiO <sub>2</sub>	3	72	-	
		6	72	-	
<i>Scenedesmus</i> sp.		12	72	-	
		24	72	-	
		48	72	-	
		96	72	-	
		192	72	-	
	TiO <sub>2</sub>	1	96	=	(D. Wang et al., 2011)
<i>Ceriodaphnia dubia</i>		10	96	=	
		50	96	=	
		100	96	=	
		200	96	=	
		300	96	=	
	CuO	0.1	72	+	(Pedroso et al., 2013a)
<i>Chlamydomonas reinhardtii</i>		1	72	+	
		10	72	+	
		100	72	=	
		1000	72	-	
	CoNP	0.5	96	-	(X. Chen et al., 2018a)
<i>Platymonas subcordiformis</i>		1	96	-	
		2	96	-	
		5	96	-	



		10	96	-	
		20	96	-	
		30	96	-	
		50	96	-	
		80	96	-	
		100	96	-	
		0.5	96	-	
		1	96	-	
		2	96	-	
		5	96	-	
	<i>Chaetoceros curvisetus</i>	10	96	-	
		20	96	-	
		30	96	-	
		50	96	-	
		80	96	-	
		100	96	-	
		0.5	96	-	
		1	96	-	
		2	96	-	
		5	96	-	
	<i>Skeletonema costatum</i>	10	96	-	
		20	96	-	
		30	96	-	
		50	96	-	
		80	96	-	
		100	96	-	
	ZnO	5	144	-	(Ji et al., 2011a)
		10	144	-	
	<i>Chlorella sp</i>	20	144	-	
		50	144	-	
		100	144	-	
		200	144	-	
		1000	144	-	
	ZnO	0.1	96	-	(Manzo et al., 2013)
		0.5	96	-	
	<i>Dunaliella tertiolecta</i>	0.75	96	-	
		1	96	-	
		3	96	-	
		5	96	-	
		7.5	96	-	
		10	96	-	

\* Biomass growth is compared to the control

\*\* (+) Indicative of biomass increase and (-) Indicative of biomass decrease.

### 3.3 Light conversion

A uniform and sustainable illumination of the cultivation system is still a challenge for microalgae growth. The conventional approach to improving the light condition is the use of nanoparticles in the photobioreactors to dilute and redistribute the intense incident light (Eroglu et al., 2013). Nanoparticles application in microalgal cultures provides several benefits in terms of light absorption. For instance, their fluid nature allows shape flexible and efficient backscattering in the cultivation system, total scattered light flux to the microalgae culture, and the frequency can be controlled by changing the concentration and size (Torkamani et al., 2010a). In the study of Sun et al. (2016), organosilicone particles were doped inside the planar waveguides as the light-scattering media. Compared with a system without waveguides, the illumination surface area per unit volume increased by 10.3 times, and the illuminated volume fractions were up to 410% higher. Likewise, a suspension of SiO<sub>2</sub> nanoparticles was used in the study of Guiannelli et al. (2012), to achieve a uniform distribution of light to *C. reinhardtii* CC124. A 23% net increase in the final chlorophyll *a* concentration was observed when the nanoparticle suspension was used (**Fig. 3.**). In another study, *C. reinhardtii* and *Cyanothece* 51142 were submitted to Ag nanoparticles coupled to localized surface plasmon resonance (LPSR) (Torkamani et al., 2010b). Results showed that the application of Ag nanoparticles could promote a high backscattering of blue light in the light spectrum, obtaining an algal growth by more than 30%.

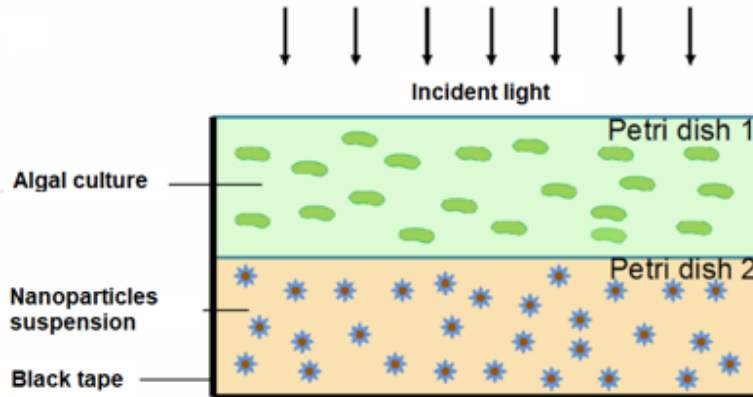


**Fig. 3.** Schematic of the plasmonic miniphotobioreactor enhanced with Ag nanoparticles (Torkamani et al., 2010b).

### 3.4 Toxicity

The toxicity of nanoparticles on microalgae is related to the damage to cellular functions leading to cell death. Toxicity can be related to particle size, crystal form, test methods, and species (Ji et al., 2011b). Navarro et al. (2008a), pointed out two types of toxic effects of nanoparticles:

- a) Direct effects, such as chemical composition and surface chemistry (cytotoxicity).
- b) Indirect effects, such as the release of toxic ions from nanoparticles.

Metal ions released have been considered as the main toxicity pathways of nanoparticles, shading effects, oxidative damage, and photocatalysis also accounted for toxicity effects. Some metallic particles increase its toxicity at the nanoscale because a reduced particle size leads to enhanced solubilization of nanoparticles into toxic metal ions. Nanoparticles also influence the photosynthetic utilization and nutrient uptake of microalgae (Chen et al., 2018b; Johari et al., 2018). Nanoparticles

---

present two main mechanisms of attack (Khezerlou et al., 2018; Miller et al., 2010a), namely (a) generation of ROS and (b) release of metal ions.

The dissolution rate of nanoparticles is influenced by several factors, including particle size surface area, surface curvature, the roughness of the particle, and the characteristics of the media (Suman et al., 2015a). Likewise, intrinsic characteristics of nanoparticles such as size, zeta potential, and extrinsic characteristics of the culture media such as pH and ionic strength have influenced nanoparticles, and in the particular case of Ag nanoparticles, dissolution, agglomeration, the interaction between cells and toxic response (Sendra et al., 2017a). Ag nanoparticles generate free radicals in microorganisms and can deteriorate cellular functions (Oukarroum & Popovic, 2012a). The Ag<sup>+</sup> is dissolved from Ag nanoparticles over time, and the speciation of the dissolved Ag<sup>+</sup> is an important factor involved in the toxicity of metallic nanoparticles in aquatic environments (Sendra et al., 2017b).

Other metal nanoparticles such as Cr<sub>2</sub>O<sub>3</sub>, ZnO, Co, CeO<sub>2</sub>, CuO and TiO<sub>2</sub> nanoparticles, have proved to be toxic in in *Pseudokirchneriella subcapitata* (Manier et al., 2013b), of *Dunaliella tertiolecta* (Miller et al., 2010b), *Chlorella* sp. (Kaliyamurthi et al., 2019b), *Chlorella vulgaris* (Suman et al., 2015b), *C. reinhartii* (Gunawan et al., 2013b), *Platymonas subcurdiformis*, *Chaetoceros curvisetus*, and *Skeletonema costatum* (Chen et al., 2018b), *Scenedesmus* sp. (Sadiq et al., 2011a). The latter suggest that the toxicity of nanoparticles is not only species specific, it also depends on the type and nature of the nanoparticle.

### **3.5 Generation of reactive oxygen species (ROS)**

Overproduction of ROS is believed to be a major mechanism of toxicity of nanoparticles when ROS are produced, chemical reactions occur leading to 1) cell structure damage such as loss of membrane fluidity and oxidation of unsaturated lipids, 2) increased formation of the superoxide radical ( $O_2^-$ ), and 3) ROS accumulation and oxidative stress (Kaliyamurthi et al., 2019a; Lau et al., 2020b; Passos, Felix, et al., 2016; Sarma et al., 2014). On the other hand, ROS at a proper amount can stimulate growth, cell size, lipid productivity, and metabolite accumulation of microalgae (Nguyen et al., 2019b). ROS oxidize proteins, lipids, and nucleic acids leading to changes in cell structure and mutagenesis (Pedroso et al., 2013b). Lipid peroxidation triggered by ROS can lead to impaired cellular function, alterations in physicochemical properties of cell membranes, *i.e.*, increasing the membrane permeability, which may disrupt vital functions such as loss of membrane selectivity, fluidity, and integrity which reduce the viable cells (Lei et al., 2016b; Oukarroum & Popovic, 2012b).

Metallic nanoparticles and ions are reported to cause an increase in the levels of ROS in microalgae. ROS production can be monitored by analyzing the enzymes involved in the management of oxidative stress (Moreno-Garrido et al., 2015b). Increased enzymatic activity is usually an indicative cellular defense against ROS (Déniel et al., 2019a). Microalgae can perform responses to pollutants allowing them to defend or adapt (Déniel et al., 2019b). The presence of ROS increases antioxidants' production, which can neutralize free radicals or their toxic effects (Pedroso et al., 2013b). Enzymes act as neutralizing species for ROS, even though they are located

in different regions of the cell. Antioxidant enzyme activity can protect cells from the adverse effects of reactive oxygen species. Superoxide dismutase (SOD), catalase (CAT), and peroxidase (POD) enzymes help to check cellular levels of ROS (Suman et al., 2015b). The production of exopolymeric substances in algae has increased upon exposure to nanoparticles and might contribute to detoxification mechanisms (Navarro et al., 2008b).

The concentration of nanoparticles plays an important role in the production of antioxidant enzymes. In general, ROS production is one toxicity pathway that causes cellular damages such as loss of membrane fluidity and oxidation of unsaturated lipids and needs to be monitored to prevent cell death (Déniel et al., 2019b). The size of the nanoparticles plays an important role in the ROS production since the large specific surface area of nanoparticles renders them highly reactive with high electron density, which leads to interaction with the biomolecules (Zhou et al., 2014b).

### **3.6 Ultrastructural alterations in algal cells**

ZnO nanoparticles cause toxicity to *C. vulgaris* due to the induction of ultrastructural alterations of the algal cells. Cell membranes can absorb ZnO, and a small amount of the nanoparticles can enter the cells, thus causing damage to the chloroplasts and membranes in the algal cells (Zhou et al., 2014b). The photosynthetic system is, in general, sensitive to the presence of nanoparticles. Some researchers have observed a drop in photosynthetic activity (Déniel et al., 2019b).

Inhibition on Photosystem II (PSII) may be due to chlorophyll degradation, probably by the formation of ROS (Pedroso et al., 2013b).

In the case of cellular structural changes, *C. reinhardtii* increased its cell size from 5  $\mu\text{m}$  to 8  $\mu\text{m}$  when it was exposed to 300  $\mu\text{g L}^{-1}$  of Ag nanoparticles (Sendra et al., 2017b). Conversely, when this specie was exposed to CuO, the CuO-aggregates appear to be in contact with some organelles, which could be the cytosol, vacuoles, and the close sites to the nucleus (Pedroso et al., 2013b). Gunawan et al. (2013b), revealed the accumulation of zinc in polyphosphate bodies in *C. reinhardtii*.

*Chlorella* sp. has also been reported to suffer structural damage when exposed to nanoparticles. In natural conditions, *Chlorella* sp. is spherically-shaped with a diameter ranging between 2-10 $\mu\text{m}$  (Kaliyamurthi et al., 2019b; Sadiq et al., 2011b). The exposure of this specie to 50  $\text{mg L}^{-1}$  ZnO increases the cell size due to an accumulation of lipids, and the cell division was barely observed. At 100  $\text{mg L}^{-1}$  of ZnO, the *Chlorella* sp. spherical shape disappeared, and a slight aggregation was observed. At 200  $\text{mgL}^{-1}$  violent aggregation was observed as well as a cell mass reduction, and the cells presented irregular shapes. The morphological changes can be attributed to oxidative stress, cell wall degradation, and leakage of cellular material (Kaliyamurthi et al., 2019b). In another study, Demir et al. (2015) revealed that exposure to  $\alpha\text{-Fe}_2\text{O}_3$  nanoparticles causes flocculation and growth depletion in *Nannochloropsis* sp., while, Chen et al. (2018b) reported that the cell sizes of *Skeletonema costatum* and *Chaetoceros curvisetus* were smaller with larger specific surface areas and *Platymonas subcordiformis* adsorbed more Co nanoparticles resulting in agglomeration. Changes in organelles, such as an increase in the number

of plastoglobuli inside the chloroplasts have been also reported. This change is suggested to occur when photosynthetic activity decreases (Henning et al., 2016b).

### **3.6.1 Internalization of nanoparticles in cells**

The cell wall plays an important role in nanoparticle-microalgae interactions. Cell walls are the primary site for interaction and a barrier for the entrance of nanoparticles (Navarro et al., 2008b). Uptake of nanoparticles by microalgae depends on the characteristics of the cell wall as the thickness ranges from 5 to 20 nm (this determines its barrier properties) (Sendra et al., 2017b). The cell wall is semi-permeable and can allow the crossing of very small particles (Déniel et al., 2019b). In this context, contact with nanoparticles can induce new pores forming in the membrane, thereby rendering it more permeable and less selective (Pedroso et al., 2013b).

Once the nanoparticles have penetrated the cell wall, the membrane and reached the cytosol, the nanoparticles can bind to cellular organelles, interfering in metabolites, photosynthetic or respiratory processes, and inducing ROS formation (Pedroso et al., 2013b). When nanoparticles penetrated the cytoplasm, growth inhibition, and photosynthetic activity inhibition were observed (Moreno-Garrido et al., 2015b). Studies have reported that when the algal cells ingest metals, two phases occur: 1) A rapid assimilation, is typically terminated within 10 minutes; 2) the transport into the cytoplasm (Suman et al., 2015b). The secretion of the extracellular matrix could mediate the particles' uptake under environmental stress (Gunawan et al., 2013b). The extracellular matrix binds to the particles, rendering them



bioavailable to phagocytotic cellular uptake. Ag nanoparticles < 80 nm, for instance, seem to be able to enter into bacterial cells (Moreno-Garrido et al., 2015b). Sendra et al. (2017b) reported toxic effects due to the internalization and adhesion of Ag nanoparticles onto the cell wall. Otherwise, Kaliamurthi et al. (2019b), reported the permeabilization of the *Spirulina platensis* cell membrane during the biosynthesis of Ag nanoparticles. Notably, the ion released, and the ROS generation is concentration-dependent; thus, a low concentration is desired to avoid severe cellular damage.

### **3.6.2 Damages in the cell membrane and cell wall**

The surface of algae contains many functional groups with high affinity for metal ions and carry a net negative charge mainly attributed to the presence of carboxylic, sulfhydryl, and phosphatic groups, which act as binding sites to transport metal ions across the cell membrane and into the cell (Suman et al., 2015b). The cell wall and the plasma membrane can be particularly affected by the physical or biochemical impact of nanoparticles (Navarro et al., 2008b; Oukarroum & Popovic, 2012b). The exposition of metallic ions in high concentrations can affect the permeability of the cell wall and the plasma membrane facilitating nanoparticle internalization (Pedroso et al., 2013b). The release of ions, such as Cr, can damage the cell wall and the cell membrane resulting in the formation of new pores with larger sizes that would allow nanoparticle penetration (Henning et al., 2016b). It has been reported that 50 nm size Ag nanoparticles are not able to pass through the cell wall but might act as a binding agent between algal cells (Oukarroum & Popovic, 2012b). The Ag

nanoparticles or  $\text{Ag}^+$  that reach the cell wall could damage the cell membrane and cause loss of membrane integrity and cell lysis (Sendra et al., 2017b).

The strong adhesion of nanoparticles on the algal cells may lead to direct physical effects, such as cell membrane disruption or indirect effects, such as the reduction of the available light necessary for algal growth or the limitation of the nutrient intake by clogging to the cell walls of the algal cells (Manier et al., 2013b; Oukarroum & Popovic, 2012b; Sadiq et al., 2011b). Surface attachment of nZVI may disturb the electronic and/or ionic transport chains of the cell membrane (Lei et al., 2016b). The adsorption of metallic nanoparticles to the cellular surface can increase cellular weight and, consequently, remove microalgae from the photic zone, which will affect photosynthesis (Moreno-Garrido et al., 2015b). Huang et al. (2005), reported that the addition of  $\text{TiO}_2$  nanoparticles caused a 2-fold-increased in cell weight on *Pseudokirchneriella subcapitata*. Aruoja et al. (2009b), reported that the adsorption of Ti nanoparticles is pH-dependent and a maximum Ti adsorption occurred when pH was 5.5, which lead to algal flocculation.

The deposition/aggregation strongly depends on the nanoparticles surface properties, mainly attributed to parameters such as temperature, ionic strength, pH, particle concentration, and size (Navarro et al., 2008b). Besides damaging the cell membrane or for interactions between the nanoparticle-cell wall, the formation of aggregates in the media is one toxicity pathway that in most cases limits the light availability of cells and can inhibit photosynthesis.

### 3.7 Shading effect

The shading effect refers to the reduction of the captured light of the algae cells (Déniel et al., 2019b). Cheloni et al. (2016), showed a correlation between photosynthesis inhibition and shading. Shading effect is considered a potential toxic mechanism of nanoparticles, which is possibly the main cause of the algal growth inhibition, rather than the cell membrane damage or DNA damage (Lei et al., 2016b). It might be attributed to the adsorbed nanoparticles to algae, which might increase cellular weight, leading to cell sedimentation and light reduction (Navarro et al., 2008b). This fact may lead to an increase in the chlorophyll content to optimize light availability as an attempt to overcome the shading effect (Pedroso et al., 2013b).

In general, results from several studies show that nanoparticles accumulation on the surface of photosynthetic organisms (nanoparticles aggregates) may reduce the light availability to the entrapped algal cells, since they inhibit photosynthetic activity, leading to inhibition of the algal growth (**Fig. 4**) (Hu et al., 2018a; Navarro et al., 2008a; Sadiq et al., 2011b). Agglomerates of Co nanoparticles reduced the light available to three studied microalgae, *Platymonas subcordiformis*, *Chaetoceros curvisetus*, and *Skeletonema costatum*, affecting the photosynthesis process and inhibiting their growth (Chen et al., 2018b).

On the other hand, the shading effect of light caused by CuO nanoparticles on *C. reinhardtii* was not significant to impel an inhibitory effect on the algae growth (Pedroso et al., 2013b). Besides, this is a result of nanoparticle aggregation, which strongly depends on the properties of the nanoparticles. Hence, it is established that larger nanoparticles/agglomerates lead to higher shading effect. As already

mentioned, the shading effect depends on the microalgae specie and the nanoparticle properties (Hu et al., 2018b).

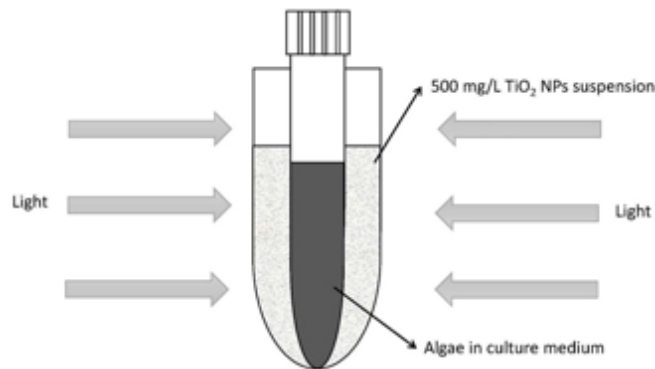


**Fig. 4.** Diagram of the shading effect of 500 mg L<sup>-1</sup> TiO<sub>2</sub> nanoparticles on microalgae (Hu et al., 2018b).

## 4. Prospects and recommendations

Research about the use of nanoparticles on microalgae cultivation is mostly focused on assessing their toxicity, it is important to make a switch and focused research on exploiting the advantages of the use of nanoparticles on microalgae cultivation to improve their growth and yield towards efficient biorefinery approach.

The use of nanoparticles on microalgae cultivation is a promising pathway to tailor biomass production and biofuels/high-value products. However, optimizing the use of nanoparticles on microalgae cultivation either by adding them in their single form, as composites (with nanofibers), or by adding them in the photobioreactors requires further research effort.

Moreover, further and intensified studies on the effect of nanoparticles on the harvesting process integrated with the growth of microalgae could render the process energy-effective (Abo Markeb et al., 2019; Bayat Tork et al., 2017; Duman et al., 2019; Hu et al., 2013). Following the biorefinery approach, to make the process more environmentally and economically friendly and sustainable, it is strongly suggested that research effort should be directed towards the addition of nanoparticles to wastewater cultivated microalgae. Since it is established that wastewater presents turbidity, which can result in a decrease in biomass production, thus the addition of nanoparticles could aid a better light distribution and CO<sub>2</sub> dilution. The later could have a positive impact on photosynthetic biogas upgrading, since CO<sub>2</sub> mass transfer is one of the major limitations of the process. In this context, the addition of NPs into bacterial-algal photobioreactors could boost photosynthetic biogas upgrading, thus resulting in a biomethane that meets international regulations coupled to an enhanced biomass production.

Finally, the viability of microalgae cultivation could be boosted by the diversified production of vast value-added products. Also, the techno-economic evaluation of the process will aid in process intensification to achieve overall energy-efficient cultivation and harvesting. Finally, on studies have been reported on the green synthesis of nanoparticles coupled to microalgae cultivation.

# Chapter 2

---

## Influence of the crystal phase of Fe<sub>2</sub>O<sub>3</sub> nanoparticles on *Chlorella* cultures and biomass production

This chapter is adapted from the publication:

- Vargas-Estrada, L. Domínguez-Espíndola, R., Rodríguez-González, C., Palma-Tirado, L., Sebastian, P.J. Submitted to Clean Technologies and Environmental Policy (2022)



## 1. Introduction

The addition of metallic oxide nanoparticles to microalgae cultures have gained popularity in the last years, and even if their use is a controversial topic and little is known of their mechanism of interaction with microalgae, and is believed that they can act as RuBisCO stimulants, nutrient supplements, ROS generators, electron transports, among others (Gunawan et al., 2013a; Kadar et al., 2012a; Rana et al., 2020; Vaz et al., 2020), resulting in improved microalgae growth and production of high-value products. Furthermore, it is known that metallic oxides react with CO<sub>2</sub> and water to form carbonates (Mulu, Arimi, et al., 2021), in this context, the interaction among NPs-water-CO<sub>2</sub> could serve as explained the beneficial interaction between microalgae and NPs. For instance, Jeon et al.(2017) demonstrated that the addition of SiO<sub>2</sub> NPs to *Chlorella vulgaris* culture improved the mass transfer of CO<sub>2</sub> to the cells, resulting in an improved k<sub>La</sub> and lipid production. Moreover, the use of nanoporous materials, such as polymeric nanofibers, has been implemented to improve the contact time between microalgae and CO<sub>2</sub>, which can serve as a technique to improve the mass transfer of CO<sub>2</sub> to the cells (Vaz et al., 2020; Vaz, Mastrantonio, et al., 2019). Furthermore, it has been demonstrated that the addition of metal oxide NPs to polymeric nanofibers can create nanocomposites that increase the CO<sub>2</sub> adsorption efficiencies (Vaz, Costa, et al., 2019; Vaz et al., 2020; Vaz, Mastrantonio, et al., 2019), resulting in an improved biomass production. Thereby, the addition of NPs can be considered as a promising option to increase the production of high value-added microalgal biomass.



Recently, Fe<sub>2</sub>O<sub>3</sub> NPs have gained popularity since they are thermodynamically stable and are non-toxic for some species, moreover, it is believed that Fe ions are dispersed in the culture media, and can serve as nutrient supplements for microalgae (Vargas-Estrada et al., 2020). Recently, Rana et al. (2020) demonstrated the potential of Fe<sub>2</sub>O<sub>3</sub> NPs on lipid production in *Chlorella pyrenoidosa*. Additionally, Bibi et al. (2021) demonstrated that Fe<sub>2</sub>O<sub>3</sub> are not available as an iron source, discharging the theory that NPs can act as nutrient supplements. However, it is known that the tolerance of NPs on microalgae is species specific (Chen et al., 2018a; Rana et al., 2020) and normally high nanoparticle concentration (>100 mg L<sup>-1</sup>) inhibits microalgae growth (Bibi et al., 2021; Pedroso et al., 2013a). Additionally, other characteristics of the NPs, such as size, crystal phase, oxidation stage, etc., of Fe<sub>2</sub>O<sub>3</sub> NPs influence differently the microalgae culture. For instance, Lei et al (2016a) studied the effect of particle size, crystal phase, oxidation state and environmental aging of different iron NPs and observed that the crystal phase of Fe<sub>2</sub>O<sub>3</sub> had a different effect on *Chlorella pyrenoidosa*. According to these authors, the  $\alpha$ - phase of Fe<sub>2</sub>O<sub>3</sub> NPs presented a higher toxicity on *C. pyrenoidosa* than the  $\gamma$ - phase, thus, the crystal phase of Fe<sub>2</sub>O<sub>3</sub> NPs should be considered to maximize beneficial effects on microalgae. Interestingly, Kayani et al (2014), synthesized Fe<sub>2</sub>O<sub>3</sub> NPs and observed that the annealing temperature (400 and 1000 °C) influenced the crystal phase of the NPs. Indeed, even if the  $\alpha$ - phase was present at both annealing temperatures, the  $\gamma$ - phase was present at higher concentrations when the annealing temperature was 400 °C. In this context, synthesized NPs can have an advantage of having both phases ( $\alpha$  and  $\gamma$ ) present, depending on the annealing temperature.

In this context, the aim of this chapter was to synthesize the optimal Fe<sub>2</sub>O<sub>3</sub> NPs to improve microalgae biomass production coupled to high-value products. Hence, the synthesized NPs were added to *Chlorella vulgaris* cultured in BG11 at different concentrations. Then, to assess the robustness of the Fe<sub>2</sub>O<sub>3</sub> NPs, the NPs were added to *Chlorella* sp. cultures without carbonate supplementation.

## 2. Methods

### 2.1 Fe<sub>2</sub>O<sub>3</sub> nanoparticle synthesis

Fe<sub>2</sub>O<sub>3</sub> NPs were prepared by sol–gel method combined with hydrothermal treatment under controlled conditions. Ferric Nitrate (Fluka), ethylene glycol (sigma Aldrich) and nitric acid (Fermont) were used without any purification treatment. Fe<sub>2</sub>O<sub>3</sub> colloidal solution was prepared by mixing ethylene glycol (50 mL) with Ferric Nitrate (3 g) in a ball flat bottom flask under constant agitation for 90 minutes. For hydrolysis, a solution of 0.1 M of citric acid in 50 mL of deionized water was mixed with 1 mL of nitric acid (used as a catalyst in the process of hydrolysis), it was added to the flask dropwise and left under constant stirring for 24 h at 50°C. After the aging period of 24 h, the solution was placed in a glass beaker and kept in vigorous stirring for 5 hours at 70°C to make stable sol. The sol was then heated at 85°C under maintained magnetic stirring until the water content was evaporated and a brown semi-solid gel was formed. This was followed by aging for 72 hours for the condensation and polymerization reactions. The formed gel was then dried by putting it in an oven at 100°C for 2 hours. The dried gel was then annealed at temperatures of 450 and 1000°C for 2 hours.

The synthesized NPs were annealed at 450 °C and 1000 °C, referred as Fe<sub>2</sub>O<sub>3</sub>-450 and Fe<sub>2</sub>O<sub>3</sub>-1000, respectively. The structural features of Fe<sub>2</sub>O<sub>3</sub> NPs were examined by TEM analyses (JEOL JEM-1400 plus, 100 kV). The elemental composition of Fe<sub>2</sub>O<sub>3</sub> nanoparticles annealed at 450 and 1000 °C were recorded using scanning electron microscopy (SEM) (Hitachi FE-SEM S-5500 integrated with an energy-dispersive X-ray spectrometer Bruker Quantax 200 for EDS elemental analysis. The phase formation and crystalline structure of the synthesized Fe<sub>2</sub>O<sub>3</sub> nanoparticles were determined by X-ray diffraction (Rigaku, DMAX 2200).

## **2.2 Nanoparticle stock solution**

Fresh stock solutions with concentrations of 200 mg L<sup>-1</sup> of each Fe<sub>2</sub>O<sub>3</sub> NPs were prepared with sterile microalgae culture media to facilitate their aggregation to microalgae cultures. Before the solution was aggregated, the stock solutions were sonicated for 15 minutes to avoid NPs agglomeration.

## **2.3 Microalgae strain and culture**

Two different microalgae strains were used in order to elucidate the viability of the Fe<sub>2</sub>O<sub>3</sub> NPs. The strain *Chlorella vulgaris* was used in this chapter because of its robustness and was kindly donated by the UNICACH, Chiapas, Mexico, and a consortium of microalgae and nitrifying bacteria mainly dominated by *Chlorella* sp., which was donated by the Metropolitan Autonomous University (UAM), Mexico City, Mexico, and was isolated from the water channels of Xochimilco, Mexico. In this particular chapter, no change in the composition of the consortium was observed, and the predominant species was *Chlorella* sp., thus we will refer to the

consortium as *Chlorella* sp. Both *C. vulgaris* and *Chlorella* sp. were kept in an incubator (Thermo Scientific) at 19 °C with light:dark cycles of 15:9 h, respectively in Erlenmeyer flasks covered with a cotton plug. *C. vulgaris* was cultivated in BG-11 and *Chlorella* sp. was cultivated in Bayfolan forte (Bayer CropScience) at a concentration of 1 mL L<sup>-1</sup>.

## 2.4 Experimental set-up

Batch cultures were carried out in Erlenmeyer flasks of 500 mL. The working volume was kept constant (500 mL) by adding sterile deionized water before taking samples to cover losses from evaporation. Each Erlenmeyer flask was inoculated with microalgae culture at a 10% (v v<sup>-1</sup>) ratio. *Chlorella vulgaris* was cultivated in BG-11 and *Chlorella* sp. was cultivated in Bayfolan forte (Bayer CropScience) at a concentration of 1 mL L<sup>-1</sup>.

This chapter was divided in two stages, in stage I, to determine the optimal Fe<sub>2</sub>O<sub>3</sub> NPs for *C. vulgaris*, the Fe<sub>2</sub>O<sub>3</sub> NPs were added to reach a final concentration of 10 mg L<sup>-1</sup> in the Erlenmeyer flasks. Three different conditions were assessed: 1) control (*C. vulgaris* without NPs); 2) 10 mg L<sup>-1</sup> Fe<sub>2</sub>O<sub>3</sub>-450; and 3) 10 mg L<sup>-1</sup> Fe<sub>2</sub>O<sub>3</sub>-1000. After obtaining the optimal Fe<sub>2</sub>O<sub>3</sub> NPs for microalgae cultivation, the selected Fe<sub>2</sub>O<sub>3</sub> NPs were added at different concentrations (5 and 20 mg L<sup>-1</sup>) to determine the optimal Fe<sub>2</sub>O<sub>3</sub> concentration for microalgae culture, a control without NPs was also ran. Each condition was run in duplicate.

In stage II, the same conditions of stage I were elucidated, but to simulate real environmental conditions, *Chlorella* sp. was used and cultivated in Bayfolan Forte (1 mL L<sup>-1</sup>) medium without carbonate supplementation.

The flasks were incubated under cool-light with an intensity of 800 lm in light:dark cycles of 12:12 hours respectively. Air was pumped to provide CO<sub>2</sub> to the cultures and to avoid culture sedimentation.

## 2.5 Analytical determinations

### 2.5.1 Biomass concentration and chlorophyll a

Microalgae biomass concentration was determined by cell density which was determined by optical microscopy with an improved Neubauer chamber. Dry weight was measured at the beginning and at the end of the experiments by filtering 10 mL of the sample through 47 mm glass fiber filters (Whatman. GE Healthcare Life Sciences) and drying them all night at 105 °C, according to standard methods (APHA-AWWA-WPCF, 1999). Chlorophyll *a* content was determined by spectrophotometry, briefly 1 mL of sample was centrifuged at 10000 rpm for 5 minutes, after that the supernatant was discarded and 1 mL of a solution of methanol:water 90:10 (v v<sup>-1</sup>) was added. Then, the sample was heated in a water bath at 75 °C for 20 minutes, and then centrifuged at 10000 rpm for 5 minutes, the supernatant was carefully removed and the optical density was measured at a wavelength of 663 nm and 645 nm. The chlorophyll *a* content was calculated according to Eq. (2):

$$\text{chlorophyll } a \text{ (mg L}^{-1}\text{)} = (12.7 * A_{663}) - (2.6 * A_{645}) \quad (2)$$

### 2.5.2 Growth parameters and CO<sub>2</sub> biofixation rate

The biomass productivity ( $P_x$ , mg L<sup>-1</sup>d<sup>-1</sup>) was calculated according to equation Eq (3):

$$P_x = \frac{X_t - X_0}{t - t_0} \quad (3)$$

where  $X_t$  is the biomass concentration (mg L<sup>-1</sup>) at time  $t$  (d) and  $X_0$  is the concentration of biomass at time  $t_0$  (d).

The specific growth rate ( $\mu$ , d<sup>-1</sup>) was calculated according to Eq (4):

$$\mu = \frac{\ln X_t - \ln X_0}{t - t_0} \quad (4)$$

The CO<sub>2</sub> biofixation rate ( $R$ , mg L<sup>-1</sup>d<sup>-1</sup>) was calculated according to Eq (5):

$$R = P_x X_{cbm} \frac{M_{CO_2}}{M_C} \quad (5)$$

where  $M_{CO_2}$  is the molar mass of CO<sub>2</sub> (g mol<sup>-1</sup>) and  $M_C$  the molar mass of carbon (g mol<sup>-1</sup>), and  $X_{cbm}$  is the carbon fraction in the microalgal biomass (50%, w w<sup>-1</sup>) (Vaz, Mastrantonio, et al., 2019).

### 2.5.3 Alkalinity and dissolved inorganic carbon (DIC)

Alkalinity was determined by acid titration at the beginning and at the end of the experiment. pH was measured using a digital pH meter (HANNA instruments) and the DIC concentration was calculated according to (Rosa et al., 2015).

#### **2.5.4 Biomass composition**

To determine the carbohydrate and lipid content in the microalgae biomass at the end of the experiment the microalgae biomass was centrifuged at 3,500 rpm for 15 minutes, frozen at -30 °C (Equitec) and finally freeze-dried (-110 °C, 0.049 hPa) (Labconco, USA). The carbohydrate content was determined by the phenol-sulfuric acid method (Dubois et al., 1956) using D-glucose as a standard and lipids were determined according to (G. Li et al., 2020a).

#### **2.5.5 Microalgae sample preparation for TEM analysis**

Microalgae were collected in Eppendorf tubes and fixed for 24 h at 40 °C with 3% glutaraldehyde in 0.1 M cacodylate buffer. Subsequently, they were washed overnight in 0.2 M cacodylate buffer and postfixed with 0.1 M OsO<sub>4</sub> in 0.1M cacodylate buffer for 1 h at 40 °C. Several washes equal to the previous ones were carried out. Pellets were obtained and transferred to smaller tubes and to dehydrate in increasing concentrations of ethanol beginning with 30%, 50%, 70%, making 2 changes of 30 min at each concentration, until reaching 96% and absolute ethanol. In the second change of absolute ethanol, the pellets were removed from the tubes and transferred to vials. This was followed by a change of solvent with propylene oxide (2 times for 30 min). For infiltration, they were left in a 1:1 mixture of epoxy resin:propylene oxide overnight at room temperature. The propylene oxide was evaporated to concentrate the resin. Several changes of resin were made under agitation until the complete extraction of the oxide. The pellets were oriented in molds with complete resin and polymerized in an oven at 60 °C for 36 h. The blocks obtained were cut in an ultramicrotome and sections with a thickness of 60 nm to

90 nm were obtained and collected on 300 mesh copper grids. The grids with the sections were counterstained with 2% uranyl acetate for 20 min and with 2% lead citrate for 15 min. Finally, the samples were observed in the JEOL Model JEM-1010 transmission electron microscope operated at 80Kv. The images were obtained with an ORIUS model GATAN camera that is coupled to the microscope and with the Digital Micrograph program.

## **2.6 Statistical analysis**

To determine the effect of the NPs on microalgae growth and biomass composition, the results were analyzed by ANOVA followed by Tuckey's test considering  $\alpha=0.05$ .

## **3. Results and discussion**

### **3.1 Characterization of the Fe<sub>2</sub>O<sub>3</sub> nanoparticles**

The structural features of Fe<sub>2</sub>O<sub>3</sub> NPs have been examined by SEM analyses and TEM analyses. Both results obtained by TEM and SEM show the good aggregation of spherical/rhombic structures between 30–50 nm diameter. Polycrystalline nature of nanoparticles with hexagonal plates and spherical shaped particles are visualized in **Fig. 5**. The peaks in EDX spectrum confirm the presence of Iron and Oxygen, their atomic percentages are shown in **Table 2**.



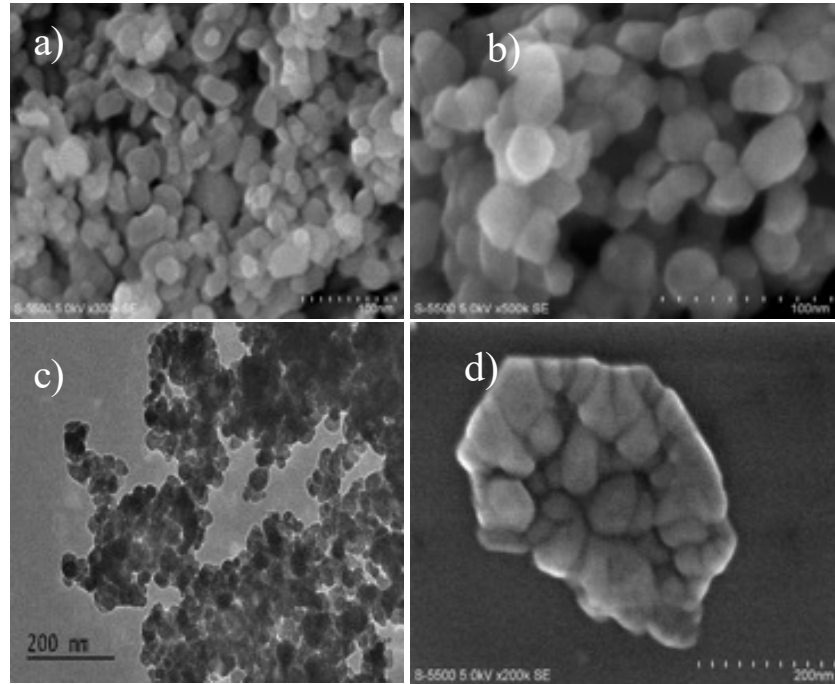


**Fig. 5.** SEM images of a)  $\text{Fe}_2\text{O}_3$ -450, b)  $\text{Fe}_2\text{O}_3$ -1000 and TEM images of c)  $\text{Fe}_2\text{O}_3$ -450, d)  $\text{Fe}_2\text{O}_3$ -1000

**Table 2.** Chemical compositions of the  $\text{Fe}_2\text{O}_3$  nanoparticles.

<i>Element</i>	<i><math>\text{Fe}_2\text{O}_3</math>-450</i>		<i><math>\text{Fe}_2\text{O}_3</math>-1000</i>	
	<i>Weight (%)</i>	<i>Atomic (%)</i>	<i>Weight (%)</i>	<i>Atomic (%)</i>
O	41.92	67.45	52.69	75.19
Fe	54.65	25.19	43.65	17.85
C	3.43	7.36	3.66	6.96

The phase formation and crystalline structure of synthesized  $\text{Fe}_2\text{O}_3$  nanoparticles was determined by X-ray diffraction recorded by scanning  $2\theta$  in the

range of  $20-70^\circ$ , with grazing incidence angle of  $0.5^\circ$  recorded at room temperature.

**Fig. 6.** shows the powder X-ray diffraction pattern of  $\alpha\text{-Fe}_2\text{O}_3$  nanoparticles.

All diffraction peaks are in agreement with Joint Committee on Powder Diffraction Standards (JCPDS) X-ray data file. At  $450^\circ\text{C}$  the major XRD peak is observed at  $2\theta = 33.08^\circ$  while the second major peak is recorded at  $2\theta = 35.54^\circ$ . Other peaks are found at  $2\theta = 53.97^\circ$ ,  $2\theta = 57.55^\circ$  and  $62.42^\circ$ . The planes for corresponding angles are (104), (311), (116), (110) and (214), respectively. When annealing temperature was raised to  $1000^\circ\text{C}$  the XRD peaks were registered at  $2\theta = 33.13^\circ$ ,  $35.60^\circ$ ,  $49.42^\circ$ ,  $54.04^\circ$ ,  $62.39^\circ$ , and  $63.95^\circ$ . At this temperature corresponding planes are (104), (311), (024), (116), (214), and (300) (Kuai & Zhang, 2019). Spectra of nanoparticles at both annealing temperatures agree with the standard card corresponding to  $\alpha$  phase of iron oxide (hematite). The peak at  $35.54^\circ$  refers to the presence of  $\gamma\text{-Fe}_2\text{O}_3$  (maghemite) phase, while the other peaks refer to the  $\alpha\text{-Fe}_2\text{O}_3$  phase. Hence, hematite structure is achieved at annealing temperature of  $450^\circ\text{C}$ , but main peaks related to this specific crystal phase are best defined when the annealing temperature is increased to  $1000^\circ\text{C}$ . Our results are in agreement with (Kayani et al., 2014; Raja et al., 2015), who observed similar peaks at similar angles. According to (Kayani et al., 2014) when  $\text{Fe}_2\text{O}_3$  nanoparticles are annealed at  $400^\circ\text{C}$  the  $\alpha$ - and  $\gamma$ - phase are present. On the other hand, when  $\text{Fe}_2\text{O}_3$  are annealed at  $1000^\circ\text{C}$  a phase change from  $\gamma$ - to  $\alpha$ - takes place, and hematite is the dominant phase, which is in agreement with our results obtained by X-ray diffraction.

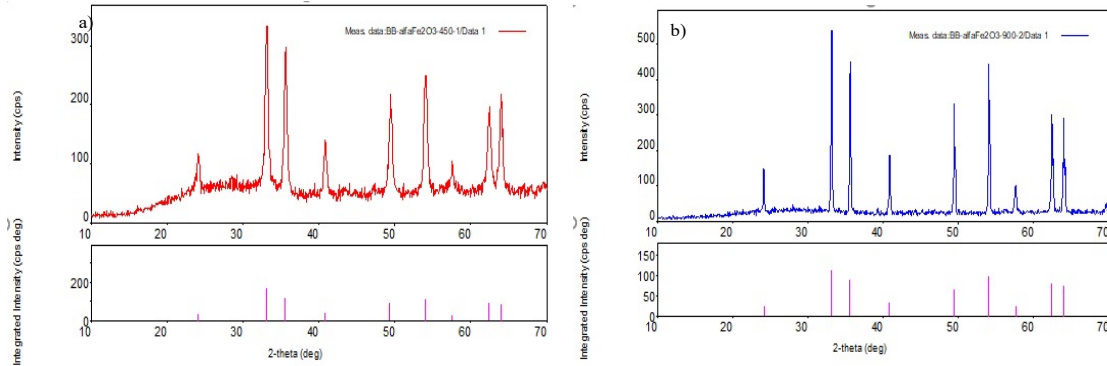


**Fig. 6.** XRD analysis results of a) Fe<sub>2</sub>O<sub>3</sub>-450; and b) Fe<sub>2</sub>O<sub>3</sub>-1000.

## 3.2 Effect of Fe<sub>2</sub>O<sub>3</sub> nanoparticles on *Chlorella vulgaris*

### 3.2.1 Biomass growth and chlorophyll content

The crystal phase of the Fe<sub>2</sub>O<sub>3</sub> NPs plays an important role on microalgae growth, interestingly, the annealing temperature of the synthesized NPs influences the crystal phase of the NPs. Thus, we assessed the addition of Fe<sub>2</sub>O<sub>3</sub> NPs annealed at different temperatures in *C. vulgaris* to find the optimum Fe<sub>2</sub>O<sub>3</sub> NPs for microalgae production and macromolecule accumulation, the results are shown in **Fig. 7**.

After 9 days of cultivation, the addition of 10 mg L<sup>-1</sup> of Fe<sub>2</sub>O<sub>3</sub>-450 to *C. vulgaris* cultures did not influence microalgae growth compared to the control, while the addition of 10 mg L<sup>-1</sup> of Fe<sub>2</sub>O<sub>3</sub>-1000 showed an inhibitory effect at day 9 (**Fig. 7a**). Indeed, we can say that the crystal composition of the Fe<sub>2</sub>O<sub>3</sub> NPs did influence *C. vulgaris* growth and our results are in agreement with (Lei et al., 2016a). However, since a mixture of both crystal phases were present in the Fe<sub>2</sub>O<sub>3</sub>-450 no significant difference in *C. vulgaris* growth was observed. Moreover, chlorophyll content is used to indicate the photosynthesis rate and/or the cell division of microalgae (Liang et

al., 2020) and in our particular study, the chlorophyll content in *C. vulgaris* decreased when Fe<sub>2</sub>O<sub>3</sub>-1000 were added while the chlorophyll content in *C. vulgaris* with Fe<sub>2</sub>O<sub>3</sub>-450 did not present a significant change (**Fig. 7c**). It has been previously stated that a loss in chlorophyll *a* content may be due to inhibition in the electron transport chain specially in the donor center, whereas an increase of chlorophyll *a* content should be due to the inhibition in the acceptor side (Sendra et al., 2017a). Thus, the reduction of chlorophyll in our study indicates that *C. vulgaris* quantum yield of PSII was interfered by the presence of Fe<sub>2</sub>O<sub>3</sub>-1000. Moreover, TEM micrographs served to observe the interactions between Fe<sub>2</sub>O<sub>3</sub> NPs and *C. vulgaris* cells (**Fig. 8**). The addition of Fe<sub>2</sub>O<sub>3</sub>-450 show NPs agglomeration and a few deformed cells (**Fig. 8b**), but no significant changes compared to the control (**Fig. 8a**). On the other hand, the addition of Fe<sub>2</sub>O<sub>3</sub>-1000 show deformed cells, agglomeration of NPs and the adhesion of NPs to the algal cells (**Fig. 8c**), the adhesion of NPs to algal cells has been considered as one toxic effect since it can lead to inhibition due to the lack of light availability or nutrient limitation (Fathi et al., 2020; Sendra et al., 2017a; Vargas-Estrada et al., 2020).

Interestingly, *C. vulgaris* cultivated with Fe<sub>2</sub>O<sub>3</sub>-1000 presented a higher biomass productivity (Px), higher biofixation rate (R), but no significant difference was observed between the assays for the specific growth rate ( $\mu$ ) (**Table 3**). Additionally, the DIC<sub>final</sub> of these assays was higher, as it has been stated elsewhere (Mulu, Arimi, et al., 2021), the presence of metallic oxides enable the CO<sub>2</sub> removal as they react with CO<sub>2</sub> and water to form carbonates, thus our results suggest that the NPs could have induced the dissolution of CO<sub>2</sub> into the culture broth in the form

of carbonates, resulting in enhanced kinetic parameters, however, the long exposure of *C. vulgaris* to these particular NPs resulted in a toxic effect leading to a cell density loss of up to 57% at day 9.

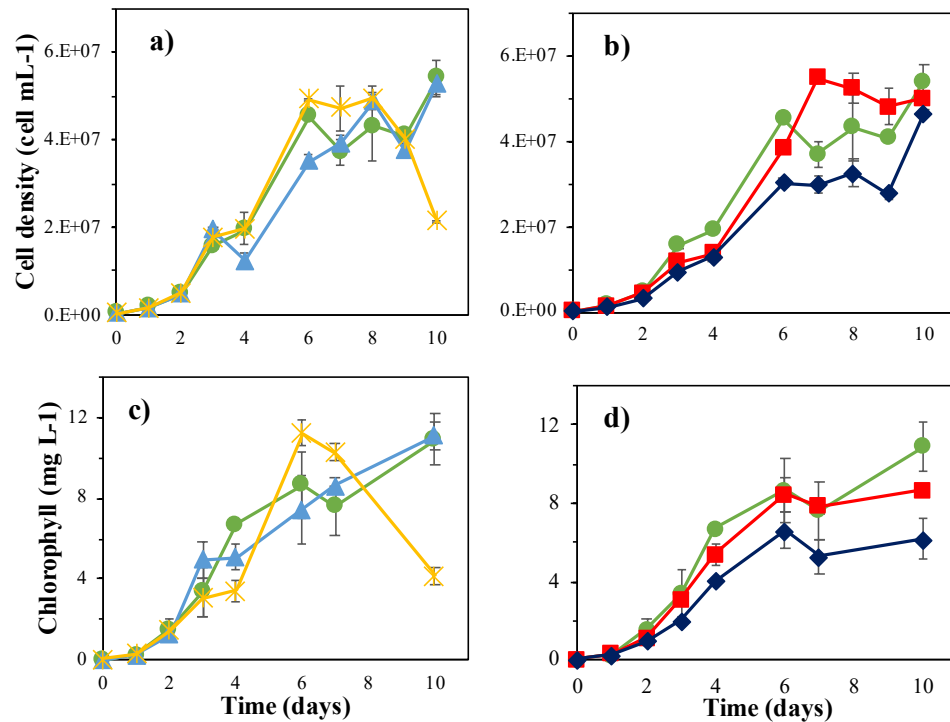


**Fig. 7.** Time course of the cell density a) and b); and chlorophyll content c) and d) of *Chlorella vulgaris* cultivated in BG-11 medium under different conditions assessed: control (green circles), 10 mg L<sup>-1</sup> Fe<sub>2</sub>O<sub>3</sub>-450 (blue triangles), 10 mg L<sup>-1</sup> Fe<sub>2</sub>O<sub>3</sub>-100 (yellow crosses); 5 mg L<sup>-1</sup> Fe<sub>2</sub>O<sub>3</sub>-450 (red squares); 20 mg L<sup>-1</sup> Fe<sub>2</sub>O<sub>3</sub>-450 (navy blue diamonds).

**Table 3.** Kinetic growth parameters of *Chlorella* sp. and *C. vulgaris* with 10 mg L<sup>-1</sup> of Fe<sub>2</sub>O<sub>3</sub>.

	<i>Chlorella vulgaris</i>			<i>Chlorella</i> sp.		
	Control	Fe <sub>2</sub> O <sub>3</sub> -450	Fe <sub>2</sub> O <sub>3</sub> -1000	Control	Fe <sub>2</sub> O <sub>3</sub> -450	Fe <sub>2</sub> O <sub>3</sub> -1000
<b>Px</b>	45.6 ± 0.8	43.1 ± 4.4	59.3 ± 0.8	72.2 ± 9.4	90.0 ± 4.7	25.0 ± 2.3
<b>μ</b>	0.35 ± 0.03	0.36 ± 0.01	0.31 ± 0.02	0.25 ± 0.02	0.25 ± 0.01	0.12 ± 0.01
<b>R</b>	83 ± 1	79 ± 8	108 ± 1	132 ± 17	164 ± 8	45 ± 4
<b>DIC<sub>i</sub></b>	80 ± 15	79 ± 4	78 ± 21	125 ± 6	120 ± 10	125 ± 1
<b>DIC<sub>f</sub></b>	522 ± 9	482 ± 20	613 ± 10	229 ± 19	223 ± 9	201 ± 19

Note: DIC<sub>i</sub> refers to initial dissolved inorganic carbon; DIC<sub>f</sub> refers to final dissolved inorganic carbon.

Indeed, Fe<sub>2</sub>O<sub>3</sub>-450 NPs were selected as the optimal NPs for *C. vulgaris* growth and subsequently different concentrations (5 and 20 mg L<sup>-1</sup>) were assessed. After 9 days of cultivation, the addition of 5 mg L<sup>-1</sup> Fe<sub>2</sub>O<sub>3</sub>-450 did not show a significant difference in cell density, however the exponential phase was prolonged (**Fig. 7b**). Moreover, the chlorophyll content was significantly lower by the addition of the NPs, suggesting that this concentration influences the pigment synthesis (**Fig. 7d**). On the other hand, the addition of 20 mg L<sup>-1</sup> resulted in lower cell density and chlorophyll content, suggesting that this particular dose can inhibit *C. vulgaris* growth, which is in accordance with (Bibi et al., 2021). Furthermore, there was no statistical difference in the Px (**Table 4**) between the assays but the assays containing 20 mg L<sup>-1</sup> of Fe<sub>2</sub>O<sub>3</sub>-450 recorded the lowest Px values. Additionally, the μ and the R values decreased as the NPs concentration increased, suggesting that the

concentration of NPs interfered in the growth of *C. vulgaris*, contrary results have been previously observed by Rana and coworkers (2020), who observed that 20 mg L<sup>-1</sup> of Fe<sub>2</sub>O<sub>3</sub> NPs enhanced the biomass productivity of *C. pyrenoidosa*, confirming that NPs tolerance is species specific.

**Table 4.** Kinetic growth parameters of *C. vulgaris* and *Chlorella* sp. with 5 mg L<sup>-1</sup> and 20 mg L<sup>-1</sup> of Fe<sub>2</sub>O<sub>3</sub>-450.

	<i>Chlorella vulgaris</i>			<i>Chlorella</i> sp.		
	Control	5 mg L <sup>-1</sup>	20 mg L <sup>-1</sup>	Control	5 mg L <sup>-1</sup>	20 mg L <sup>-1</sup>
<b><i>Px</i></b>	45.6 ± 0.8	43.7 ± 3.54	33.7 ± 1.7	52.2 ± 3.2	56.1 ± 7.1	62.2 ± 3.1
<b><i>μ</i></b>	0.35 ± 0.03	0.26 ± 0.02	0.19 ± 0.02	0.17 ± 0.02	0.18 ± 0.03	0.18 ± 0.01
<b><i>R</i></b>	83 ± 1	80 ± 6	62 ± 3	96 ± 6	103 ± 13	114 ± 6

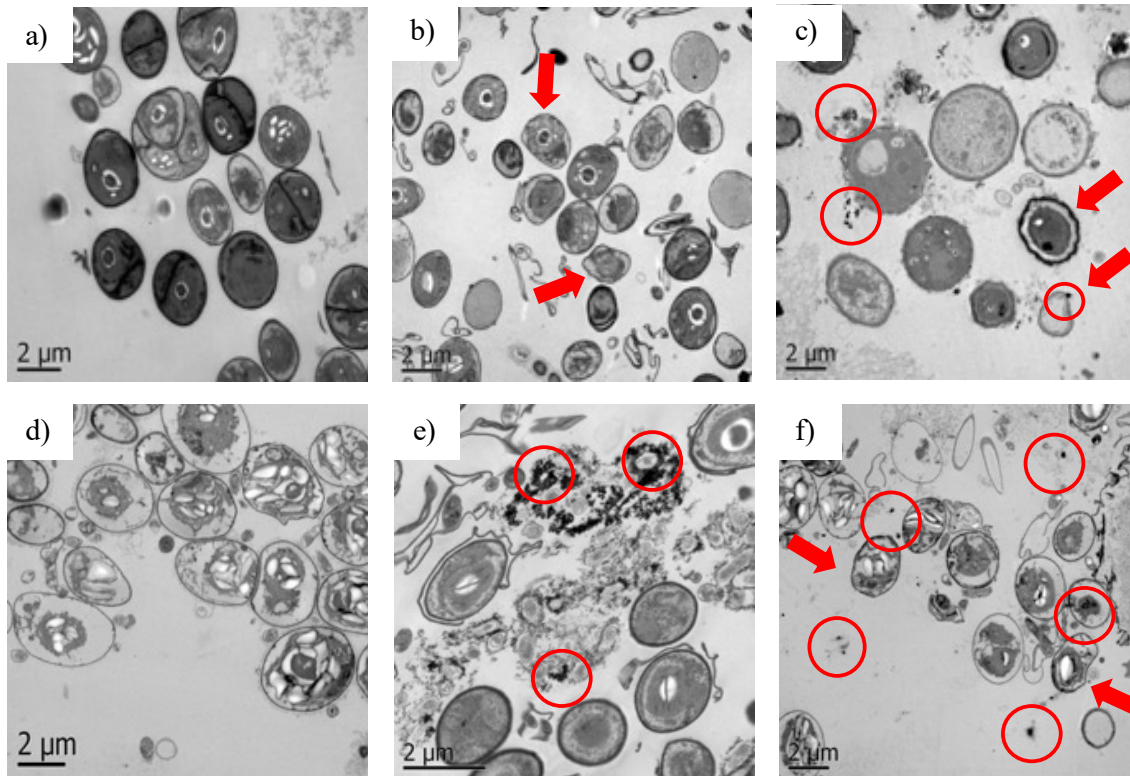


**Fig. 8.** TEM micrographs of *Chlorella vulgaris*. a) Control; b)  $\text{Fe}_2\text{O}_3$ -450; c)  $\text{Fe}_2\text{O}_3$ -1000; and *Chlorella* sp. d) Control; e)  $\text{Fe}_2\text{O}_3$ -450; f)  $\text{Fe}_2\text{O}_3$ -1000. Red arrows indicate deformed cells, red circles indicate the presence of nanoparticles.

### 3.2.2 Biomass composition

The addition of  $\text{Fe}_2\text{O}_3$  NPs stimulated carbohydrate content of *C. vulgaris* regarding the NPs added (**Fig. 9**). *C. vulgaris* carbohydrate content increased from 18.67% to 41.27% and 44.83% (% dw) when  $10 \text{ mg L}^{-1}$  of  $\text{Fe}_2\text{O}_3$ -450 and  $\text{Fe}_2\text{O}_3$ -1000 respectively were added. Interestingly, the carbohydrate content did not present a statistical difference compared to the control (18.67% dw) when  $5 \text{ mg L}^{-1}$  were added, whereas the carbohydrate content significantly increased up to 53.09% (% dw) when  $20 \text{ mg L}^{-1}$  of  $\text{Fe}_2\text{O}_3$ -450 were added. Thus, the carbohydrate content in *C. vulgaris* increased with the increasing concentrations of  $\text{Fe}_2\text{O}_3$ -450. Indeed, our results



suggest that concentrations  $\geq 10 \text{ mg L}^{-1}$  stimulate carbohydrate accumulation in *C. vulgaris*.

On the other hand, the lipid content of *C. vulgaris* increased from 11.25% (control) to 14.8 % and 21.5% when  $10 \text{ mg L}^{-1}$  of  $\text{Fe}_2\text{O}_3$ -450 and  $\text{Fe}_2\text{O}_3$ -1000 respectively were added. Moreover, the lipid content was statistically higher than the control when  $5 \text{ mg L}^{-1}$  and  $20 \text{ mg L}^{-1}$  of  $\text{Fe}_2\text{O}_3$ -450 were added to the culture, increasing from 11.25% (control) to 16.9% and 17.6% for  $5 \text{ mg L}^{-1}$  and  $20 \text{ mg L}^{-1}$  respectively. Notwithstanding, the lipid content in *C. vulgaris* presented contradictory results, the higher lipid content was recorded when  $20 \text{ mg L}^{-1}$  of  $\text{Fe}_2\text{O}_3$ -450 NPs was added, suggesting that the higher concentration of NPs stimulated the lipid content. It was probably due to the formation of ROS (Rana et al., 2020), since the interaction of light and oxygen in presence of moisture produces oxidizing radicals and ROS, and higher concentrations of NPs led to higher concentration of generated ROS.

Indeed, even if the addition of  $\text{Fe}_2\text{O}_3$ -450 NPs resulted in a carbohydrate and lipid enhancement, the carbohydrate enhancement was significantly higher, suggesting that the NPs influenced *C. vulgaris* metabolism. Carbohydrate's and lipid's main component is carbon, hence providing a source of this element can increase their production (Varaprasad et al., 2021). Thus, high  $\text{CO}_2$  concentration improves the carboxylase activity of RuBisCO enzyme, which is known as the key enzyme for  $\text{CO}_2$  fixation, resulting in an improved photosynthetic activity (González-Fernández & Ballesteros, 2012). Additionally, the RuBisCO enzyme can transform the  $\text{CO}_2$  into precursors of carbohydrates, which are accumulated as a reserve of

energy for cell growth (Vaz et al., 2020). Thereby, from the results obtained in our study, we can say that the addition of NPs improved *C. vulgaris* metabolism probably by the formation of carbonated species. However, at this point it is important to mention that the  $DIC_{final}$  did not present a significant change between the assays but the significantly higher carbohydrate content in *C. vulgaris* containing 10 and 20 mg L<sup>-1</sup> of Fe<sub>2</sub>O<sub>3</sub>-450 NPs suggest that the addition of these NPs could have enhanced the CO<sub>2</sub> source to *C. vulgaris*. Vaz et al. (2019) reported similar findings when nanofibers containing Fe<sub>2</sub>O<sub>3</sub> NPs were added to *Chlorella fusca* cultures. Thus, the use of Fe<sub>2</sub>O<sub>3</sub> NPS played a crucial role in the enhancement of the charge separation efficiency, which is beneficial for the *C. vulgaris* metabolism.

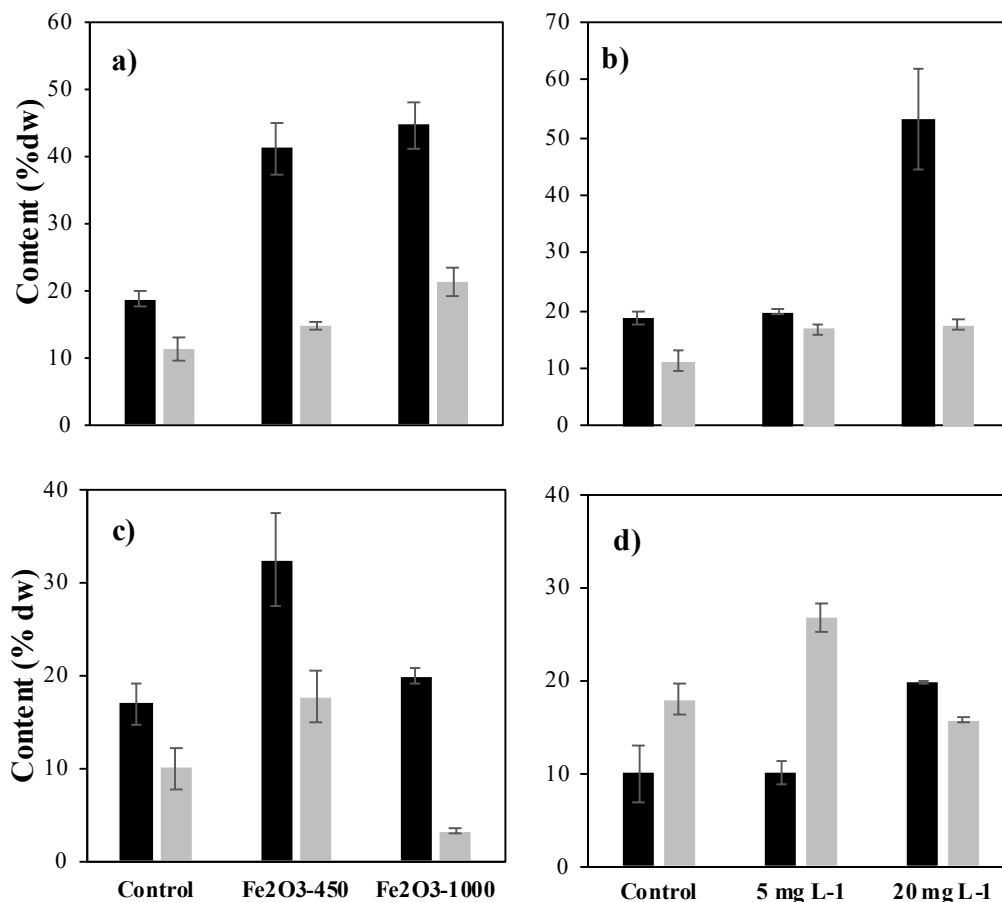


**Fig. 9.** Carbohydrate (black) and lipid (light grey) content of *Chlorella vulgaris* cultivated with and 10 mg L<sup>-1</sup> of the corresponding Fe<sub>2</sub>O<sub>3</sub> NPs; b) *C. vulgaris* cultivated with 5 mg L<sup>-1</sup> and 20 mg L<sup>-1</sup> of Fe<sub>2</sub>O<sub>3</sub>-450; c) *Chlorella* sp. cultivated with and 10 mg L<sup>-1</sup> of the corresponding Fe<sub>2</sub>O<sub>3</sub> NPs; d) *Chlorella* sp. cultivated with 5 mg L<sup>-1</sup> and 20 mg L<sup>-1</sup> of Fe<sub>2</sub>O<sub>3</sub>-450.

### 3.3 Effect of Fe<sub>2</sub>O<sub>3</sub> nanoparticles on *Chlorella* sp.

#### 3.3.1 Biomass growth and chlorophyll content

After 9 days of cultivation, *Chlorella* sp. cultivated in Bayfolan Forte presented an increment in cell density from 1.46 E+07 cells mL<sup>-1</sup> to 2.27 E+07 cells mL<sup>-1</sup> when 10 mg L<sup>-1</sup> of Fe<sub>2</sub>O<sub>3</sub>-450 was added. On the other hand, the addition of 10 mg L<sup>-1</sup> of Fe<sub>2</sub>O<sub>3</sub>-

1000 did not show a significant difference in cell density ( $1.61 \text{ E}+07 \text{ cell mL}^{-1}$ ). Even if the cell density of *Chlorella* sp. cultivated with  $\text{Fe}_2\text{O}_3$ -1000 was lower compared to the  $\text{Fe}_2\text{O}_3$ -450, the growth was not statistically different compared to the control (**Fig. 10a**).

On the other hand, the chlorophyll content of *Chlorella* sp. suffered a decay from  $4.28 \text{ mg L}^{-1}$  to almost negligible ( $0.05 \text{ mg L}^{-1}$ ) when  $10 \text{ mg L}^{-1}$   $\text{Fe}_2\text{O}_3$ -1000 NPs were added, however, when  $\text{Fe}_2\text{O}_3$ -450 were added, *Chlorella* sp. presented a higher chlorophyll content ( $14.68 \text{ mg L}^{-1}$ ) compared to the control ( $4.28 \text{ mg L}^{-1}$ ) (**Fig. 10c**). Thus, we can say that both  $\text{Fe}_2\text{O}_3$  NPs interfered in the quantum yield of PSII of *Chlorella* sp., but  $\text{Fe}_2\text{O}_3$ -1000 have a more toxic effect on *Chlorella* sp. since they led to a chlorophyll loss. Moreover, TEM micrographs show the interactions between *Chlorella* sp. and the two types of  $\text{Fe}_2\text{O}_3$  NPs (**Fig. 8**). The addition of  $10 \text{ mg L}^{-1}$  of  $\text{Fe}_2\text{O}_3$ -450 show the agglomeration of NPs (**Fig. 8e**) but no significant changes in the morphology of the cells were observed compared to the control (**Fig. 8d**). On the other hand, the addition of  $10 \text{ mg L}^{-1}$  of  $\text{Fe}_2\text{O}_3$ -1000 show the adhesion of NPs to microalgal cells as well as deformed cells (**Fig. 8f**). Indeed, our results obtained with *Chlorella* sp. confirmed that  $\text{Fe}_2\text{O}_3$ -1000 NPs have a toxic influence on microalgae, mainly by their crystal composition and this is in agreement with (Lei et al., 2016a).

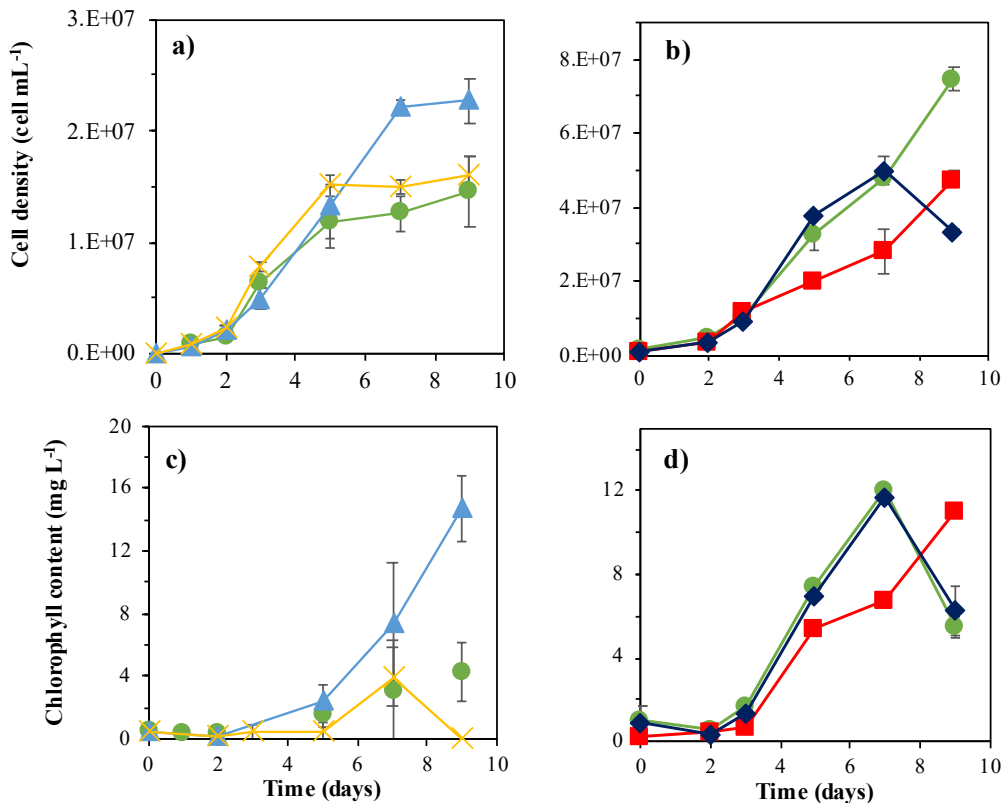


**Fig. 10.** Time course of the cell density a) and b); and chlorophyll content c) and d) of *Chlorella* sp. cultivated in Bayfolan forte medium under different conditions assessed: control (green circles), 10 mg L<sup>-1</sup> Fe<sub>2</sub>O<sub>3</sub>-450 (light blue triangles), 10 mg L<sup>-1</sup> Fe<sub>2</sub>O<sub>3</sub>-100 (yellow cruces); 5 mg L<sup>-1</sup> Fe<sub>2</sub>O<sub>3</sub>-450 (red squares); 20 mg L<sup>-1</sup> Fe<sub>2</sub>O<sub>3</sub>-450 (navy blue diamonds).

Furthermore, the Px of *Chlorella* sp. significantly decreased by 65% when 10 mg L<sup>-1</sup> of Fe<sub>2</sub>O<sub>3</sub>-1000 NPs was added to the culture, as well as the  $\mu$  and the R values (**Table 3**). On the other hand, the addition of 10 mg L<sup>-1</sup> of Fe<sub>2</sub>O<sub>3</sub>-450 NPs did not present a significant difference compared to the control. Moreover, the DIC<sub>f</sub> did not present a significant difference between the assays, however at this point is important to highlight that the assays containing 10 mg L<sup>-1</sup> of Fe<sub>2</sub>O<sub>3</sub>-450 NPs increased their cell density, which can be attributed to the fact that the Fe<sub>2</sub>O<sub>3</sub>-450

NPs stimulated *Chlorella* sp. growth, either by the formation of carbonates that were rapidly consumed by *Chlorella* sp. or by the released of iron ions that could have stimulated *Chlorella* sp. metabolism (Cheng et al., 2020; Vaz, Costa, et al., 2019).

Therefore, Fe<sub>2</sub>O<sub>3</sub>-450 NPs were selected as the optimal NPs for *Chlorella* sp. culture, and different concentrations (5 and 20 mg L<sup>-1</sup>) were elucidated to find the optimum concentration for enhanced *Chlorella* sp. growth. The addition of 5 mg L<sup>-1</sup> Fe<sub>2</sub>O<sub>3</sub>-450 did not present a biomass enhancement and the addition of 20 mg L<sup>-1</sup> resulted in biomass loss at day 7 (**Fig. 10b**). Even if the addition of 20 mg L<sup>-1</sup> Fe<sub>2</sub>O<sub>3</sub>-450 resulted in a cell density loss, the Px,  $\mu$  and the R values between the different assays did not show a statistical difference (**Table 4**). Interestingly, the chlorophyll content in the control and the assays containing 20 mg L<sup>-1</sup> of Fe<sub>2</sub>O<sub>3</sub>-450 NPs behaved similarly and suffered a decay on day 7 (**Fig. 10d**), but the addition of 5 mg L<sup>-1</sup> of Fe<sub>2</sub>O<sub>3</sub>-450 NPs resulted in a chlorophyll enhancement, suggesting that low doses Fe<sub>2</sub>O<sub>3</sub>-450 NPs stimulate pigment synthesis in *Chlorella* sp. The behavior observed with *Chlorella* sp. is in accordance with the results reported by Bibi et al. (2021), where the addition of low concentrations of Fe<sub>2</sub>O<sub>3</sub> NPs showed similar growth patterns on *C. vulgaris* than the control (without NPs)

### 3.3.2 Biomass composition

The addition of 10 mg L<sup>-1</sup> of Fe<sub>2</sub>O<sub>3</sub>-1000 did not present a significant difference in the carbohydrate content of *Chlorella* sp. On the other hand, the addition of 10 mg L<sup>-1</sup> of Fe<sub>2</sub>O<sub>3</sub>-450 NPs to *Chlorella* sp. culture resulted in a significant carbohydrate enhancement of 91%, increasing from 16.98% to 32.50% (% dw) (**Fig. 9c**). It has

been previously stated that microalgae possesses a carbon concentrating mechanism that prepares the cells to gather and accumulate inorganic carbon from surroundings and the concentration of CO<sub>2</sub> in the culture broth affects the starch content (Chandra et al., 2020; González-Fernández & Ballesteros, 2012). Hence, since the culture media was not carbonate supplemented and the only carbon source was provided by the sparged air, our results suggest that the addition of Fe<sub>2</sub>O<sub>3</sub>-450 NPs influenced the carbohydrate metabolism of *Chlorella* sp. Moreover, the lipid content of *Chlorella* sp. did not present a significant change when 10 mg L<sup>-1</sup> of Fe<sub>2</sub>O<sub>3</sub>-450 NPs were added to the culture. Nevertheless, the addition of 10 mg L<sup>-1</sup> of Fe<sub>2</sub>O<sub>3</sub>-1000 resulted in a lipid decrement from 11.25 to 3.25 % (dw). The production of ROS has been stated as one toxicity pathway that causes cellular damages such as loss of membrane fluidity and the oxidation of unsaturated lipids (Déniel et al., 2019a; Vargas-Estrada et al., 2020). Therefore, the reduction in the lipid content can be mainly attributed to cell-self-protection from ROS generated by the Fe<sub>2</sub>O<sub>3</sub>-1000 NPs. Indeed, our results obtained with *Chlorella* sp. confirm the fact that Fe<sub>2</sub>O<sub>3</sub>-1000 NPs have a toxic effect on microalgae, mainly by the crystal composition, and the higher  $\alpha$ -phase content present in the Fe<sub>2</sub>O<sub>3</sub>-1000 NPs had a higher toxicity in both strains used.

Interestingly, the addition of 5 mg L<sup>-1</sup> Fe<sub>2</sub>O<sub>3</sub>-450 resulted in a lipid enhancement from 18% (control) to 26.75% (% dw) (**Fig. 9d**). At this point it is important to mention that the chlorophyll content in the assays with 5 mg L<sup>-1</sup> of Fe<sub>2</sub>O<sub>3</sub>-450 was increased by the addition of the NPs, and the lipid enhancement in the latter assays is correlated to the chlorophyll content and to the cell density

decrement since, typically, the lipid production increases at the expense of the growth rate (Mulgund, 2022). On the other hand, the addition of 20 mg L<sup>-1</sup> Fe<sub>2</sub>O<sub>3</sub>-450 NPs resulted in a lipid decrement, which can be related to lipid oxidation resulting from an oxidative stress created by the formation of ROS. Indeed, from our results we could say that Fe<sub>2</sub>O<sub>3</sub>-450 NPs created a stressful environment for *Chlorella* sp., however low doses (5 mg L<sup>-1</sup>) of Fe<sub>2</sub>O<sub>3</sub>-450 NPs were tolerable for *Chlorella* sp. and stimulated lipid production, while the addition of higher doses ( $\geq$  10 mg L<sup>-1</sup>) did not present a significant change compared to the control.

Finally, the addition of 20 mg L<sup>-1</sup> of Fe<sub>2</sub>O<sub>3</sub>-450 NPs increased the carbohydrate content from 9.92% to 19.75% (% dw) while no significant enhancement was observed when 5 mg L<sup>-1</sup> of Fe<sub>2</sub>O<sub>3</sub>-450 NPs were added. Nonetheless, 10 mg L<sup>-1</sup> of Fe<sub>2</sub>O<sub>3</sub>-450 NPs was the optimal dose for carbohydrate production. Indeed, Fe<sub>2</sub>O<sub>3</sub>-450 NPs influenced *Chlorella* sp. metabolism as well, and our results suggest that the addition of these NPs stimulated the carbohydrate metabolism of *Chlorella* sp. as discussed in section 3.2.2. Thus, our results suggest that low doses of Fe<sub>2</sub>O<sub>3</sub>-450 NPs support the production of high-value biomass even at low CO<sub>2</sub> concentrations.

## 4. Conclusions

The annealing temperature of the Fe<sub>2</sub>O<sub>3</sub> nanoparticles influenced the crystal phase formation of the nanoparticles. Indeed, Fe<sub>2</sub>O<sub>3</sub>-450 nanoparticles presented a higher concentration of the  $\gamma$ -phase than the Fe<sub>2</sub>O<sub>3</sub>-1000 nanoparticles. The crystal phase played an important role in *Chlorella vulgaris* and *Chlorella* sp. growth, but the



Fe<sub>2</sub>O<sub>3</sub>-1000 nanoparticles presented a higher toxicity in both species. On the other hand, Fe<sub>2</sub>O<sub>3</sub>-450 nanoparticles influenced the carbohydrate content of *C. vulgaris* at concentrations  $\geq 10$  mg L<sup>-1</sup>. Moreover, the addition of 5 mg L<sup>-1</sup> of Fe<sub>2</sub>O<sub>3</sub>-450 induced lipid accumulation on *Chlorella* sp. while concentrations  $\geq 10$  mg L<sup>-1</sup> influenced microalgae growth and carbohydrate production. Indeed, Fe<sub>2</sub>O<sub>3</sub> nanoparticles can be used as a strategy to produce high-value biomass even at low concentrations of CO<sub>2</sub>.

# Chapter 3

---

## Effect of wastewater composition on microalgae growth, nutrient uptake, biomass composition and energy recovery

This chapter is adapted from the publication:

- Vargas-Estrada, L., Longoria, A., Okoye, P. U., & Sebastian, P. J. (2021). Energy and nutrients recovery from wastewater cultivated microalgae: Assessment of the impact of wastewater dilution on biogas yield. *Bioresource Technology*, 341 doi:10.1016/j.biortech.2021.125755



---

## 1. Introduction

The world's population is expected to increase to approximately 9 billion in the year 2050, with a consequent high demand for cleaner energy supply and clean water (Shahid et al., 2020a). Since clean energy and water are two of the sustainable development goals, many efforts have been made to meet these goals. These objectives converge in a single point, microalgae. Microalgae have demonstrated to have the potential to accumulate different macromolecules when exposed to different stress environments (carbohydrates, lipids, and/or proteins) (Chen et al., 2011a; Li et al., 2020a; Qiu et al., 2020; Rosa et al., 2018; Toledo-Cervantes et al., 2018). These macromolecules can be used to produce biofuels such as biodiesel, bioethanol, biohydrogen, biogas, etc.

The interest in using microalgae to produce biofuels has increased because microalgae can grow in wastewater (Arias et al., 2018; Fernández-Linares et al., 2017a; Iasimone et al., 2018; Mounghmoon et al., 2020), which normally contains nutrients such as nitrogen and phosphorous that are essential for microalgae growth. Besides, if these compounds are not removed from wastewater discharges, they can cause environmental damages such as eutrophication, leading to oxygen depletion, loss of species, and an increase in the turbidity and toxicity of water (Hernández-García et al., 2019).

The integration of microalgae growth to wastewater treatment is a sustainable process that removes nutrients from wastewater and produces biomass that can be valorized and transformed into biofuels at a low cost (Jiang et al., 2018a). For instance, Chang et al. (2018) used microalgae to treat landfill leachate, while at the

same time produce bio-lipid in a membrane photobioreactor. They showed that nitrogen and phosphorus reclamation efficiencies could reach above 50% and 70%, respectively. In a similar study, phytoremediation of reverse osmosis concentrate with microalgae was implemented as a strategy for the treatment of the concentrate, reduction of CO<sub>2</sub>, and biolipid production (Chang et al., 2020). Firstly, electrooxidation was used to pretreat the reverse osmosis concentrate that contains high free ammonia and chromaticity that could impact the process efficiency. Then, the macroalgae were used to remediate the concentrate, to reclaim nutrients and to produce biolipid. This strategy could realize a maximum biolipid yield of 491.5 mg L<sup>-1</sup> with a biomass concentration of 1.27 g L<sup>-1</sup> under a current density of 3.25 mA cm<sup>-2</sup>.

Although microalgae cultivation in wastewater presents many advantages, there are still some challenges, such as high COD (Terán Hilaes et al., 2021) and NH<sub>4</sub><sup>+</sup> content, toxicity, turbidity, presence of microalgae predators, etc., that need to be surmounted to enhance biomass productivity and macromolecules production. COD concentration in wastewater is one of the key parameters that need to be account for in microalgae cultivation in wastewater since high COD concentrations could inhibit microalgae growth. Several authors have assessed the effect of initial COD in wastewater on microalgae growth. evaluating initial COD concentrations ranging from 300–3200 mg COD L<sup>-1</sup>, observing contrary results (Gao et al., 2018; Molinuevo-Salces et al., 2016a; Nguyen et al., 2020a). Guo et al. (2017) observed that the dilution by 10% of anaerobically digested swine wastewater (corresponding to 289.98 ± 11.05 mg COD L<sup>-1</sup>) was the best dilution ratio for fungal-algal cultivation.

On the other hand, (Xu et al., 2015) observed that *Scenedesmus obliquus* grew faster in the media containing 1200 and 1600 mg COD L<sup>-1</sup>.

Moreover, high NH<sub>4</sub><sup>+</sup> concentrations presented in wastewater can inhibit microalgae growth and some techniques, such as water dilution have been implemented to reduce the NH<sub>4</sub><sup>+</sup> concentration (Jiang et al., 2018b). The dilution of wastewater could lead to nutrient depletion creating stress conditions that could change microalgae metabolic pathways towards lipids synthesis, triglyceride accumulation, protein content reduction and increased carotenogenesis (Chen et al., 2011b; Shahid et al., 2020b). Hernández-García et al. (2019) reported the highest biomass yield (1.95 ± 0.3 g L<sup>-1</sup>) of *Desmodesmus* spp. when cultivated during nutrient limitation. They revealed that *Desmodesmus* spp. accumulated up to 20% and 41% of lipids and carbohydrates, respectively. In another study made by Fernández-Linares et al. (2017b), the species *Chlorella vulgaris* UTEX, *Chlorella vulgaris* CICESE and an indigenous consortium presented increased lipid contents (25.70 ± 1.24%, 23.35 ± 3.01%, and 20.54 ± 1.23%, respectively) when cultivated in treated wastewater with limited nitrogen in the medium. Although nitrogen starvation has led to higher lipid content in microalgae, the lipid content depends on the species, because *Desmodesmus* spp. accumulated a higher lipid content compared to *C. vulgaris* UTEX and *C. vulgaris* CICESE. Furthermore, there is no study on the lipid production of mixed microalgae cultures grown in wastewater with low nitrogen content.

The use of mixed cultures of microalgae-bacteria for wastewater treatment is a noteworthy research line because the presence of bacteria not only removes organic

matter but helps the growth of microalgae (Luo et al., 2020), however, other factors such as temperature need to be controlled to achieve better performance. For instance, González-Camejo et al. (2019a) reported that temperature plays an important role in the growth of the microalgae-nitrifying bacteria consortium. They revealed that temperatures in the range of 15 – 30 °C had no significant effect on microalgae cultivation, but when the temperature increased to 30 – 35 °C, microalgae viability was significantly reduced. Also, using mixed culture for nutrients recovery from wastewater could limit the lipids accumulation, in this way anaerobic digestion for biogas production is the most viable option to recover energy from the produced biomass.

Hence, in this chapter, the biomass composition of a mixed culture of microalgae cultivated in different dilutions of wastewater was investigated and compared. The biomass was subsequently assessed for the production of biogas. Statistical analysis was performed to elucidate the significance of the process variables and the experimental data was model to investigate the process kinetics.

## **2. Methods**

### **2.1 Description of the Wastewater**

Wastewater was collected from the wastewater treatment plant (WWTP) located inside the Institute of Renewable Energy (IER) located in Temixco, Morelos, Mexico. The WWTP treats wastewater generated in the IER including the cafeteria, laboratories, and bathrooms. WWTP consists of a screening collection tank, which is then directed to a primary settler where sedimentary solids are separated. Then,

wastewater is channeled to two aerobic digesters and then to a high load solids separator to separate secondary sludge. Secondary sludge is recirculated to the primary settler and the treated water is directed to a disinfection tank where sodium hypochlorite is added. Finally, treated water goes through a sand and gravel filter for final disposal. Wastewater samples for microalgae culture were collected after the aerobic treatment. Microalgae growth was assessed in two different wastewater dilutions of 10% (v v<sup>-1</sup>) and 50% (v v<sup>-1</sup>), and 100% (v v<sup>-1</sup>) wastewater, to compare if the nutrient content of each PBR affects the biomass composition. The dilutions were carried out with filtered tap water.

## **2.2 Microalgae culture**

The microalgae strain used in this chapter corresponds to a consortium of different species of microalgae and nitrifying bacteria, but the culture is mainly dominated by *Chlorella* sp., and was donated by the Metropolitan Autonomous University (UAM), Mexico City, Mexico. The microalgae mixture was isolated from the water channels of Xochimilco, Mexico. In this chapter, to simplify the terms, we will refer to the mixed culture as “microalgae”. The microalgae are kept in an incubator (Thermo Scientific) at 19 °C with light:dark cycles of 15:9 h, respectively in Erlenmeyer flasks covered with a cotton plug. As a culture medium, Bayfolan forte (Bayer CropScience) is used in a concentration of 1mL L<sup>-1</sup>.

## **2.3 Experimental set-up**

Microalgae cultivation was carried out under environmental conditions in flat plate photobioreactors (PBR) with dimensions of 60 cm length × 10 cm width × 50 cm



height, and a working volume of 20 L. Air was pumped (Elite 800) to provide CO<sub>2</sub> and to avoid the sedimentation of the culture. The solar intensity was measured with a light meter (Field Scout TM 3415FXSE). The temperature was measured with a submersible thermometer (4339, Control Company) and pH was not controlled.

Microalgae were cultivated in different wastewater dilutions as described above, a control in filtered tap water with Bayfolan forte (1 mL L<sup>-1</sup>) was also cultivated adding a total of 4 assays: PBR1: Control; PBR2: 10% (v v<sup>-1</sup>) wastewater; PBR3: 50% (v v<sup>-1</sup>) wastewater and PBR4: 100% wastewater, each assay was run in duplicate. Before inoculating with the microalgae, the PBRs were sterilized with a submergible UV lamp (13 W, 110 v) for 20 minutes to avoid the presence of predators.

## **2.4 Biochemical methane potential test**

The biochemical methane (BMP) tests were carried out to assess the biogas production from the different microalgae biomass obtained and to know if the wastewater dilution affects the biogas production. To carry out the BMP tests, an inoculum from an anaerobic reactor that treats sludge from the Polytechnic University of the State of Morelos (UPEMOR) was used. BMP tests were carried out in serum bottles of 120 mL, the liquid phase occupied a volume of 80 mL. The bottles were prepared in a substrate:inoculum ratio of 0.5 gVS<sub>s</sub>: gVS<sub>r</sub><sup>-1</sup>, each bottle contained 5 gVS according to (Alzate et al., 2012). The missing volume was made up with distilled water to reach 80 mL and nitrogen was used to purge for 1 minute to ensure anaerobic conditions. Thereafter, the bottles were sealed with rubber stoppers and aluminum caps and then incubated at 35 °C until biogas production ceased. In total,

the BMP of the following types of biomass was assessed: control (Bayfolan forte); 10% (v v<sup>-1</sup>) wastewater; 50% (v v<sup>-1</sup>) wastewater, and 100% wastewater. In addition, a blank containing inoculum was prepared to quantify the methane produced by endogenous respiration, each assay was run in triplicates. The total volume of biogas produced was calculated by subtracting the volume of the blank from each of the tests.

#### 2.4.1 Biogas production and composition

The volume of the produced biogas in each bottle was determined by the pressure difference inside the bottle. Once the pressure was measured, the gas was released until atmospheric pressure was reached. The biogas composition was determined using a gas detector Altair 5x, MSA.

#### 2.4.2 Kinetic model

The experimental data obtained from the BMP test were modeled by the modified Gompertz model (Eq 6).

$$B = B_0 \cdot e \left\{ -e \left[ \frac{R_m e}{B_0} (\lambda - t) + 1 \right] \right\} \quad (6)$$

where  $B$  is the cumulative methane yield ( mL<sub>CH<sub>4</sub></sub> gVS<sup>-1</sup>),  $B_0$  is the methane yield potential (mL<sub>CH<sub>4</sub></sub> gVS<sup>-1</sup>),  $R_m$  is the maximum methane yield rate (mL<sub>CH<sub>4</sub></sub> gVS<sup>-1</sup>),  $\lambda$  is the lag time (d),  $t$  is the digestion time (d), and  $e$  is the Euler number.

## 2.5 Analytical procedures

### 2.5.1 Microalgae and nitrifying bacteria growth

Microalgae growth was assessed by 1) dry weight (DW) method by filtering 10 mL of the sample through glass fiber filters 47 mm (Whatman. GE Healthcare Life Sciences), followed by drying all night at 105 °C, according to standard methods (APHA-AWWA-WPCF, 1999); and 2) cell density (CD) method, which was determined by optical microscopy with an improved Neubauer chamber. The DW and CD were measured every day. Biomass productivity ( $P$ ) and specific growth rate ( $\mu$ ) were calculated according to Eqs. (7) and (8), respectively (J. Cheng et al., 2020):

$$P = \frac{DW_1 - DW_0}{t_1 - t_0} \quad (7)$$

where  $P$  is biomass productivity ( $\text{g L}^{-1} \text{d}^{-1}$ ),  $DW_1$  and  $DW_0$  are the biomass dry weight ( $\text{g L}^{-1}$ ) at time  $t_1$  and  $t_0$  (d).

$$\mu = \frac{\ln DW_1 - \ln DW_0}{t_1 - t_0} \quad (8)$$

where  $\mu$  is the specific growth rate ( $\text{d}^{-1}$ ),  $\ln DW_1$  and  $\ln DW_0$  are the natural logarithm of biomass dry weight at time  $t_1$  and  $t_0$  (d).

The growth of nitrifying bacteria was quantified by the nitrification rate according to Eq. (9) (González-Camejo et al., 2019b):

$$NO_X R = \frac{NO_{x1} - NO_{x0}}{t_1 - t_0} \quad (9)$$

where  $NO_{xR}$  ( $\text{mg N L}^{-1} \text{ d}^{-1}$ ) is the nitrification rate;  $NO_{x1}$  ( $\text{mg N L}^{-1}$ ) is the concentration of nitrates plus nitrites at time  $t_1$  (d) and  $NO_{x0}$  ( $\text{mg N L}^{-1}$ ) is the concentration of nitrates plus nitrites at time  $t_0$  (d).

The nitrogen uptake by nitrifying bacteria was calculated according to Eq. (10).

$$N_{uptake} = NO_{x1} - NO_{x0} \quad (10)$$

where  $N_{uptake}$  ( $\text{mg N L}^{-1}$ ) is the nitrogen uptake,  $NO_{x1}$  ( $\text{mg N L}^{-1}$ ) is the final concentration of nitrates plus nitrites and  $NO_{x0}$  ( $\text{mg N L}^{-1}$ ) is the initial concentration of nitrates plus nitrites.

### 2.5.2 Nutrient removal

The concentration of nutrients was determined as follows: ammonium concentration ( $\text{NH}_4^+$ ) was measured according to (Solórzano, 1969), nitrates ( $\text{NO}_3^-$ ) were measured by the cadmium reduction method (method 8171MR, HACH). The nitrites ( $\text{NO}_2^-$ ) were measured by the diazotization method (method 8507, HACH), total inorganic nitrogen (TIN) was calculated as the sum of  $\text{NH}_4^+$ ,  $\text{NO}_3^-$  and  $\text{NO}_2^-$ . The total phosphorous (TP) was measured by the phospho-vanadium-molybdate method according to standard methods (APHA-AWWA-WPCF, 1999) and the chemical oxygen demand (COD) was measured by tests kits (method 8000, HACH). All the tests were run in duplicates. To determine the concentration of  $\text{NH}_4^+$ ,  $\text{NO}_3^-$ ,  $\text{NO}_2^-$ , TP, and COD, a volume of each PBR was collected and centrifuged at 2300 RPM for 15 min and the supernatant was carefully extracted for characterization.

### **2.5.3. Biomass composition and statistical analysis**

Microalgae biomass composition was determined as follows: carbohydrates content was determined by the phenol-sulfuric method (Dubois et al., 1956), lipids were determined by the methanol-chloroform method according to (Tongprawhan et al., 2014), ash was determined according to NREL determination of ash in algal biomass (Van Wychen & Laurens, 2016). Proteins were calculated as the subtraction of carbohydrates, lipids, and ashes. Statistical analysis was performed and analyzed by ANOVA followed by Tuckey's test considering  $\alpha=0.05$ . The results were presented as mean  $\pm$  standard deviation.

## **3. Results and discussion**

### **3.1 Microalgae and nitrifying bacteria growth**

Wastewater cultivated microalgae have been considered as an economic and environmentally friendly option to recover nutrients and produce biomass since wastewater contains nutrients such as ammonium nitrogen ( $\text{NH}_4^+\text{-N}$ ) and phosphorous, which are essential nutrients for microalgae growth. **Table 5** shows the chemical composition of each PBR at the beginning of the study.

**Table 5.** Chemical composition of each PBR at the beginning of the experiment

	<b>PBR1</b>	<b>PBR2</b>	<b>PBR3</b>	<b>PBR4</b>
COD (mg L <sup>-1</sup> )	69.00 ± 1.41	8.00 ± 2.83	70.00 ± 8.49	158.00 ± 36.77
TP (mg L <sup>-1</sup> )	49.14 ± 1.63	7.32 ± 2.51	21.01 ± 5.64	40.00 ± 12.73
NH <sub>4</sub> <sup>+</sup> (mg L <sup>-1</sup> )	31.21 ± 1.21	9.52 ± 0.67	45.42 ± 1.10	87.57 ± 2.64
NO <sub>3</sub> <sup>-</sup> (mg L <sup>-1</sup> )	8.50 ± 2.12	6.50 ± 0.71	15.50 ± 2.12	18.50 ± 0.71
NO <sub>2</sub> <sup>-</sup> (mg L <sup>-1</sup> )	0.02 ± 0.01	0.43 ± 0.01	2.29 ± 0.05	5.25 ± 0.35
TIN (mg L <sup>-1</sup> )	39.73 ± 1.11	16.45 ± 0.46	63.21 ± 1.09	106.07 ± 1.675
pH	8.17 ± 0.05	8.72 ± 0.58	8.73 ± 0.73	8.54 ± 0.57

Note: COD: chemical oxygen demand; TP: total phosphorous; TIN: Total Inorganic Nitrogen.

After 10 days of cultivation under environmental conditions, no change in the proliferation of microorganisms was observed, and the dominant species was the microalgae *Chlorella* sp., concomitantly, there was no statistical difference in microalgae biomass production between the culture mediums. The PBR1 and PBR3 behaved very similarly, and the PBR3 presented a maximum cell density at day 9 (8.11E+07 cell mL<sup>-1</sup>), followed by PBR1 (6.95E+07 cell mL<sup>-1</sup>) and PBR2 (6.68E+07 cell mL<sup>-1</sup>), while PBR4 showed the lowest cell density (2.56E+07 cell mL<sup>-1</sup>) (**Fig. 11a**). During the cultivation period, all the cultures suffered a drop in their cell density on day 5 of cultivation, however, the cultures managed to recover. This behavior could be attributed to the adaptation phase of the microalgae to wastewater and to the

depletion of essential nutrients in the medium, such as ammonium and phosphorous, which limited the culture growth. Regarding dry weight, the PBRs presented the same trend as the cell density (**Fig. 11b**); the dry weight is considered only as the weight of algae cells.

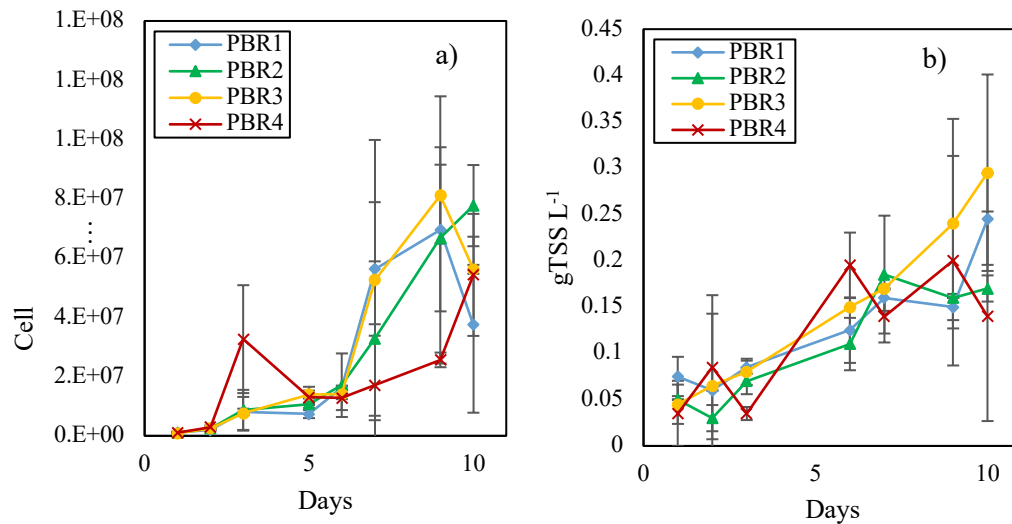


**Fig. 11.** Microalgae growth. a) cell density (cell mL<sup>-1</sup>); b) dry weight (TSS L<sup>-1</sup>).

The results suggest that the wastewater concentration did not significantly affect the biomass production, however, when wastewater proportion was increased to 50% (v v<sup>-1</sup>), a higher biomass production (in terms of cell density and dry weight) was observed with higher biomass productivity (g L<sup>-1</sup> d<sup>-1</sup>) (**Table 6**). Conversely, when the wastewater concentration decreased to 10% (v v<sup>-1</sup>) the biomass productivity and specific growth rate decreased as well. The decrease in  $P$  and  $\mu$  can be attributed to the low nutrient content in PBR2, which limited the microalgae growth. The results reported concerning wastewater dilution for microalgae culture vary from

municipal wastewater, digestate, agro-industrial wastewater, landfill leachate, or a combination of two or more types of wastewater (Arias et al., 2018; Gupta et al., 2019a; Li et al., 2020b; Porto et al., 2020). Li et al., (2020b) evaluated the growth of microalgae in original piggery effluent (OPE). They reported that anaerobically digested piggery effluent (DPE) in different dilutions depends on the  $\text{NH}_4^+\text{-N}$  concentration (20, 40, and 80  $\text{mg L}^{-1}$ ). They observed an increase in biomass productivity as the  $\text{NH}_4^+\text{-N}$  concentration increased for DPE. In this chapter, the biomass productivity decreased when 100% of wastewater was used, which could be attributed to 1) the nutrient and micronutrient depletion, since the wastewater used came from biological treatment and essential micronutrients could have been consumed, and 2) the wastewater turbidity, which has been widely reported as one of the main factors that influence microalgae growth in wastewater (Jiang et al., 2018b). Comparably, the specific growth rate obtained was greater than the reported specific growth rate of  $0.11 \pm 0.01 \text{ day}^{-1}$  by (Paskuliakova et al., 2016), cultivating *Chlamydomonas* sp. at 15 °C, 14:10 h light:dark cycles, and  $22 \mu\text{mol m}^{-2} \text{ s}^{-1}$ . This shows a great promise for the microalgae used under environmental conditions.

The microalgae biomass production may have been affected by nitrifying bacteria since both microorganisms compete for ammonia nitrogen. The  $\text{NO}_x\text{R}$ s obtained were  $1.57 \pm 0.16$ ;  $0.53 \pm 0.03$ ;  $2.42 \pm 0.20$  and  $3.08 \pm 0.05 \text{ mg N L}^{-1} \text{ d}^{-1}$  for PBR1, PBR2, PBR3 and PBR4, respectively. The  $\text{NO}_x\text{R}$  values obtained are below the range reported by (González-Camejo et al., 2019b) ( $3\text{-}6 \text{ mg N L}^{-1} \text{ d}^{-1}$ ) where the activity of nitrifying bacteria increases, which suggests that there is a competition for ammonia nitrogen between the two microorganisms, limiting the growth of



microalgae. In addition, the  $N_{\text{uptake}}$  of the nitrifying bacteria for PBR1, PBR2, PBR3, and PBR4 was  $13.08 \pm 1.44$ ,  $4.77 \pm 0.27$ ,  $21.82 \pm 1.79$ , and  $27.70 \pm 0.42$  mg L<sup>-1</sup>, respectively. Although PBR4 presented the highest  $N_{\text{uptake}}$ , this value represents 31.65% of the initial NH<sub>4</sub> concentration in the wastewater. Nitrifying bacteria contained in PBR3, PBR1, and PBR2 consumed 47.96%, 41.81%, and 50.10% of the initial NH<sub>4</sub> concentration, respectively. Hence the results reveal that the activity of nitrifying bacteria increased as the NH<sub>4</sub> in the medium decreased, and as the NH<sub>4</sub> concentration in the media increased, microalgae proliferated.

**Table 6.** Microalgae biomass productivity ( $P$ ) and specific growth rate ( $\mu$ )

<b>Parameter</b>		
<b>Culture conditions</b>	<b><math>P</math> (g L<sup>-1</sup>d<sup>-1</sup>)</b>	<b><math>\mu</math> (d<sup>-1</sup>)</b>
Control	$0.019 \pm 0.008$	$0.133 \pm 0.054$
10% (v v <sup>-1</sup> ) wastewater	$0.015 \pm 0.001$	$0.187 \pm 0.063$
50% (v v <sup>-1</sup> ) wastewater	$0.028 \pm 0.014$	$0.212 \pm 0.095$
100% (v v <sup>-1</sup> ) wastewater	$0.015 \pm 0.004$	$0.210 \pm 0.093$

### 3.2 Nutrient removal

The operation of the flat plate photobioreactors is considered as a tertiary treatment with the main objective of remove/recycle nutrients such as nitrogen and phosphorous. The microalgae growth and nutrient removal from three different

wastewater concentrations (10% (v v<sup>-1</sup>); 50% (v v<sup>-1</sup>) and 100% (v v<sup>-1</sup>)) were assessed. Since microalgae composition varies depending on the nutrients present in the culture media, the changes in microalgae composition depending on wastewater dilution were investigated.

Wastewater is characterized by high concentrations of nitrogen in the form of ammonium, nitrate, and nitrite, and phosphorous (Gupta et al., 2019b). The two nutrients of N and P are essential for microalgae growth and if they are not removed from wastewater before being discharged to the environment, they can cause eutrophication. **Fig. 12** shows the result of nutrient removal.

Observably, the COD increased after 10 days of cultivation for PBR1, PBR2, and PBR3 (**Fig. 12a**). This behavior has been previously reported by some authors (Lima et al., 2020a; Uggetti et al., 2018) and was mainly attributed to the release of compounds from microalgae. Notably, when microalgae are cultivated using CO<sub>2</sub> as a carbon source they excrete small molecular organic substances such as glycolic acid as a product of the photosynthetic carbon reduction cycle (Wang et al., 2010). In addition, the increase in COD concentration has been related to endogenous respiration of microalgae and bacteria when the biomass growth reaches the death phase (Nguyen et al., 2020b), which is agrees with the behavior observed in PBR1 and PBR3. Thus, the decrease in the COD concentration in PBR4 could be explained by 1) PBR4 did not reach the death phase, therefore there was no endogenous respiration, and 2) PBR4 biomass productivity was lower than PBR2, leading to less released compounds, and lower COD.

Phosphorous is an essential nutrient for microalgae growth as it is the component of various metabolic activities, energy, lipid, protein, and coenzymes of the body (Hussain et al., 2021a). The TP was completely removed for all the PBRs containing wastewater (**Fig. 12b**). In PBR2 TP was not detected from day 2, which could impact microalgae, limiting their growth. This finding agrees with the study of González-Camejo et al. (2017), which reported a culture decay when phosphorous was not detected in the medium. Lima et al. (2020b) also reported that phosphorous was the limiting nutrient for microalgae growth, thus, the phosphorous depletion limited microalgae growth.

Nitrogen is a very vital nutrient for microalgae growth (Hussain et al., 2021b), and are available in the form of  $\text{NH}_4^+$ ,  $\text{NO}_3^-$ , and  $\text{NO}_2^-$ . The most common inorganic source of nitrogen,  $\text{NH}_4^+$  used by eukaryotic algae, is the preferred nitrogen form due to the less energetic cost during its assimilation, followed by  $\text{NO}_3^-$ ,  $\text{NO}_2^-$ , and urea (Su, 2021). The  $\text{NH}_4^+$  reached removals up to 97.85% in PBR2, 89.59% in PBR3, and 71.69% in PBR4 (**Fig. 12c**). The  $\text{NH}_4^+$  reached removals above 71.69%, it is important to mention that  $\text{NO}_2^-$  and  $\text{NO}_3^-$  concentration suffered an augmentation at the end of the study (**Fig. 12d** and **12e**), which can be attributed to the mixed culture microalgae used in this study. Thus, nitrifying bacteria competed with microalgae for  $\text{NH}_4^+$  uptake, augmenting the  $\text{NO}_3^-$  and  $\text{NO}_2^-$  concentrations.

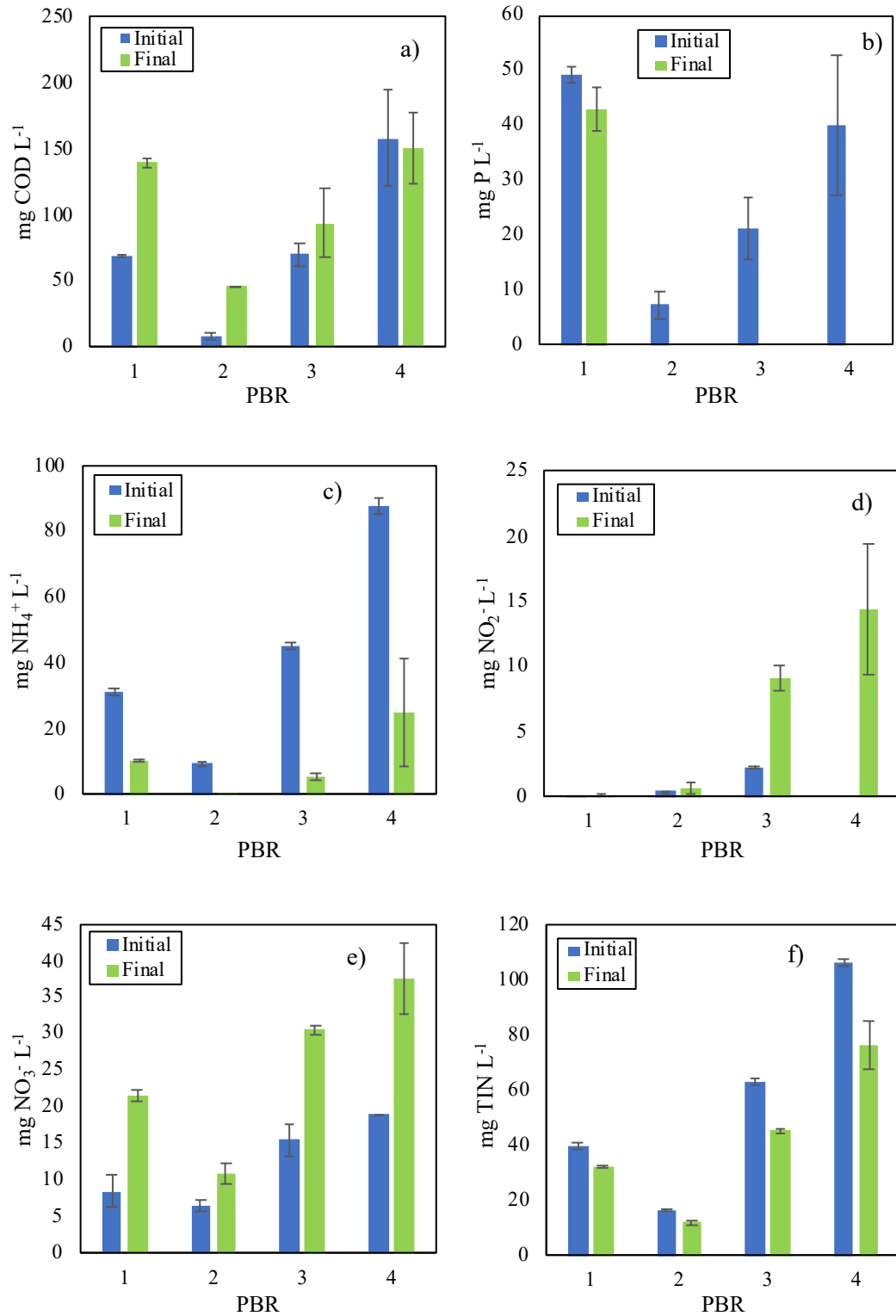


**Fig. 12.** Nutrient content at the beginning and at the end of the study a) COD; b) TP; c) NH<sub>4</sub><sup>+</sup>; d) NO<sub>2</sub><sup>-</sup> and e) NO<sub>3</sub><sup>-</sup>; f) TIN.

González-Camejo et al. (2019b) investigated the effect of ambient temperature variations on an indigenous microalgae-nitrifying bacteria culture dominated by *Chlorella*. They observed that ammonium-oxidizing bacteria (AOB) can reduce microalgae growth by depleting the  $\text{NH}_4^+$  concentration in the media, and the temperature plays an important role since AOB growth increases at temperatures above 25 °C. The temperature of the PBRs was maintained at an average of  $22.18 \pm 0.73$  °C, which is in the range temperature for microalgae proliferation. Albeit the microalgae proliferated, nitrifying bacteria competed for the  $\text{NH}_4^+$  present in the medium limiting microalgae growth. Despite  $\text{NO}_2^-$  and  $\text{NO}_3^-$  increased at the end of our study, the TIN concentration was decreased after 10 days of cultivation (**Fig. 12f**) under environmental conditions confirming the  $\text{NH}_4^+$  uptake by microalgae and nitrifying bacteria.

### 3.3 Biomass composition

Microalgae can produce different macromolecules (lipids, proteins, and carbohydrates) as well as pigments and carotenoids depending on the species and the environmental growth conditions. Stress methods have been used to optimize different macromolecule or pigments accumulation. In previous studies, it has been postulated that nitrogen depletion might lead to lipid accumulation (Chen et al., 2011b; Li et al., 2020b; Shahid et al., 2020b). In this chapter, initial  $\text{NH}_4^+$  concentrations were similar to those assessed by Li et al. (2020b) but contrary results were observed. As shown in **Fig. 13**,  $\text{NH}_4^+$  concentration did not influence the lipid production of the microalgae. The PBR2 presented the lowest  $\text{NH}_4^+$  content,

which was completely removed, however, the microalgae presented a lipid content of  $8.78 \pm 4.50$  (% DW), indicating that  $\text{NH}_4^+$  starvation did not lead to lipid accumulation. The same behavior was observed in PBR3 with a lipid content of  $10.48 \pm 3.28$ . Nevertheless, both PBR2 and PBR3 reached  $\text{NH}_4^+$  removals of 97.85% and 89.59% respectively. Notably, the presence of nitrogen was still detected in the form of  $\text{NO}_3^-$ , which could have affected the lipid production since a no-nitrogen-starvation environment was achieved. This is in agreement with the study of Chen et al. (2011b), which revealed that the species *Dunaliella tertiolecta* was able to use either ammonium or nitrate as a nitrogen source. On the other hand, PBR4 presented a slightly higher lipid content of  $19.67 \pm 4.90$  %, but the results in this study were still below the results reported by Sakthi Vignesh et al. (2020), where lipid contents up to 44% and 52% for *Dictyococcus* sp. and *Coelastrella* sp., respectively were observed when the strains were cultivated under nitrogen starvation.

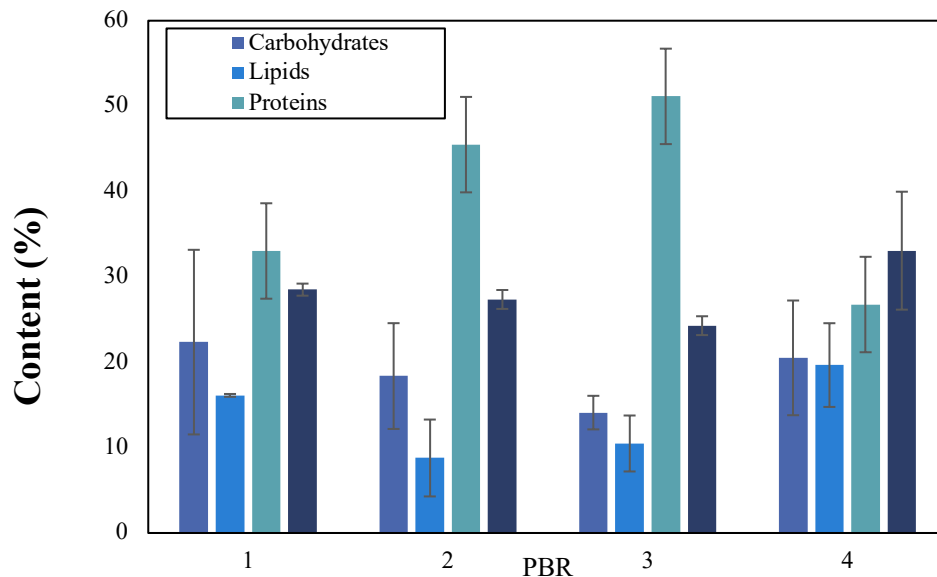


**Fig. 13.** Microalgae biomass composition at the end of the study.

Although the accumulated lipids are not very high, the stored energy and the nutrients recovered by the microalgae can still be used by transforming them into biogas. According to Wang et al. (2016), the VS/TS ratio is a parameter that indicates the content of organic materials, and normally substrates with VS/TS ratio greater than 0.5 are considered high in organic matter, making them more suitable for biogas production Wang et al. (2017). **Table 7** shows the TS, VS, and VS/TS ratio of the different microalgae biomass obtained in our study. The VS/TS ratio ranged between  $0.71 \pm 0.07$  and  $0.82 \pm 0.03$  hence, the biomass produced is suitable for anaerobic digestion.

**Table 7.** Total solids (TS), volatile solids (VS) and VS/TS ratio of the microalgae biomass.

	<b>TS (%)</b>	<b>VS (%)</b>	<b>VS/TS</b>
PBR1	96.45±1.65	73.08±14.37	0.76±0.14
PBR2	95.75±0.55	73.82±0.91	0.77±0.01
PBR3	93.70±1.42	77.24±1.37	0.82±0.03
PBR4	96.13±0.59	68.20±6.82	0.71±0.07

### 3.4 Biogas production

Anaerobic digestion of microalgae has gained attention because it is considered the most straightforward technology to recover energy from microalgae biomass without energy-intensive drying or extraction techniques (Norouzi & Nezamzadeh-Ejhi, 2020)(Passos, Hom-Diaz, et al., 2016). The cumulative biogas and methane

production from wastewater-cultivated microalgae at different percentages of wastewater content was assessed. The results are presented in **Fig. 14**. After 33 days of incubation under mesophilic conditions, no statistical difference was observed between the assays. Hence, the different microalgae culture conditions did not statistically affect biogas production. The biomass from PBR4 presented the highest accumulated biogas volume (204.47 mL<sub>biogas</sub>) followed by PBR2 and PBR3, with lower biogas and methane-accumulated volume. This can be explained by the high protein content of PBR2 and PBR3 during anaerobic digestion. Proteins are mainly degraded to ammonium and its accumulation could inhibit the anaerobes activity (Mahdy et al., 2015).

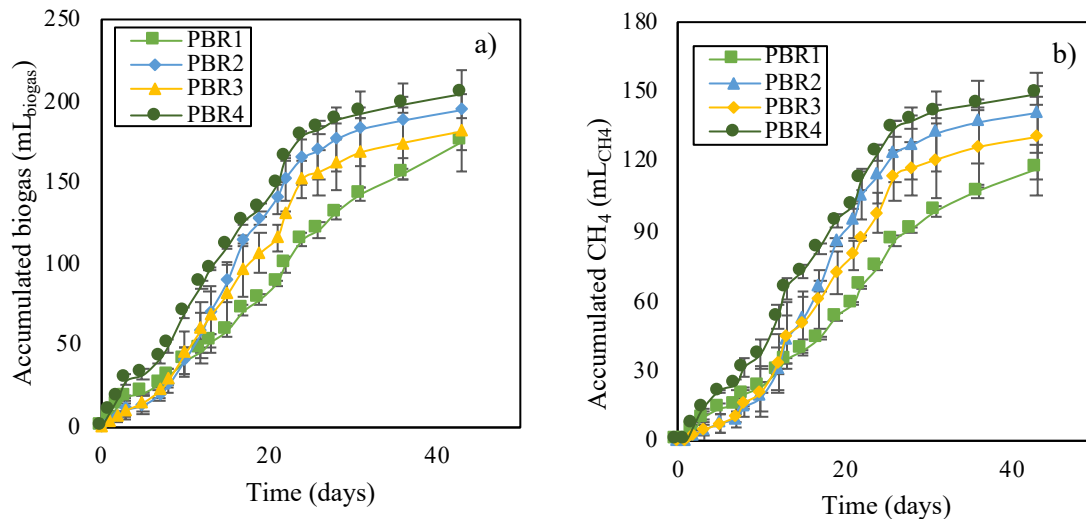


**Fig. 14.** a) Accumulated biogas and b) accumulated methane production after 33 days of incubation under mesophilic conditions.



After 33 days of mesophilic incubation, the anaerobic digestate of PBR1, PBR2, PBR3, and PBR4 presented  $\text{NH}_4^+$  concentrations of  $617.64 \pm 76.29$ ,  $421.53 \pm 60.94$ ,  $502.28 \pm 95.49$  and  $389.12 \pm 7.12$   $\text{mg L}^{-1}$ , respectively. The high protein content in PBR1, PBR2, and PBR3 led to higher  $\text{NH}_4^+$  concentrations compared to PBR4. Since concentrations of  $\text{NH}_4^+$  around 1700-1800  $\text{mg L}^{-1}$  are considered inhibitory (Mahdy et al., 2015), the low biogas production of PBR1, PBR2, and PBR3 is mainly attributed to the recalcitrance of microalgae biomass. Conversely, the higher cumulative biogas volume in PBR4 can be attributed to the lipid content, since lipids have the highest specific methane yield, where specific yields of 1.014  $\text{mL CH}_4 \text{gVS}^{-1}$ , 0.851  $\text{mL CH}_4 \text{gVS}^{-1}$ , and 0.415  $\text{mL CH}_4 \text{gVS}^{-1}$  can be achieved for lipids, proteins, and carbohydrates, respectively (Molinuevo-Salces et al., 2016b; Montingelli et al., 2015). Among the PBRs, PBR4 presented the highest lipid content.

The results obtained from the BMP tests were analyzed using the modified Gompertz model (**Table 8**) and the results suggest that PBR4 increased its  $R_m$  by 65.11% and the lag phase was reduced by 38.53%, which is mainly attributed to the biomass composition. Although PBR4 presented the highest biogas volume, the VS removal was the lowest. These results suggest that pretreatment is required to recover more energy from wastewater cultivated microalgae, but since the lag phase in PBR4 was 2.03 days, a facile pretreatment, *i.e.*, thermal pretreatment at low temperature, could be enough to recover energy from this biomass. Finally, the results suggest that wastewater dilution does not affect statistically the biogas production, but higher methane and biogas volume was achieved when microalgae cultivated in 100% of wastewater was used.

**Table 8.** Kinetic parameters and anaerobic digestion efficiency of the different microalgae biomass.  $B_0$  methane yield potential;  $R_m$  maximum methane yield rate;  $\lambda$  is the lag time; VS volatile solids.

Conditions	Kinetic parameters			AD Efficiency
	$B_0$ (mL CH <sub>4</sub> )	$R_m$ (mL CH <sub>4</sub> d <sup>-1</sup> )	$\lambda$ (d)	% VS removed
PBR1	157.87	3.99	3.29	32.16
PBR2	149.50	7.66	5.99	31.06
PBR3	143.16	6.02	4.70	20.84
PBR4	160.86	6.59	2.03	10.89

## 4. Conclusions

Microalgae cultivated in wastewater exhibited high nutrient removals, reaching 100% and 97.85% removal of TP and NH<sub>4</sub><sup>+</sup>, respectively. When microalgae were cultivated in 100% of wastewater, higher lipid content was accumulated in PBR4, however, the presence of nitrifying bacteria in the culture facilitated partial oxidation of the ammonium to nitrates and nitrites, thus no-nitrogen-starvation was induced in the media. This resulted in lower lipid accumulation in PBR2 and PBR3. The high lipid content in PBR4 resulted in higher biogas production of 204.47 mL<sub>biogas</sub>. Hence, the results suggested that 100% wastewater cultivated microalgae are more feasible for biomass production and energy recovery.



# Chapter 4

---

## Effect of long-term exposure to Fe<sub>2</sub>O<sub>3</sub> nanoparticles on microalgae growth, nutrient uptake and biomass composition

This chapter is adapted from the publication:

- Vargas-Estrada, L., Okoye, P.U., Muñoz, R., Novelo, E., Sebastian, P.J. In preparation. Effect of long term exposure to Fe<sub>2</sub>O<sub>3</sub> nanoparticles on microalgae growth, composition and nutrient uptake.



## 1. Introduction

Microalgae have been considered as a promising feedstock for wastewater treatment, CO<sub>2</sub> capture and biofuel production (Miyawaki et al., 2021). However, their biomass productivities and biofuels production yields *i.e.* biodiesel is low, several techniques have been implemented to overcome these particular drawbacks (Magalhães et al., 2021). Recently, the use of nanotechnology in microalgae cultures is gaining attention since it has been demonstrated that the addition of some metallic nanoparticles (NPs) can enhance biomass productivities, lipid production, carbohydrates accumulation, CO<sub>2</sub> sequestration and light absorption (Vargas-Estrada et al., 2020).

Notwithstanding NPs represent a promising technique to improve microalgae cultivation, most of the literature is focused on their toxic effect since some NPs, such as Ag (Moreno-Garrido et al., 2015a), TiO<sub>2</sub> (J. Hu et al., 2018b), Co (Chen et al., 2018a), ZnO (Manzo et al., 2013). However, NPs such as SiO<sub>2</sub>, Fe<sub>2</sub>O<sub>3</sub> and mesoporous carbons have been reported to have beneficial effects on microalgae (Bibi et al., 2021; Jeon et al., 2017; Rana et al., 2020; Vargas-Estrada et al., 2022, 2023). In this regard, if the attention is focused on the beneficial effects of NPs, interesting results could be obtained.

For instance, Jeon et al. (2017) observed that the addition of SiO<sub>2</sub> NPs increased the biomass production of *Chlorella vulgaris* by 177%, additionally, the lipid content was increased by 340% as well. Moreover, Fe<sub>2</sub>O<sub>3</sub> NPs also demonstrated beneficial effects on some microalgae species. Rana et al. (2020) observed that the biomass concentration of *Chlorella pyrenoidosa* increased by

33.75% when 20 mg L<sup>-1</sup> of Fe<sub>2</sub>O<sub>3</sub> NPs were added, additionally, a lipid content up to 16.89% (dw) was observed when 30 mg L<sup>-1</sup> were added. Additionally, Bibi et al. (2021) observed that the addition of 50 and 100 mg L<sup>-1</sup> of Fe<sub>2</sub>O<sub>3</sub> NPs increased the lipid content by 39.7% and 25.5% respectively. Even if NPs have demonstrated to have beneficial effects in some microalgae species, their reported studies are limited to batch conditions, synthetic and controlled mineral mediums and time exposures up to 35 days. However, Xia et al., (2021) recently evaluated the effect of Fe<sub>2</sub>O<sub>3</sub> NPs addition to synthetic wastewater cultivated *C. vulgaris* cultures for 100 days. These authors reported that the addition of 50 mg L<sup>-1</sup> of these particular NPs led to biomass yields of 2.02 g L<sup>-1</sup> and lipid contents up to 12.3%. Notwithstanding, literature on the exposure of NPs under real wastewater and environmental conditions is scarce.

In this regard, this chapter aimed at assessing the long-term exposure to Fe<sub>2</sub>O<sub>3</sub> NPs if a mixed microalgae-cyanobacterial consortium cultivated in pristine wastewater under environmental conditions. The effect of the NPs was elucidated in terms on biomass production, nutrient uptake and biomass composition.

## **2. Materials and methods**

### **2.1 Nanoparticles**

Fe<sub>2</sub>O<sub>3</sub> nanoparticles were synthesized according to (Norouzi & Nezamzadeh-Ejhi, 2020). A nitrogen physisorption analysis was conducted in an ASAP 2050 (Micromeritics, USA) at 77 K to determine the surface area, pore volume and average pore diameter of the NPs. The specific surface area and pore characteristics were determined by the BET method and BJH equation. Scanning electron microscopy

(SEM) (JEOL JSM-6490LV) and energy-dispersive spectroscopy (EDS) (EDX-700/800, Hitachi, Japan) were carried out to determine the surface morphology and elemental composition of the target NPs. Four different concentrations of Fe<sub>2</sub>O<sub>3</sub> NPs were assessed: 10, 20, 30 and 70 mg L<sup>-1</sup>.

## 2.2 Microalgae and culture media

The microalgae used for inoculation of the photobioreactors (PBRs) was a *Chlorella vulgaris* strain which was kindly donated by the UAM. An inoculum was grown in SK medium enriched with peptone, glucose and yeast extract according to (Vargas-Estrada et al., 2023). The PBRs were inoculated with 200 mg L<sup>-1</sup> of *C. vulgaris* in wastewater which was obtained from the WWTP of the Institute of Renewable Energies, Temixco, Mexico. The PBRs were let to stabilize for 30 days before the experimentation began. After the stabilization period, a change in the composition of the biomass was observed, and the microorganisms dominating the culture was the cyanobacteria *Leptolyngbya foveolarum*, followed by the microalgae *Scenedesmus obtusus* and *Desmodesmus abundans*.

## 2.3 Experimental set-up

The experiments were carried out under environmental conditions at the outdoors of the Hydrogen Laboratory, of the Institute of Renewable Energies in Temixco, Mexico using two closed tubular photobioreactors (PBR) of 15 cm of diameter, 50 cm of height and a working volume of 7 L (**Fig. 15**). The PBRs were daily fed with 1 L of wastewater by means of peristaltic pumps to have a hydraulic retention time of 7 days. Additionally, air was pumped to provide CO<sub>2</sub> and to prevent culture



sedimentation. The output liquor was collected in a settler and weekly harvested. One PBR was used as a control (PBR-Control) and was only fed with wastewater while the other PBR was used to elucidate the effect of the  $\text{Fe}_2\text{O}_3$  NPs (PBR-NPs) on the microalgae culture.

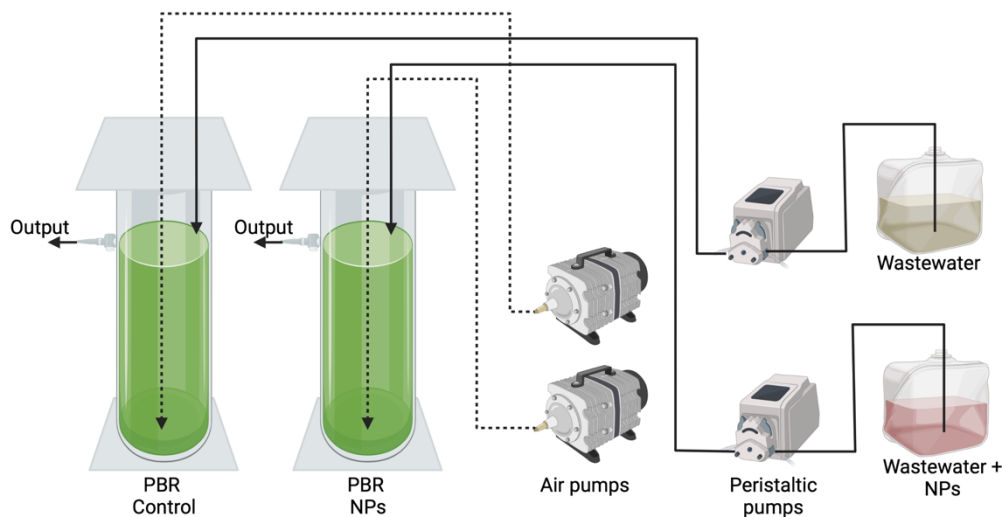


**Fig. 15.** Schematic diagram of the experimental set up. Dotted lines represent air flow, continuous lines represent liquid flow.

## 2.4 Sampling procedures and operational conditions

The PBRs were initially operated for 30 days to acclimate and stabilize the microalgae-cyanobacteria culture. Subsequently, stage I (days 0-10) was intended as a control condition to discharge differences in biomass growth and PBR performance. Then, in stage II (days 11-50)  $\text{Fe}_2\text{O}_3$  NPs were added to the PBR-NPs to reach a final concentration of  $10 \text{ mg L}^{-1}$ , afterwards the NPs were daily fed through the fed wastewater. In stage III (days 51- 81) the concentration of NPs was increased to  $20 \text{ mg L}^{-1}$  in both the PBR-NPs and the fed wastewater. In stage IV (days 82-120)

the concentration in the PBR-NPs and in the fed wastewater was increased up to 30 mg L<sup>-1</sup>. Finally, in stage V (days 121-150) the concentration was increased to 70 mg L<sup>-1</sup> in the PBR-NPs and in the fed wastewater.

The pH of the PBRs were daily measured in the morning while the temperature of the PBRs was daily measured twice day (morning and afternoon), PAR was measured (Field Scout TM 3415FXSE) twice a day as well. Twice a week, aliquots of 100 mL of the PBRs broth and wastewater were taken to measure the concentration of N-NH<sub>4</sub><sup>+</sup>, N-NO<sub>2</sub><sup>-</sup>, N-NO<sub>3</sub><sup>-</sup>, P-PO<sub>4</sub><sup>3-</sup>, total suspended solids (TSS) and volatile suspended solids (VSS).

The collected biomass in the settler was harvested, frozen at -30 °C (Equitec) and finally freeze-dried (-110 °C, 0.049 hPa) (Labconco, USA) for its subsequently characterization.

## 2.5 Analytical procedures

The pH was measured with a Orion Star A211 sensor (ThermoFisher Scientific, US), the temperature was measured with a submersible thermometer (4339, Control Company). N-NH<sub>4</sub><sup>+</sup> was measured according to (Solórzano, 1969), N-NO<sub>3</sub><sup>-</sup> were measured by the cadmium reduction method (method 8171MR, HACH), N-NO<sub>2</sub><sup>-</sup> were measured by the diazotization method (method 8507, HACH), P-PO<sub>4</sub><sup>3-</sup> was measured by the phospho-vanadium-molybdate method according to standard methods (APHA-AWWA-WPCF, 1999) and TSS and VSS were determined according to standard methods (APHA-AWWA-WPCF, 1999). The harvested biomass was characterized in terms of carbohydrates and lipid content according to (Vargas-

Estrada, Longoria, Okoye, et al., 2021). Finally, the identification of the microalgae cultures was carried out by microscopic examination in a Nikon E600 microscope (Japan), with differential interference contrast, photographs were taken with a Nikon DXM1200 digital camera.

## **2.6 Statistical analysis**

The results were analyzed by ANOVA followed by Tuckey's test considering  $\alpha=0.05$  to determine the effect of the NPs on microalgae growth and biomass composition.

## **3. Results and discussions**

### **3.1 Nanoparticles characterization**

The Fe<sub>2</sub>O<sub>3</sub> NPs exhibited a particle size of 25 nm and nanorod morphology (**Fig. 16**), this particular morphology exhibits a high specific surface area, and better electrochemical and magnetic properties compared to other Fe<sub>2</sub>O<sub>3</sub> morphologies (Bazrafshan et al., 2017; Powell et al., 2021; Rao et al., 2015). The chemical composition of these particular NPs was O: 59%, Fe: 37.40% and Na: 3.44% (in atomic percentage). The presence of Na in the NPs is due to trace levels of the catalyst used for their synthesis.

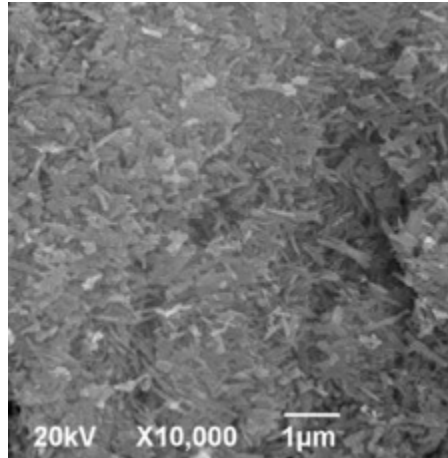


**Fig. 16.** SEM micrograph of the Fe<sub>2</sub>O<sub>3</sub> nanoparticles.

### 3.2 Microalgae growth

After 150 days of cultivation, the composition of the microalgae changed in each PBR. At the beginning of the study, in both PBRs there was an abundant growth of *Leptolyngbya foveolarum* that formed clusters on which other Cyanoprokaryota (such as *Gloeocapsa atrata*) and isolated coenobium of *Scenedesmus obtusus* and *Desmodesmus abundans* were incorporated, additionally in PBR-NPs there was also a tenuous growth of *Stigeoclonium tenue*. At the end of the study, PBR-Control culture was composed by *Scenedesmus obtusus*, *Merismopedia punctata*, *Desmodesmus abundans*, *Closteriopsis acicularis*, *Phormidium aerugineo-coeruleum*, *Leptolyngbya foveolarum*, *Choricysits parasítica*, *Pectinodesmus javanensis* and ciliates. On the other hand, the species observed in PBR-NPs were *Scenedesmus obtusus*, *Desmodesmus abundans*, *Merismopedia punctata*, *Closteriopsis acicularis* and ciliates. Interestingly, in PBR-NPs the presence of *Leptolyngbya foveolarum* was not observed. The latter is mainly attributed to the fact that the Fe<sub>2</sub>O<sub>3</sub> NPs formed agglomerates and were deposited in the filamentous

species (**Fig. 17**). The agglomeration of NPs has been previously reported as one of the major factors that inhibits microalgae growth (Vargas-Estrada et al., 2020), moreover the agglomeration of NPs comes along with the shading effect that has also been established as one of the factors affecting microalgae growth (Cheloni et al., 2016). Additionally, Demir et al. (2015) previously reported that  $\text{Fe}_2\text{O}_3$  NPs caused the flocculation and growth depletion of *Nannochloropsis* sp. Similarly, Chen et al. (2018) reported a similar behavior with Co NPs and *Skeletonema costatum*. In this regard, the absence of *L. foveolarum* is in agreement with the previous reported studies suggesting that the interaction of the  $\text{Fe}_2\text{O}_3$  NPs and the culture was a physical effect rather than a cell or DNA damage.

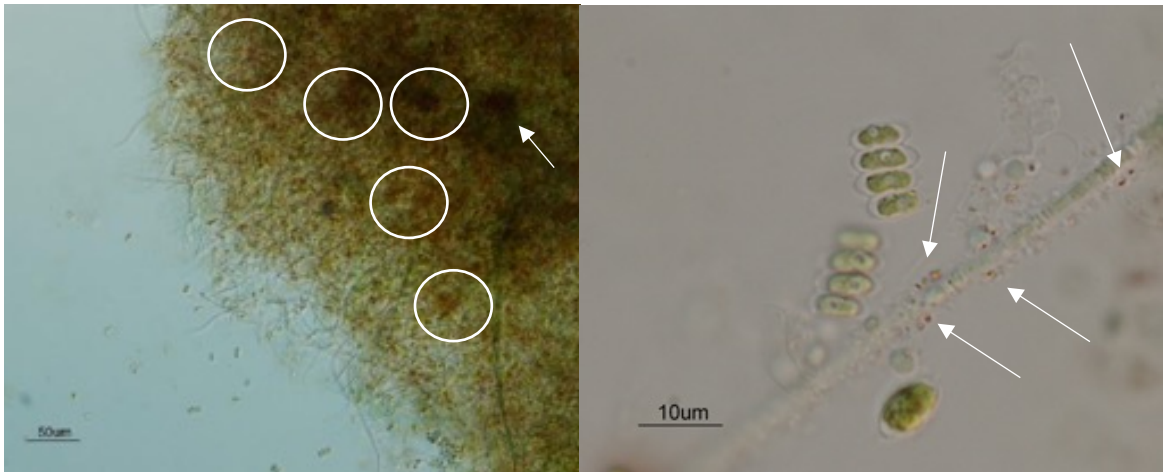


**Fig. 17.**  $\text{Fe}_2\text{O}_3$  nanoparticles deposited in the filamentous species contained in PBR-NPs. The circles and arrows indicate the presence of  $\text{Fe}_2\text{O}_3$  nanoparticles.

The mean biomass concentration during stage I did not present significant changes and was  $0.42 \pm 0.14$  and  $0.46 \pm 0.15$  for PBR-Control and PBR-NPs respectively (**Fig. 18**). Moreover, stage II presented the same behavior and did not

present a significant difference and was  $0.56 \pm 0.28$  and  $0.51 \pm 0.25$  for PBR-Control and PBR-NPs respectively.

On the other hand, the biomass production in PBR-NPs was significantly reduced, compared to the PBR-Control, by 36% and 18% during stage III and IV respectively, which corresponds to the concentrations of 20 and 30 mg L<sup>-1</sup> of Fe<sub>2</sub>O<sub>3</sub> NPs respectively. Even if the biomass production during these two stages was significantly lower than the recorded in the control, in stage IV the biomass concentration in PBR-NPs presented the maximum value recorded (1.21 g L<sup>-1</sup>). The later could be attributed to the fact that the Fe<sub>2</sub>O<sub>3</sub> NPs were deposited to *L. foveolarum*, causing biomass sedimentation and cell death however, since most part of the NPs were attached to *L. foveolarum*, the culture media presented a lower concentration of suspended Fe<sub>2</sub>O<sub>3</sub> NPs, which did not inhibit the growth of the other microalgae species. Whether this theory is truth, the fact is that in stage IV the biomass concentration in PBR-NPs manage to recover either by the acclimatation of the microalgae to the NPs, the sedimentation of the *L. foveolarum* + Fe<sub>2</sub>O<sub>3</sub> NPs flocs, or by the environmental conditions that could have stimulated the microalgae growth. The later can be confirmed by the fact that the PBR-Control presented the same growth tendency, and whereas one PBR contained NPs and the other did not, both PBRs presented the same growth tendency.

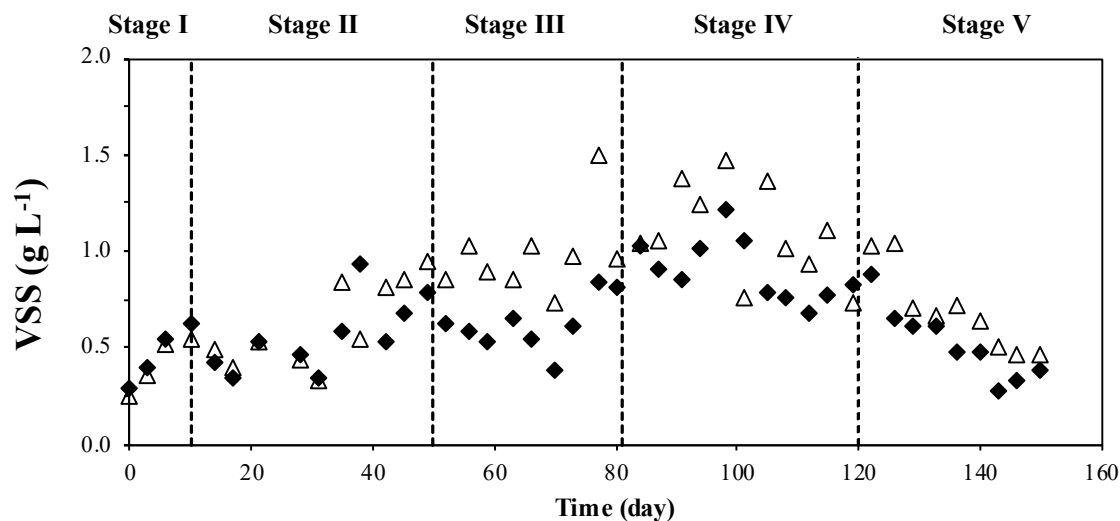


**Fig. 18.** Time course of biomass production in PBR-Control (empty triangles) and PBR-NPs (dark diamonds).

### 3.3 Nutrient uptake and PBRs performance

The environmental parameters of both PBRs are presented in **Table 9**. The pH of both PBRs did not present a significant change during the experiment, and remind above 8.5 for 150 days. Concomitantly, the temperature in the PBRs decreased as the time passed. This is mainly attributed to the environmental conditions, since the ambient temperature was, in average,  $35.4 \pm 0.9$  °C in stage I, and by stage V the ambient temperature decreased to  $27.3 \pm 0.9$  °C. The same behavior was observed in the morning PAR. In this regard, the decreased in both temperature and PAR could explain the fact that by stage V the biomass concentration in both PBRs decreased.

**Table 9.** Environmental parameters of the PBRs during the experiment

Stage	PBR	Temperature (°C)		PAR ( $\mu\text{mol m}^{-2}\text{s}^{-1}$ )		pH
		Morning	Afternoon	Morning	Afternoon	
<b>I</b>	<i>Control</i>	24.2 ± 2.3	35.1 ± 0.3	115.4 ± 42.7	286.3 ± 159.1	8.9 ± 0.4
	<i>NPs</i>	24.4 ± 2.1	35.1 ± 0.3	110.7 ± 42.3	280.2 ± 146.1	9.0 ± 0.5
<b>II</b>	<i>Control</i>	27.7 ± 2.1	32.1 ± 2.3	78.8 ± 20.2	178.5 ± 59.4	8.9 ± 0.4
	<i>NPs</i>	22.7 ± 2.1	32.4 ± 2.6	75.1 ± 21.4	177.6 ± 162.9	8.8 ± 0.4
<b>III</b>	<i>Control</i>	21.7 ± 1.7	28.9 ± 1.3	61.3 ± 20.4	168.1 ± 43.5	8.8 ± 0.4
	<i>NPs</i>	21.7 ± 1.5	28.9 ± 1.3	59.9 ± 18.8	165.4 ± 42.2	8.5 ± 0.3
<b>IV</b>	<i>Control</i>	21.1 ± 1.3	28.0 ± 1.6	57.9 ± 13.4	187.7 ± 97.5	8.7 ± 0.5
	<i>NPs</i>	21.1 ± 1.4	29.1 ± 1.2	57.9 ± 13.5	186.8 ± 96.0	8.8 ± 0.6
<b>V</b>	<i>Control</i>	21.2 ± 1.0	27.5 ± 1.5	67.2 ± 27.3	226.8 ± 289.6	9.3 ± 0.9
	<i>NPs</i>	21.2 ± 1.0	27.5 ± 1.4	67.4 ± 27.6	237.2 ± 334.1	9.2 ± 0.7

$\text{PO}_4^{3-}$  concentration in the wastewater decreased during stage II and remained stable until by the beginning of stage V (**Fig. 19a**). This can be explained by the constant changes in the population and activities in the Institute. On the other hand the  $\text{PO}_4^{3-}$  in the PBRs gradually decreased during stage II, and remain  $\leq 2 \text{ mg L}^{-1}$  and no significant differences in the P- $\text{PO}_4^{3-}$  concentrations of both PBRs were observed during the study.

N- $\text{NH}_4^+$  concentration in wastewater ranged  $\approx 10$  to  $50 \text{ mg L}^{-1}$  (**Fig. 19b**). Even if the concentrations of N- $\text{NH}_4^+$  in the wastewater remained low compared to



those previously reported by Vargas-Estrada et al. (2021) it is in the range of the amount of  $\text{N-NH}_4^+$  uptake of some microalgae species ( $42 - 49 \text{ mg L}^{-1}$ ) (Cheng et al., 2019). On the other hand, the  $\text{N-NH}_4^+$  concentrations in the PBRs remained almost negligible since the middle of stage II and until the end of the study. The later suggest that the addition of  $\text{Fe}_2\text{O}_3$  NPs did not influence the nutrient uptake of PBR-NPs, contrary to the previously reported by Xia et al. (2021) who observed that the addition of  $\text{Fe}_2\text{O}_3$  NPs influenced the  $\text{N-NH}_4^+$  uptake by *Chlorella vulgaris*.

$\text{N-NO}_2^-$  (**Fig. 19d**) concentrations remained almost negligible and in stage IV and V some maximum concentrations were recorded for the wastewater and the PBRs which can be explained by the variations in the wastewater and the denitrification process. The latter is explained by the fact that  $\text{N-NO}_3^-$  (**Fig 19c**) was present in the wastewater, and microalgae in the PBRs could have used it as a source of nitrogen since the  $\text{N-NH}_4^+$  was rapidly consume as a result of their growth (Méndez et al., 2022). Interestingly, the  $\text{N-NO}_3^-$  in PBR-Control was lower than in PBR-NPs, which is related to the lower biomass concentration in the PBRs, confirming the uptake by microalgae. In this regard, the  $\text{N-NO}_2^-$  maximum values during stage IV and V is correlated to the denitrification of  $\text{N-NO}_3^-$ .

In this regard, the  $\text{Fe}_2\text{O}_3$  NPs did not influence negatively the nutrient uptake nor acted as nutrient competitors for microalgae. Thus, it can be said that the slight decrement in the biomass concentration is related to the deposition of the NPs into the filamentous microorganisms.

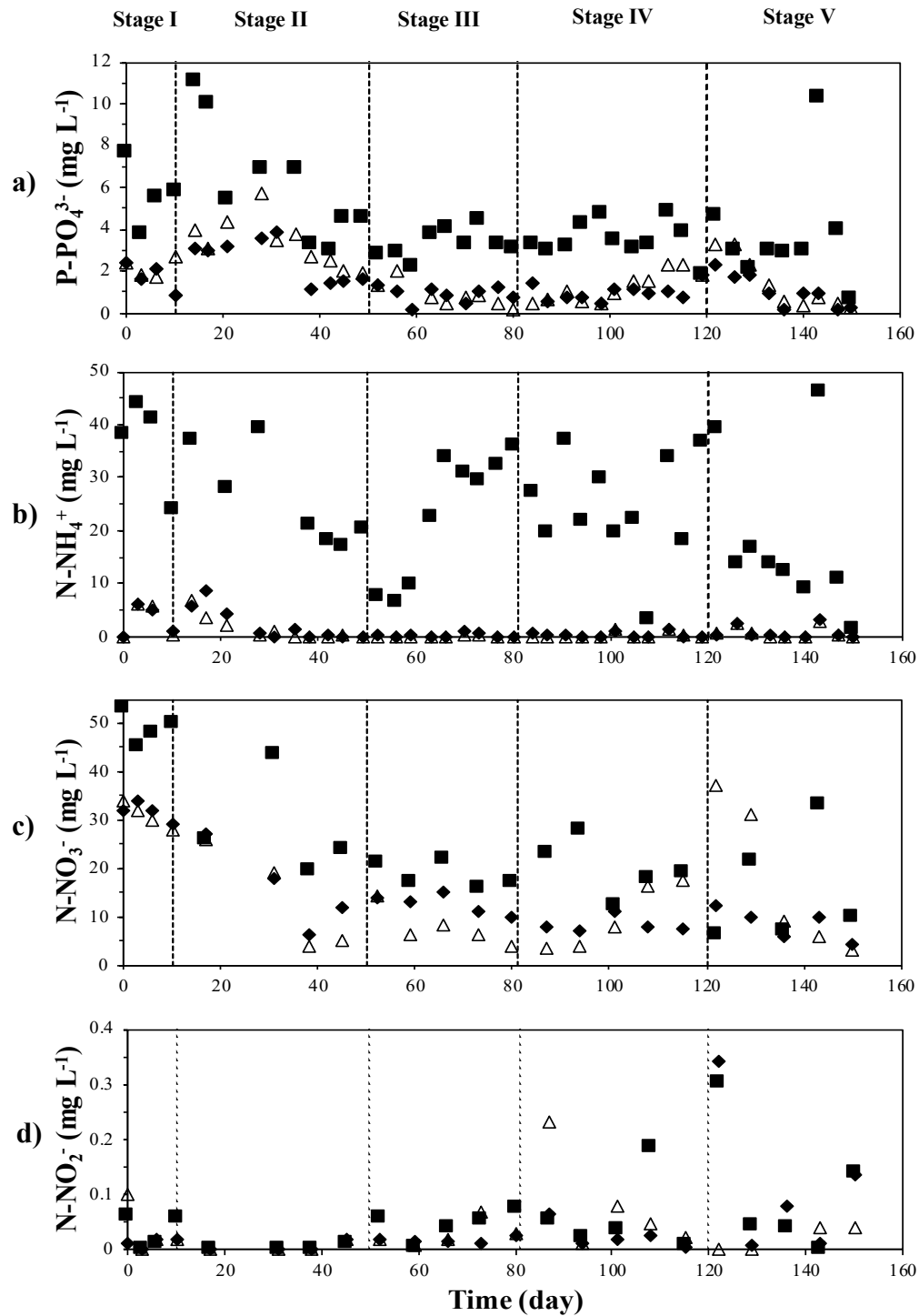


**Fig. 19.** Time course of a) P-PO<sub>4</sub><sup>3-</sup>; b) N-NH<sub>4</sub><sup>+</sup>; N-NO<sub>3</sub><sup>-</sup>; N-NO<sub>2</sub><sup>-</sup> concentrations in the PBR-Control (empty triangles), PBR-NPs (dark diamonds) and wastewater (dark squares)

### 3.4 Biomass composition

The changes in the biomass composition of each PBR is shown in **Fig. 20**. The lipid content on both PBRs remained under 12% (dw) through the study, and is mainly attributed to the strains present in the cultures. It has been widely stated that Fe<sub>2</sub>O<sub>3</sub> NPs can stimulate the lipid content in microalgae mainly by the formation of ROS species (Vargas-Estrada et al., 2020), and even Bibi et al. (2021) previously reported that *C. vulgaris* recorded a lipid enhancement of 39.7 and 25.5 % when 50 and 100 mg L<sup>-1</sup> of Fe<sub>2</sub>O<sub>3</sub> NPs were added to the culture. On the other hand, Vargas-Estrada et al. (2022) and Vargas-Estrada et al. (2022) recently reported that the addition of Fe<sub>2</sub>O<sub>3</sub> to a mixed culture of microalgae-bacteria and to *Chlorella sorokiniana* cultures respectively, did not stimulate the lipid production in both species. The effect of Fe<sub>2</sub>O<sub>3</sub> NPs on microalgae species strongly depends on the concentration, the crystal phase, the time of exposure and the microalgae strain, and at this point is important to mention that at the beginning of stage I, the dominant species in both PBRs was the cyanobacteria *L. foveolarum*. Cyanobacteria are known for their high protein or glycogen and polyhydroxybutyrate and usually nitrogen starvation leads to high concentrations of polyhydroxybutyrate (González-Fernández & Ballesteros, 2012). Interestingly, no significant changes were observed in the carbohydrate content of the PBRs during stages I and II, even if these two stages presented a low N-NH<sub>4</sub><sup>+</sup> and N-NO<sub>2</sub><sup>-</sup> concentrations during these particular stages. However, the N-NO<sub>3</sub><sup>-</sup> concentrations remained ≈ 10 mg L<sup>-1</sup>, and it has been stated elsewhere (Vargas-Estrada, Longoria, Okoye, et al., 2021) that even when NH<sub>4</sub><sup>+</sup> is negligible in the culture media the presence of other nitrogen species stimulate the nitrification/denitrification process. Additionally, the dominant species changed

through the study, which could have directly influenced the macromolecule accumulation. Interestingly, by the middle of stage IV, the carbohydrate content in PBR-NPs significantly increased up to 38%, similar findings were recently reported by Vargas-Estrada et al. (2022) who assessed the influence in a mixed microalgae-bacteria consortium and observed that the addition of Fe<sub>2</sub>O<sub>3</sub> NPs under UV-visible light stimulated the carbohydrates content of the consortium. In this chapter, the increased carbohydrates content can be attributed to the fact that by the end of stage V, the presence of *L. foveolarum* was not observed in PBR-NPs, and the presence of the Fe<sub>2</sub>O<sub>3</sub> NPs could have influenced the metabolism of the present microalgae to produce carbohydrates. However, in stage V the concentration of the Fe<sub>2</sub>O<sub>3</sub> NPs increased to 70 mg L<sup>-1</sup> and the carbohydrate content of the PBR-NPs was significantly reduced. Moreover, during stage V the carbohydrates content in PBR-NPs continued to gradually decreased mainly attributed to the presence of the NPs.

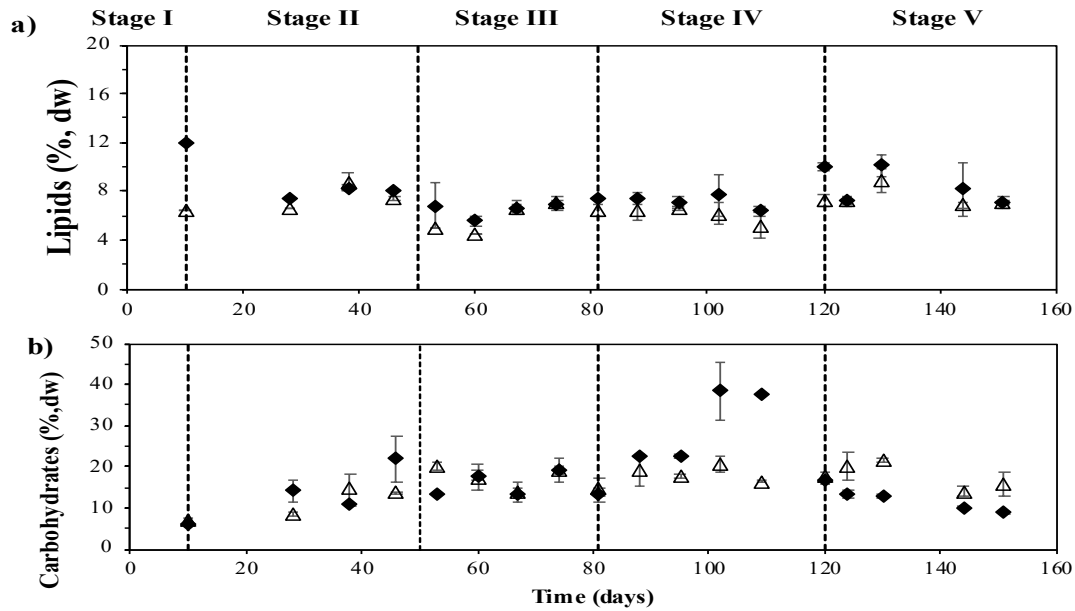


**Fig. 20.** Time course of the a) Lipids and b) carbohydrates content of PBR-Control (empty triangles) and PBR-NPs (dark diamonds).

## 4. Conclusions

The long-term exposure to  $\text{Fe}_2\text{O}_3$  NPs decreased the biomass production when the concentrations in the culture media were 20 and 30  $\text{mg L}^{-1}$ . The biomass concentration was reduced mainly by a physical effect of the NPs on the microalgae-cyanobacteria consortium rather than a chemical or DNA interaction. Additionally, the NPs did not interfere in the nutrient uptake, and the nutrient removals on the wastewater was similar to those recorded in the control. Finally, the NPs did not significantly increase the carbohydrates or lipids content of the microalgae. In this regard, it can be said that the addition up to 70  $\text{mg L}^{-1}$  of  $\text{Fe}_2\text{O}_3$  NPs did not inhibit the microalgae growth, however, the cyanobacteria was completely inhibited in the PBR-NPs mainly by physical interactions.

# Chapter 5

---

## Effect of iron based nanoparticles on *Chlorella sorokiniana* metabolism and biogas upgrading

This chapter is adapted from the publication:

- Vargas-Estrada, L., Hoyos, E. G., Sebastian, P. J., & Muñoz, R. (2023). Influence of mesoporous iron based nanoparticles on *Chlorella sorokiniana* metabolism during photosynthetic biogas upgrading. *Fuel*, 333 doi:10.1016/j.fuel.2022.126362



## 1. Introduction

Photosynthetic biogas upgrading is based on a solar-driven CO<sub>2</sub> fixation by microalgae that has emerged as an attractive, cost-effective and environment friendly option for CO<sub>2</sub> and H<sub>2</sub>S removal from biogas (Ángeles et al., 2021; Rodero, Carvajal, et al., 2020; Rodero et al., 2019). This technology has demonstrated to be feasible in algal-bacterial photobioreactors interconnected to an absorption column (Franco-Morgado et al., 2018; Marín et al., 2020; Meier et al., 2015; Posadas et al., 2015; Rodero, Carvajal, et al., 2020; Toledo-Cervantes et al., 2016; Xu et al., 2015), reaching CO<sub>2</sub> removals up to 98.6% at pilot and demo scale (Rodero, Carvajal, et al., 2020; Rodero, Severi, et al., 2020). However, there are some challenges and limitations that need to be addressed: i) low CO<sub>2</sub> mass transfer to the culture medium, ii) variations in the liquid and gas flow rates, pH and alkalinity, and iii) diurnal and seasonal variability of environmental parameters influencing photosynthetic activity (Bose et al., 2019). Thus, innovative operational strategies are required to enhance CO<sub>2</sub> biofixation during photosynthetic biogas upgrading.

The use of nanoporous materials has recently attracted a renewed attention in the field of CO<sub>2</sub> capture because they exhibit key advantages such as a large surface area to volume ratio, high reactivity, abundant active sites and high adsorption capacity (Kumar et al., 2020). Metal oxide nanoparticles (NPs) and nanoporous carbons rank among the most popular nanomaterials for CO<sub>2</sub> capture (Kumar et al., 2020). Three potential mechanisms have been hypothesized to explain the CO<sub>2</sub> capture enhancement by the addition of NPs: 1) bubble braking effect, where NPs induce a small sized bubble and hence the diffusion area increases; 2) shuttle effect,



where the gas is adsorbed to the NPs surface and then is released into the liquid; 3) hydrodynamic effect, where the NPs collide, inducing turbulence and refreshing the liquid-gas boundary layer (Choi et al., 2015). The mechanism of interaction will depend on operational factors, such as the type of reactor, agitation and the liquid phase (Kluytmans et al., 2003). The shuttle and the hydrodynamic effect have been previously observed in stirred tanks (Alper & Öztürk, 1986; Kluytmans et al., 2003), although the results reported are contradictory, in both cases the mass transfer was increased. Thus, mesoporous NPs of metal oxides and carbon could represent an innovative tool to enhance CO<sub>2</sub> fixation during photosynthetic biogas upgrading.

The addition of metal oxide NPs to microalgae culture is a controversial topic and the majority of the studies are focused on their toxic effect (Liang et al., 2020), and the number of studies assessing the benefits of NPs addition on microalgae metabolism is scarce (He et al., 2017). He et al. (2017) reported that Fe<sub>2</sub>O<sub>3</sub> NPs improved biomass and lipid production up to 39.6% in *Scenedesmus obliquus* at concentrations < 20 mg L<sup>-1</sup>. Jeon et al. (2017) studied the addition of SiO<sub>2</sub> NPs (0.3% wt) to *C. vulgaris* cultures and observed that NPs enhanced the gas-liquid mass transfer rate of CO<sub>2</sub> by 31%, and the biomass cell dry weight was increased from 0.48 g L<sup>-1</sup> (without the NPs) to 1.33 g L<sup>-1</sup> (with the SiO<sub>2</sub> NPs). The addition of 0.3 g L<sup>-1</sup> of polymeric nanofibers containing Fe<sub>2</sub>O<sub>3</sub> NPs enhanced CO<sub>2</sub> fixation up to 310.9 mg L<sup>-1</sup> in *Chlorella fusca* LEB 111 cultures (Vaz et al., 2020). Finally, the addition of 100 mg L<sup>-1</sup> of graphene quantum dots under UV radiation to *Chlorella pyrenoidosa* cultures enhanced its growth and lipid production by 17% and 34% respectively (Yang et al., 2022). The effect of NPs has been studied in microalgae growth and

macromolecular composition but little information is available in literature on the influence of metal oxide NPs and carbon NPs on photosynthetic biogas upgrading and on microalgae composition.

This chapter assessed the influence of three types of iron based NPs on *Chlorella sorokiniana* cultures devoted to biogas upgrading: Fe<sub>2</sub>O<sub>3</sub> and two different carbon-coated zero-valent NPs. This chapter also investigated the effect of these NPs and the type of irradiation (visible *versus* visible+UV) on CO<sub>2</sub> removal kinetics and on the growth kinetics and composition of *C. sorokiniana*.

## **2. Materials and methods**

### **2.1 Nanoparticles and stock solutions**

Carbon coated zero-valent iron (ZVI) (31.38% of Fe, wt.%) NPs were kindly donated by SMALLOPS and carbon coated ZVI (7.26% of Fe, wt.%) NPs were kindly donated by CALPECH. The surface area and morphology, pore volume, average pore diameter and elemental composition of the three NPs was determined. Fresh stock solutions of 200 mg L<sup>-1</sup> of each nanoparticle were prepared in microalgae culture medium and sonicated for one hour to prevent nanoparticle agglomeration in order to facilitate the addition of the NPs.

### **2.2 Microalgae culture and biogas**

The microalgae used in this study was *C. sorokiniana* 211/8k, which was originally purchased from the Culture Centre of Algae and Protozoa (Cambridge, UK). *C.*

*sorokiniana* was stored at 4 °C on sterile agar plates in SK medium enriched with glucose (3.125 g L<sup>-1</sup>), peptone (0.0625 g L<sup>-1</sup>) and yeast extract (0.0625 g L<sup>-1</sup>) according to (Borde et al., 2003; Guieysse et al., 2002). An inoculum of *C. sorokiniana* was grown at 25 °C in enriched SK medium under continuous illumination (900 μE m<sup>-2</sup>s<sup>-1</sup>) and shaken at 300 rpm. When the culture reached the exponential growth, the culture was centrifuged (10000 rpm, 4 °C), washed several times and resuspended in distilled water to reach a final concentration of 24 g L<sup>-1</sup> of total suspended solids (TSS).

To elucidate the effect of nanoparticles on *C. sorokiniana* cultures devoted to biogas upgrading, two different synthetic biogas mixtures were used: Biogas A composed of CO<sub>2</sub> (30%) and CH<sub>4</sub> (70%) (Carbueros Metalicos; Spain), and Biogas B composed of CO<sub>2</sub> (29.5%), H<sub>2</sub>S (0.5%) and CH<sub>4</sub> (70%) (Abello Linde; Spain).

### **2.3 Experimental set-up**

Batch assays were conducted in 1.2 L gas tight glass bottles to evaluate the effect of the three types of nanoparticles (Fe<sub>2</sub>O<sub>3</sub>, CALLPECH NPs, SMALLOPS NPs) at different concentrations (0, 20, 40 and 70 mg L<sup>-1</sup>) and under different light sources (visible *versus* visible + UV) on biogas upgrading by *C. sorokiniana*. The bottles were prepared containing 1 L of the corresponding synthetic biogas in the headspace and 0.2 L of mineral salt medium rich in carbonates as described elsewhere (Marín et al., 2020) and the corresponding NP concentration. The mineral medium and the corresponding nanoparticle concentration were added to the bottles, which were then closed with butyl septa and plastic caps. The bottles were initially flushed with

helium for 5 min and subsequently the corresponding synthetic biogas was flushed for 5 min using inlet and outlet needles to replace the helium headspace. After one hour of stabilization (300 rpm, 25 °C), the bottles were inoculated with *C. sorokiniana* at an initial concentration of 200 mg L<sup>-1</sup> of TSS, and immediately, the gas composition of the headspace was determined by gas chromatography-thermal conductivity detection (GC-TCD). Then, the bottles were incubated at 25 °C under continuous magnetic stirring (300 rpm) to prevent microalgae sedimentation. Light intensity of 900 μE m<sup>-2</sup>s<sup>-1</sup> was continuously provided by visible LED lights (PHILLIPS, Spain).

In the test series I, four operational conditions were evaluated for each nanoparticle: 1) *C. sorokiniana* biomass and synthetic biogas A; 2) *C. sorokiniana* biomass with 10 mg L<sup>-1</sup> of nanoparticles and biogas A; 3) *C. sorokiniana* and synthetic biogas B; 4) *C. sorokiniana* biomass with 10 mg L<sup>-1</sup> of nanoparticles and biogas B. Each condition was run in triplicate. In test series II, the influence of different NPs concentrations (20 mg L<sup>-1</sup>, 40 mg L<sup>-1</sup>, and 70 mg L<sup>-1</sup>) was assessed under biogas A headspace, 25 °C, magnetic stirring (300 rpm) and visible light 900 μE m<sup>-2</sup>s<sup>-1</sup>. A control containing only *C. sorokiniana* and biogas A was conducted. Each condition was run in triplicate. Finally, in test series III, the influence of different NPs concentrations (20 mg L<sup>-1</sup>, 40 mg L<sup>-1</sup>, and 70 mg L<sup>-1</sup>) was assessed under biogas A headspace, 25 °C, magnetic stirring (300 rpm) and visible light (900 μE m<sup>-2</sup>s<sup>-1</sup>) + UV light (λ 315-350 nm, 10 W m<sup>-2</sup>). A control containing only *C. sorokiniana* biomass and biogas A was conducted. Each condition was run in triplicate.

## 2.4 Analytical procedures

Microalgae Biomass productivity (Px) was calculated according to Eq. (11):

$$Px = \frac{DW_1 - DW_0}{t_1 - t_0} \quad (11)$$

where Px is biomass productivity (g L<sup>-1</sup> d<sup>-1</sup>),  $DW_1$  and  $DW_0$  are the biomass dry weight (g L<sup>-1</sup>) at time  $t_1$  and  $t_0$  (d).

The biogas composition in the headspace of the bottles (CH<sub>4</sub>, CO<sub>2</sub>, H<sub>2</sub>S and O<sub>2</sub>) was determined two times per day by GC-TCD (Bruker) according to (Posadas et al., 2015). pH was determined at the beginning and at the end of the experiment (SensION™ + PH3 pHmeter, HACH, Spain). The dissolved IC concentrations were determined at the beginning and at the end of the experiments using a Shimadzu TOC-VCSH analyzer (Japan) equipped with a TNM-1 chemiluminescence module. Microalgae growth was determined daily by optical density at 750 nm (OD<sub>750</sub>) using a Shimadzu spectrophotometer (Japan). TSS concentrations were determined according to standard methods (APHA-AWWA-WPCF, 1999). The biomass obtained from test series II and III was harvested (10000 rpm, 4 °C) and freeze-dried for further macromolecular characterization. The carbohydrate content was determined according to (Dubois et al., 1956), while the lipid content was determined gravimetrically following biomass extraction with chloroform: methanol (2:1 v v<sup>-1</sup>) as described elsewhere (Ángeles et al., 2020). Physisorption analysis was conducted in an ASAP 2050 (Micromeritics, USA) at 77 K using nitrogen. Scanning electron microscopy (SEM) (JEOL JSM-6490LV) and energy-dispersive spectroscopy (EDS)

(EDX-700/800, Hitachi, Japan) were carried out to determine the surface morphology and elemental composition of the target NPs.

## 2.5 Statistical analysis

The results are presented as mean values  $\pm$  standard deviation. An analysis of variance (ANOVA) followed by Tuckey's test considering  $\alpha=0.05$  was performed to assess the influence of NPs on microalgae metabolism.

## 3. Results and discussion

### 3.1 Characterization of nanoparticles

SEM micrographs show the morphology of the NPs herein used (**Fig. 21**). The  $\text{Fe}_2\text{O}_3$  NPs exhibited a particle size of 25 nm and nanorod morphology, which has been previously reported to exhibit a high specific surface area, and better electrochemical and magnetic properties compared to other  $\text{Fe}_2\text{O}_3$  morphologies (Bazrafshan et al., 2017; Powell et al., 2021; Rao et al., 2015). The CALPECH NPs presented particle size ranging from 50-70 nm and were agglomerated, which is in accordance to (Correcher et al., 2021; Munoz et al., 2021). Finally, the SMALLOPS NPs exhibited the highest particle size (150 nm) and were also agglomerated. The EDS analysis showed the presence of elements such as Na, in  $\text{Fe}_2\text{O}_3$  NPs (**Fig A1**), and P, K, Ca and S in CALPECH and SMALLOPS NPs (**Fig. A2 and A3**, respectively), which could play a key role to stimulate microalgae growth. Additionally, the EDS analysis revealed a Fe content of 7.26% (wt. %) in CALPECH NPs, whereas a Fe content of 31.38 (wt. %) was recorded in SMALLOPS NPs. At this point, it is important to

highlight that the difference in Fe content between the CALPECH and SMALLOPS NPs could influence differently *C. sorokiniana* growth and metabolism.

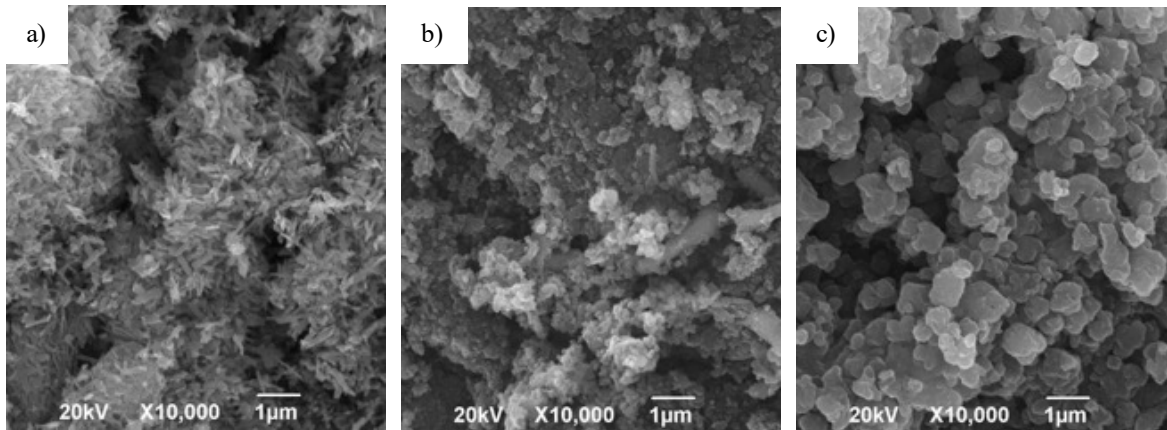


**Fig. 21.** SEM micrographs of a) Fe<sub>2</sub>O<sub>3</sub>, b) CALPECH and c) SMALLOPS nanoparticles.

The BET surface area is a typical parameter for the selection of adsorbents, and the higher the surface area, the better the adsorbent capacity (Zhang et al., 2022). The BET surface areas of the NPs herein used were 32.07, 27.26 and 5.45 m<sup>2</sup>g<sup>-1</sup> for Fe<sub>2</sub>O<sub>3</sub>, CALPECH and SMALLOPS respectively, suggesting that Fe<sub>2</sub>O<sub>3</sub> and CALPECH NPs could act as better gas adsorbents than SMALLOPS NPs. The lowest surface area of the SMALLOPS NPs can be attributed to the higher particle size, and the agglomeration of the NPs due to Van Der Waals forces (Raja et al., 2015). Additionally, the pore volume of a material has been more strongly correlated to its adsorption capacity (Zhang et al., 2022). In this particular study, the pore volume of the NPs used was 0.38, 0.28 and 0.03 cm<sup>3</sup>g<sup>-1</sup> for Fe<sub>2</sub>O<sub>3</sub>, CALPECH and SMALLOPS NPs, respectively. Thus, the latter also suggested that Fe<sub>2</sub>O<sub>3</sub> NPs can act as better

adsorbents than CALPECH and SMALLOPS NPS. Finally, the pore diameter of Fe<sub>2</sub>O<sub>3</sub>, CALPECH and SMALLOPS NPs was 47.46, 41.47 and 27.45 nm, respectively. According to the IUPAC classification, the three NPs herein used represented mesoporous materials. Fe<sub>2</sub>O<sub>3</sub> and mesoporous carbon materials are known for their CO<sub>2</sub> adsorption capacities (Hakim, Marliza, Abu Tahari, Yusop, et al., 2016; Li et al., 2021). The properties observed in the materials herein used suggest that Fe<sub>2</sub>O<sub>3</sub> NPs closely followed by CALPECH NPs could positively impact CO<sub>2</sub> adsorption, thus resulting in an increased *C. sorokiniana* growth rate due to a higher CO<sub>2</sub> availability. However, the nature of the NPs could play an important role on microalgae metabolism.

### **3.2 Influence of biogas composition on *C. sorokiniana* growth and CO<sub>2</sub> removal**

The cumulative CO<sub>2</sub> consumption and cumulative O<sub>2</sub> production in the headspace of the bottles and the cumulative OD<sub>750</sub> served as indicators of *C. sorokiniana* growth (**Fig. 22**). *C. sorokiniana* growth was inhibited in all the assays containing biogas B in the headspace. Indeed, the presence of sulfur oxidizing bacteria is necessary to create a symbiosis with microalgae and prevent H<sub>2</sub>S toxicity, since sulfur oxidizing bacteria utilize the O<sub>2</sub> produced by microalgae to oxidize the H<sub>2</sub>S contained in biogas into SO<sub>4</sub><sup>2-</sup> (Franco-Morgado et al., 2018; Posadas et al., 2016). It has been stated elsewhere (Meier et al., 2018) that the high dissolved oxygen concentrations achieved in algal cultures can mediate the oxidation of H<sub>2</sub>S. In the present study, the



low *C. sorokiniana* concentrations could not release enough oxygen to oxidize the H<sub>2</sub>S contained in biogas B, resulting in biomass inhibition.

On the other hand, biogas A did not inhibit the growth of *C. sorokiniana*. The addition of Fe<sub>2</sub>O<sub>3</sub>, CALPECH and SMALLOPS NPs did not support an enhancement in the cumulative CO<sub>2</sub> consumption likely due to the low NPs concentration tested. Interestingly, the addition of Fe<sub>2</sub>O<sub>3</sub> and CALPECH NPs induced a slightly higher cumulative O<sub>2</sub> production of 7 ( $p = 0.007$ ) and 5% ( $p = 0.016$ ), respectively (**Fig. 22d** and **22e**), confirming that these NPs positively influenced *C. sorokiniana* growth. The OD<sub>750</sub> of the culture broths containing Fe<sub>2</sub>O<sub>3</sub> increased by 33% (**Fig. 22g**), whereas the assays containing CALPECH NPs experienced an increase in OD<sub>750</sub> during the exponential phase (**Fig. 22h**). Lei and collaborators (2016a) investigated the effect of iron NPs on green algae and observed that Fe oxidation state played an important role on microalgae growth and growth inhibition decreased with the oxidation of NPs. Vaz and collaborators (2020) demonstrated that the addition of polymeric nanofibers containing Fe<sub>2</sub>O<sub>3</sub> NPs improved CO<sub>2</sub> biofixation of *Chlorella fusca*. In the present study, the enhancement in O<sub>2</sub> production and cumulative OD<sub>750</sub> induced by the addition of Fe<sub>2</sub>O<sub>3</sub> NPs can be attributed to the fact that the NPs stimulated the growth of *C. sorokiniana*, since iron is one essential micronutrient for microalgae growth and acts as a cofactor in the electron transport system (Rana & Prajapati, 2021). CALPECH and SMALLOPS NPs contained ZVI, whose addition to microalgae cultures induce contradictory effect in different microalgae species (*i.e.* *Chlorella pyrenoidosa* and *Desmodesmus subspicatus*) (Lei et al., 2016a; Pádrová et al., 2015). In this chapter, the addition of

CALPECH NPs mediated a significant increment in O<sub>2</sub> production of 5.80% ( $p = 0.016$ ), and both O<sub>2</sub> production and OD<sub>750</sub> were significantly enhanced ( $p = 0.029$ ), during the exponential growth phase. The addition of SMALLOPS NPs did not induce an enhancement in O<sub>2</sub> production or in OD<sub>750</sub> (**Fig. 22f** and **22i**). The results herein obtained suggest that the ZVI content in the NPs can play a key role in microalgae growth, and the higher Fe content in SMALLOPS NPs could have interfered *C. sorokiniana* growth.

Biomass productivity (Px) was significantly enhanced ( $p = 0.012$ ) when CALPECH NPs were added (**Table 10**). Significant increases in the pH of the culture broths were recorded in the assays containing CALPECH ( $p = 0.002$ ) and Fe<sub>2</sub>O<sub>3</sub> ( $p = 0.037$ ) NPs (**Table 10**). These results were in agreement with those of Pádrová and coworkers (2015), who observed that low concentrations of ZVI NPs, ranging between 1.70 and 5.10 mg L<sup>-1</sup>, stimulated the growth of *Desmodesmus subspicatus*, *Dunaliella salina*, *Parachlorella kessleri*, *Raphidocelis subcapitata*, *Nannochloropsis limnetica*, *Trachydiscus minutus* and *Arthrospira maxima*. The results herein obtained suggest that iron NPs influenced microalgal assimilation of CO<sub>2</sub>.

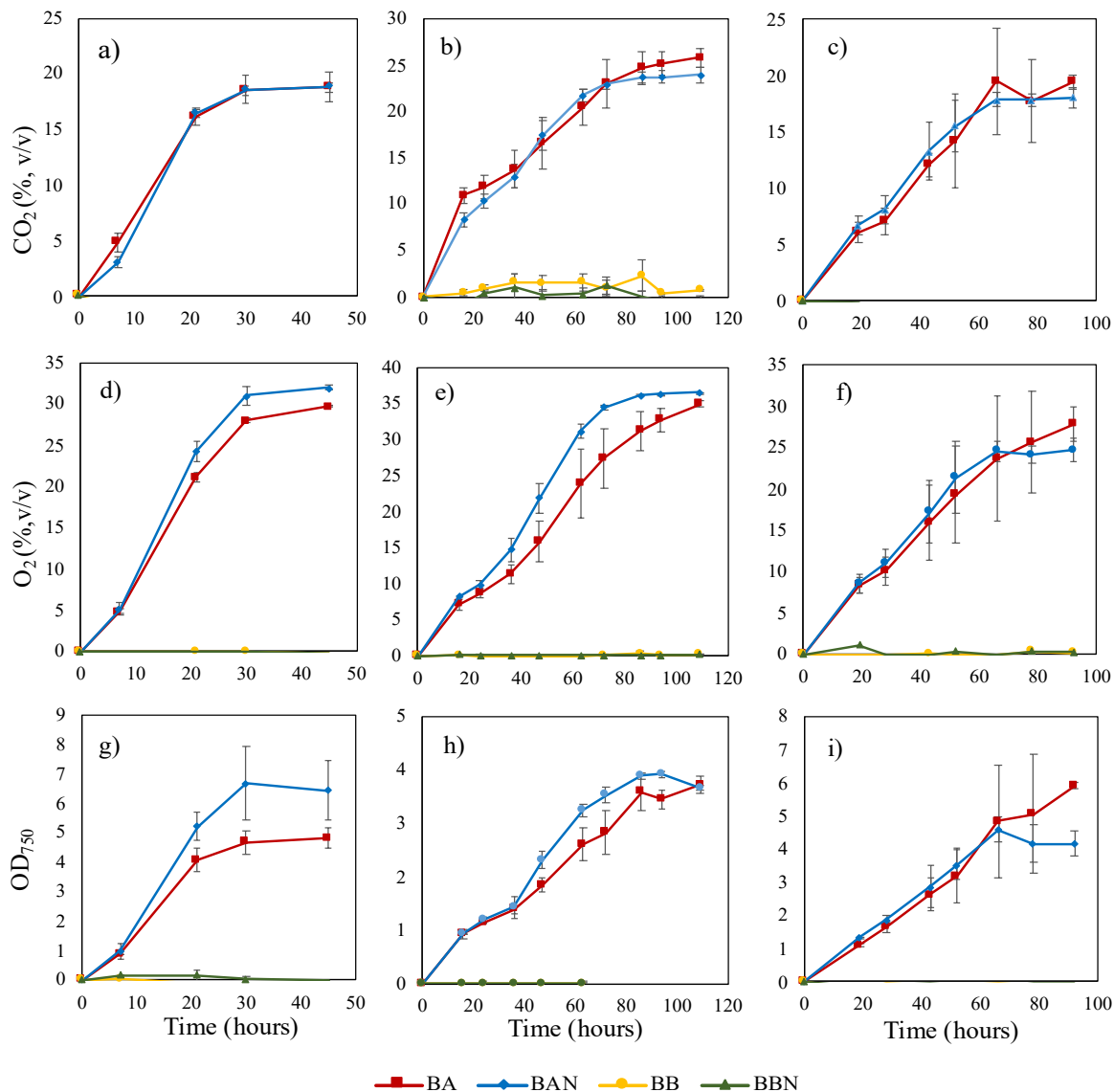


**Fig. 22.** Time course of the cumulative CO<sub>2</sub> consumption in the assays with 10 mg L<sup>-1</sup> of a) Fe<sub>2</sub>O<sub>3</sub> NPs, b) CALPECH NPs, c) SMALLOPS NPs; of the cumulative O<sub>2</sub> production in the assays with 10 mg L<sup>-1</sup> of d) Fe<sub>2</sub>O<sub>3</sub> NPs, e) CALPECH NPs, f) SMALLOPS NPs; and of culture absorbance (OD<sub>750</sub>) in the assays with 10 mg L<sup>-1</sup> of g) Fe<sub>2</sub>O<sub>3</sub> NPs, h) CALPECH NPs, i) SMALLOPS NPs. NPs refers to the addition of nanoparticles; BA (squares) refers to the assays with biogas A; BAN (diamonds) refers to assays with biogas A and NPs; BB (circles) refers to the assays with biogas B; and BBN (triangles) refers to the assays with biogas B and NPs.

**Table 10.** Biomass productivity and initial and final IC concentration in the *Chlorella sorokiniana* assays supplemented with 10 mg L<sup>-1</sup> of the different NPs.

	<i>Fe<sub>2</sub>O<sub>3</sub></i>		<i>CALPECH</i>		<i>SMALLOPS</i>	
	<i>Control</i>	<i>10 mg L<sup>-1</sup></i>	<i>Control</i>	<i>10 mg L<sup>-1</sup></i>	<i>Control</i>	<i>10 mg L<sup>-1</sup></i>
<b><i>Px (g L<sup>-1</sup>d<sup>-1</sup>)</i></b>	0.56±0.07	0.79±0.16	0.35±0.08	0.59±0.05	0.97±0.12	0.76±0.04
<b><i>IC<sub>inicial</sub> (mg L<sup>-1</sup>)</i></b>	1417±29	1426±46	1468±6	1486±23	1497±9	1453±16
<b><i>IC<sub>final</sub> (mg L<sup>-1</sup>)</i></b>	1108±18	1036±81	1203±14	1144±46	793±12	819±22
<b><i>pH<sub>inicial</sub></i></b>	7.86±0.07	7.81±0.05	8.01±0.84	7.84±0.06	7.78±0.02	7.75±0.01
<b><i>pH<sub>final</sub></i></b>	9.00±0.08	9.26±0.13	8.93±0.02	9.06±0.03	8.79±0.10	8.56±0.12

### 3.3 Influence of nanoparticle concentration on *C. sorokiniana* growth and CO<sub>2</sub> removal under visible light

The addition of 40 and 70 mg L<sup>-1</sup> of Fe<sub>2</sub>O<sub>3</sub> NPs resulted in a significantly increased cumulative CO<sub>2</sub> consumption by 10% and 26%, respectively ( $p = 0.00001$ ) (**Fig. 23a**). The cumulative O<sub>2</sub> production (**Fig. 23d**) and the OD<sub>750</sub> (**Fig. 23g**) in the assay with 70 mg Fe<sub>2</sub>O<sub>3</sub> L<sup>-1</sup> were 19% and 35% higher than the control. No significant difference was observed in Px ( $p = 0.143$ ) (**Table 11**) or in IC ( $p = 0.847$ ) concentration and pH ( $p = 0.079$ ) (**Table A1, A2**) among the assays. These results disagreed with the observations of Rana and coworkers (2020), who reported that the addition of Fe<sub>2</sub>O<sub>3</sub> NPs resulted in growth inhibition of *C. sorokiniana* even at low concentrations (2 mg L<sup>-1</sup>). The results herein obtained suggest that the toxicity of

NPs in microalgae are not only species specific, but also the morphology and characteristics of the NPs can play a key role on microalgae growth (Lei et al., 2016a). The special morphology of the Fe<sub>2</sub>O<sub>3</sub> NPs herein used neither inhibited microalgae growth nor delayed the exponential phase. On the contrary, the cumulative O<sub>2</sub> production increased at increasing NPs concentrations. This study confirmed that Fe<sub>2</sub>O<sub>3</sub> NPs acted as CO<sub>2</sub> adsorbents and the higher CO<sub>2</sub> consumption in the 70 mg L<sup>-1</sup> assays can be explained by the fact that CO<sub>2</sub> was adsorbed to the NP surface and more readily available for *C. sorokiniana* consumption. The addition of 70 mg L<sup>-1</sup> of Fe<sub>2</sub>O<sub>3</sub> increased the carbohydrate content of *C. sorokiniana* by 47% compared to the control (10%, dw) (**Fig. 24a**). The lipid content of *C. sorokiniana* decreased regardless of the concentration of NPs added. The latter suggest that the stress conditions caused by the addition of Fe<sub>2</sub>O<sub>3</sub> induced lipid oxidation by reactive oxygen species (ROS) and the accumulation of carbohydrates as a protective response. These results were in agreement with Marchello and coworkers (2018) who observed that the exposure of *C. sorokiniana* to TiO<sub>2</sub> NPs caused stress in microalgae cells, which resulted in a 140% carbohydrate enhancement. Romero and coworkers (2020) also observed a carbohydrate enhancement of up to 80% in *Chlorella vulgaris* when exposed to Ag NPs.

The addition of 40 and 70 mg L<sup>-1</sup> of CALPECH NPs resulted in a significantly enhanced CO<sub>2</sub> consumption ( $p = 0.0006$ ) of 5 and 11 %, respectively (**Fig. 24b**). The O<sub>2</sub> production was significantly enhanced by 13, 15 and 16% when dosing 20, 40 and 70 mg L<sup>-1</sup>, respectively ( $p = 0.00008$ ) (**Fig. 24e**). The OD<sub>750</sub> underwent enhancements of 33, 41 and 47% when 20, 40 and 70 mg L<sup>-1</sup> were added, respectively

( $p = 0.0001$ ) (**Fig. 24h**). The Px was significantly higher ( $p = 0.002$ ) when  $70 \text{ mg L}^{-1}$  were added (**Table 11**). The final IC concentrations and pH (**Table A1, A2**) confirmed the accelerated growth of *C. sorokiniana* mediated by the addition of CALPECH NPs. The addition of CALPECH NPs resulted in a positive effect on *C. sorokiniana* regardless of the concentration added. However,  $70 \text{ mg L}^{-1}$  supported the highest enhancements among all the concentrations tested. The carbohydrate content and the lipid content of *C. sorokiniana* was 12% and 11% (% dw) respectively, without the addition of NPs. The addition of  $70 \text{ mg L}^{-1}$  of CALPECH NPs significantly increased ( $p = 0.0006$ ) the carbohydrate and lipid content by 56% and 25% respectively, whereas no significant changes were observed in the presence of the other concentrations tested (**Fig. 24b**). This suggested that CALPECH NPs were not toxic to *C. sorokiniana* likely due to the low iron content of the NPs. The main iron source of these particular NPs is ZVI which has previously shown to be less toxic for microalgae species compared to other iron NPs, also provides a source of iron that increases cell growth and induces metabolic changes in some microalgae species (Kadar et al., 2012a; Pádrová et al., 2015). Pádrová and coworkers (2015) observed that  $5.1 \text{ mg L}^{-1}$  of ZVI stimulated the growth of *Arthrospira maxima*. In another study, Kadar and coworkers (2012a) showed that *Pavlova lutheri*, *Isochrysis galbana* and *Tetraselmis suecica* preferred ZVI NPs over EDTA-Fe. Thus, it can be hypothesized that CALPECH NPs accelerated the metabolism of *C. sorokiniana*. The high  $\text{CO}_2$  availability, induced by the high  $\text{CO}_2$  concentrations in the headspace of the bottles, led to an activation of the RuBisCO enzyme, which is the rate-limiting enzyme in the Calvin cycle (Cheng et al., 2020). The activation of the latter enzyme can result in an increased photosynthetic efficiency and  $\text{CO}_2$  fixation (Vargas-

Estrada et al., 2020). This enhanced CO<sub>2</sub> availability was mainly attributed to the porosity of the NPs, since part of the CO<sub>2</sub> remained adhered to the surface of the NPs and was released by the so-called “shuttle” effect (Kluytmans et al., 2003).

The addition of 70 mg L<sup>-1</sup> of SMALLOPS NPs entailed an increased cumulative CO<sub>2</sub> (12% higher than the control) consumption ( $p = 0.005$ ). The O<sub>2</sub> production in tests supplied with 40 mg L<sup>-1</sup> was 15% higher than the control, while the assays containing 70 mg L<sup>-1</sup> of SMALLOPS NPs did not experience an O<sub>2</sub> production enhancement. It is well known that iron NPs exhibit the potential to induce the formation of ROS by Fenton reactions, Fenton-like reactions, Haber-Weiss reactions or even more complex reactions (Rana et al., 2020; Rana & Prajapati, 2021). In these reactions O<sub>2</sub> reacts with the released Fe<sup>+</sup> ions to form ROS, hence, the O<sub>2</sub> photosynthetically produced could have led to the formation of ROS. The OD<sub>750</sub> was 19, 22 an 15% higher than the control when 20, 40 and 70 mg L<sup>-1</sup> were added ( $p = 0.003$ ) respectively, confirming the increased *C. sorokiniana* growth by the addition of SMALLOPS NPs. However, Px did not experience significant differences ( $p = 0.276$ ) among the assays. The final IC concentrations and pH values (**Table A1** and **A2**) confirmed that the addition of 40 mg L<sup>-1</sup> of SMALLOPS NPs stimulated *C. sorokiniana* growth, suggesting that this concentration could be the optimal for *C. sorokiniana*. The carbohydrates content of *C. sorokiniana* without NPs was 7% (dw) and increased by 66, 42 and 91% when 20, 40 and 70 mg L<sup>-1</sup> were added, respectively. The lipid content of the microalgal biomass without NPs was 14% (dw) and increased as well with the addition of NPs. The assays containing 40 mg L<sup>-1</sup> experienced an increase of 32% (**Fig. 24c**), which was the higher lipid content herein recorded. The

latter suggest that the addition of SMALLOPS NPs resulted in accelerated microalgae metabolism and in the production of high value biomass. The addition of SMALLOPS NPs seems to have induced a formation of ROS directly proportional to the percentage of iron content in the NPs, which influenced lipid accumulation in *C. sorokiniana*. The lipid content in the assays provided with 70 mg L<sup>-1</sup> decreased, likely because the concentration of ROS was higher than the tolerated by *C. sorokiniana*, resulting in the oxidation of lipids as a mechanism of defense. The higher iron content in SMALLOPS NPs induced lipid accumulation in *C. sorokiniana*, which represents an innovative strategy to produce lipid-enriched biomass at relatively low NPs concentrations.

**Table 11.** Influence of the type and concentration of nanoparticles on biomass productivity as a function of the type of light source: visible light (white background) and visible light + UV light (grey background)

	$P_X$ (g L <sup>-1</sup> d <sup>-1</sup> )		
	<i>Fe<sub>2</sub>O<sub>3</sub></i>	<i>CALPECH</i>	<i>SMALLOPS</i>
<b>Control</b>	1.24 ± 0.12	0.81 ± 0.02	2.15 ± 0.16
<b>20 mg L<sup>-1</sup></b>	1.12 ± 0.09	1.75 ± 0.21	2.10 ± 0.41
<b>40 mg L<sup>-1</sup></b>	1.27 ± 0.35	1.10 ± 0.14	2.00 ± 0.27
<b>70 mg L<sup>-1</sup></b>	1.75 ± 0.49	1.67 ± 0.22	1.72 ± 0.13
<b>Control</b>	1.37 ± 0.19	2.01 ± 0.09	1.81 ± 0.19
<b>20 mg L<sup>-1</sup></b>	1.36 ± 0.33	1.92 ± 0.08	1.84 ± 0.05
<b>40 mg L<sup>-1</sup></b>	1.27 ± 0.16	2.15 ± 0.31	1.67 ± 0.11
<b>70 mg L<sup>-1</sup></b>	1.60 ± 0.43	2.07 ± 0.10	1.70 ± 0.25



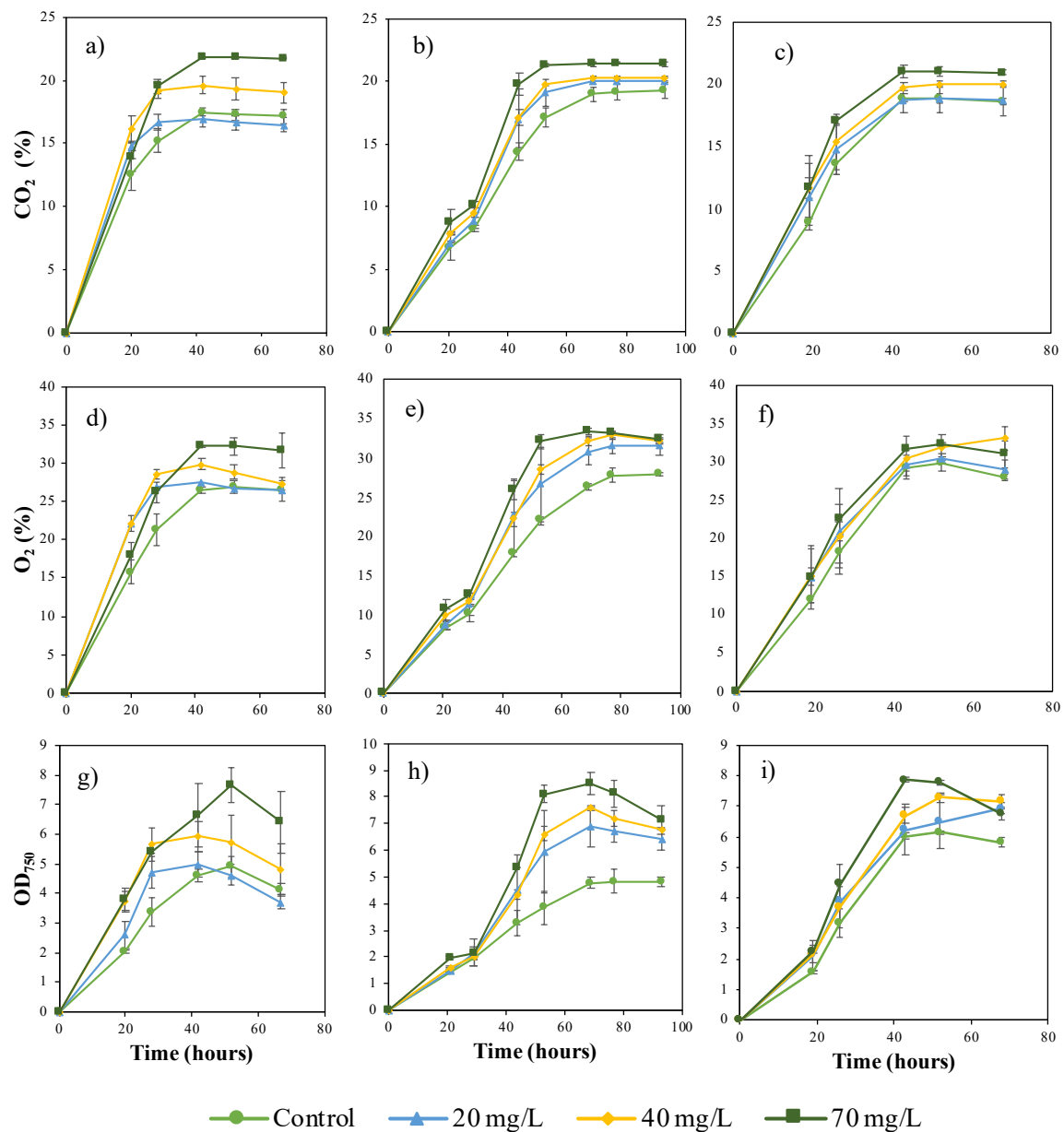


**Fig. 23.** Time course of the cumulative CO<sub>2</sub> consumptions in assays supplied with a) Fe<sub>2</sub>O<sub>3</sub>, b) CALPECH, c) SMALLOPS; of the cumulative O<sub>2</sub> production in the assays supplied with d) Fe<sub>2</sub>O<sub>3</sub>, e) CALPECH, e) SMALLOPS; and of the cumulative OD<sub>750</sub> in the assays supplied with d) Fe<sub>2</sub>O<sub>3</sub>, e) CALPECH, e) SMALLOPS. The assays were carried out under visible light.

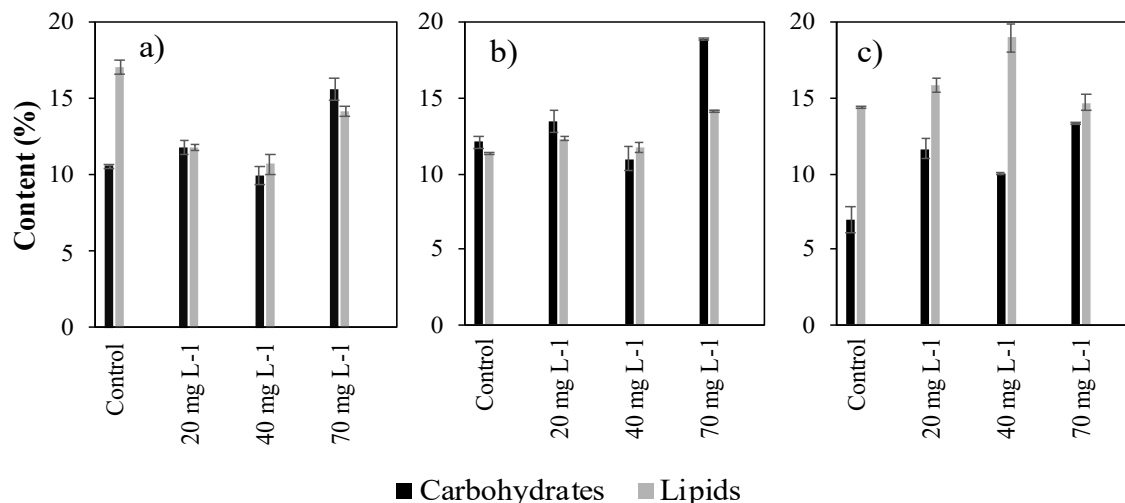


**Fig. 24.** Influence of the concentration of a) Fe<sub>2</sub>O<sub>3</sub> NPs; b) CALPECH NPs; c) SMALLOPS NPs on the carbohydrate (black) and lipid (grey) content of microalgae biomass at the end of the assays under visible light.

### 3.4 Influence of nanoparticle concentration on *C. sorokiniana* growth and CO<sub>2</sub> removal under visible + UV light

Yang and coworkers (2022) recently studied the effect of graphene oxide quantum dots on *Chlorella pyrenoidosa* under UV light and observed a positive effect of the growth and lipid production of this microalgae. Similarly, Dinc and coworkers (2022) demonstrated that the addition of Se NPs to microalgae reduced UV-stress effects in *C. vulgaris*. The present study assessed the influence of UV light supplementation to visible light at different concentrations of the Fe<sub>2</sub>O<sub>3</sub>, CALPECH and SMALLOPS NPs.

The addition of Fe<sub>2</sub>O<sub>3</sub> NPs under visible light supplemented with UV light exerted the same effects than visible light. Indeed, the concentrations of 40 and 70

mg L<sup>-1</sup> resulted in an increase in the cumulative CO<sub>2</sub> consumption of 13 and 23%, respectively ( $p = 0.00004$ ) (**Fig. 25a**). However, while the assays containing 40 mg L<sup>-1</sup> led to an enhanced O<sub>2</sub> production ( $p = 0.019$ ) (**Fig. 25d**), the assays with 70 mg L<sup>-1</sup> did not show a significant difference compared to the control tests ( $p = 0.162$ ). The OD<sub>750</sub> ( $p = 0.148$ ) (**Fig. 25g**), Px ( $p = 0.602$ ) (**Table 11**) and the final IC concentration ( $p = 0.585$ ) (**Table A1**) did not show any significant differences among the assays. The obtained results suggested that the exposure to *UV* light in the presence of Fe<sub>2</sub>O<sub>3</sub> NPs did not exert a toxic effect on *C. sorokiniana* since the growth was not inhibited and no retarded exponential growth was observed, contrary to the results obtained by Bibi and coworkers (2021). The carbohydrate content was significantly increased ( $p = 0.00003$ ) by 300, 190 and 530% under 20, 40 and 70 mg Fe<sub>2</sub>O<sub>3</sub> L<sup>-1</sup>, respectively (**Fig. 26a**), while the lipid content decreased regardless of the concentration of Fe<sub>2</sub>O<sub>3</sub> NPs. The addition of Fe<sub>2</sub>O<sub>3</sub> NPs under *UV* + visible light mediated the same mechanisms than visible light. Fe<sub>2</sub>O<sub>3</sub> NPs under *UV* light exposure (<260 nm) increased their oxidation effectiveness (Photo-Fenton process) (Shokri & Fard, 2022) however, in the present study, the *UV* light exposure coupled to the addition of Fe<sub>2</sub>O<sub>3</sub> NPs resulted in lower lipid contents in *C. sorokiniana* compared to the lipid contents under visible light. The lower lipid content in *C. sorokiniana* (<16%, dw) was herein attributed to a response to *UV* radiation. The significant increase in carbohydrate content compared to the control (2%, dw) ( $p = 0.00003$ ) suggested the occurrence of stress conditions caused by the NPs, regardless of the type of light, and can be attributed to an increased respiration and higher carbohydrates requirements for energy production (Romero et al., 2020).

The addition of 40 and 70 mg L<sup>-1</sup> of CALPECH NPs resulted in a 4 and 9% higher cumulative CO<sub>2</sub> consumption compared to the control assays ( $p = 0.0004$ ), respectively (**Fig. 25b**). The O<sub>2</sub> production increased with NPs concentration, with enhancements of 7, 11 and 17% at 20, 40 and 70 mg L<sup>-1</sup> respectively ( $p = 0.0009$ ), compared to the control assays (**Fig. 25e**). The increased photosynthetic activity of *C. sorokiniana* was also supported by the final OD<sub>750</sub>, which were 33, 34 and 47% higher at 20, 40 and 70 mg L<sup>-1</sup> ( $p = 0.009$ ) respectively, compared to the control tests (**Fig. 25h**). Even though Px (**Table 11**) did not exhibit a significant difference among the assays ( $p = 0.448$ ), the exponential growth phase was slightly increased by the addition of 70 mg L<sup>-1</sup> of CALPECH NPs. The final IC ( $p = 0.029$ ) and pH ( $p = 0.0000009$ ) (**Table A1 and A2**) supported the accelerated growth of *C. sorokiniana*. The carbohydrate and lipid contents of the control were 8.5% and 17% (% dw) respectively, and did not exhibit significant differences by the addition of NPs ( $p = 0.179$ ) (**Fig. 26b**). From the results herein obtained, it can be said that the *UV* light exposure reduced the beneficial effects of CALPECH NPs in terms of accumulation of macromolecules. However, since the cumulative CO<sub>2</sub>, O<sub>2</sub> and OD<sub>750</sub> were similar to the assays carried out under visible light, the results under *UV* light exposure support the theory that the enhanced CO<sub>2</sub> availability by the addition of CALPECH NPs was likely due to the adhesion of the gas to the surface of the NPs. The enhancement in the lipid content can be attributed to the formation of ROS mediated by the iron source of the NPs. Even though the mechanism of interaction of the NPs under *UV* light is not very clear, *UV* light exposure could have reduced the activity of the iron source explaining the reduced lipid and carbohydrate accumulation under *UV* exposure. Moreover, Dinc and coworkers (2022) observed that Se NPs is effective

at scavenging free radicals under UV exposure, thus the iron source of the CALPECH NPs could have the same response under UV radiation as well.

The addition of SMALLOPS NPs resulted in an increased cumulative CO<sub>2</sub> consumption of 10% and 17% when 40 and 70 mg L<sup>-1</sup> were added, respectively ( $p = 0.003$ ) (**Fig. 25c**). The O<sub>2</sub> production was increased regardless of the concentration of NPs, with enhancements of 8, 11 and 12 % for 20, 40 and 70 mg L<sup>-1</sup>, respectively ( $p = 0.002$ ) (**Fig. 25f**). The cumulative OD<sub>750</sub> confirmed the enhanced growth of *C. sorokiniana*, where the addition of 40 and 70 mg L<sup>-1</sup> resulted in 25 and 20 % higher cumulative OD<sub>750</sub> than the control ( $p = 0.002$ ) (**Fig. 25i**). Even if no significant differences in Px were recorded ( $p = 0.577$ ) (**Table 11**), the final IC ( $p = 0.0008$ ) concentration and pH ( $p = 0.0002$ ) values (**Table A1 and A2**) confirmed the accelerated microalgae growth in the assays containing 40 and 70 mg L<sup>-1</sup> of SMALLOPS NPs. SMALLOPS NPs supported similar *C. sorokiniana* growth patterns under visible light and UV-visible light, which suggested that the stimulated *C. sorokiniana* growth can be attributed to the interaction between the carbon coat of the NPs and the gaseous CO<sub>2</sub>. The iron content of the NPs is the responsible of the lipid/carbohydrate content, since the iron ions can led to the formation of ROS through the Fenton process (Rana & Prajapati, 2021). SMALLOPS NPs lipid content without the NPs was 19% (dw). The addition of 40 and 70 mg L<sup>-1</sup> of NPs induced lipid oxidation (**Fig. 26a and 26b**, respectively), whereas the lipid content of *C. sorokiniana* was enhanced by 11% with the addition of 20 mg L<sup>-1</sup> ( $p = 0.0004$ ) (**Fig. 26c**). The latter suggest that the iron source of SMALLOPS NPs enhanced their oxidative activity by the exposure of UV light (Shokri & Fard, 2022), and 20 mg L<sup>-1</sup>

of NPs induced an increase in *C. sorokiniana* lipid content as a mechanism of protection. Lipid oxidation could have occurred at 40 and 70 mg L<sup>-1</sup> due to the higher ROS concentration present in the culture media. It has been previously reported that ZVI NPs act as electron donors to catalyze a wide range of different reactions, and this particular NPs exhibit a better bioavailability compared to other iron NPs (Pádrová et al., 2015). Positive effects of ZVI NPs have been reported at concentrations below 5.1 mg L<sup>-1</sup> (Kadar et al., 2012a; Pádrová et al., 2015), thus, the latter explains the fact that the higher content of Fe in SMALLOPS NPs lead to the formation of ROS whereas the low concentration of Fe in CALPECH NPs resulted in biomass enhancements. Under *UV* radiation, the iron source of CALPECH NPs could act as *UV* scavengers, whereas the high concentration of Fe in SMALLOPS NPs under *UV* light likely mediated the formation of ROS.

Finally, the results obtained from *UV*-light exposure confirmed the fact that the increased CO<sub>2</sub> availability was due to the porosity of the NPs, and the CO<sub>2</sub> concentration was directly correlated to the NPs concentration. The increased CO<sub>2</sub> accumulation in the headspace did not increase IC concentration in the bottles containing NPs, suggesting that both shuttle and hydrodynamic effect could have occurred. Indeed, the CO<sub>2</sub> could have been adhered to the NPs surface and then released to the headspace of the bottles. Then, the presence of the NPs created an hydrodynamic effect as described in (Kluytmans et al., 2003), which facilitated the transfer of CO<sub>2</sub> to microalgae. On the other hand, the iron source was the responsible for the macromolecule accumulation/decrease in *C. sorokiniana*.

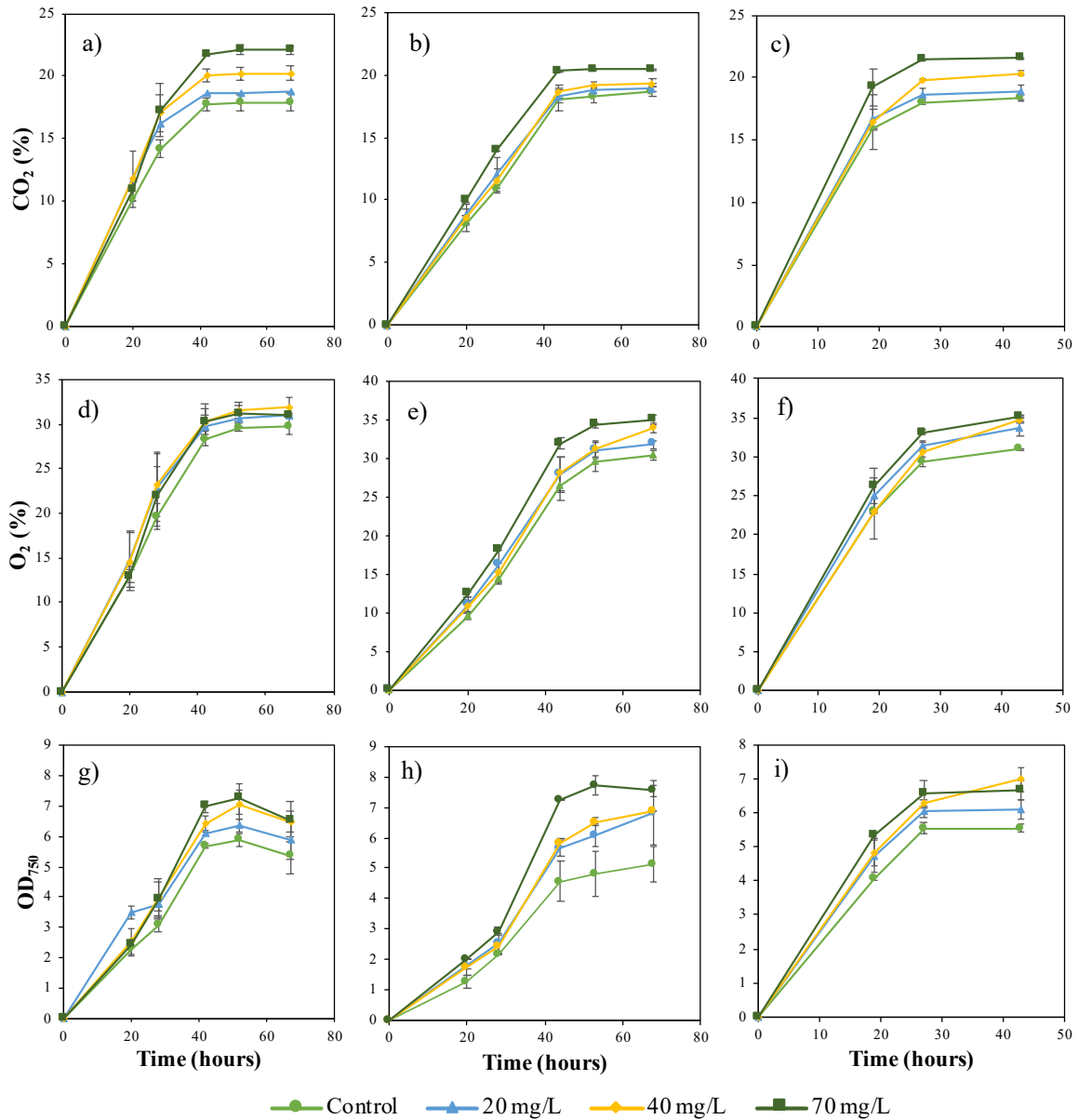


**Fig. 25.** Time course of the cumulative CO<sub>2</sub> consumptions in assays with a) Fe<sub>2</sub>O<sub>3</sub>, b) CALPECH, c) SMALLOPS; cumulative O<sub>2</sub> production in assays with d) Fe<sub>2</sub>O<sub>3</sub>, e) CALPECH, e) SMALLOPS; and cumulative OD<sub>750</sub> in assays with d) Fe<sub>2</sub>O<sub>3</sub>, e) CALPECH, e) SMALLOPS. The assays were carried out under visible light + UV light.

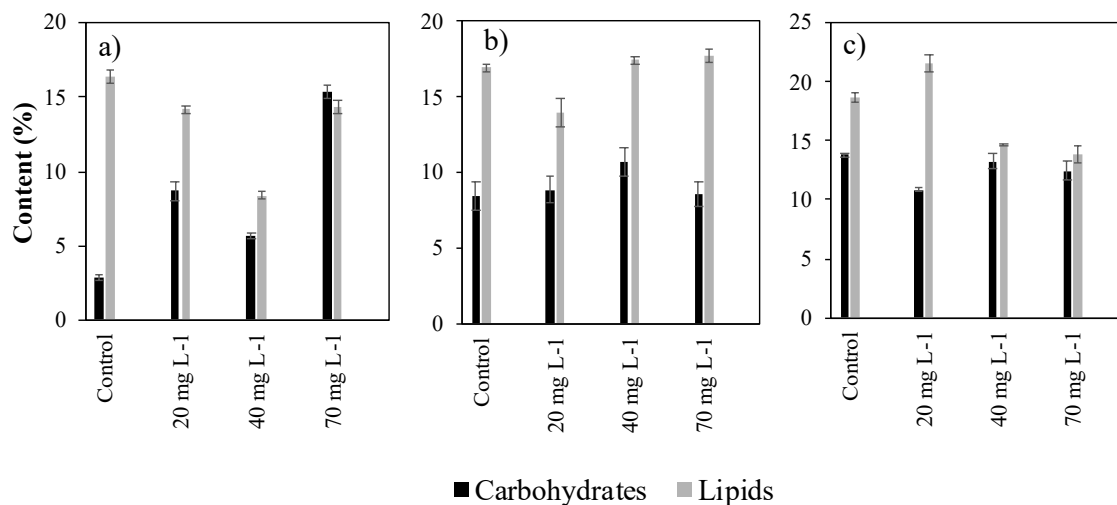


**Fig. 26.** Influence of the concentration of a) Fe<sub>2</sub>O<sub>3</sub> NPs; b) CALPECH NPs; c) SMALLOPS NPs on the carbohydrate (black) and lipid (grey) content of microalgae biomass at the end of the assays under visible light + UV light.

## 4. Conclusions

The mesoporous nature of the three different nanoparticles improved CO<sub>2</sub> availability and adsorption to *Chlorella sorokiniana* cultures regardless of their chemical composition. The addition of iron nanoparticles resulted in an enhanced *C. sorokiniana* growth regardless of the concentration and the type of nanoparticles tested. The results obtained suggest that both shuttle and hydrodynamic effects could have occurred during the cultivation of *C. sorokiniana*. The different iron sources of each nanoparticle influenced differently *C. sorokiniana* metabolism and was the responsible for carbohydrates/lipids accumulation. UV light exposure confirmed the fact that the higher CO<sub>2</sub> availability was likely due to the physical properties of the nanoparticles. However, UV light exposure induced lipid oxidation when Fe<sub>2</sub>O<sub>3</sub> and SMALLOPS nanoparticles were added as a result of their higher iron



content. Mesoporous nanoparticles can be considered as an effective technology to improve CO<sub>2</sub> consumption during photosynthetic biogas upgrading.

# Chapter 6

---

## Effect of nanoparticles on a mixed microalgae-bacteria consortium's metabolism and biogas upgrading

This chapter is adapted from the publication:

- Vargas-Estrada, L., Hoyos, E. G., Sebastian, P. J., & Muñoz, R. (2022). Elucidating the role of nanoparticles on photosynthetic biogas upgrading: Influence of biogas type, nanoparticle concentration and light source. *Algal Research*, 68 doi:10.1016/j.algal.2022.102899



## 1. Introduction

Biogas has become a relevant renewable energy source with the potential to substitute natural gas in the context of the World's Ecological Transition. Biogas is typically produced *via* anaerobic digestion of organic matter and its composition varies depending on the redox state of the substrates, environmental and operational conditions in the digesters. This green gas vector is mainly composed of CH<sub>4</sub> (45-75%), CO<sub>2</sub> (25-55%) and H<sub>2</sub>S (0.005-2%) (Haider et al., 2022). In this context, the removal of contaminants such as CO<sub>2</sub> and H<sub>2</sub>S is mandatory prior to its use as a vehicle fuel or to its injection to the natural gas grid (Marín et al., 2021). Today, several physical and chemical methods are commercially available for biogas upgrading, including membrane separation, cryogenic separation, pressure swing adsorption, water scrubbing, organic solvent scrubbing, chemical absorption (Mulu, M'Arimi, et al., 2021). The high operating costs and environmental impacts of these physical/chemical technologies have triggered research in biological methods such hydrogenotrophic and photosynthetic biogas upgrading.

Photosynthetic biogas upgrading in microalgae-bacteria photobioreactors has been validated at pilot and demo-scale, and widely reported to be an economically and environmentally friendly option to upgrade biogas into biomethane coupled to nutrient recovery from the liquid fraction of digestates (Rodero, Carvajal, et al., 2020). Despite algal-bacterial photobioreactors interconnected to external biogas absorption columns have reached CO<sub>2</sub> removals of up to 98.6% at pilot (Rodero, Severi, et al., 2020) and demo scale (Rodero, Carvajal, et al., 2020), there are still some challenges that need to be addressed to maintain a robust biogas upgrading

performance. Recently, Bose et al (2021) compared seven different factors affecting the bubble column performance in photosynthetic biogas upgrading. The main process limitations identified to date are i) the low  $\text{CO}_2$  mass transfer to the culture medium, ii) the high sensitivity of biomethane quality to variations in the gas and liquid flow rates and pH, and iii) the diurnal and seasonal variability of environmental parameters influencing photosynthetic activity (Bose et al., 2019). Indeed, this process requires the development of innovative operational strategies to enhance  $\text{CO}_2$  absorption and fixation.

During the past years, the use of nanomaterials in environmental applications is gaining attention due to their unique physicochemical properties such as size, morphology, high reactivity, chemical stabilization, high surface area-to-volume ratio, abundant active sites and high adsorption capacity (Vargas-Estrada et al., 2020). Indeed, nanomaterials and nanoparticles can play a key role in  $\text{CO}_2$  capture technologies, biogas production and biogas upgrading processes (Kumar et al., 2020). To date, many solid adsorbents, mainly porous materials, have been effectively used to remove  $\text{CO}_2$  from biogas, such as activated carbons and metal oxides (Golmakani et al., 2022). Moreover, it is known that the use of metal oxide NPs mediates the formation of carbonates, bicarbonates and carboxylates when  $\text{CO}_2$  interacts with the NPs surfaces (Mulu, Arimi, et al., 2021). In this context, the addition of nanoporous materials to microalgae cultures devoted to biogas upgrading can create a symbiosis where the materials adsorb  $\text{CO}_2$  to form carbonates and bicarbonate species that can be further fixed *via* photosynthesis by microalgae. This would result in enhancements in biomass production and in the performance

of biogas purification. In addition, it has been recently demonstrated that the supplementation of graphene oxide quantum dots under *UV*-light exposure stimulated the CO<sub>2</sub> capture and lipid production in *Chlorella pyrenoidosa* (Yang et al., 2022). Thus, NPs can be also used as a strategy to scavenge the damage of solar *UV* radiation to microalgae.

The addition of metal oxide NPs to microalgae culture is still a controversial topic, since NPs can be toxic to some microalgae species or stimulate their growth and lipid production (**Table 12**). Even if there is very little information on how the NPs addition to microalgae culture can improve the CO<sub>2</sub> adsorption, the reported studies present promising results (Vaz et al., 2020). In this way, the physico-chemical properties of the NPs can represent an advantage to improve CO<sub>2</sub> adsorption since they can act as electron donors/acceptors and light conversion aids, or form carbonates when CO<sub>2</sub> interacts with their surface, among others. Jeon et al. (2017) reported that SiO<sub>2</sub> NPs enhanced the gas-liquid mass transfer rate of CO<sub>2</sub> in *C. vulgaris* cultures, resulting in an enhanced growth and lipid production. Similarly, the use of polymeric nanofibers containing Fe<sub>2</sub>O<sub>3</sub> NPs has been reported as a promising technique to enhance CO<sub>2</sub> fixation of *Chlorella fusca* LEB 111 cultures (Vaz et al., 2020). On the other hand, the addition of zero-valent iron NPs have proved to have beneficial effects on microalgae species like *Pavlova lutheri*, *Isochrysis galbana*, *Tetraselmis suecica*, (Kadar et al., 2012c) *Desmodesmus subcapicatus*, *Dunaliella salina*, *Parachlorella kessleri* and *Trachydiscus minutus* (Pádrová et al., 2015). However, to the best of our knowledge, little is known about the effect of carbon NPs on microalgae culture. The literature on the effect of carbon-

coated zero-valent iron NPs on microalgae and the number studies devoted to investigate the potential of NPs during photosynthetic biogas upgrading is scarce.

This chapter aimed at assessing the effect of two metal oxides NPs ( $\text{Fe}_2\text{O}_3$  and  $\text{SiO}_2$ ) and one magnetic NP (carbon coated zero-valent iron) on microalgae growth and photosynthetic biogas upgrading efficiency at laboratory scale in batch enclosed photobioreactors. Additionally, the influence of NPs concentration and light source (visible *versus* visible + UV) on the parameters above mentioned were also investigated.

**Table 12.** Effect of nanoparticles on microalgae growth. PAN: polyacrylonitrile; DMF: dimethylformamide (DMF); NFs: nanofibers.

<i>NP</i>	<i>Strain</i>	<i>CO<sub>2</sub> source</i>	<i>Effect</i>	<i>Reference</i>
$\text{Fe}_2\text{O}_3$	<i>Chlorella vulgaris</i>		At concentrations of 50 and 100 mg L <sup>-1</sup> biomass growth was reduced by 41.2% and 83.7% whereas total lipid contents increased by 39.7% and 25.5% respectively.	(Bibi et al., 2021)
g-C <sub>3</sub> N <sub>4</sub>	<i>Scenedesmus</i> sp.		Improved biomass and lipid accumulation	(Ren et al., 2020)
PAN/DMF NFs with 4% (w v <sup>-1</sup> ) $\text{Fe}_2\text{O}_3$ NPs	<i>Chlorella fusca</i> LEB 111	15% v v <sup>-1</sup> CO <sub>2</sub> gas	Assays with 0.3 g L <sup>-1</sup> nanofibers supported 10.9% greater lipid production than the assays without nanofiber	(Vaz et al., 2020)
SiC	<i>Scenedesmus</i> sp.		Improved biomass and lipid accumulation	(Ren et al., 2020)

TiC		Inhibitory effect	
TiO <sub>2</sub>			
TiO <sub>2</sub>	<i>Dunaliella tertiolecta</i>	No evidence of NPs mediated inhibition of the growth or pigment content at concentrations up to 10 mg L <sup>-1</sup>	(Morelli et al., 2018)
ZnO	<i>Dunaliella tertiolecta</i>	Growth was reduced at concentration of 1 mg L <sup>-1</sup>	(Manzo et al., 2013)
ZnO	<i>Skeletonema costatum</i>	Growth was inhibited at 0.5 mg L <sup>-1</sup>	(C. Zhang et al., 2016)
	<i>Arthrospira maxima</i>	Growth and lipid accumulation were stimulated at concentrations between 1.7-5.1 mg L <sup>-1</sup>	
	<i>Desmodesmus subspicatus</i>		
ZVI	<i>Dunaliella salina</i>		(Pádrová et al., 2015)
	<i>Nannochloropsis limnetica</i>	Growth and lipid accumulation were stimulated at a concentration of 5.1 mg L <sup>-1</sup>	
	<i>Parachlorella kessleri</i>		
	<i>Raphidocelis subcapitata</i>		
	<i>Trachydiscus minutus</i>		
	<i>Isochrysis galbana</i>	Preference to nanoparticles over EDTA-Fe	
ZVI	<i>Pavlova lutheri</i>	Increase in lipid content	(Kadar et al., 2012c)
	<i>Tetraselmis suecica</i>	Increased total cellular lipid content	



## **2. Materials and methods**

### **2.1 Nanoparticles and stock solutions**

Three different metal nanoparticles were investigated. Fe<sub>2</sub>O<sub>3</sub> NPs were synthesized according to (Norouzi & Nezamzadeh-Ejhi, 2020), while SiO<sub>2</sub> nanopowder was purchased from Sigma Aldrich. The CaCO<sub>3</sub> nanoparticles were kindly donated by CALPECH. Fresh stock solutions of 200 mg L<sup>-1</sup> of each nanoparticle were prepared in microalgae mineral medium, and sonicated for one hour to prevent nanoparticle agglomeration and facilitate the addition of the NPs to the microalgae culture. To determine the surface area, pore volume and average pore diameter of the NPs herein used, a nitrogen physisorption analysis was conducted in an ASAP 2050 (Micromeritics, USA) at 77 K. The specific surface area and pore characteristics were determined by the BET method and BJH equation. Scanning electron microscopy (SEM) (JEOL JSM-6490LV) and energy-dispersive spectroscopy (EDS) (EDX-700/800, Hitachi, Japan) were carried out to determine the surface morphology and elemental composition of the target NPs.

### **2.2 Microalgae culture and biogas**

The microalgae culture used in our study consisted of a consortium of microalgae and cyanobacteria composed of *Chlorella* sp. (91.30 %), *Nitzschia* sp. (7.56 %) and *Pseudanabaena* sp. (1.16%) (percentages expressed in number of cells). The consortium was obtained from an outdoors 180 L pilot experimental plant treating real biogas and digestate from a 100 L sewage sludge digester located at the Institute of Sustainable Processes (Valladolid, Spain). The detailed description of the pilot

plant can be found elsewhere (Marín, Posadas, Cano, Pérez, Blanco, et al., 2018; Posadas et al., 2017). To elucidate the effect of NPs on photosynthetic biogas upgrading, two different synthetic biogas mixtures were used: Biogas A composed of CO<sub>2</sub> (30%) and CH<sub>4</sub> (70%) (Carbueros Metalicos; Spain), and Biogas B composed of CO<sub>2</sub> (29.5%), H<sub>2</sub>S (0.5%) and CH<sub>4</sub> (70%) (Abello Linde; Spain).

### **2.3 Experimental set-up**

Batch assays to quantitatively evaluate the effect of the different nanoparticles at different concentrations and under different light sources on biogas upgrading by microalgae were conducted in 1.2 L glass bottles. The bottles were prepared with 1 L of synthetic biogas headspace and 0.2 L of working volume, which was composed of mineral salt medium rich in carbonates as described elsewhere (Marín et al., 2020) and the corresponding nanoparticle concentration. The bottles were closed with butyl septa and plastic caps, flushed with helium for 5 min and, subsequently, the corresponding synthetic biogas was flushed for 5 min using inlet and outlet needles to replace the helium headspace. After one hour of stabilization, the bottles were inoculated with the mixed algal culture at an initial concentration of 200 mg L<sup>-1</sup> of TSS. Then, the bottles were incubated at 25 °C under continuous magnetic stirring (300 rpm) to avoid microalgae sedimentation. Light intensity of 900 μE m<sup>-2</sup> s<sup>-1</sup> was continuously provided by visible LED lights.

This chapter was divided in three tests series. In the tests series I, four operational conditions were evaluated for each nanoparticle: 1) Microalgae biomass and synthetic biogas A; 2) Microalgae biomass with 10 mg L<sup>-1</sup> of nanoparticles and

biogas A; 3) Microalgae biomass and synthetic biogas B; 4) Microalgae biomass with 10 mg L<sup>-1</sup> of nanoparticles and biogas B. Each condition was run in triplicate. In tests series II, the influence of different concentrations (20, 40, and 70 mg L<sup>-1</sup>) of each nanoparticle was assessed under biogas A headspace, 25 °C, magnetic stirring (300 rpm) and visible light 900 μE m<sup>-2</sup>s<sup>-1</sup>. A control containing only algal biomass and biogas A was conducted. Each condition was run in triplicate. In test series III, the influence of different concentrations (20, 40, and 70 mg L<sup>-1</sup>) of each nanoparticle was assessed under biogas A headspace, 25 °C, magnetic stirring (300 rpm) and visible light 900 μE m<sup>-2</sup>s<sup>-1</sup> + UV light (λ 315-350 nm, 10 W m<sup>-2</sup>). The UV light exposure was added to simulate real solar radiation. A control containing only algal biomass and biogas A was conducted. Each condition was run in triplicate.

## **2.4 Analytical procedures**

The biogas composition in the headspace of the bottles was determined two times per day by gas chromatography-TCD (Bruker) to quantify the gas concentration of CH<sub>4</sub>, CO<sub>2</sub>, H<sub>2</sub>S and O<sub>2</sub> in the headspace according to (Posadas et al., 2015). Microalgae growth was daily determined by optical density at 750 nm using a Shimadzu spectrophotometer (Japan), microalgae samples were daily taken and properly diluted to obtain an absorbance under 1, then the obtained absorbance was multiplied by the dilution factor. The initial CO<sub>2</sub> and O<sub>2</sub> content in the headspace along with the OD<sub>750</sub> were normalized and are presented as cumulative values. pH was determined at the beginning and at the end of the experiment (SensION™ + PH3 pHmeter, HACH, Spain). TSS concentrations were determined according to

standard methods (APHA-AWWA-WPCF, 1999). The biomass obtained from test series II and II was harvested (10000 rpm, 4 °C) and freeze-dried for further macromolecular characterization. The carbohydrate content was determined according to (Dubois et al., 1956), while the lipid content was determined gravimetrically following biomass extraction with chloroform:methanol (2:1 v v<sup>-1</sup>) as described elsewhere (Ángeles et al., 2020).

## 2.5 Statistical analysis

The results are presented as mean values  $\pm$  standard deviation. An analysis of variance (ANOVA) followed by Tuckey's test considering  $\alpha=0.05$  was performed to assess the influence of nanoparticles on microalgae growth.

## 3. Results and discussion

### 3.1 Nanoparticle characterization

The SEM micrographs show the morphology of the three NPs used in this study (**Fig. 27**). The Fe<sub>2</sub>O<sub>3</sub> NPs presented a nanorod morphology, which has been previously reported to exhibit a high specific surface area and better electrochemical and magnetic properties compared to other Fe<sub>2</sub>O<sub>3</sub> morphologies (Powell et al., 2021). The CACOI NPs were characterized by agglomerated NPs in accordance with (Munoz et al., 2021). Finally, the SiO<sub>2</sub> NPs presented the smallest particle size among the three NPs tested. Moreover, the chemical composition of each NPs is presented in **Table 13**. The presence of Na in the Fe<sub>2</sub>O<sub>3</sub> NPs was attributed to trace levels of the catalyst used for their synthesis. Interestingly, the CACOI NPs exhibited low levels

of essential minerals for microalgae growth, which could serve as nutrients and promote microalgae growth.

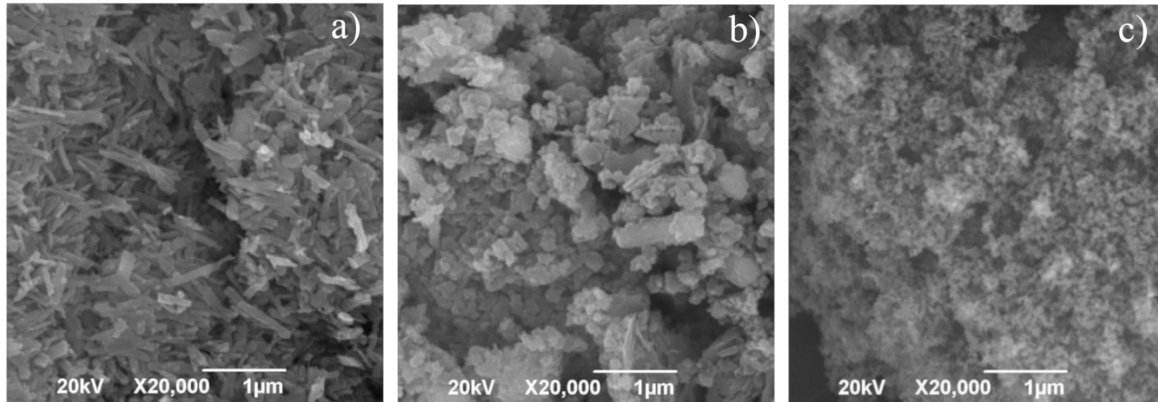


**Fig. 27.** Scanning Electron Microscope micrographs of a)  $\text{Fe}_2\text{O}_3$ , b) CACOI; carbon coated zero valent iron, and c)  $\text{SiO}_2$  nanoparticles.

**Table 13.** Chemical composition of the different nanoparticles used. The values represent the atomic percentage. CACOI: carbon coated zero valent iron

Element	$\text{Fe}_2\text{O}_3$	CACOI	$\text{SiO}_2$
Si (%)			19.70
O (%)	59.20	12.90	80.30
Na (%)	3.44		
Fe (%)	37.40	1.74	
C (%)		85.10	
P (%)		0.09	
K (%)		0.23	
Ca (%)		0.03	

Furthermore, the BET surface area, pore volume and average pore diameter of the target NPs are shown in **Table 14**. The three NPs herein used presented pore diameters  $<50$  nm, and according to the IUPAC classification, the three NPs represent mesoporous materials. In this context, the NPs can serve as gas adsorbents and promote a higher CO<sub>2</sub> biofixation. It is known that Fe<sub>2</sub>O<sub>3</sub> NPs represent an effective adsorbent of CO<sub>2</sub> (Hakim, Marliza, Abu Tahari, Wan Isahak, et al., 2016), Hakim et al. (2016), reported that the CO<sub>2</sub> adsorption capacity of Fe<sub>2</sub>O<sub>3</sub> increased up to four times when the particle size decreased from 160.5 nm (bulk form) to 24.5-56 nm. In this particular chapter, the synthesized Fe<sub>2</sub>O<sub>3</sub> NPs exhibited an average particle size of 24 nm, which are in the range reported by (Hakim, Marliza, Abu Tahari, Yusop, et al., 2016). Moreover, the morphology of the Fe<sub>2</sub>O<sub>3</sub> NPs herein synthesized resulted in a higher BET surface area, which could eventually support a high CO<sub>2</sub> adsorption from biogas. On the other hand, the CaCO<sub>3</sub> NPs presented slightly lower pore volume (0.28 cm<sup>3</sup> g<sup>-1</sup>), surface area (27.30 m<sup>2</sup> g<sup>-1</sup>) and average pore diameter (41.50 nm), than the Fe<sub>2</sub>O<sub>3</sub> NPs, suggesting that both Fe<sub>2</sub>O<sub>3</sub> and CaCO<sub>3</sub> NPs can behave similarly as adsorbents. Finally, the SiO<sub>2</sub> NPs presented the highest BET surface area, pore volume and average pore diameter. The values obtained in our particular study ranged between the results reported by (Liao et al., 2018) and (Krishnan et al., 2022), suggesting that SiO<sub>2</sub> NPs could support superior adsorption properties than CaCO<sub>3</sub> and Fe<sub>2</sub>O<sub>3</sub> NPs. Thus, the results of the adsorption/desorption analysis confirmed that nanopowders exhibited a high surface area (Ilves et al., 2018), but the nature of the CaCO<sub>3</sub> and Fe<sub>2</sub>O<sub>3</sub> NPs,

inherently containing essential trace metals for microalgae growth, could play a key role in microalgae metabolism.

**Table 14.** BET surface area, pore volume and average pore diameter of the nanoparticles used in this study. BET: Brunauer-Emmett-Teller; CACOI: carbon coated iron

<b>Nanoparticles</b>	<b>BET surface area (m<sup>2</sup> g<sup>-1</sup>)</b>	<b>Pore volume (cm<sup>3</sup> g<sup>-1</sup>)</b>	<b>Average pore diameter (nm)</b>
<i>Fe<sub>2</sub>O<sub>3</sub></i>	32.10	0.38	47.50
<i>CACOI</i>	27.30	0.28	41.50
<i>SiO<sub>2</sub></i>	981	6.97	28.40

### **3.2 Influence of type of biogas and nanoparticle addition on microalgae growth**

The CO<sub>2</sub> consumption and O<sub>2</sub> production recorded in the headspace of the bottles served as indicators of microalgae growth, along with the optical density of the culture broth (**Fig. 28**). The addition of biogas B resulted in microalgae inhibition regardless of the presence of NPs, and can be mainly attributed to the absence of sulfur-oxidizing bacteria responsible for the rapid oxidation of H<sub>2</sub>S to SO<sub>4</sub><sup>2-</sup> (Franco-Morgado et al., 2018).

On the other hand, biogas A did not induce microalgae inhibition likely due to the absence of H<sub>2</sub>S. The cultures containing Fe<sub>2</sub>O<sub>3</sub> NPs and SiO<sub>2</sub> NPs exhibited similar cumulative O<sub>2</sub> productions, CO<sub>2</sub> consumptions and culture densities than their controls (in the absence of NPs). Interestingly, Fe<sub>2</sub>O<sub>3</sub> NPs have been previously

reported as microalgal photosynthesis stimulants, resulting in enhancement in biomass growth and lipid/carbohydrate contents (Xia et al., 2021). In our particular study, the addition of 10 mg L<sup>-1</sup> of Fe<sub>2</sub>O<sub>3</sub> NPs did not support any significant improvement in CO<sub>2</sub> cumulative consumptions but a slight enhancement of 5% in O<sub>2</sub> production was observed.

The addition of NPs at 10 mg L<sup>-1</sup> did not enhance Px under biogas A atmosphere in any of the conditions tested. This can be attributed to the microalgae species used in this study, since the effect of the NPs is species specific (**Table 11**) (Vargas-Estrada et al., 2020). Nonetheless, the microalgae cultivated with Fe<sub>2</sub>O<sub>3</sub> NPs presented a statistically higher OD<sub>750</sub>, likely supported by slightly higher O<sub>2</sub> production compared to the control tests. Indeed, the addition of 10 mg L<sup>-1</sup> of Fe<sub>2</sub>O<sub>3</sub> NPs stimulated the production of microalgal-bacterial biomass, which is in accordance with (Xia et al., 2021). At this point it is important to mention that Xia et al (2021) observed higher biomass growth enhancements at higher Fe<sub>2</sub>O<sub>3</sub> NPs concentrations (50 mg L<sup>-1</sup>), which suggested that the concentrations herein assessed were too low, and higher concentrations of Fe<sub>2</sub>O<sub>3</sub> NPs can be added to observe an effect on photosynthetic biogas upgrading. Moreover, despite the addition of CaCO<sub>3</sub> NPs resulted in a lower final OD<sub>750</sub> at the end of the experiment, the reduced lag phase in terms of O<sub>2</sub> production, CO<sub>2</sub> consumption and biomass growth suggested that CaCO<sub>3</sub> NPs stimulated the activity of the algal consortium herein used. Even if little is known about the effect of CaCO<sub>3</sub> NPs on microalgae, our results suggest that these particular NPs do not represent a threat for microalgae growth. Finally, the addition of 10 mg L<sup>-1</sup> SiO<sub>2</sub> under a biogas A atmosphere did not support any



statistical difference in the monitored parameters compared to the control tests. SiO<sub>2</sub> NPs were previously reported as stimulants of *Chlorella vulgaris* metabolism, and final dry cell weight of 1.33 g L<sup>-1</sup> were recorded by the addition of SiO<sub>2</sub> NPs (Jeon et al., 2017). Moreover, the same authors also observed that fatty acid methyl esters productivity was increased up to 0.62 g L<sup>-1</sup> d<sup>-1</sup> by the addition of the SiO<sub>2</sub> NPs. However, in our study no significant change was observed neither in the final dry weight nor in Px by the addition of SiO<sub>2</sub> NPs, probably because the study of Jeon et al (2017) used a concentration of 0.2 wt% SiO<sub>2</sub> NPs, which is much higher than the concentrations herein used. Thus, the absence of impact of SiO<sub>2</sub> NPs on algal metabolism compared to literature can be explained by the significant lower concentration herein used.

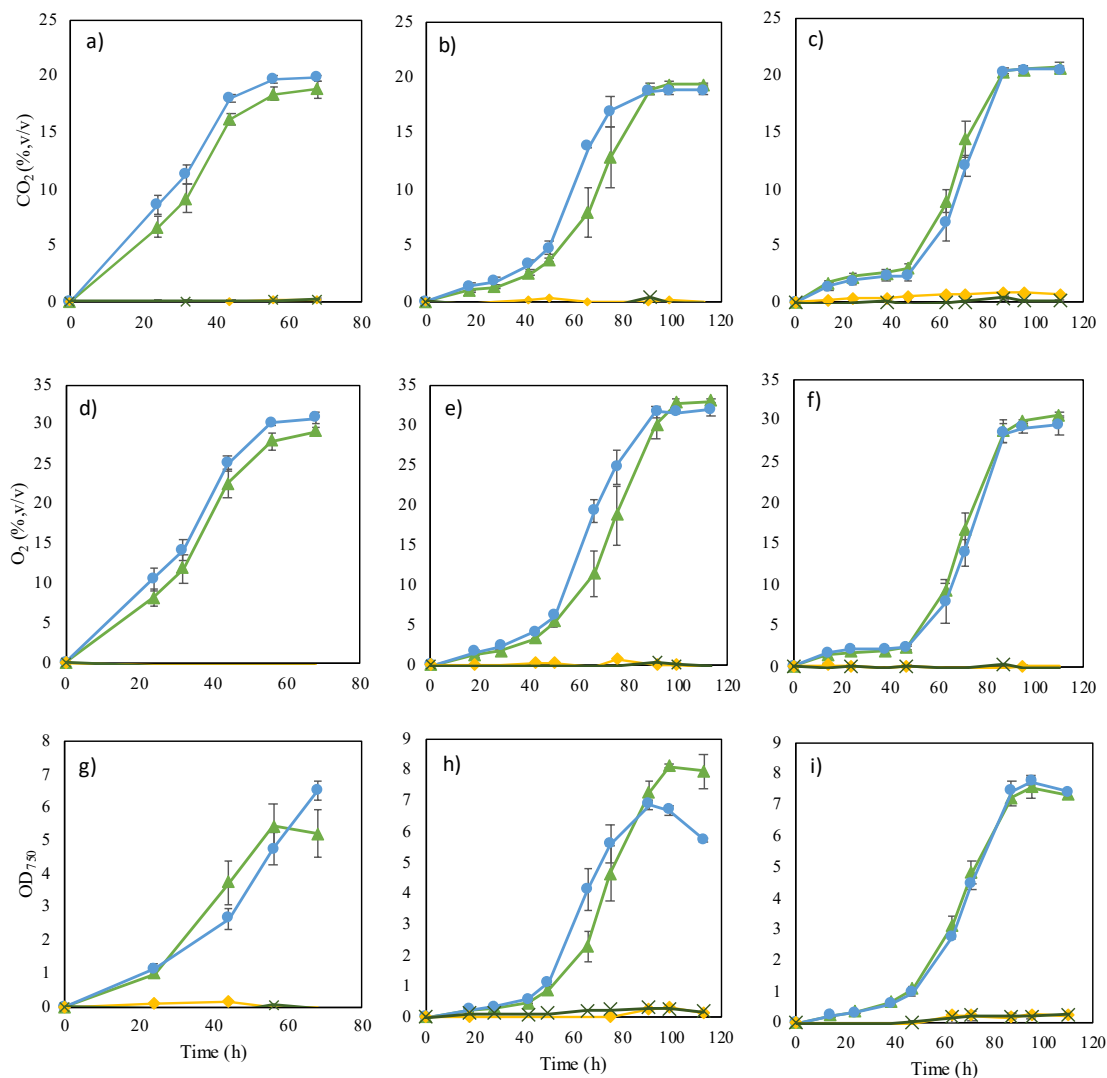


**Fig. 28.** Time course of the cumulative CO<sub>2</sub> consumption in the assays supplied with a) Fe<sub>2</sub>O<sub>3</sub> NPs, b) CACO<sub>1</sub> NPs, c) SiO<sub>2</sub> NPs; cumulative O<sub>2</sub> production in the assays supplemented with d) Fe<sub>2</sub>O<sub>3</sub> NPs, e) CACO<sub>1</sub> NPs, f) SiO<sub>2</sub> NPs; and culture absorbance of the algal consortium supplied with g) Fe<sub>2</sub>O<sub>3</sub> NPs, h) CACO<sub>1</sub> NPs, i) SiO<sub>2</sub> NPs. NPs: nanoparticles; BA (triangles): assays with biogas A; BAN (circles): assays with biogas A and NPs; BB (diamonds): assays with biogas B; BBN (cross): assays with biogas B and NPs; CACO<sub>1</sub>: carbon coated zero valent iron.

The addition of NPs at 10 mg L<sup>-1</sup> did not enhance Px under biogas A atmosphere in any of the conditions tested. This can be attributed to the microalgae species used in this study, since the effect of the NPs is species specific (**Table 15**) (Vargas-Estrada et al., 2020). Nonetheless, the microalgae cultivated with Fe<sub>2</sub>O<sub>3</sub> NPs presented a statistically higher OD<sub>750</sub>, likely supported by slightly higher O<sub>2</sub> production compared to the control tests. Indeed, the addition of 10 mg L<sup>-1</sup> of Fe<sub>2</sub>O<sub>3</sub> NPs stimulated the production of microalgal-bacterial biomass, which is in accordance with (Xia et al., 2021). At this point it is important to mention that Xia et al (2021) observed higher biomass growth enhancements at higher Fe<sub>2</sub>O<sub>3</sub> NPs concentrations (50 mg L<sup>-1</sup>), which suggested that the concentrations herein assessed were too low, and higher concentrations of Fe<sub>2</sub>O<sub>3</sub> NPs can be added to observe an effect on photosynthetic biogas upgrading. Moreover, despite the addition of CaCO<sub>3</sub> NPs resulted in a lower final OD<sub>750</sub> at the end of the experiment, the reduced lag phase in terms of O<sub>2</sub> production, CO<sub>2</sub> consumption and biomass growth suggested that CaCO<sub>3</sub> NPs stimulated the activity of the algal consortium herein used. Even if little is known about the effect of CaCO<sub>3</sub> NPs on microalgae, our results suggest that these particular NPs do not represent a threat for microalgae growth. Finally, the addition of 10 mg L<sup>-1</sup> SiO<sub>2</sub> under a biogas A atmosphere did not support any statistical difference in the monitored parameters compared to the control tests. SiO<sub>2</sub> NPs were previously reported as stimulants of *Chlorella vulgaris* metabolism, and final dry cell weight of 1.33 g L<sup>-1</sup> were recorded by the addition of SiO<sub>2</sub> NPs (Jeon et al., 2017). Moreover, the same authors also observed that fatty acid methyl esters productivity was increased up to 0.62 g L<sup>-1</sup> d<sup>-1</sup> by the addition of the SiO<sub>2</sub> NPs. However, in our study no significant change was observed neither in the

final dry weight nor in Px by the addition of SiO<sub>2</sub> NPs, probably because the study of Jeon et al (2017) used a concentration of 0.2 wt% SiO<sub>2</sub> NPs, which is much higher than the concentrations herein used. Thus, the absence of impact of SiO<sub>2</sub> NPs on algal metabolism compared to literature can be explained by the significant lower concentration herein used.

**Table 15.** Biomass productivity (Px) and pH of the algal consortium broth supplemented with 10 mg L<sup>-1</sup> of the different nanoparticles. CACOI: carbon coated zero valent iron.

	<i>Fe<sub>2</sub>O<sub>3</sub></i>		<i>CACOI</i>		<i>SiO<sub>2</sub></i>	
	Control	10 mg L <sup>-1</sup>	Control	10 mg L <sup>-1</sup>	Control	10 mg L <sup>-1</sup>
<i>P<sub>x</sub></i> (g L <sup>-1</sup> d <sup>-1</sup> )	0.78±0.005	0.87±0.07	1.30±0.07	1.29±0.032	1.32±0.03	1.38±0.06
<i>pH<sub>initial</sub></i>	7.65±0.04	7.74±0.02	7.86±0.03	7.89±0.01	7.76±0.02	7.70±0.04
<i>pH<sub>final</sub></i>	8.85±0.05	8.89±0.10	9.33±0.13	9.28±0.04	9.23±0.10	9.13±0.06

CACOI NPs are covered with carbon, and this particular material has been widely used for CO<sub>2</sub> capture (Kumar et al., 2020). The mechanism of interaction between the NPs and the CO<sub>2</sub> capture is not well understood yet, but one of the main mechanism of interaction is the “shuttle effect”, which can be described as follows: CO<sub>2</sub> is adsorbed by the NPs and then the loaded NPs release the adsorbed CO<sub>2</sub> into the aqueous medium, or the algal broth in this case (Choi et al., 2015). Thus, the reduced lag phase achieved in the presence of CACOI NPs could be explained by the adsorption capacity of activated carbon (Munoz et al., 2021). Hence, the CO<sub>2</sub> present in the biogas atmosphere was adsorbed to the surface of the NPs and rapidly released

in the aqueous broth for microalgae consumption, thus stimulating an early algal metabolism.

### 3.3 Influence of nanoparticle concentration under visible light

The addition of 20, 40 and 70 mg L<sup>-1</sup> of Fe<sub>2</sub>O<sub>3</sub> NPs resulted in higher cumulative CO<sub>2</sub> consumption and higher Px during the exponential growth phase (**Table 16**) (**Fig. 29**). Indeed, the addition of Fe<sub>2</sub>O<sub>3</sub> NPs resulted in up to 38% Px enhancement. The higher Px values herein obtained can be mainly attributed to: 1) the culture media composition, which is a synthetic centrate supporting high biomass productions due to its rich nutrients content compared to other types of wastewater (Tan et al., 2021); 2) the high CO<sub>2</sub> concentration in the headspace of the bottle, which resulted in accelerated microalgae growth; 3) the biostimulant nature of the nanoparticles used and 4) the high photosynthetic active radiation and the high illuminated surface to volume ratio. However, the higher the Fe<sub>2</sub>O<sub>3</sub> NPs concentration, the higher the lag phase in the assays (**Fig. 29a, 29d, 29g**). This matched the observations of Bibi and co-workers (2021), who reported that concentrations of Fe<sub>2</sub>O<sub>3</sub> NPs between 50-100 mg L<sup>-1</sup> delayed the exponential growth phase of microalgae. Although the cumulative CO<sub>2</sub> consumption and biomass productivity increased with increasing concentrations of Fe<sub>2</sub>O<sub>3</sub> NPs, the cumulative O<sub>2</sub> production decreased as the NPs concentration increased. This phenomenon was likely due to the interactions between O<sub>2</sub> and Fe<sub>2</sub>O<sub>3</sub> NPs *via* Fenton reactions, Photo-Fenton reactions, Haber-Weiss reactions or even more complex reactions (Shokri & Fard, 2022), where the Fe<sup>2+</sup> ions released by the Fe<sub>2</sub>O<sub>3</sub> NPs react with peroxide, water and O<sub>2</sub> to form ROS.

Even though the formation of ROS has been considered as one of the major factors that induce toxicity in microalgae (Vargas-Estrada et al., 2020), the use of  $\text{Fe}_2\text{O}_3$  NPs presents contradictory results and the tolerance to  $\text{Fe}_2\text{O}_3$  NPs is species specific. Thus, the retarded exponential phase could be attributed to the presence of ROS. Rana et al (2020) reported that the biomass concentration of *Chlorella pyrenoidosa* was enhanced by 33.7% when  $20 \text{ mg L}^{-1}$  of  $\text{Fe}_2\text{O}_3$  NPs were added, which is similar to the biomass enhancements obtained in our study.

**Table 16.** Biomass productivity (Px) as a function of the type of nanoparticles and light source, at different concentrations. CACOI: carbon coated zero valent iron.

	<b><math>\text{Fe}_2\text{O}_3</math></b>		<b>CACOI</b>		<b><math>\text{SiO}_2</math></b>	
	<i>Visible light</i>	<i>Visible + UV light</i>	<i>Visible light</i>	<i>Visible + UV light</i>	<i>Visible light</i>	<i>Visible + UV light</i>
<i>Control</i>	1.98±0.30	0.94±0.06	1.24±0.07	2.04±0.10	1.68±0.24	0.90±0.07
<i>20 mg L<sup>-1</sup></i>	1.44±0.18	1.45±0.13	1.69±0.48	2.00±0.14	1.89±0.08	0.88±0.05
<i>40 mg L<sup>-1</sup></i>	2.63±0.14	1.41±0.09	2.25±0.55	1.92±0.06	1.89±0.08	0.86±0.05
<i>70 mg L<sup>-1</sup></i>	2.75±0.23	1.48±0.15	3.12±0.65	2.14±0.03	1.81±0.13	0.85±0.08

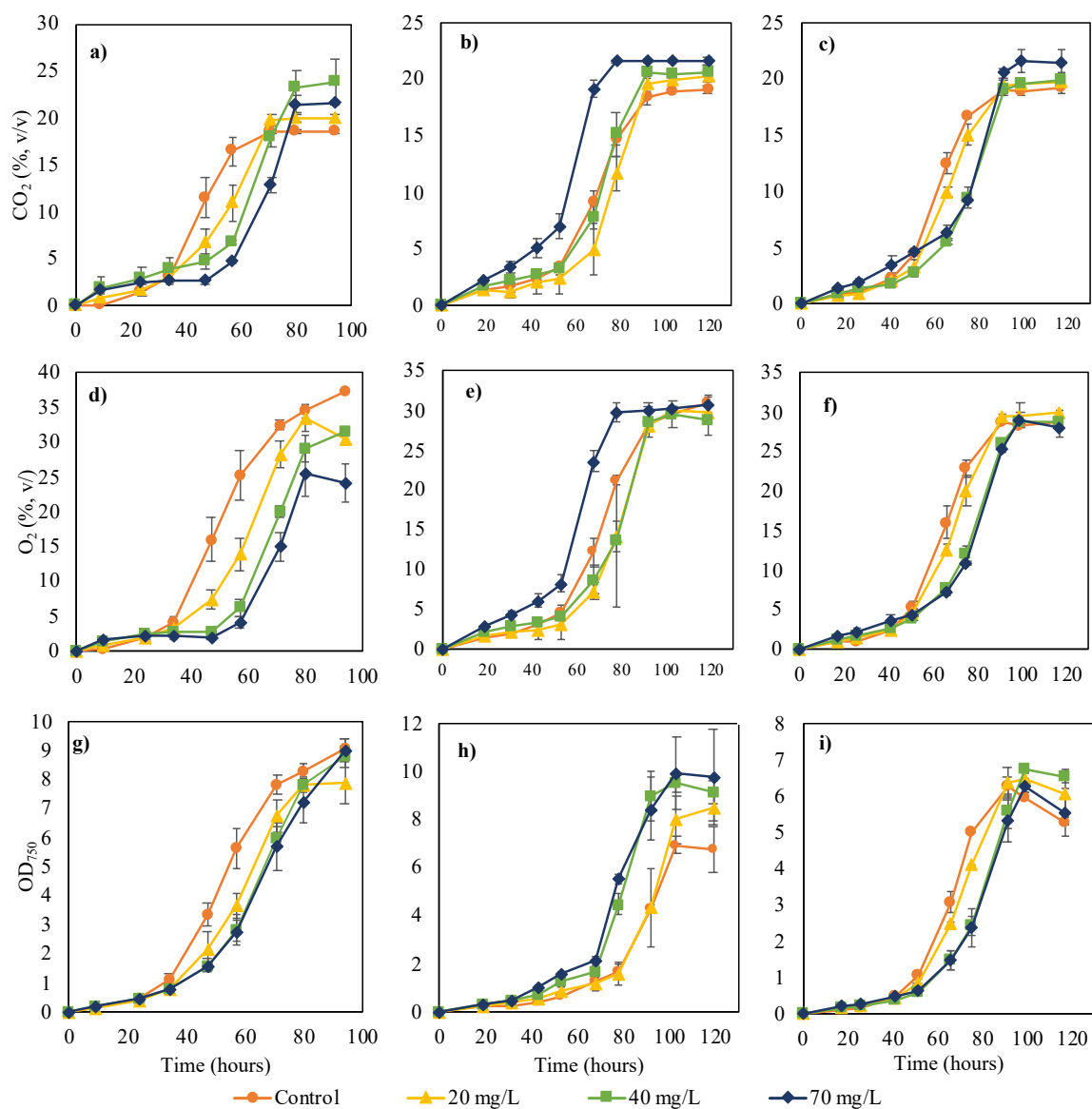


**Fig. 29.** Time course of the cumulative CO<sub>2</sub> consumption in the assays supplied with different concentrations of a) Fe<sub>2</sub>O<sub>3</sub> NPs, b) CaCOI NPs, c) SiO<sub>2</sub> NPs; of the cumulative O<sub>2</sub> production in the tests supplemented with different concentrations of d) Fe<sub>2</sub>O<sub>3</sub> NPs, e) CaCOI NPs, f) SiO<sub>2</sub> NPs; and culture absorbance of the algal consortium supplied with different concentrations of g) Fe<sub>2</sub>O<sub>3</sub> NPs, h) CaCOI NPs, i) SiO<sub>2</sub> NPs. The assays were run under visible light. CaCOI: carbon coated zero valent iron; NPs: nanoparticles.

The addition of Fe<sub>2</sub>O<sub>3</sub> NPs did not enhance the carbohydrates or lipids content of the algal biomass (**Fig. 30a**) as previously reported by Bibi and co-workers (2021). However, these authors observed that the total lipid content of *C. vulgaris* depends on the time of exposure, and the long term exposure to high Fe<sub>2</sub>O<sub>3</sub> NPs concentration resulted in a lipid degradation mediated by a defense mechanism of microalgae against ROS. Thus, the lower lipid content recorded in the assays containing 70 mg L<sup>-1</sup> of Fe<sub>2</sub>O<sub>3</sub> NPs is supported by the long term exposure to Fe<sub>2</sub>O<sub>3</sub> and to the presence of ROS (Bibi et al., 2021). Finally, the results herein obtained suggests that Fe<sub>2</sub>O<sub>3</sub> NPs acted as CO<sub>2</sub> adsorbents and increased CO<sub>2</sub> availability in the cultivation broth, a phenomenon which has been previously observed in a larger extent at increasing CO<sub>2</sub> concentrations (Hakim, Marliza, Abu Tahari, Wan Isahak, et al., 2016). However, the nature of Fe<sub>2</sub>O<sub>3</sub> NPs to Fenton reactions and the formation of ROS interfered in the biomass production and macromolecular accumulation in the microalgae herein used.

Compared to the assays with Fe<sub>2</sub>O<sub>3</sub> NPs, the addition of CACOI NPs did not increase the lag phase of algal metabolism. Indeed, the addition of 70 mg L<sup>-1</sup> of CACOI NPs enhanced both P<sub>x</sub> and the rates of CO<sub>2</sub> consumption, and reduced the lag phase (**Fig. 29b, 29e, 29h**). The cumulative CO<sub>2</sub> consumption in the 70 mg L<sup>-1</sup> CACOI assays was 13% higher than in the control tests. The latter confirms the fact that CACOI NPs stimulated the CO<sub>2</sub> adsorption mainly by the nature of the material, and the increased CO<sub>2</sub> consumption could be mainly attributed to the higher CO<sub>2</sub> availability in the headspace of the bottles. Notwithstanding, the increasing concentrations of CACOI NPs did not impact significantly on the cumulative O<sub>2</sub>



production and  $OD_{750}$ . However the lag phase was significantly increased by the addition of the CACOI NPs, and was related to the increasing concentration. On the other hand, the carbohydrate content of the algal biomass increased by a factor of 2.6 when the cultivation broth was supplemented with  $70 \text{ mg L}^{-1}$ , which can be explained by the superior  $\text{CO}_2$  biofixation mediated by the NPs (Vargas-Estrada et al., 2020). Thus, the higher  $\text{CO}_2$  availability mediated by CACOI NPs at  $70 \text{ mg L}^{-1}$  stimulated the activity of the RuBisCO enzyme, which is widely known to be the catalyst of  $\text{CO}_2$  biofixation (Vaz et al., 2020). Therefore, an enhanced  $\text{CO}_2$  biofixation resulted in an increased biomass productivity during the logarithmic growth phase, and in the accumulation of high-value products (Vaz et al., 2020). Hence, the improved logarithmic phase coupled to the accumulation of carbohydrates confirms that the biofixation capacity of microalgae was significantly improved by the addition of  $70 \text{ mg L}^{-1}$  of CACOI NPs.

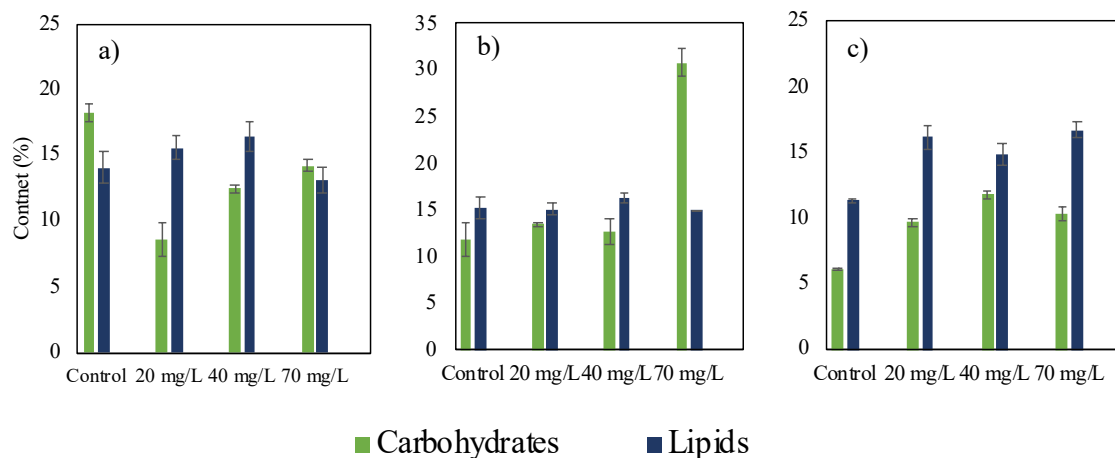


**Fig. 30.** Influence of the concentration of a)  $\text{Fe}_2\text{O}_3$  NPs; b) CACOI NPs; c)  $\text{SiO}_2$  NPs on the carbohydrate (green) and lipid (blue) content of microalgae biomass at the end of the assays under visible light. CACOI: carbon coated zero valent iron; NPs: nanoparticles.

Finally, the addition of 70 mg L<sup>-1</sup> of SiO<sub>2</sub> NPs led to a cumulative CO<sub>2</sub> consumption 11.50% higher than that of the control, thus confirming that SiO<sub>2</sub> NPs acted as CO<sub>2</sub> adsorbents mediating a faster CO<sub>2</sub> dissolution in the algal broth. Notwithstanding, the addition of 40 and 70 mg L<sup>-1</sup> of SiO<sub>2</sub> NPs resulted in a longer lag phase while no statistical difference was observed on the P<sub>x</sub>. Even if the addition of SiO<sub>2</sub> NPs induced higher cumulative CO<sub>2</sub> consumptions, no statistical difference was observed neither in the cumulative O<sub>2</sub> production nor in OD<sub>750</sub>, which did not agree with the observations of Jeon and co-workers (2017). The latter confirms the fact that the exposure to NPs is species specific and even if the addition of SiO<sub>2</sub> NPs has been reported to enhanced biomass and lipid production in *Chlorella vulgaris*, the mixed culture used in this chapter did not experience the same beneficial effects. Interestingly, the addition of SiO<sub>2</sub> NPs enhanced both the carbohydrate and lipid content of the final biomass regardless of the NPs concentration tested. For instance, the addition of 40 mg L<sup>-1</sup> SiO<sub>2</sub> NPs supported the highest carbohydrate content, which was 1.91-fold higher than that in the control assays. Similarly, enhancements in the lipid content ranging by a factor 1.3- 1.5 were obtained when SiO<sub>2</sub> NPs were supplemented to the algal broth. Thus, the superior accumulation of carbohydrates and lipids can be explained by the fact that the addition of SiO<sub>2</sub> NPs created a stress environment to the microalgae and, as a response, carbohydrates were accumulated as an energy reserve (Romero et al., 2020). On the other hand, lipid accumulation can be explained by the fact that the SiO<sub>2</sub> NPs induced an oxidative stress to microalgae, resulting in a lipid accumulation as a nonenzymatic antioxidant mechanism of defense to scavenge the excessive ROS (Wang et al., 2021). Similar findings have been reported by Jeon et al (Jeon et al., 2017), who reported lipid

enhancements of up to 340% compared to the control mainly attributed to the environmental stress created by the NPs. Thus, our results suggest that the SiO<sub>2</sub> NPs served as CO<sub>2</sub> adsorbents, however the nature of the NPs to created stress conditions that limited the growth of microalgae. Nonetheless, the SiO<sub>2</sub> NPs can be used as a technique to improve the value of the produced biomass.

### **3.4 Influence of nanoparticle concentration under UV-visible light**

Solar *UV* radiation can seriously affect microalgae integrity and biological function, since it induces the production of ROS (Rastogi et al., 2020). However, Yang et al. (Yang et al., 2022) recently proved that *UV*-light mediated a positive effect on CO<sub>2</sub> capture and lipid production in *C. pyrenoidosa* when graphene oxide quantum dots were added. In this context, NPs could act as *UV* protectors and/or spectrum converters to promote microalgae growth and macromolecule accumulation.

In our study, the addition of Fe<sub>2</sub>O<sub>3</sub> NPs supported an enhancement of up to 50% in Px compared to the control (**Table 12**). However, no statistical difference was observed in the cumulative CO<sub>2</sub> consumption between the assays (**Fig. 31**). Furthermore, the cumulative O<sub>2</sub> decreased as the NPs concentration increased. Interestingly, despite the cumulative O<sub>2</sub> concentration was reduced by 30% at 70 mg L<sup>-1</sup> Fe<sub>2</sub>O<sub>3</sub> NPs, the OD<sub>750</sub> and Px were 26% and 5% higher than in the control, respectively. The latter suggests that when Fe<sub>2</sub>O<sub>3</sub> NPs were added, the reduction in O<sub>2</sub> content in the headspace did not entail a lower cell growth and this particular behavior can be attributed to the interactions between O<sub>2</sub> and the NPs, which likely caused the formation of ROS. Additionally, the presence of 70 mg L<sup>-1</sup> of Fe<sub>2</sub>O<sub>3</sub> NPs

resulted in a carbohydrate enhancement of up to 94% compared to the control assays. However, no statistical difference in term of lipid content was observed among the assays (**Fig. 32**). Moreover, the supply of *UV* light in this test series led to a higher lipid production compared to the assays conducted exclusively with visible light regardless of the addition of NPs. Thus, our results are in agreement with the observations of Yang et al. (2022), who reported that the addition of graphene quantum dots enhanced the photosynthetic activity and the CO<sub>2</sub> fixation of *Chlorella pyrenoidosa* when exposed to *UV*-light. Additionally, Dinc et al (2022) has also observed beneficial effects on *C. vulgaris* growth by the addition of Se NPs under *UV* light, mainly because the NPs scavenge the *UV* radiation, protecting the microalgal cells. Thus, the Fe<sub>2</sub>O<sub>3</sub> NPs herein used stimulated microalgae growth at the highest concentration tested, suggesting that Fe<sub>2</sub>O<sub>3</sub> can scavenge the harmful effect of *UV* radiation resulting in high-value biomass productivity.

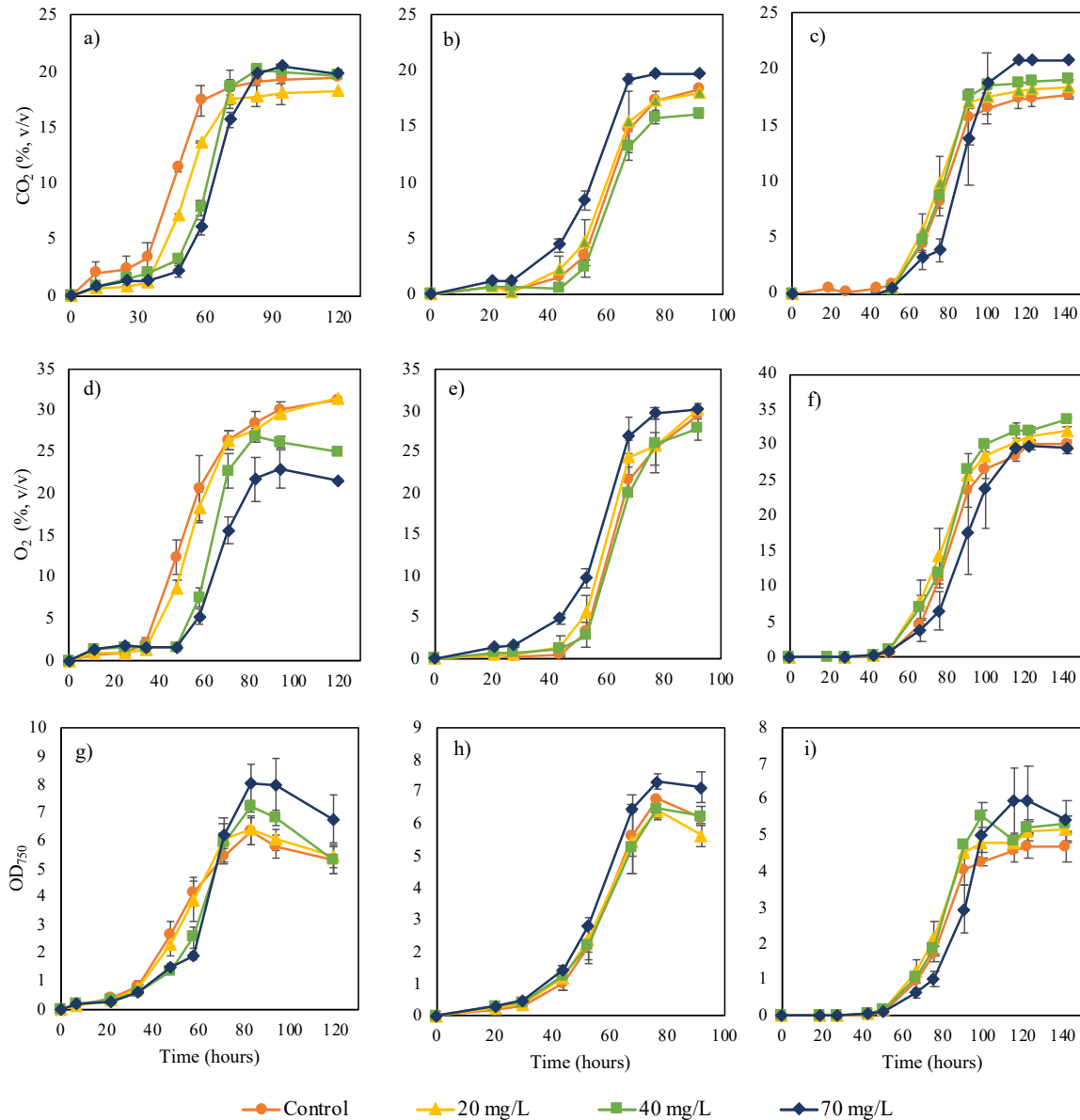


**Fig. 31.** Time course of the cumulative CO<sub>2</sub> consumption in the assays supplied with different concentrations of a) Fe<sub>2</sub>O<sub>3</sub> NPs, b) CaCOI NPs, c) SiO<sub>2</sub> NPs; of the cumulative O<sub>2</sub> production in the tests supplemented with different concentrations of d) Fe<sub>2</sub>O<sub>3</sub> NPs, e) CaCOI NPs, f) SiO<sub>2</sub> NPs; and culture absorbance of the algal consortium supplied with different concentrations of g) Fe<sub>2</sub>O<sub>3</sub> NPs, h) CaCOI NPs, i) SiO<sub>2</sub> NPs. The assays were run under UV+visible light. CaCOI: carbon coated zero valent iron; NPs: nanoparticles.

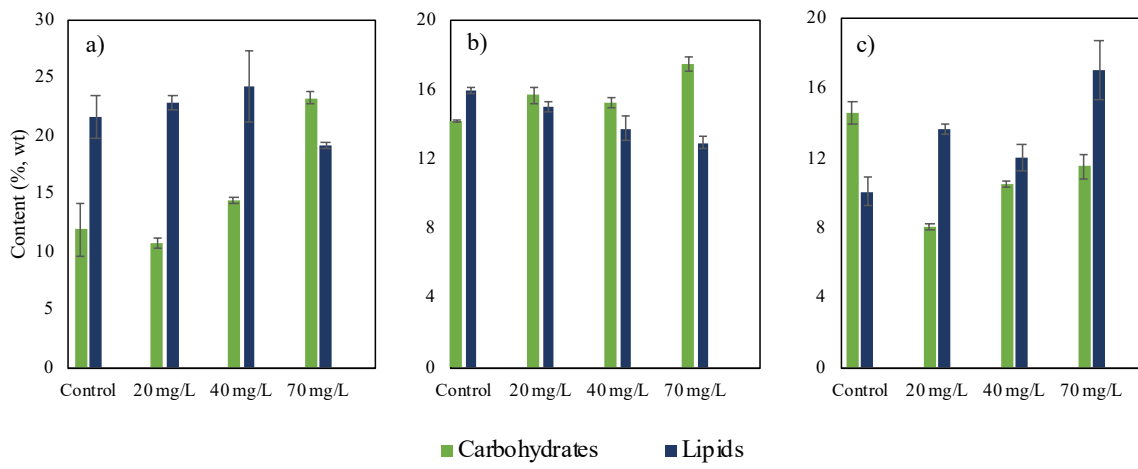


**Fig. 32.** Influence of the concentration of a) Fe<sub>2</sub>O<sub>3</sub> NPs; b) CACOI NPs; c) SiO<sub>2</sub> NPs on the carbohydrate (green) and lipid (blue) content of microalgae biomass at the end of the assays under *UV*+visible light. CACOI: carbon coated zero valent iron; NPs: nanoparticles.

On the other hand, despite the increase in CACOI NPs concentration from 20 to 70 mg L<sup>-1</sup> did not enhance Px, the addition of 70 mg L<sup>-1</sup> of NPs resulted in a faster exponential phase and a statistically significant CO<sub>2</sub> consumption enhancement. Interestingly, there was no statistical difference in the cumulative O<sub>2</sub> production between the assays, and the lipid production slightly decreased as the NPs concentration increased. Since this behavior was not observed in the assays carried out only with visible light, the latter suggest that lipid peroxidation in this particular test series was induced by ROS formation mediated by the interaction of the zero valent iron contained in the NPs and the *UV* light exposure (Yang et al., 2022). However, the addition of 70 mg L<sup>-1</sup> induced a carbohydrate content enhancement of up to 22% and an OD<sub>750</sub> 15% higher than the control. The results herein obtained confirm the fact that CACOI NPs effect of microalgae are mainly as CO<sub>2</sub> adsorbents, resulting in enhanced CO<sub>2</sub> availability in the headspace of the bottles. Moreover, the

increased CO<sub>2</sub> led to an activation of microalgae metabolism and storage as carbohydrates under both visible and visible + *UV* light.

Finally, the addition of SiO<sub>2</sub> NPs did not support an enhancement in Px despite the addition of 70 mg L<sup>-1</sup> SiO<sub>2</sub> NPs led to a CO<sub>2</sub> consumption 18% higher than that recorded in the control tests. Moreover, the addition of 20 and 40 mg L<sup>-1</sup> of SiO<sub>2</sub> NPs led to 11% and 6% higher O<sub>2</sub> cumulative productions compared to the control tests, respectively. Additionally, OD<sub>750</sub> increased as the NPs concentration increased, and the addition of 70 mg L<sup>-1</sup> SiO<sub>2</sub> induced a OD<sub>750</sub> enhancement of 16%. Furthermore, the addition of 70 mg L<sup>-1</sup> SiO<sub>2</sub> mediated a 69% enhancement in the lipid content compared to the control. Finally, our results indicate that the *UV*-light exposure induce a higher lipid accumulation in microalgae likely due to a mechanism of defense against the generation of ROS (Nguyen et al., 2019a). Interestingly, SiO<sub>2</sub> NPs and *UV* radiation can induce an oxidative stress on microalgae (Jeon et al., 2017). However, in our particular study, neither biomass loss nor lipid peroxidation by the combination of SiO<sub>2</sub> NPs and *UV* radiation was observed. Therefore, our results suggest that the oxidative stress caused by SiO<sub>2</sub> NPs did not increase with *UV* exposure. Thus, even if no biomass enhancements were observed with the addition of SiO<sub>2</sub> NPs neither under visible and visible + *UV* light exposure, contrary to the observed by Jeon et al (2017), these NPs still can be used as a strategy to produce high-value biomass even under *UV* radiation.

## 4. Conclusions and future prospective

$\text{Fe}_2\text{O}_3$ ,  $\text{CaCO}_3$  and  $\text{SiO}_2$  NPs addition to microalgae cultures devoted to biogas upgrading boosted  $\text{CO}_2$  adsorption resulting in high-value biomass. Under visible light, the cumulative  $\text{CO}_2$  consumptions increased as the NPs concentrations increased.  $\text{SiO}_2$  NPs stimulated carbohydrates and lipids production,  $\text{CaCO}_3$  NPs supported both increased  $\text{CO}_2$  consumptions, higher biomass productivities, shorter lag phases and carbohydrate productions. *UV* light supply reduced the beneficial effects of NPs, however, the addition of  $\text{Fe}_2\text{O}_3$  NPs stimulated biomass productivities and carbohydrates, whereas  $\text{CaCO}_3$  NPs supported shorter lag phases, increased  $\text{CO}_2$  consumption and carbohydrates productions. Finally, the addition of  $\text{SiO}_2$  NPs supported lipid production enhancements. Promising results to improve the  $\text{CO}_2$  adsorption couple to biomass production and high-value products were obtained in this chapter. However, it is important to highlight that these particular results were obtained under controlled conditions. In this regard, future studies should be directed to assess the effect of the NPs on microalgae under uncontrolled conditions, *i.e.* real centrate and environmental conditions. Moreover, life cycle assessments, exergy analyses, techno-economic analyses and energy analyses as described in (Aghbashlo et al., 2022), should be considered to assess the sustainability of the process. Finally, the results herein obtained can be scaled-up to pilot plants to boost  $\text{CO}_2$  consumption coupled to microalgae growth. The later could represent a feasible technique to improve the performance of the established technology for photosynthetic biogas upgrading.





# Chapter 7

---

## Effect of carbon coated zero-valent iron nanoparticles on photosynthetic biogas upgrading at pilot-scale

This chapter is adapted from the publication

- Vargas-Estrada, L., Hoyos, E. G., Méndez, L., Sebastian, P. J., & Muñoz, R. Send to Sustainable Chemistry and Pharmacy. Boosting photosynthetic biogas upgrading via carbon-coated zero-valent iron nanoparticle addition: a pilot proof of concept study.



## 1. Introduction

The recent announcement by the European Commission to reduce at least 50% of the European greenhouse gas emissions by 2030 rely on a decarbonized economy based on renewable electricity and biomethane (Brémond et al., 2021). Gas infrastructure, which has been considered as the battery of the future European energy system, will play a key role to reach these environmental targets (Brémond et al., 2021). In the past decade, biogas production via anaerobic digestion has experienced a rapid growth based its potential to generate a renewable energy source while sustainably managing organic wastes (Ángeles et al., 2021; Brémond et al., 2021; Ferreira et al., 2019; Mulu, M'Arimi, et al., 2021). The typical composition of biogas is 55-75% methane ( $\text{CH}_4$ ), 30-50% carbon dioxide ( $\text{CO}_2$ ),  $\leq 3\%$  hydrogen sulfide ( $\text{H}_2\text{S}$ ),  $\leq 10\%$  ammonia ( $\text{NH}_3$ ), hydrogen ( $\text{H}_2$ ),  $\leq 1\%$ , nitrogen ( $\text{N}_2$ ),  $\leq 1\%$  and trace levels of halogenated compounds and volatile organic compounds (Aghel et al., 2022; Mulu, M'Arimi, et al., 2021). In this context, biogas upgrading to biomethane has become mandatory prior to its use as fuel for vehicles or its injection into the natural gas grid (Marín et al., 2021; Rodero, Carvajal, et al., 2020). Indeed, the recently enforced European biomethane standard (EN 16723:2018) requires a biogas composed of  $\text{CH}_4 \geq 90\%$ ,  $\text{CO}_2 \leq 2\%$ ,  $\text{O}_2 \leq 1\%$  and negligible amounts of  $\text{H}_2\text{S}$  (Marín et al., 2019).

Nowadays, only physicochemical processes such as cryogenic separation, chemical scrubbing, pressure swing adsorption, organic solvent scrubbing, membrane separation and water scrubbing are available at commercial scale for biogas upgrading (Aghel et al., 2022; Mulu, M'Arimi, et al., 2021). However, these

technologies entail a high energy demand and ecological impacts (Rodero et al., 2018). Thereby, biological processes such as hydrogenotrophic biogas upgrading and upgrading of biogas based on bacterial-algal symbiosis have become a promising eco-friendly option for biogas purification.

Upgrading of biogas based on bacterial-algal symbiosis consist in the CO<sub>2</sub> fixation by microalgae through photosynthesis, which generates valuable biomass that can later be used as raw material for the manufacturing of biofuels of biofertilizers (Ángeles et al., 2021; Rodero, Carvajal, et al., 2020; Rodero et al., 2019). The oxygen released during photosynthesis is used to oxidize the H<sub>2</sub>S contained in biogas by chemolitotrophic bacteria. The nutrients required to support bacterial-algal growth can be supplied by the liquid fraction of digestates. To date upgrading of biogas based on bacterial-algal symbiosis has been widely investigated at pilot and demo-scale (Franco-Morgado et al., 2018; Marín et al., 2020; Meier et al., 2015; Posadas et al., 2015; Rodero, Carvajal, et al., 2020; Toledo-Cervantes et al., 2016; Xu et al., 2015) using algal open ponds interconnected to external biogas purification columns. This technology has supported CO<sub>2</sub> removals of up to 98.6% at both pilot and demo-scale (Rodero, Carvajal, et al., 2020; Rodero, Severi, et al., 2020). However, few technical challenges need to be addressed before moving this green biogas upgrading technology to a commercial level: i) the low CO<sub>2</sub> mass-transfer to the culture broth, ii) the high sensitivity of biomethane quality to variations in the pH of the culture broth and in the liquid and gas flow rates inside the PC, and iii) the diurnal and seasonal variability of environmental parameters influencing photosynthetic activity (Bose et al., 2019).

The low-cost mass transfer of CO<sub>2</sub> from biogas to a scrubbing liquid phase has been a critical limitation in biogas upgrading, and many efforts have been made to overcome this challenge, including the use of nanoporous materials such as metal oxide nanoparticles (NPs) and mesoporous carbons (Dong et al., 2017; Golmakani et al., 2022; Hemmati et al., 2019; Kumar et al., 2020; Ndiaye et al., 2018; Wang et al., 2021). NPs present certain advantages among which are abundant active sites, large surface area-volume ratio, high reactivity, abundant active sites and high adsorption capacity (Anwar et al., 2018; Kumar et al., 2020). Notwithstanding, the addition of NPs to microalgae cultures is a controversial field. Recently, studies have demonstrated that the supplementation of metal NPs and carbon NPs can enhance CO<sub>2</sub> gas-liquid mass transfer and ultimately enhance the biofixation rate of CO<sub>2</sub>. For instance, Jeon et al. (2017) proved that SiO<sub>2</sub> NPs augmented the gas-liquid mass transfer of CO<sub>2</sub>, in *Chlorella vulgaris* cultures, resulting in higher microalgae concentrations. Moreover, the addition of polymeric nanofibers containing Fe<sub>2</sub>O<sub>3</sub> NPs has also been validated as a promising tool to enhance CO<sub>2</sub> biofixation by *Chlorella fusca* (Vaz, Costa, et al., 2019; Vaz et al., 2020; Vaz, Mastrantonio, et al., 2019). Additionally, Kluytmans and co-workers demonstrated that the addition of carbon particles enhanced the interfacial area of the gas-liquid phases in a 2D bubble column (Kluytmans et al., 2003). Despite the fact that the gas-liquid mass transfer of CO<sub>2</sub> is complex and depends on the type of photobioreactor, agitation and gas sparging device, there are three potential mechanisms of NP interaction: 1) gas bubble breaking effect, where NPs promote smaller gas bubble diameters and the gas-liquid diffusion area increases; 2) shuttle effect, where CO<sub>2</sub> is rapidly adsorbed to the NPs surface and then slowly released into the aqueous medium; 3)

hydrodynamic effect, where NPs collide, inducing turbulence and refreshing the liquid-gas boundary layer (Choi et al., 2015). In this context, the addition of NPs into bacterial-algal photobioreactors could boost photosynthetic biogas upgrading, thus resulting in a biomethane that meets international regulations coupled to an enhanced biomass production.

This chapter aimed to elucidate for the first time the effect of carbon-coated zero-valent iron NPs addition to bacterial-algal cultures devoted to upgrading of biogas based on bacterial-algal symbiosis in an indoors pilot scale plant using synthetic biogas.

## **2. Materials and methods**

### **2.1 Nanoparticles**

Carbon-coated zero-valent iron nanoparticles were kindly donated by CALPECH, Spain and will be referred as CALPECH NPs. The surface area, pore volume and average pore diameter of the NPs was determined by a nitrogen physisorption analysis in an ASAP 2050 (Micromeritics, USA) at 77 K. The specific surface area and pore characteristics were determined by the BET method and BJH equation. Scanning electron microscopy (SEM) (JEOL JSM-6490LV) and energy-dispersive spectroscopy (EDS) (EDX-700/800, Hitachi, Japan) were carried out to determine the surface morphology and elemental composition of the target NPs. Moreover, the NPs were added to the bacterial-microalgae consortium at a concentration of 70 mg L<sup>-1</sup>. This concentration was obtained from previous experiments carried out at the

Institute of Sustainable Processes and was considered as the optimal concentration to enhance microalgae growth and CO<sub>2</sub> absorption (data not shown).

## 2.2 Gas-liquid mass transfer rate calculation

The volumetric mass transfer coefficient ( $k$ ) was calculated to elucidate the CO<sub>2</sub> mass transfer with and without the addition of the CALPECH NPs. The liquid-mass transfer assays were carried out in serum bottles of 120 mL with a working volume of 80 mL. The CALPECH NPs were added at a concentration of 70 mg L<sup>-1</sup>, according to (Vargas-Estrada et al., 2022), a control only containing distilled water was also run. Then, the bottles were sealed with butyl rubber seals and aluminum caps, and N<sub>2</sub> was sparged to ensure an oxygen-free headspace, and after that CO<sub>2</sub> was injected until the pressure in the headspace was 151.325 kPa. The bottles were agitated at 300 rpm and the pressure in the headspace was measure to calculate the CO<sub>2</sub> concentration.

## 2.3 Experimental set-up

The indoor pilot system was located in the Institute of Sustainable Processes at the University of Valladolid, Spain. The system was composed of a 180 L algal open pond with an illuminated area of 1.2 m<sup>2</sup>, which was interconnected to a 8 L conical settler, which itself was interconnected to a 2.5 L purification column (PC) (165 cm height × 4.4 cm internal diameter). The algal open pond was agitated at 20 cm s<sup>-1</sup> by a paddle wheel composed of six blades, and was continuously illuminated at a photosynthetic active radiation (PAR) of 1550 ± 70 μmol m<sup>-2</sup> s<sup>-1</sup> by six LED PCBs (Phillips SA, Spain)



of high intensity (**Fig. 33**). The algal open pond was initially inoculated with a microalgal broth composed of *Chlorella* sp. from a similar outdoors experiment as described elsewhere (Méndez et al., 2022). The system was daily fed with 5 L d<sup>-1</sup> of centrate kindly donated by the wastewater treatment plant of Valladolid, Spain. The mean composition of the centrate was: 487 ± 40 mg L<sup>-1</sup> inorganic carbon (IC), 575 ± 32 mg L<sup>-1</sup> total nitrogen (TN) and 76 ± 26 mg L<sup>-1</sup> total organic carbon (TOC). Synthetic biogas with a composition of 0.5% H<sub>2</sub>S, 29.5% CO<sub>2</sub> and 70% CH<sub>4</sub> (Abello, Linde; Spain) was sparged at the bottom of the PC by a stainless steel gas diffuser (pore size 2 μm) at a flow rate of 50 L d<sup>-1</sup>. The PC was maintained at a recirculating L/G ratio of 2. Biomass was daily removed from the settler to establish a continuous productivity of biomass of 22.5 g m<sup>-2</sup> d<sup>-1</sup> to provide a constant microalgae growth according to (Méndez et al., 2022). The settled biomass withdrawn was centrifuged (10000 rpm, 4 °C) and to prevail a zero-effluent process the supernatant was returned to the algal open pond. To counterbalance losses of evaporation, tap water was continuously added to the algal open pond.

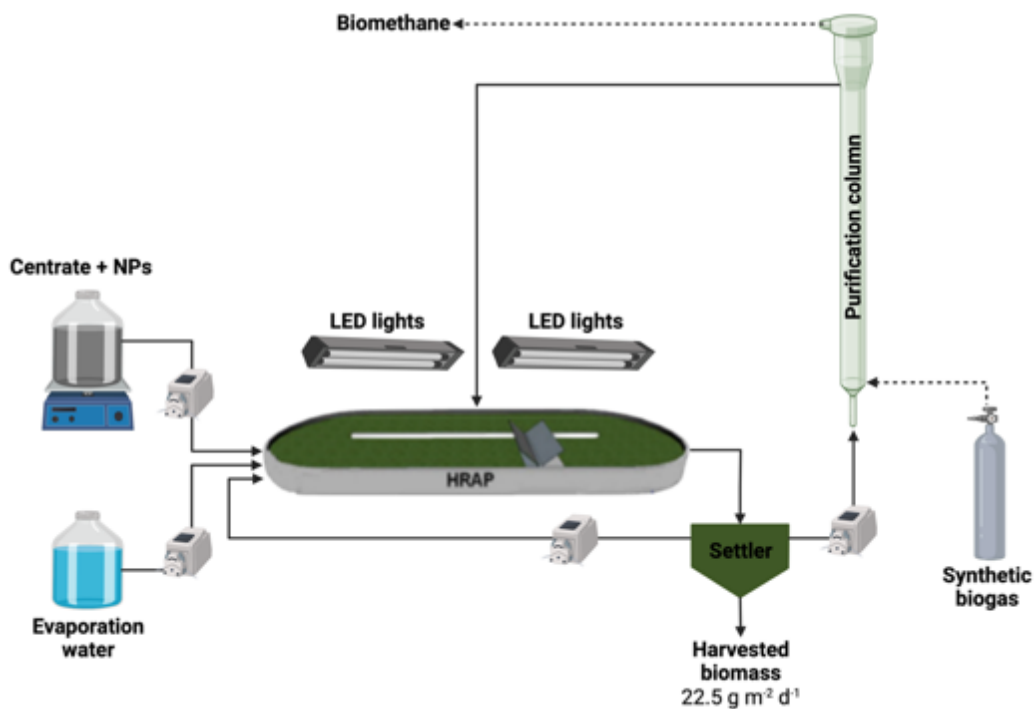


**Fig. 33.** Schematic diagram of the experimental set-up. Continuous and dotted lines represent liquid and gas flow, respectively.

## 2.4 Sampling procedures and operational conditions

The system was initially operated for 20 days with the purpose of acclimate the algal-bacterial communities to indoor conditions. Afterwards, scenario I (days 0-16) was dedicated as a control condition to evaluate the performance of the upgrading of biogas based on bacterial-algal symbiosis in the algal open pond under continuous irradiation in indoors conditions. In scenario II (days 17-46), carbon-coated zero valent iron NPs, kindly provided by CALPECH, Spain, were added to the system at a concentration of  $70 \text{ mg L}^{-1}$  (day 17). CALPECH NPs were daily added at a concentration of  $70 \text{ mg L}^{-1}$  to the centrate fed to the algal open pond. The centrate-

NPs solution was sonicated for one hour to avoid NPs agglomeration and subsequently the centrate-NPs solution was constantly agitated with a magnetic stirrer.

The dissolved oxygen (DO), pH and temperature of the algal open pond culture broth, and the ambient temperature were daily measured. Twice a week, gas samples were taken to determine the content of CO<sub>2</sub>, CH<sub>4</sub>, N<sub>2</sub>, O<sub>2</sub> and H<sub>2</sub>S in the raw biogas and upgraded biomethane in the inlet and outlet of the PC, respectively. Aliquots of 150 mL of the algal open pond culture broth and centrate were taken twice a week in order to obtain the concentration of TN, TOC, IC, , N-NO<sub>2</sub><sup>-</sup>, N-NO<sub>3</sub><sup>-</sup>, S-SO<sub>4</sub><sup>2-</sup>, P-PO<sub>4</sub><sup>3-</sup>, microalgae population structure, volatile suspended solids (VSS) and total suspended solids (TSS).

## **2.5 Analytical procedures**

The temperature and DO of the culture broth were monitored by an OXI 3310 oximeter (WTW, Germany). The pH was measured with a SensION™ + PH3 pHmeter (HACH, Spain). The biogas and biomethane composition was measured in a gas chromatograph with thermal conductivity detection (Bruker, USA) to quantify the content of CO<sub>2</sub>, CH<sub>4</sub>, N<sub>2</sub>, O<sub>2</sub> and H<sub>2</sub>S according to (Posadas et al., 2015). The IC, TN and TOC concentrations were obtained by a Shimadzu TOC-VCSH analyzer (Japan) equipped with a TNM-1 chemiluminescence module. TSS and VSS concentrations were obtained according to standard methods (APHA-AWWA-WPCF, 1999). PAR was monitored by a Li-250 A light meter (Li-COR Biosciences, Germany). N-NH<sub>4</sub><sup>+</sup> concentration was obtained by the Nessler method using a UV-

2550 spectrophotometer Shimadzu, Japan. The concentration of S-SO<sub>4</sub><sup>2-</sup>, N-NO<sub>2</sub><sup>-</sup>, N-NO<sub>3</sub><sup>-</sup>, P-PO<sub>4</sub><sup>3-</sup> were determined by HPLC-IC (Waters 432, conductivity detector, USA). Finally, the quantification and identification of microalgae concentration was carried out by microscopic examination of the algal open pond culture broths, which were fixed with lugol acid at 5% and stored at 4°C before the analysis following standard procedures described elsewhere (Sournia, 1978).

## 2.6 Statistical analysis

One-way ANOVA analysis was conducted to elucidate the effect of NPs. The results are shown as mean values ± standard deviation.

## 3. Results and discussion

### 3.1 Nanoparticles characterization

The CALPECH NPs exhibited a particle size ranging from 50-70 nm and were agglomerated, which is in accordance to (Correcher et al., 2021; Munoz et al., 2021) (**Fig. A4**). Moreover, the EDS analysis showed the presence of elements such as P, K, Ca and S in CALPECH NPs (**Fig. A2**), which could play a key role to stimulate microalgae growth. Additionally, the EDS analysis revealed a Fe content of 8.68% (wt. %). Furthermore, the BET surface area is a typical parameter for the selection of adsorbents, and the higher the surface area, the better the adsorbent capacity (Zhang et al., 2022). However, the pore volume of a material has been more strongly correlated to its adsorption capacity (Zhang et al., 2022). In this particular study, the surface area of the NPs was 27.26 m<sup>2</sup>g<sup>-1</sup>, while the pore volume of the NPs used

accounted for  $0.28 \text{ cm}^3\text{g}^{-1}$ . Finally, the pore diameter of the CALPECH NPs was 41.47 nm. According to the IUPAC classification, the NPs herein used represented mesoporous materials. In this context, the properties observed in the material herein used suggest that CALPECH NPs can act as gas absorbents and positively impact on  $\text{CO}_2$  absorption, resulting in an increased microalgae growth due to a higher  $\text{CO}_2$  availability.

### 3.2 Effect of nanoparticles on the gas-liquid mass transfer rate

The volumetric mass transfer rate of  $\text{CO}_2$  was calculated according to Eq (12) (Jeon et al., 2017; Tseng et al., 2010):

$$q_t = q_e(1 - e^{-kt}) \quad (12)$$

where  $q_t$  is the concentration of  $\text{CO}_2$  adsorbed ( $\text{mg L}^{-1}$ ) at time  $t$  (min),  $q_e$  the concentration of  $\text{CO}_2$  adsorbed at equilibrium ( $\text{mg L}^{-1}$ ), and  $k$  the first-order rate constant of adsorption ( $\text{min}^{-1}$ ).

Eq (12) can be rearranged according to Eq (13):

$$\frac{q_t}{q_e} = 1 - e^{-kt} \quad (13)$$

The changes in the  $\text{CO}_2$  concentration in the headspace of the bottles is shown in **Fig. 34**. The estimated  $k$  values were  $0.18$  and  $0.26 \text{ min}^{-1}$  for the control and CALPECH assays, respectively. Thus,  $k$  was increased by 44% by the addition of the CALPECH NPs. The latter can be attributed to the fact that the NPs induced shuttle effects and hydrodynamic effects that enhanced the  $\text{CO}_2$  transfer to the liquid phase.

Similar findings have been reported elsewhere by (Jeon et al., 2017; Kluytmans et al., 2003). Even if the mechanism of interaction between the NPs and the liquid phase is uncertain, the results herein obtained suggest that CALPECH NPs can promote the CO<sub>2</sub> mass transfer to the liquid phase, which can be beneficial for microalgae CO<sub>2</sub> consumption and biogas upgrading.

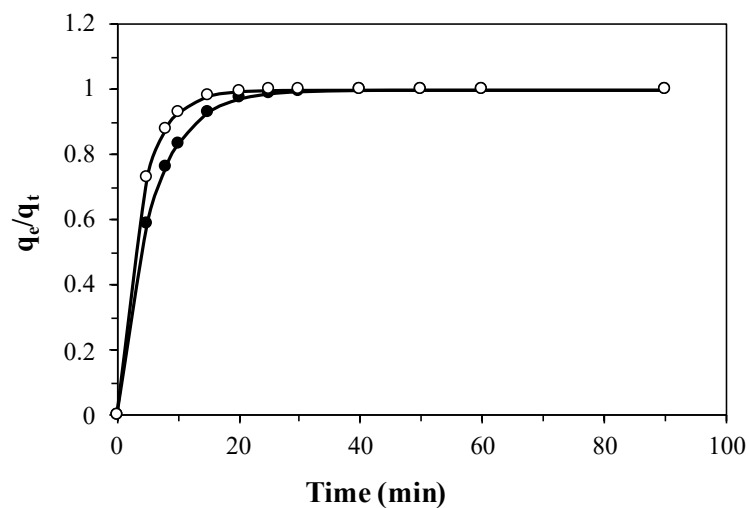


**Fig. 34.** Time course of CO<sub>2</sub> concentration without CALPECH NPs (dark circles) and with CALPECH NPs (empty circles)

### 3.3 Effect of nanoparticles on algal open pond performance

The microalgae population inside the algal open pond remained constant, with *Chlorella* sp. as the dominant species detected during the entire time of the experiment. The dominance of this green microalgae species confirmed its tolerance to the presence of NPs. Interestingly, the number of individuals increased from

$2.7 \times 10^9$  in scenario I to  $2.05 \times 10^{10}$  in scenario II, confirming that the addition of NPs stimulated the growth of *Chlorella* sp. The algal open pond was first inoculated at 2 g VSS L<sup>-1</sup>, but the biomass concentration was gradually reduced to 1.56 g VSS L<sup>-1</sup> during scenario I as a consequence of the adaptation to indoor conditions. The addition of CALPECH NPs during scenario II resulted in a gradual increment in the concentration of the biomass up to 3.26 g VSS L<sup>-1</sup> (**Fig. 35**). Interestingly, the addition of NPs stimulated microalgae growth, causing the accumulation of microalgae biomass inside the algal open pond despite the bacterial-algal biomass withdrawal rate remained constant at 22.5 g m<sup>-2</sup> d<sup>-1</sup>. Interestingly, biomass concentration herein achieved in the presence of NPs were significantly higher than the observed by Marín et al. (2022), Marín et al. (2018) and Méndez et al. (2022) in a similar experimental set-up upgrading synthetic or real biogas (0.55-1.80 g VSS L<sup>-1</sup>). Thus, the enhancement in the concentration of biomass observed in our particular study suggest that biomass productivity can be increased to prevent biomass accumulation in the algal open pond in the presence of NPs.

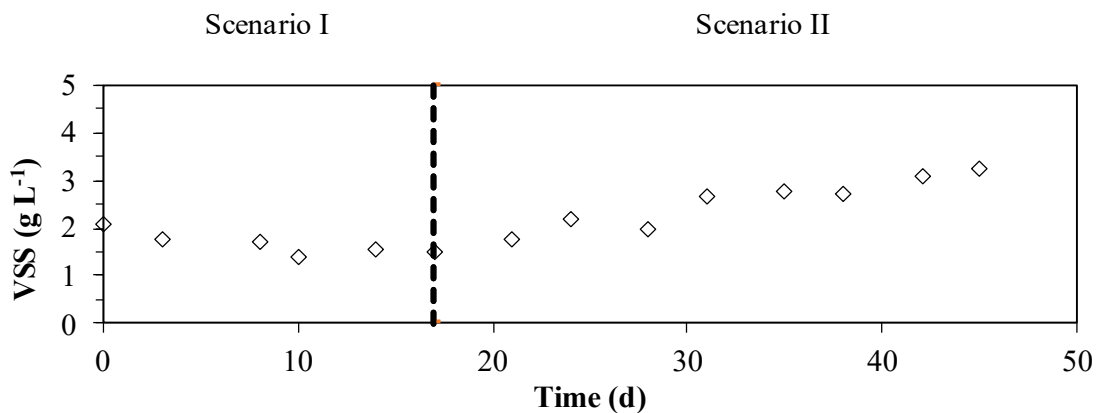


**Fig. 35.** Time course of biomass concentration (VSS g L<sup>-1</sup>) in the algal open pond.

The pH of the algal open pond averaged  $8.55 \pm 0.10$  and  $9.08 \pm 0.15$  in scenario I and II, respectively (**Fig. 36a**). Likewise, the pH at the top of the PC significantly increased from  $7.61 \pm 0.07$  in scenario I to  $7.89 \pm 0.13$  in scenario II (**Fig. 36a**). The lower pH always registered in the PC, in comparison to the pH in the algal open pond, was attributed to medium acidification due to the transfer of  $\text{CO}_2$  and  $\text{H}_2\text{S}$  to the recirculating culture broth (Méndez et al., 2022). This pH increase was correlated to the enhanced photosynthetic activity in the algal open pond (**Fig. 36b**), which also entailed a decrease in IC concentration from an average value of  $699 \pm 255$  in scenario I to  $437 \pm 53$  mg/L in scenario II. In this context, green microalgae such as *Chlorella* preferred  $\text{CO}_2$  and  $\text{HCO}_3^-$  under photoautotrophic growth, and alkaline pHs of 8.5-9 induce the dominance of  $\text{HCO}_3^-$  species (Vargas-Estrada et al., 2020). Indeed, an alkaline pH and sufficient  $\text{CO}_2$  supply activate the RuBisCO enzyme, responsible for  $\text{CO}_2$  biofixation (Vargas-Estrada et al., 2020). Thus, our results suggest that photosynthetic activity and  $\text{CO}_2$  biofixation were increased by the addition of NPs. Moreover, the low concentration of IC of the algal open pond culture broth recorded in our particular study ( $<1000$  mg  $\text{L}^{-1}$ ) were related to the low IC concentration in the centrate,  $464 \pm 29$  and  $504 \pm 38$  mg  $\text{L}^{-1}$  in scenario I and II, respectively. Interestingly, even if IC concentrations in our particular study were lower than the optimal values previously reported to maintain the high pH and buffer capacity needed for an effective biogas upgrading performance (IC  $> 1000$  mg  $\text{L}^{-1}$ ) (Marín et al., 2021; Marín, Posadas, Cano, Pérez, Blanco, et al., 2018; Méndez et al., 2022; Rodero, Severi, et al., 2020), the pH in the algal open pond culture broth prevailed above 9 during scenario II without the need of any external  $\text{NaHCO}_3$  or



$\text{Na}_2\text{CO}_3$  supplementation. In this context, the addition of CALPECH NPs played a key role in the algal open pond performance, not only by enhancing biomass productivity but also by maintaining a satisfactory biogas upgrading performance (see section 3.4 of this chapter) at low IC concentrations. Nevertheless, it is important to highlight that the concentration of IC in the algal open pond suffered declined from 530 to 374  $\text{mg L}^{-1}$  at the end of scenario II, mainly due to the increased photosynthetic activity induced by the addition of NPs. Likewise, the pH in the algal open pond culture broth experienced a slight pH drop to 8.86. This decrease in the pH of the algal open pond, together with the reduced buffer capacity of the recirculating broth, mediated a decrease in the pH of PC from 8.29 to 7.67.

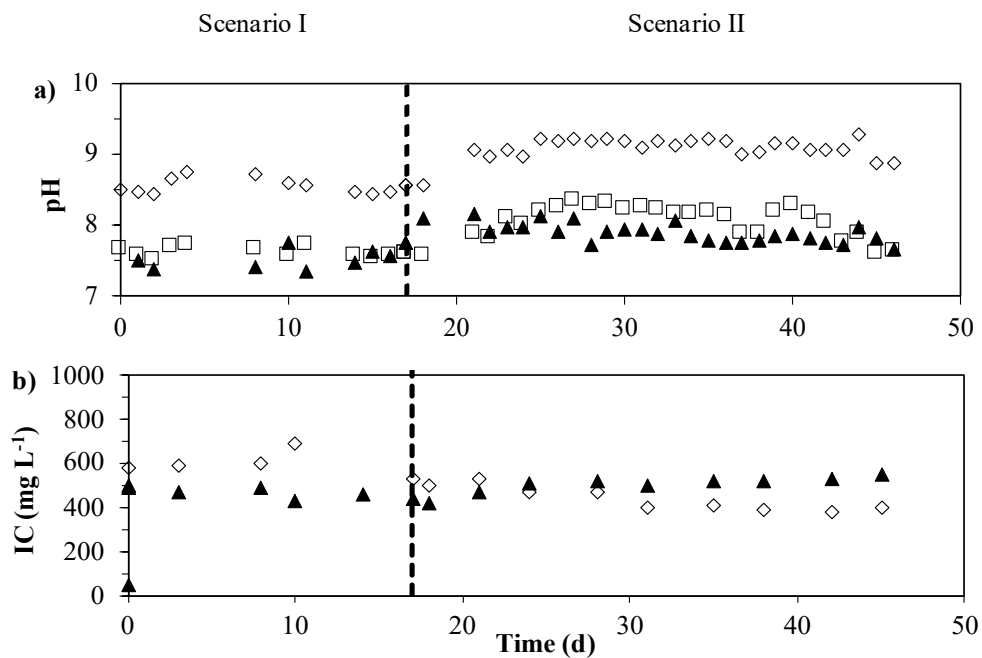


**Fig. 36.** Time course of a) pH and b) inorganic carbon concentration in the cultivation broth of the algal open pond (empty diamonds), purification column (empty squares) and centrate (solid triangles).

The DO concentrations of the algal open pond culture broth augmented from average values of  $11.23 \pm 3.20$  mg L<sup>-1</sup> in scenario I to  $16.51 \pm 4.61$  mg L<sup>-1</sup> in scenario II (**Fig. 37a**). The DO concentration is highly sensitive to light and temperature, which remained constant under indoor conditions, and therefore, the significant variations in DO herein recorded can be attributed to the presence of NPs (**Table 17**). Thus, the increase in DO in our particular study was attributed to the enhanced photosynthetic activity.

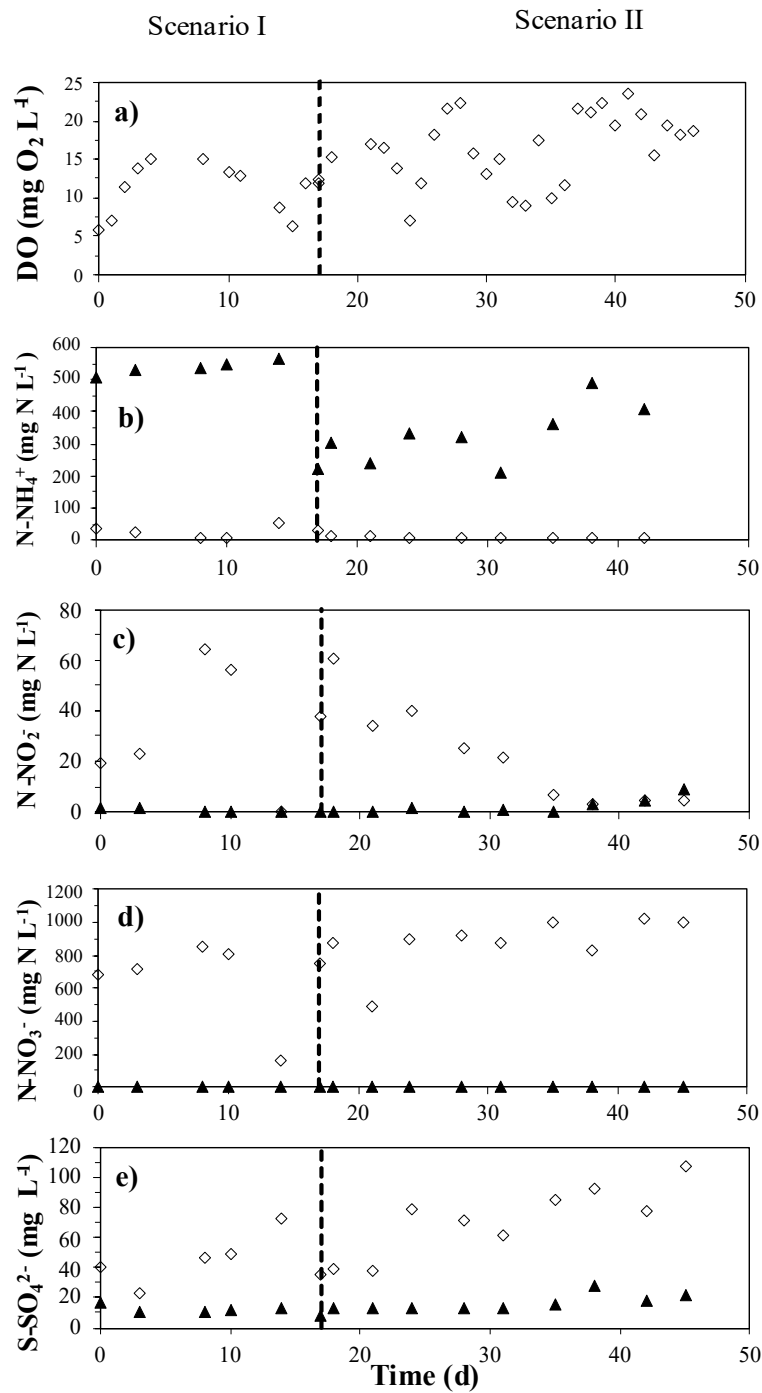


**Fig. 37.** Time course of a) dissolved oxygen, b) N-NH<sub>4</sub><sup>+</sup>, c) N-NO<sub>2</sub><sup>-</sup>, d) N-NO<sub>3</sub><sup>-</sup> and e) S-SO<sub>4</sub><sup>2-</sup> concentrations in the cultivation broth of the algal open pond (empty diamonds) and centrate (solid triangles).

**Table 17.** Environmental and operational parameters of algal open pond during the experiment

	<b>Scenario I</b>	<b>Scenario II</b>
Algal open pond Temperature ( °C)	24.1 ± 0.8	23.9 ± 1.5
Ambient Temperature (°C)	20.9 ± 1.0	20.2 ± 0.8
Light intensity (mol m <sup>-2</sup> s <sup>-1</sup> )	1719 ± 312	1590 ± 32
Evaporation (L m <sup>-2</sup> d <sup>-1</sup> )	8.5 ± 1.0	7.8 ± 0.7
Biomass withdrawal (g m <sup>-2</sup> d <sup>-1</sup> )	22.5	22.5

The dissolved TOC concentrations, which averaged  $291 \pm 58$  mg L<sup>-1</sup> and  $77 \pm 27$  mg L<sup>-1</sup> in the culture broth of the algal open pond and the centrate, respectively, remained constant between scenarios. The accumulation of TOC in the culture broth under zero effluent operation, even at low TOC concentrations in the centrate, has been previously observed by Posadas et al. (2016) and can be explained by the recalcitrant properties of the organic compounds and cell lysis of the culture broth (Méndez et al., 2022; Posadas et al., 2016). At this point it should be stressed that the addition of NPs did not have an impact neither in the TOC concentration of the centrate nor in the culture broth, despite the fact that CALPECH NPs are covered with carbon, and activated carbon can remove soluble organic compounds from wastewater (Jeswani et al., 2015). However, the CALPECH NPs herein used are covered by a non-activated mesoporous carbon (Correcher et al., 2021) and its effectiveness has only be assessed with micropollutants such as diclofenac, sulfamethoxazole and metronidazole (Munoz et al., 2021). In this context, the pore

volume and average pore diameter ( $0.28 \text{ cm}^3 \text{ g}^{-1}$  and  $41.47 \text{ nm}$  respectively) of the CALPECH NPs herein used were higher than those previously reported by Munoz and collaborators (Munoz et al., 2021), which could have influenced the organic matter removal performance of the CALPECH NPs.

TN concentrations in the algal open pond culture broth prevailed unchanged throughout the study (**Table 18**), reaching mean concentrations of  $825 \pm 243 \text{ mg L}^{-1}$  and  $982 \pm 83 \text{ mg L}^{-1}$  in scenario I and II, respectively. Moreover, the TN concentration in the centrate prevailed constant at  $552 \pm 23 \text{ mg L}^{-1}$  and  $591 \pm 30 \text{ mg L}^{-1}$ , respectively (**Table 18**). Moreover, the concentration of  $\text{N-NH}_4^+$  in the centrate significantly decreased from scenario I ( $484 \pm 129 \text{ mg L}^{-1}$ ) to scenario II ( $333 \pm 90 \text{ mg L}^{-1}$ ) (**Fig. 37b**), whereas the concentration of  $\text{N-NH}_4^+$  remained almost negligible in the culture broth of the algal open pond. This intensive  $\text{N-NH}_4^+$  consumption was likely supported by microalgae growth, since  $\text{N-NH}_4^+$  is the preferred nitrogen source of green microalgae, and by the nitrification of  $\text{N-NH}_4^+$  to  $\text{N-NO}_3^-$  and  $\text{N-NO}_2^-$ . Interestingly, the concentration of  $\text{N-NO}_2^-$  (**Fig. 37c**) and  $\text{N-NO}_3^-$  (**Fig. 37d**) in the culture broth of the algal open pond confirmed the prevailing nitrification process. Hence,  $\text{N-NO}_2^-$  concentrations averaged  $40 \pm 20 \text{ mg L}^{-1}$  during scenario I, and gradually decreased from  $60.35 \text{ mg L}^{-1}$  to  $4.16 \text{ mg L}^{-1}$  along scenario II. Moreover, the  $\text{N-NO}_3^-$  concentrations remained constant in both scenarios, with mean concentrations of  $791 \pm 223 \text{ mg L}^{-1}$ . The recorded depletion of  $\text{N-NO}_2^-$  was attributed to its oxidation to  $\text{N-NO}_3^-$  driven by the enhanced DO and IC prevailing in the culture broth.

**Table 18.** TN, TOC and P-PO<sub>4</sub><sup>3-</sup> concentrations in the centrate and cultivation broth of the algal open pond during the experiment

	<b>Scenario I</b>	<b>Scenario II</b>
Centrate TN (mg L <sup>-1</sup> )	552 ± 23	591 ± 30
Algal open pond TN (mg L <sup>-1</sup> )	825 ± 243	982 ± 83
Centrate TOC (mg L <sup>-1</sup> )	75 ± 32	78 ± 24
Algal open pond TOC (mg L <sup>-1</sup> )	278 ± 89	299 ± 26
Centrate P-PO <sub>4</sub> <sup>3-</sup> (mg L <sup>-1</sup> )	152 ± 10	119 ± 25
Algal open pond P-PO <sub>4</sub> <sup>3-</sup> (mg L <sup>-1</sup> )	116 ± 12	105 ± 17

P-PO<sub>4</sub><sup>3-</sup> content in the centrate significantly decreased from 152 ± 10 mg L<sup>-1</sup> in scenario I to 119 ± 25 mg L<sup>-1</sup> in scenario II as a result of variations in the operation of Valladolid wastewater treatment plant. Interestingly, even if the photosynthetic activity increased in scenario II, the concentration of P-PO<sub>4</sub><sup>3-</sup> in the culture broth of the algal open pond did not present a significant difference between both scenarios, averaging 110 ± 16 mg L<sup>-1</sup>. Praveen and coworkers (2018) observed that microalgae cultivated in the presence of N-NO<sub>3</sub><sup>-</sup> resulted in a lower demand for P-PO<sub>4</sub><sup>3-</sup>. In our study, the concentration of N-NO<sub>3</sub> in the algal open pond culture broth was around 1000 mg L<sup>-1</sup>, thus supporting the reduced P-PO<sub>4</sub><sup>3-</sup> uptake by microalgae.

Finally, S-SO<sub>4</sub><sup>2-</sup> concentration in the centrate prevailed constant during both scenarios, with mean concentrations of 15 ± 5 mg L<sup>-1</sup>. Nevertheless, the concentration of S-SO<sub>4</sub><sup>2-</sup> in the algal open pond culture broth increased from an average of 45 ± 17 in scenario I to 73 ± 23 mg L<sup>-1</sup> in scenario II (**Fig. 37e**). The later increase can be

explained by the constant supply of H<sub>2</sub>S via biogas sparging in PC and to the high DO concentrations recorded during scenario II (induced by the addition of CALPECH NPs), the latter supporting H<sub>2</sub>S oxidation to SO<sub>4</sub><sup>2-</sup> (Rodero, Severi, et al., 2020).

### 3.4 Effect of nanoparticles on biogas upgrading performance

CH<sub>4</sub> content in the biomethane averaged  $83.9 \pm 5.0$  % and  $90.8 \pm 2.2$  % in scenario I and II, respectively (**Fig. 38a**), with a maximum content of 93.7 % recorded during scenario II. Marín and coworkers (Marín et al., 2020) reported similar CH<sub>4</sub> contents in photosynthetically upgraded biomethane at similar L/G ratios but in systems operated with highly carbonated (IC > 1200 mg L<sup>-1</sup>) mineral salt medium. Concomitantly, the CO<sub>2</sub> content in the upgraded biomethane significantly decreased from  $6.3 \pm 0.5$  % in scenario I to  $3.6 \pm 1.5$  % in scenario II (**Fig. 38b**), corresponding to CO<sub>2</sub> removal efficiencies (REs) of  $86.2 \pm 1.1$  % and  $92.1 \pm 3.1$  %, respectively. Similar CO<sub>2</sub>-REs (> 80%) have been reported by Posadas and coworkers (2017) and Marín and coworkers (2021) at a relatively higher alkalinity (IC > 1300 mg L<sup>-1</sup>). It has been widely observed that high alkalinities in the algal open pond culture broth (> 1000 mg L<sup>-1</sup>), along with pH values > 9, support an enhanced CO<sub>2</sub> mass transfer to the recirculation culture broth in PC (Franco-Morgado et al., 2018). Posadas and coworkers (2017) and Méndez and coworkers (2022) reported that digestate supplementation with NaHCO<sub>3</sub> and Na<sub>2</sub>CO<sub>3</sub> was needed to increase the concentration of IC in the culture broth > 1600 mg L<sup>-1</sup>. In our particular study, the

addition of CALPECH NPs supported high CO<sub>2</sub>-REs during scenario II due to the improved upgrading of biogas based on bacterial-algal symbiosis, which raised the pH in both the algal open pond and PC. However, the gradual drop of pH at the end of scenario II, attributed to the active photosynthetic IC consumption, resulted in a CO<sub>2</sub> content of 4.9%, and a CO<sub>2</sub>-REs of 88.4 %. Moreover, H<sub>2</sub>S was not detected in the biomethane in scenario I or II, suggesting that the H<sub>2</sub>S present in the raw biogas was oxidized to SO<sub>4</sub><sup>2-</sup> (Ángeles et al., 2021).

Furthermore, O<sub>2</sub> content in the biomethane significantly decreased by 50% in scenario II, averaging  $1.6 \pm 0.6$  % in scenario I and  $0.8 \pm 0.3$  % in scenario II (**Fig. 38c**). Moreover, the N<sub>2</sub> concentration in biomethane significantly decreased from  $7.9 \pm 4.3$  % in scenario I to  $4.4 \pm 0.9$  % in scenario II (**Fig. 38d**). At this point, is important to mention that the operational L/G ratio of 2 used in scenario I and II typically result in high O<sub>2</sub> and N<sub>2</sub> contents in the upgraded biomethane, that are in between 3 to 6.7 % and 0.5 to 2.8 %, respectively (Marín et al., 2020; Méndez et al., 2022; Posadas et al., 2017). Interestingly, the concentrations of O<sub>2</sub> and N<sub>2</sub> recorded in the upgraded biomethane suggested that the addition of CALPECH NPs played an important role in the O<sub>2</sub> and N<sub>2</sub> stripping to the biomethane. Indeed, CALPECH NPs herein used exhibited a mesoporous surface (**Fig. A1**) where both N<sub>2</sub> and O<sub>2</sub> could have been adsorbed, thus reducing the levels of these biogas pollutants.

Even if the mechanisms governing the interactions between NPs and microalgae still remains uncertain, Choi and coworkers (2015) described three potential mechanisms underlying the observed CO<sub>2</sub> capture enhancement by SiO<sub>2</sub> NPs: breaking effect, shuttle effect and the hydrodynamic effect. Kluytmans and



coworkers (2003) also showed that CO<sub>2</sub> mass transfer in a 2D bubble column containing activated carbon particles was enhanced by an increased interfacial area of the gas-liquid phases, mainly caused by the addition of the particles and the electrolyte. In this context, the results obtained in our particular study suggested that the mass-transfer of CO<sub>2</sub> in PC during scenario II was enhanced by the addition of CALPECH NPs. However, the IC in the HRAP was not increased by the addition of CALPECH NPs, which suggest that 1) the CO<sub>2</sub> could have been adhered to the NPs surface or 2) microalgae rapidly consumed the CO<sub>2</sub>, thus resulting in an increased biomass concentration. Anyhow, the addition of CALPECH NPs entailed an enhancement in the pH of the culture broth in the algal open pond, boosting the performance in both biomass production and biogas upgrading. The addition of CALPECH NPs can be a promising technique to overcome one of the major limitations of photosynthetic biogas upgrading such as the CO<sub>2</sub> mass transfer from the biogas.

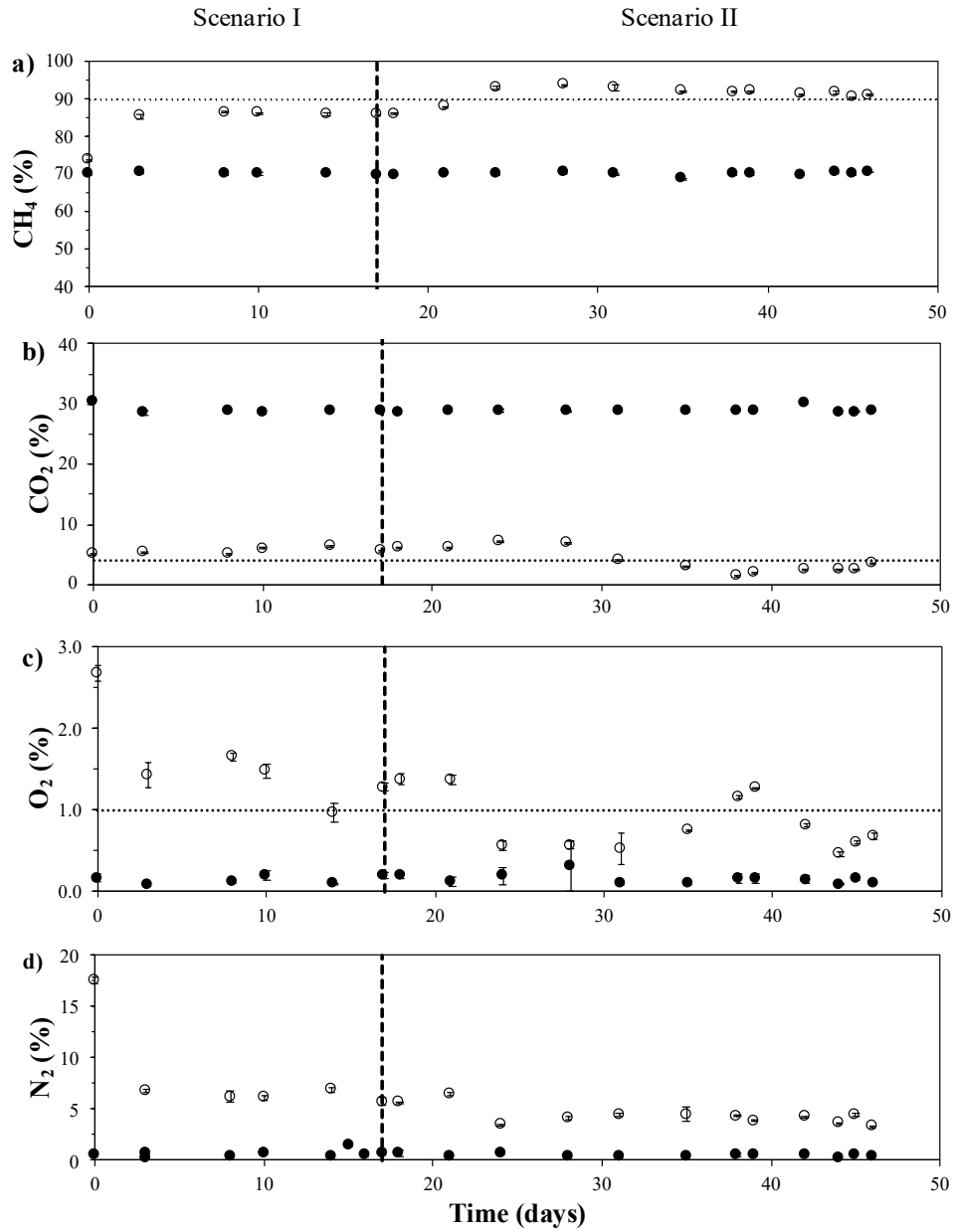


**Fig. 38.** Time course of the concentration of a) CH<sub>4</sub>, b) CO<sub>2</sub>, c) O<sub>2</sub>, d) N<sub>2</sub> in the synthetic biogas (solid circles) and in biomethane (empty circles). Note: the dotted lines denote the limits of the European regulations.

## 4. Conclusions

The addition of carbon-coated zero-valent NPs boosted the performance of photosynthetic biogas upgrading at low alkalinities ( $IC < 1000 \text{ mg L}^{-1}$ ), supporting  $\text{CO}_2$ -REs and  $\text{CH}_4$  contents  $> 90 \%$ . Microalgae biomass productivity was enhanced by the addition of the NPs, resulting in biomass concentrations of  $3.26 \text{ gVSS L}^{-1}$ . However, this enhanced photosynthetic activity might result in a reduction of the buffer capacity and the pH of the algal open pond culture broth. For the first time, this study proved that the addition of NPs can be used as a viable strategy to improve biogas upgrading coupled to microalgae production.

# Chapter 8

---

## Discussion



In this chapter the most relevant findings obtained from the experiments carried out for this thesis are discussed. The main points herein discussed are focused on 1) the effect of NPs on microalgae growth and metabolism; 2) the effect of NPs on CO<sub>2</sub> availability; and 3) the effect of NPs on photosynthetic biogas upgrading at pilot scale. It is important to mention that in this chapter, the results obtained in the thesis will not be compared with previous studies since they have been compared and discussed through the thesis. To simplify the comparison of the results, only the results obtained under visible light will be deeply discussed, and the results obtained when visible light was supplemented with *UV* light will serve as a confirmation of the results obtained with visible light (in terms of physical interactions between microalgae and NPs).

### **1. Effect of nanoparticles on microalgae metabolism**

Microalgae growth and macromolecule accumulation (*i.e.* carbohydrates and lipids) highly depend on the environmental conditions under which microalgae are grown. Typically, microalgae growth is limited by the low photosynthesis efficiency either due to low CO<sub>2</sub> diffusion or to low light availability. On the other hand, when the accumulation of high value products such as lipids and carbohydrates is desired, biomass growth is limited. In this regard, NPs have emerged as promising technology that can enhance both biomass and high-value product production. While the mechanism of interaction between microalgae and NPs remains uncertain, the experiments carried out in this thesis can serve to explain the effect of NPs on microalgae metabolism (**Table 19**).

For instance, **Chapter 2** showed that the crystal phase of the NPs influences differently microalgae metabolism in terms of biomass productivity and carbohydrates or lipids accumulation. When the  $\alpha$ - phase was dominant in the NPs, a toxic effect was observed in *Chlorella* spp. Interestingly, the  $\gamma$ -phase showed stimulation of *Chlorella* spp. metabolism under environments with and without carbonates supplementation. From the later results, this chapter induced the theory that  $\text{Fe}_2\text{O}_3$  NPs could have some interactions with  $\text{CO}_2$ , since *Chlorella* sp. growth was not only supported in culture media without carbonate supplementation, but biomass productivities enhancements were observed when concentrations of 10 and 20  $\text{mgL}^{-1}$  were added to the cultures.

To confirm if  $\text{Fe}_2\text{O}_3$  could support microalgae growth under real conditions, **Chapter 4** was devoted to elucidate the long-term exposure to  $\text{Fe}_2\text{O}_3$  NPs. Firstly, 10  $\text{mg L}^{-1}$  of  $\text{Fe}_2\text{O}_3$  nanoparticles were added to microalgae culture, however contrary to the results obtained from the batch experiments, the biomass productivity and the carbohydrates content was neither enhanced nor inhibited. Thus the concentration of  $\text{Fe}_2\text{O}_3$  NPs was increased to 20  $\text{mg L}^{-1}$ , but no significant difference was either observed. At this point, it is important to mention that the species inside the photobioreactors (PBRs) used in this chapter was a mixed microalgae-cyanobacteria consortium, which was the major factor that limited the carbohydrates accumulation. Afterwards,  $\text{Fe}_2\text{O}_3$  concentrations were increased to 30  $\text{mg L}^{-1}$  and finally to 70  $\text{mg L}^{-1}$ . Interestingly, the presence of the NPs affected the growth of cyanobacteria mainly by the deposition of the NPs into the flocs of the filamentous microorganism, leading to sedimentation and shading effects and finally cell death.

Nevertheless, microalgae growth was not inhibited by the high concentrations of the Fe<sub>2</sub>O<sub>3</sub> NPs. Interestingly, concentrations of 30 mg L<sup>-1</sup> of these particular NPs increased carbohydrates content of wastewater cultivated microalgae and did not influence nutrient uptake. In fact, the PBR containing Fe<sub>2</sub>O<sub>3</sub> NPs presented similar growth pattern than the PBR without NPs. In this regard, **Chapter 4** confirmed the fact that Fe<sub>2</sub>O<sub>3</sub> can support microalgae growth and carbohydrates accumulation without the supplementation of carbonates. Moreover, the addition of NPs could serve as a strategy to improve biomass quality of wastewater cultivated microalgae. However, from these results the use of other metallic NPs that enhance CO<sub>2</sub> mass transfer was encouraged.

Fe<sub>2</sub>O<sub>3</sub>, SiO<sub>2</sub> and mesoporous carbon (**Chapter 5** and **6**) NPs were selected to studied their effect on microalgae cultures devoted to biogas upgrading, since these particular NPs have proved to enhanced the CO<sub>2</sub> mass transfer in CO<sub>2</sub> capture systems. The experiments were carried out in batch PBRs under a synthetic biogas atmosphere, and different light sources, and regardless of the environmental conditions, the nature of the nanoparticles influenced differently on microalgae metabolism. Firstly, the influence of two different mesoporous carbon and Fe<sub>2</sub>O<sub>3</sub> NPs were assessed in pure cultures of *Chlorella sorokiniana*. The results obtained with the Fe<sub>2</sub>O<sub>3</sub> NPs under a synthetic biogas atmosphere presented the same tendency than the experiments carried put in **Chapter 4**, and no significant differences were observed in the biomass productivities when 10 mg L<sup>-1</sup> were added. However, microalgae growth increased with increasing concentrations of 40 and 70 mgL<sup>-1</sup> of Fe<sub>2</sub>O<sub>3</sub> NPs. Additionally, the carbohydrate content was increased when the



concentration of the  $\text{Fe}_2\text{O}_3$  NPs increased up to  $70 \text{ mg L}^{-1}$ . The same behavior was observed with the mixed microalgae-bacteria consortium, and biomass productivities were enhanced when  $\text{Fe}_2\text{O}_3$  NPs were added. However, the consortium used in **Chapter 6** presented the same effect than the consortium used in **Chapter 4**, and no lipid or carbohydrate enhancement were observed. Indeed, the effect of NPs on microalgae highly depends on the species, however the results obtained in this thesis suggest that pure cultures are better candidates to accumulate carbohydrates or lipids even when NPs are added.

$\text{SiO}_2$  NPs presented contrary results from the previous reports in literature, and no biomass enhancements were observed. However, these particular NPs served as stimulants for lipid production, regardless of the concentration tested, which is in agreement with the literature. The same behavior was observed under *UV* light, suggesting that in this thesis, these particular  $\text{SiO}_2$  NPs created a stressful environmental that resulted in lipid accumulation. Thus,  $\text{SiO}_2$  can serve as a strategy to produce lipid rich biomass.

Finally, the two mesoporous carbon coated zero valent iron ( $\text{Fe}^0$ ) NPs (CALPECH and SMALLOPS) presented the most interesting and promising results. Firstly, it is important to remember that CALPECH NPs presented a lower  $\text{Fe}^0$  content than SMALLOPS, 7 and 31% (wt), respectively, which played a key role in the microalgae metabolism. It is known that  $\text{Fe}^0$  is one of the most reactive species of Fe, and is usually used to produce Fenton reactions. In this regard, the higher  $\text{Fe}^0$  content in SMALLOPS NPs could induced the formation of reactive oxygen species (ROS). The addition of SMALLOPS NPs did not enhance the biomass productivity of

*C. sorokiniana* regardless of the concentration added. Additionally, as the NPs concentration increased, the cumulative O<sub>2</sub> in the headspace of the PBRs decreased. On the other hand, the addition of SMALLOPS NPs led to higher lipid content in *C. sorokiniana*. This confirms the fact that the higher Fe<sup>0</sup> content in these particular NPs induced the formation of ROS and could have limited the biomass productivity of *C. sorokiniana*. Moreover, the addition of CALPECH NPs significantly enhanced biomass productivities not only on *C. sorokiniana* but on the mixed microalgae-bacteria consortium as well. Interestingly, as the CALPECH NPs concentration increased the biomass productivities and the carbohydrates accumulation increased as well. In this regard, the low concentration of Fe<sup>0</sup> in CALPECH NPs prevent the reactive nature of the Fe<sup>0</sup>. Thus, it can be said that interaction between the CALPECH NPs and microalgae was likely due to their physical characteristics, but this will be discussed in the next section.

**Table 19.** Effect of the nanoparticles on microalgae metabolism. Note +refers to the control,

<b>Strain</b>	<b>NPs</b>	<b>Concentration (mg L<sup>-1</sup>)</b>	<b>Px (mgL<sup>-1</sup>d<sup>-1</sup>)</b>	<b>Carbohydrates (% dw)</b>	<b>Lipid (%dw)</b>
<i>Chlorella vulgaris</i>	Fe <sub>2</sub> O <sub>3</sub>	0	45	19	11
		5	44	19	17
		10	43	41	15
		20	34	53	18
<i>Chlorella</i> sp.	Fe <sub>2</sub> O <sub>3</sub>	0	72*, 52**	17	18
		5	56**	17	27
		10	90*	32.	18
		20	62**	20	15
<i>Chlorella sorokiniana</i>	Fe <sub>2</sub> O <sub>3</sub>	0	1240	11	17
		20	1120	12	19
		40	1270	10	11
		70	1750	16	14
	CALPECH	0	810	12	11
		20	1750	13	12
		40	1100	11	12
		70	1670	19	14
	SMALLOPS	0	2150	7	14
		20	2100	12	16
		40	20000	10	19
		70	1720	13	15
Mixed microalgae-cyanobacteria	Fe <sub>2</sub> O <sub>3</sub>	10	16+, 14	12+, 15	7+, 8
		20	35+, 22	17+, 15	6+, 6
		30	31+, 25	18+, 30	6+, 7
		70	2+, 2	17+, 12	7+, 8
Mixed microalgae-bacteria	Fe <sub>2</sub> O <sub>3</sub>	0	1890	18.3	14
		20	1440	7	16
		40	2630	12	16
		70	2750	14	13
	SiO <sub>2</sub>	0	1680	6	11
		20	1890	10	16
		40	1890	12	15
		70	1810	10	17
	CACOI	0	1240	12	15
		20	1690	13	15
		40	2250	13	16
		70	3120	30	15

## 2. Effect of nanoparticles on CO<sub>2</sub> availability

The experiments carried out under synthetic biogas atmosphere (**Chapter 5** and **6**) serve to explain the effect between NPs and CO<sub>2</sub>. The addition of NPs to microalgae cultures has been focused on their chemical activity and toxic effect, however, their physical properties such as porosity, surface area, conferred them specific properties that could represent an advantage to improve CO<sub>2</sub> transfer. **Table 20** summarizes the effect of NPs on the cumulative consumed CO<sub>2</sub> and produced O<sub>2</sub>.

The cumulative CO<sub>2</sub> in the headspace of the bottles was directly related to the concentration of the NPs and as the concentration of NPs increased, the cumulative CO<sub>2</sub> (%) increased as well, regardless of the type of NPs added. At this point, it is important to mention that all the NPs herein used presented a mesoporous surface, and was the key parameter for CO<sub>2</sub> adsorption. Additionally, the pore volume and the surface area of the NPs also influenced the CO<sub>2</sub> concentration and even if CALPECH and SMALLOPS NPs were similar (zero-valent iron covered by carbon) their physical properties and chemical composition made them completely different. For instance, SMALLOPS NPs presented the lowest surface area and pore volume (5.45 m<sup>-2</sup> g<sup>-1</sup> and 0.03 cm<sup>3</sup> g<sup>-1</sup>, respectively) of all the NPs tested in this thesis, and it was observed that these particular NPs did not significantly influence the cumulative CO<sub>2</sub> or the biomass productivity.

On the other hand, SiO<sub>2</sub> NPs presented the highest surface area and pore volume (981 m<sup>-2</sup> g<sup>-1</sup> and 6.97 cm<sup>3</sup> g<sup>-1</sup>, respectively) and were expected to increase the cumulative CO<sub>2</sub> coupled to biomass productivity. However, these particular NPs retarded the exponential phase when concentrations  $\geq 40$  mg L<sup>-1</sup> were added whilst

no significant difference in CO<sub>2</sub> and biomass productivity was observed with concentrations < 40 mg L<sup>-1</sup>.

Fe<sub>2</sub>O<sub>3</sub> and CALPECH NPs presented similar characteristics (surface area: 27-32 m<sup>2</sup> g<sup>-1</sup>, and pore volume 0.30-0.40 cm<sup>3</sup> g<sup>-1</sup>) interestingly, the higher cumulative CO<sub>2</sub> consumptions coupled to biomass productivities were obtain with both NPs. The later confirms that the physical characteristics of the NPs influence differently the CO<sub>2</sub> availability, probably by the shuttle effect or by a hydrodynamic effect. The first is referred to the adhesion of CO<sub>2</sub> to the surface of the NPs, and then the CO<sub>2</sub> is release to the culture medium and rapidly consumed by microalgae. On the other hand, the hydrodynamic effect refers to an increased in the interfacial area by the presence of the NPs in the culture medium.

Literature on which mechanism of interaction happens when NPs are added to a system for CO<sub>2</sub> capture are contradictory and both mechanism of interaction have been proposed. Nevertheless, the later studies have been proposed with water and alkaline medium, and the literature on the mechanism of interaction using microalgae is scarce. In this way, the results obtain in this thesis suggest that both mechanisms of interaction (shuttle and hydrodynamic) could have occurred in the batch systems. The shuttle effect was easily identified by the increasing CO<sub>2</sub> concentrations in the headspace of the PBRs as the NPs concentration increased as well. On the other hand, and hydrodynamic effect also can be attributed to the magnetic stirring, causing colliding of the NPs and increasing the interfacial area of contact between the microalgae and CO<sub>2</sub>. Either case, the higher CO<sub>2</sub> availability in

---

the medium activated the metabolism of microalgae, resulting in increased biomass productivities and even some carbohydrates accumulation.

The experiments carried out under *UV* light, confirmed the fact that the increased CO<sub>2</sub> availability in the headspace of the PBRs was likely due to the physical properties of the NPs. Nevertheless, the addition of *UV* light led to the formation of ROS when, Fe<sub>2</sub>O<sub>3</sub>, SiO<sub>2</sub> and SMALLOPS NPs were added, likely due to the higher iron content.

In this regard, it can be said that the physical characteristics of NPs played an important role in CO<sub>2</sub> transfer, and from the results obtained in this thesis, NPs with surface area and a pore diameter in the range of 27-32 m<sup>2</sup> g<sup>-1</sup> 0.30-0.40 cm<sup>3</sup> g<sup>-1</sup> respectively, can be considered to enhance CO<sub>2</sub> transfer to microalgae. Nevertheless, the chemical composition of the NPs is responsible for the toxicity (or not) on microalgae and even if one selected NP can be in the range for optimal CO<sub>2</sub> transfer, their chemical composition could negatively affect microalgae and result in growth inhibition.

**Table 20.** Effect of nanoparticles on cumulative CO<sub>2</sub> and produced O<sub>2</sub>.

Strain	NPs	Concentration (mg L <sup>-1</sup> )	CO <sub>2</sub> (%)	O <sub>2</sub> (%)
<i>Chlorella sorokiniana</i>	Fe <sub>2</sub> O <sub>3</sub>	0	17	26
		20	16	26
		40	19	27
		70	21	32
	CALPECH	0	19	28
		20	20	31
		40	20	32
		70	21	32
	SMALLOPS	0	18	28
		20	19	29
		40	20	33
		70	20	31
Mixed microalgae- bacteria	Fe <sub>2</sub> O <sub>3</sub>	0	18	37
		20	20	30
		40	24	32
		70	22	24
	SiO <sub>2</sub>	0	19	29
		20	20	30
		40	29	29
		70	21	28
	CACOI	0	19	31
		20	20	30
		40	21	29
		70	22	30

### 3. Effect of nanoparticles on photosynthetic biogas upgrading at pilot scale

According to the results obtained at laboratory scale, CALPECH NPs were selected as the optimal NPs to elucidate at a pilot scale system devoted to photosynthetic biogas upgrading (**Chapter 7**). CALPECH NPs were added at a concentration of 70

mgL<sup>-1</sup> to a high rate algal pond (HRAP) interconnected to a purification column (PC) where synthetic biogas was sparged. Interestingly, enhancements in biomass production and in the quality of the upgraded biomethane were observed.

Biomass production increased from 1.56 to 3.26 g VSS L<sup>-1</sup>, these results were in agreement with the observed in **Chapter 5** and **6**, where microalgae biomass productivities were also increased. In this regard, the pilot-scale experiments confirmed the fact that these particular NPs stimulated microalgae metabolism probably due to a higher CO<sub>2</sub> availability.

The quality of the upgraded biomethane significantly change by the addition of the NPs, and the CO<sub>2</sub> removals efficiencies (REs) were 86.2 % and 92.1% without and with the addition of the NPs. This CO<sub>2</sub>-REs have been previously reported in similar systems but at high alkaline culture mediums with inorganic carbon (IC) concentrations > 1000 mg L<sup>-1</sup>. Interestingly, in the experiments carried out in **Chapter 8** the IC concentration was < 600 mg L<sup>-1</sup>, and high CO<sub>2</sub>-REs were achieved by the addition of the NPs.

The high biomass production and CO<sub>2</sub>-REs are in agreement with the previously observed in the batch experiments, and this suggest that indeed the NPs improve the CO<sub>2</sub> removal. Previous studies using bubble columns and activated carbon particles suggest that the increased CO<sub>2</sub> transfers is likely due to an hydrodynamic effect, but again the reported studies did not use microorganism. Interestingly, observations in the HRAP flow (**Fig. 39**) suggest that an hydrodynamic effect is being carried out in the system.



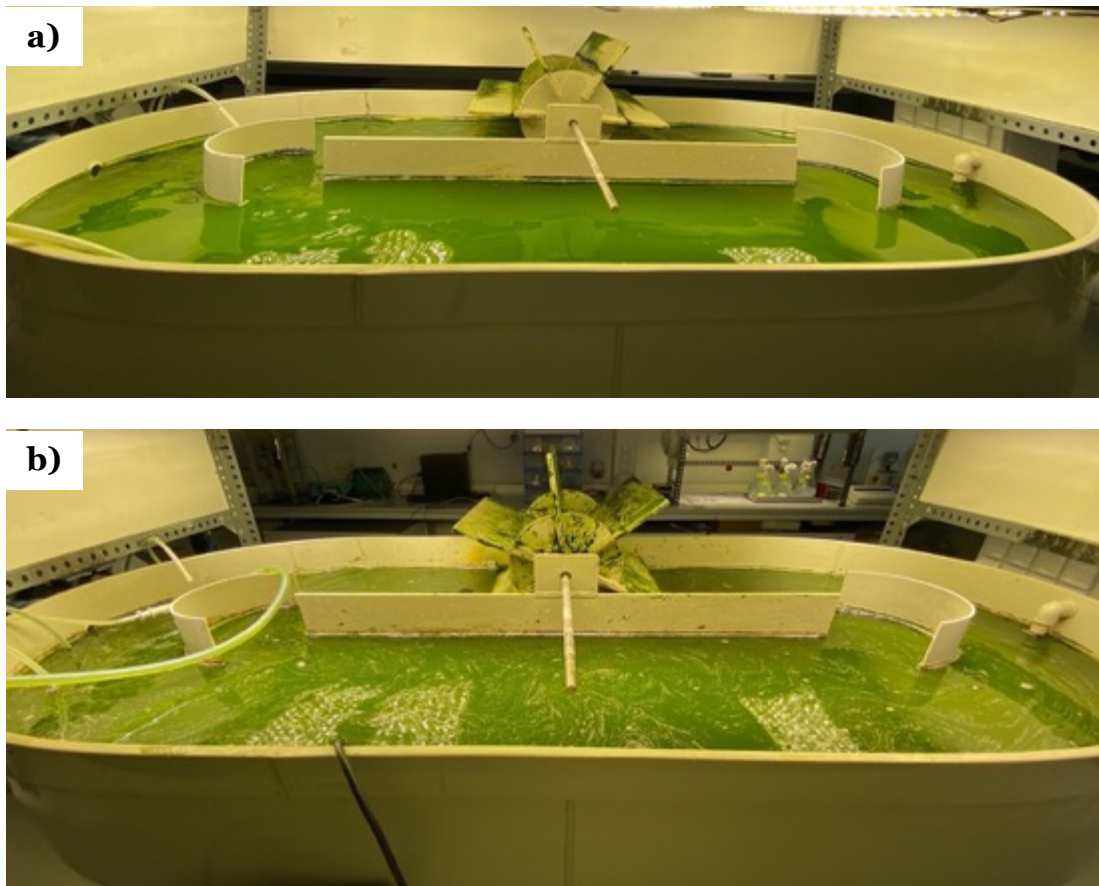


**Fig.39.** Flow inside the HRAP a) before and b) after the addition of the CALPECH nanoparticles.

Interestingly, after the addition of CALPECH NPs it can be clearly observed the presence of vortices inside the HRAP (**Fig. 39b**). It is important to highlight that these vortices are the result of the liquid flow by the agitation through the paddle wheel. However, the addition of the NPs makes the flow more noticeable and suggest that some hydrodynamic phenomenon is happening inside the HRAP. Thus, the latter led to a higher CO<sub>2</sub> availability to microalgae metabolism that resulted in an increased biomass production.

# Chapter 9

---

## Conclusions and Future Prospects



This thesis is focused on the effect of different nanoparticles on microalgae cultures and CO<sub>2</sub> adsorption. Interesting results have been obtained from the experiments and the conclusions are presented in this chapter. Additionally, future prospects and suggestions are also presented.

## 1. Conclusions

### 1.1 Effect of nanoparticles on microalgae metabolism

The influence of nanoparticles on microalgae metabolism highly depends on the microalgae species, the chemical composition of the nanoparticles, the physical properties of the nanoparticles, the concentration of nanoparticles and the environmental conditions. From the four nanoparticles herein studied (Fe<sub>2</sub>O<sub>3</sub>, SiO<sub>2</sub>, CALPECH and SMALLOPS), it can be concluded that:

- The crystal phase of Fe<sub>2</sub>O<sub>3</sub> nanoparticles influences differently microalgae metabolism, and when the  $\alpha$ -phase is dominant a toxic effect was observed in *Chlorella* spp. Cultures, whereas the dominant  $\gamma$ -phase resulted in enhanced biomass productivities.
- Low concentrations (<20 mg L<sup>-1</sup>) of Fe<sub>2</sub>O<sub>3</sub> nanoparticles did not presented significant changes in microalgae growth, but concentration >30 mg L<sup>-1</sup> retarded the exponential growth phase of microalgae.
- Concentrations >30 mg L<sup>-1</sup> of Fe<sub>2</sub>O<sub>3</sub> increased the carbohydrate content of *Chlorella* spp. cultures.
- SiO<sub>2</sub> nanoparticles increased the lipid content of microalgae-bacteria culture regardless of the concentration tested.

- The different content of Fe<sup>0</sup> in CALPECH and SMALLOPS NPs differently interfered in microalgae metabolism. The higher Fe<sup>0</sup> content in SMALLOPS NPs led to a higher lipid content in microalgae likely due to the formation of reactive oxygen species.
- Fe<sub>2</sub>O<sub>3</sub> nanoparticles and CALPECH nanoparticles significantly increased biomass productivity of microalgae, however the chemical composition of the nanoparticles influenced differently microalgae.
- Fe<sub>2</sub>O<sub>3</sub> retarded the exponential growth phase of microalgae at concentrations >40 mg L<sup>-1</sup>.
- CALPECH nanoparticles significantly increased the biomass productivities and accelerated the exponential growth phase of *Chlorella sorokiniana* and a mixed microalgae-bacteria consortium.

## 1.2 Effect of nanoparticles on CO<sub>2</sub> availability

The physical properties of the nanoparticles *i.e.* surface area and pore volume, significantly influenced the CO<sub>2</sub> adsorption and availability to microalgae. The most remarkable findings and conclusion can be listed as follows:

- The mesoporous nature of the nanoparticles influenced in the CO<sub>2</sub> available for microalgae, and as the nanoparticles concentration the CO<sub>2</sub> content increased as well.
- The biomass productivity of microalgae increased as a function of the available CO<sub>2</sub>.

- SiO<sub>2</sub> nanoparticles presented the highest surface area and pore volume among all the nanoparticles used, however these nanoparticles did not record enhancements in biomass productivities likely due to their chemical composition and interactions.
- SMALLOPS nanoparticles presented the lowest surface area and pore volume among all the nanoparticles used, and as a consequence, no significant difference in biomass productivities were observed.
- CALPECH and Fe<sub>2</sub>O<sub>3</sub> nanoparticles presented similar surface area and pore volume and presented enhancements in biomass productivities and consumed CO<sub>2</sub>. However, the nature of the nanoparticles influenced microalgae growth.
- Nanoparticles with surface area and a pore diameter in range of 27-32 m<sup>2</sup> g<sup>-1</sup> 0.30-0.40 cm<sup>3</sup> g<sup>-1</sup> respectively, can be considered to enhance CO<sub>2</sub> transfer to microalgae.

### **1.3 Effect of nanoparticles on photosynthetic biogas upgrading at pilot scale**

The addition of CALPECH nanoparticles enhanced the performance of the biogas upgrading system, with a high CO<sub>2</sub> removals efficiencies of 92.1% and biomass production up to 3.26 gVSS L<sup>-1</sup> mainly driven by and hydrodynamic effect caused by the addition of the nanoparticles.

Finally, the overall results confirm that CALPECH NPs are a promising technology to improve CO<sub>2</sub> transfer and biomass production in a photosynthetic biogas upgrading system.

## 2. Future prospects

In this thesis, the effect of CALPECH nanoparticles was assessed at a pilot scale system of 180 L under indoors conditions. The concentration assessed was 70mg L<sup>-1</sup> and promising results were obtained. However, the effect of increasing concentrations should be studied to optimize the quality of the upgraded biomethane as a function of the concentration of CALPECH nanoparticles.

The L/G ratio is one important factor in upgrading biogas systems, in this regard, the influence of L/G ratio and the CALPECH nanoparticles could also be studied to optimized the process.

Finally, the scaling of the system under environmental conditions (**Fig. 40**) can also serve to study the viability of the process.



**Fig. 40.** Photosynthetic biogas upgrading system under environmental conditions at the Institute of Renewable Energies, Temixco, Mexico.





# References

---

- Abo Markeb, A., Llimós-Turet, J., Ferrer, I., Blázquez, P., Alonso, A., Sánchez, A., Moral-Vico, J., & Font, X. (2019). The use of magnetic iron oxide based nanoparticles to improve microalgae harvesting in real wastewater. *Water Research*, 159, 490–500. <https://doi.org/10.1016/j.watres.2019.05.023>
- Aghbashlo, M., Hosseinzadeh-Bandbafha, H., Shahbeik, H., & Tabatabaei, M. (2022). The role of sustainability assessment tools in realizing bioenergy and bioproduct systems. *Biofuel Research Journal*, 9(3), 1697–1706. <https://doi.org/10.18331/BRJ2022.9.3.5>
- Aghel, B., Behaein, S., Wongwises, S., & Shadloo, M. S. (2022). A review of recent progress in biogas upgrading: With emphasis on carbon capture. *Biomass and Bioenergy*, 160(March), 106422. <https://doi.org/10.1016/j.biombioe.2022.106422>
- Alper, E., & Öztürk, S. (1986). The effect of activated carbon loading on oxygen absorption into aqueous sodium sulphide solutions in a slurry reactor. *The Chemical Engineering Journal*, 32(2), 127–130. [https://doi.org/10.1016/0300-9467\(86\)80061-2](https://doi.org/10.1016/0300-9467(86)80061-2)
- Alzate, M. E., Muñoz, R., Rogalla, F., Fdz-Polanco, F., & Pérez-Elvira, S. I. (2012). Biochemical methane potential of microalgae: Influence of substrate to inoculum ratio, biomass concentration and pretreatment. *Bioresource Technology*, 123, 488–494. <https://doi.org/10.1016/J.BIORTECH.2012.06.113>
- Ángeles, R., Arnaiz, E., Gutiérrez, J., Sepúlveda-Muñoz, C. A., Fernández-Ramos, O., Muñoz, R., & Lebrero, R. (2020). Optimization of photosynthetic biogas upgrading in closed photobioreactors combined with algal biomass production. *Journal of Water Process Engineering*, 38(July). <https://doi.org/10.1016/j.jwpe.2020.101554>
- Ángeles, R., Vega-Quiel, M. J., Batista, A., Fernández-Ramos, O., Lebrero, R., & Muñoz, R. (2021). Influence of biogas supply regime on photosynthetic biogas upgrading performance in an enclosed algal-bacterial photobioreactor. *Algal Research*, 57(April). <https://doi.org/10.1016/j.algal.2021.102350>
- Anwar, M. N., Fayyaz, A., Sohail, N. F., Khokhar, M. F., Baqar, M., Khan, W. D., Rasool, K., Rehan, M., & Nizami, A. S. (2018). CO<sub>2</sub> capture and storage: A way forward for sustainable environment. *Journal of Environmental*

- Management*, 226(August), 131–144.  
<https://doi.org/10.1016/j.jenvman.2018.08.009>
- APHA-AWWA-WPCF. (1999). Standard Methods for the Examination of Water and Wastewater. In *American Journal of Public Health and the Nations Health* (20th ed.). <https://doi.org/10.2105/ajph.56.4.684-a>
- Arias, D. M., Solé-Bundó, M., Garfí, M., Ferrer, I., García, J., & Uggetti, E. (2018). Integrating microalgae tertiary treatment into activated sludge systems for energy and nutrients recovery from wastewater. *Bioresource Technology*, 247, 513–519. <https://doi.org/10.1016/J.BIORTECH.2017.09.123>
- Aruoja, V., Dubourguier, H. C., Kasemets, K., & Kahru, A. (2009). Toxicity of nanoparticles of CuO, ZnO and TiO<sub>2</sub> to microalgae *Pseudokirchneriella subcapitata*. *Science of the Total Environment*, 407(4), 1461–1468. <https://doi.org/10.1016/j.scitotenv.2008.10.053>
- Bayat Tork, M., Khalilzadeh, R., & Kouchakzadeh, H. (2017). Efficient harvesting of marine *Chlorella vulgaris* microalgae utilizing cationic starch nanoparticles by response surface methodology. *Bioresource Technology*, 243, 583–588. <https://doi.org/10.1016/j.biortech.2017.06.181>
- Bazrafshan, H., Alipour Tesieh, Z., Dabirnia, S., Shajareh Touba, R., Manghabati, H., & Nasernejad, B. (2017). Synthesis of novel  $\alpha$ -Fe<sub>2</sub>O<sub>3</sub> nanorods without surfactant and its electrochemical performance. *Powder Technology*, 308, 266–272. <https://doi.org/10.1016/j.powtec.2016.12.015>
- Besha, A. T., Liu, Y., Bekele, D. N., Dong, Z., Naidu, R., & Gebremariam, G. N. (2020). Sustainability and environmental ethics for the application of engineered nanoparticles. *Environmental Science and Policy*, 103(October 2019), 85–98. <https://doi.org/10.1016/j.envsci.2019.10.013>
- Bibi, M., Zhu, X., Munir, M., & Angelidaki, I. (2021). Bioavailability and effect of  $\alpha$ -Fe<sub>2</sub>O<sub>3</sub> nanoparticles on growth, fatty acid composition and morphological indices of *Chlorella vulgaris*. *Chemosphere*, 282(June), 131044. <https://doi.org/10.1016/j.chemosphere.2021.131044>
- Borde, X., Guieysse, B., Delgado, O., Muoz, R., Hatti-Kaul, R., Nugier-Chauvin, C., Patin, H., & Mattiasson, B. (2003). Synergistic relationships in algal-bacterial microcosms for the treatment of aromatic pollutants. *Bioresource Technology*, 86(3), 293–300. [https://doi.org/10.1016/S0960-8524\(02\)00074-3](https://doi.org/10.1016/S0960-8524(02)00074-3)
- Bose, A., Lin, R., Rajendran, K., O’Shea, R., Xia, A., & Murphy, J. D. (2019). How to optimise photosynthetic biogas upgrading: a perspective on system design and

- microalgae selection. *Biotechnology Advances*, 107444.  
<https://doi.org/10.1016/J.BIOTECHADV.2019.107444>
- Bose, A., O'Shea, R., Lin, R., & Murphy, J. D. (2021). A comparative evaluation of design factors on bubble column operation in photosynthetic biogas upgrading. *Biofuel Research Journal*, 8(2), 1351–1373.  
<https://doi.org/10.18331/BRJ2021.8.2.2>
- Brémond, U., Bertrandias, A., Steyer, J. P., Bernet, N., & Carrere, H. (2021). A vision of European biogas sector development towards 2030: Trends and challenges. *Journal of Cleaner Production*, 287.  
<https://doi.org/10.1016/j.jclepro.2020.125065>
- Capaldi Arruda, S. C., Diniz Silva, A. L., Moretto Galazzi, R., Antunes Azevedo, R., & Zezzi Arruda, M. A. (2015). Nanoparticles applied to plant science: A review. *Talanta*, 131, 693–705. <https://doi.org/10.1016/j.talanta.2014.08.050>
- Chandra, N., Shukla, P., & Mallick, N. (2020). Role of cultural variables in augmenting carbohydrate accumulation in the green microalga *Scenedesmus acuminatus* for bioethanol production. *Biocatalysis and Agricultural Biotechnology*, 26(March), 101632.  
<https://doi.org/10.1016/j.bcab.2020.101632>
- Chang, H., Hu, R., Zou, Y., Quan, X., Zhong, N., Zhao, S., & Sun, Y. (2020). Highly efficient reverse osmosis concentrate remediation by microalgae for biolipid production assisted with electrooxidation. *Water Research*, 174, 115642.  
<https://doi.org/10.1016/j.watres.2020.115642>
- Chang, H., Quan, X., Zhong, N., Zhang, Z., Lu, C., Li, G., Cheng, Z., & Yang, L. (2018). High-efficiency nutrients reclamation from landfill leachate by microalgae *Chlorella vulgaris* in membrane photobioreactor for bio-lipid production. *Bioresource Technology*, 266(June), 374–381.  
<https://doi.org/10.1016/j.biortech.2018.06.077>
- Cheloni, G., Marti, E., & Slaveykova, V. I. (2016). Interactive effects of copper oxide nanoparticles and light to green alga *Chlamydomonas reinhardtii*. *Aquatic Toxicology*, 170, 120–128.  
<https://doi.org/https://doi.org/10.1016/j.aquatox.2015.11.018>
- Chen, M., Tang, H., Ma, H., Holland, T. C., Ng, K. Y. S., & Salley, S. O. (2011a). Effect of nutrients on growth and lipid accumulation in the green algae *Dunaliella tertiolecta*. *Bioresource Technology*, 102(2), 1649–1655.  
<https://doi.org/10.1016/j.biortech.2010.09.062>

- Chen, M., Tang, H., Ma, H., Holland, T. C., Ng, K. Y. S., & Salley, S. O. (2011b). Effect of nutrients on growth and lipid accumulation in the green algae *Dunaliella tertiolecta*. *Bioresource Technology*, *102*(2), 1649–1655.  
<https://doi.org/10.1016/j.biortech.2010.09.062>
- Chen, X., Zhang, C., Tan, L., & Wang, J. (2018a). Toxicity of Co nanoparticles on three species of marine microalgae. *Environmental Pollution*, *236*, 454–461.  
<https://doi.org/10.1016/J.ENVPOL.2018.01.081>
- Chen, X., Zhang, C., Tan, L., & Wang, J. (2018b). Toxicity of Co nanoparticles on three species of marine microalgae. *Environmental Pollution*, *236*, 454–461.  
<https://doi.org/10.1016/J.ENVPOL.2018.01.081>
- Cheng, D. L., Ngo, H. H., Guo, W. S., Chang, S. W., Nguyen, D. D., & Kumar, S. M. (2019). Microalgae biomass from swine wastewater and its conversion to bioenergy. *Bioresource Technology*, *275*, 109–122.  
<https://doi.org/10.1016/J.BIORTECH.2018.12.019>
- Cheng, J., Zhu, Y., Li, K., Lu, H., & Shi, Z. (2020). Calcinated MIL-100(Fe) as a CO<sub>2</sub> adsorbent to promote biomass productivity of *Arthrospira platensis* cells. *Science of the Total Environment*, *699*.  
<https://doi.org/10.1016/j.scitotenv.2019.134375>
- Choi, I. D., Lee, J. W., & Kang, Y. T. (2015). CO<sub>2</sub> Capture/Separation Control by SiO<sub>2</sub> Nanoparticles and Surfactants. *Separation Science and Technology (Philadelphia)*, *50*(5), 772–780.  
<https://doi.org/10.1080/01496395.2014.965257>
- Choi, W., Kim, G., & Lee, K. (2012). Influence of the CO<sub>2</sub> absorbent monoethanolamine on growth and carbon fixation by the green alga *Scenedesmus* sp. *Bioresource Technology*, *120*, 295–299.  
<https://doi.org/10.1016/j.biortech.2012.06.010>
- Correcher, R., Budyk, Y., & Fullana, A. (2021). Role of Gallic Acid in the Synthesis of Carbon-Encapsulated Iron Nanoparticles by Hydrothermal Carbonization: Selecting Iron Oxide Composition. *ACS Omega*.  
<https://doi.org/10.1021/acsomega.1c03692>
- Das, J., Ravishankar, H., & Lens, P. N. L. (2022a). Biological biogas purification: Recent developments, challenges and future prospects. *Journal of Environmental Management*, *304*(November 2021), 114198.  
<https://doi.org/10.1016/j.jenvman.2021.114198>

- Das, J., Ravishankar, H., & Lens, P. N. L. (2022b). Biological biogas purification: Recent developments, challenges and future prospects. *Journal of Environmental Management*, *304*(November 2021), 114198. <https://doi.org/10.1016/j.jenvman.2021.114198>
- Demir, V., Ates, M., Arslan, Z., Camas, M., Celik, F., Bogatu, C., & Can, Ş. S. (2015). Influence of alpha and gamma-iron oxide nanoparticles on marine microalgae species. *Bulletin of Environmental Contamination and Toxicology*, *95*(6), 752–757. <https://doi.org/10.1007/s00128-015-1633-2>
- Déniel, M., Errien, N., Daniel, P., Caruso, A., & Lagarde, F. (2019a). Current methods to monitor microalgae-nanoparticle interaction and associated effects. *Aquatic Toxicology*, *217*, 105311. <https://doi.org/10.1016/J.AQUATOX.2019.105311>
- Déniel, M., Errien, N., Daniel, P., Caruso, A., & Lagarde, F. (2019b). Current methods to monitor microalgae-nanoparticle interaction and associated effects. *Aquatic Toxicology*, *217*, 105311. <https://doi.org/10.1016/J.AQUATOX.2019.105311>
- Dinc, S. K., Vural, O. A., Kayhan, F. E., & San Keskin, N. O. (2022). Facile biogenic selenium nanoparticle synthesis, characterization and effects on oxidative stress generated by UV in microalgae. *Particuology*, *70*, 30–42. <https://doi.org/10.1016/j.partic.2021.12.005>
- Dong, B., Yuan, X. G., & Yu, K. T. (2017). Determination of liquid mass-transfer coefficients for the absorption of CO<sub>2</sub> in alkaline aqueous solutions in structured packing using numerical simulations. *Chemical Engineering Research and Design*, *124*, 238–251. <https://doi.org/10.1016/j.cherd.2017.06.017>
- Dubois, Michel., Smith, Fred., Rebers, P. A., Gilles, K. A., & Hamilton, J. K. (1956). Colorimetric Method for Determination of Sugars and Related Substances. *Analytical Chemistry*, *28*(3), 350–356. <https://doi.org/10.1021/ac60111a017>
- Duman, F., Sahin, U., & Atabani, A. E. (2019). Harvesting of blooming microalgae using green synthesized magnetic maghemite (γ-Fe<sub>2</sub>O<sub>3</sub>) nanoparticles for biofuel production. *Fuel*, *256*, 115935. <https://doi.org/10.1016/J.FUEL.2019.115935>
- Eroglu, E., Eggers, P. K., Winslade, M., Smith, S. M., & Raston, C. L. (2013). Enhanced accumulation of microalgal pigments using metal nanoparticle solutions as light filtering devices. *Green Chemistry*, *15*(11), 3155–3159. <https://doi.org/10.1039/c3gc41291a>

- Fathi, P., Sadeghi, G., Hosseini, M.-J., Farahmandkia, Z., & Mehrasbi, M. R. (2020). Effects of copper oxide nanoparticles on the *Chlorella* algae in the presence of humic acid. *SN Applied Sciences*, 2(2).  
<https://doi.org/10.1007/s42452-019-1812-6>
- Fernández-Linares, L. C., Guerrero Barajas, C., Durán Páramo, E., & Badillo Corona, J. A. (2017a). Assessment of *Chlorella vulgaris* and indigenous microalgae biomass with treated wastewater as growth culture medium. *Bioresource Technology*, 244(July), 400–406.  
<https://doi.org/10.1016/j.biortech.2017.07.141>
- Fernández-Linares, L. C., Guerrero Barajas, C., Durán Páramo, E., & Badillo Corona, J. A. (2017b). Assessment of *Chlorella vulgaris* and indigenous microalgae biomass with treated wastewater as growth culture medium. *Bioresource Technology*, 244(July), 400–406.  
<https://doi.org/10.1016/j.biortech.2017.07.141>
- Ferreira, A. F., Toledo-Cervantes, A., de Godos, I., Gouveia, L., & Muñoz, R. (2019). Life cycle assessment of pilot and real scale photosynthetic biogas upgrading units. *Algal Research*, 44(September), 101668.  
<https://doi.org/10.1016/j.algal.2019.101668>
- Franco-Morgado, M., Toledo-Cervantes, A., González-Sánchez, A., Lebrero, R., & Muñoz, R. (2018). Integral (VOCs, CO<sub>2</sub>, mercaptans and H<sub>2</sub>S) photosynthetic biogas upgrading using innovative biogas and digestate supply strategies. *Chemical Engineering Journal*, 354(August), 363–369.  
<https://doi.org/10.1016/j.cej.2018.08.026>
- Gao, S., Hu, C., Sun, S., Xu, J., Zhao, Y., & Zhang, H. (2018). Performance of piggery wastewater treatment and biogas upgrading by three microalgal cultivation technologies under different initial COD concentration. *Energy*, 165, 360–369. <https://doi.org/10.1016/j.energy.2018.09.190>
- Giannelli, L., & Torzillo, G. (2012). Hydrogen production with the microalga *Chlamydomonas reinhardtii* grown in a compact tubular photobioreactor immersed in a scattering light nanoparticle suspension. *International Journal of Hydrogen Energy*, 37(22), 16951–16961.  
<https://doi.org/10.1016/J.IJHYDENE.2012.08.103>
- Golmakani, A., Ali Nabavi, S., Wadi, B., & Manovic, V. (2022). Advances, challenges, and perspectives of biogas cleaning, upgrading, and utilisation. *Fuel*, 317(November 2021), 123085.  
<https://doi.org/10.1016/j.fuel.2021.123085>

- González-Camejo, J., Aparicio, S., Ruano, M. V., Borrás, L., Barat, R., & Ferrer, J. (2019a). Effect of ambient temperature variations on an indigenous microalgae-nitrifying bacteria culture dominated by *Chlorella*. *Bioresource Technology*, *290*, 121788. <https://doi.org/10.1016/J.BIORTECH.2019.121788>
- González-Camejo, J., Aparicio, S., Ruano, M. V., Borrás, L., Barat, R., & Ferrer, J. (2019b). Effect of ambient temperature variations on an indigenous microalgae-nitrifying bacteria culture dominated by *Chlorella*. *Bioresource Technology*, *290*, 121788. <https://doi.org/10.1016/J.BIORTECH.2019.121788>
- González-Camejo, J., Serna-García, R., Viruela, A., Pachés, M., Durán, F., Robles, A., Ruano, M. V., Barat, R., & Seco, A. (2017). Short and long-term experiments on the effect of sulphide on microalgae cultivation in tertiary sewage treatment. *Bioresource Technology*, *244*(June), 15–22. <https://doi.org/10.1016/j.biortech.2017.07.126>
- González-Fernández, C., & Ballesteros, M. (2012). Linking microalgae and cyanobacteria culture conditions and key-enzymes for carbohydrate accumulation. *Biotechnology Advances*, *30*(6), 1655–1661. <https://doi.org/10.1016/j.biotechadv.2012.07.003>
- Guieysse, B., Borde, X., Muñoz, R., Hatti-Kaul, R., Nugier-Chauvin, C., Patin, H., & Mattiasson, B. (2002). Influence of the initial composition of algal-bacterial microcosms on the degradation of salicylate in a fed-batch culture. *Biotechnology Letters*, *24*(7), 531–538. <https://doi.org/10.1023/A:1014847616212>
- Gunawan, C., Sirimanoonphan, A., Yang, W., Marquis, C. P., & Amal, R. (2013a). Submicron and nano formulations of titanium dioxide and zinc oxide stimulate unique cellular toxicological responses in the green microalga *Chlamydomonas reinhardtii*. *Journal of Hazardous Materials*, *260*, 984–992. <https://doi.org/10.1016/j.jhazmat.2013.06.067>
- Gunawan, C., Sirimanoonphan, A., Yang, W., Marquis, C. P., & Amal, R. (2013b). Submicron and nano formulations of titanium dioxide and zinc oxide stimulate unique cellular toxicological responses in the green microalga *Chlamydomonas reinhardtii*. *Journal of Hazardous Materials*, *260*, 984–992. <https://doi.org/10.1016/j.jhazmat.2013.06.067>
- Guo, G., Cao, W., Sun, S., Zhao, Y., & Hu, C. (2017). Nutrient removal and biogas upgrading by integrating fungal–microalgal cultivation with anaerobically digested swine wastewater treatment. *Journal of Applied Phycology*, *29*(6), 2857–2866. <https://doi.org/10.1007/s10811-017-1207-2>



- Gupta, S., Pawar, S. B., & Pandey, R. A. (2019a). Current practices and challenges in using microalgae for treatment of nutrient rich wastewater from agro-based industries. *Science of the Total Environment*, 687, 1107–1126. <https://doi.org/10.1016/j.scitotenv.2019.06.115>
- Gupta, S., Pawar, S. B., & Pandey, R. A. (2019b). Current practices and challenges in using microalgae for treatment of nutrient rich wastewater from agro-based industries. *Science of the Total Environment*, 687, 1107–1126. <https://doi.org/10.1016/j.scitotenv.2019.06.115>
- Haider, J., Abdul Qyyum, M., Riaz, A., Naquash, A., Kazmi, B., Yasin, M., Nizami, A. S., Byun, M., Lee, M., & Lim, H. (2022). State-of-the-art process simulations and techno-economic assessments of ionic liquid-based biogas upgrading techniques: Challenges and prospects. *Fuel*, 314(December 2021), 123064. <https://doi.org/10.1016/j.fuel.2021.123064>
- Hakim, A., Marliza, T. S., Abu Tahari, M. N., Yusop, M. R., Mohamed Hisham, M. W., & Yarmo, M. A. (2016). Development of  $\alpha$ -Fe<sub>2</sub>O<sub>3</sub> as adsorbent and its effect on CO<sub>2</sub> capture. *Materials Science Forum*, 840, 421–426. <https://doi.org/10.4028/www.scientific.net/MSF.840.421>
- Hakim, A., Marliza, T. S., Abu Tahari, N. M., Wan Isahak, R. W. N., Yusop, R. M., Mohamed Hisham, W. M., & Yarmo, A. M. (2016). Studies on CO<sub>2</sub> Adsorption and Desorption Properties from Various Types of Iron Oxides (FeO, Fe<sub>2</sub>O<sub>3</sub>, and Fe<sub>3</sub>O<sub>4</sub>). *Industrial and Engineering Chemistry Research*, 55(29), 7888–7897. <https://doi.org/10.1021/acs.iecr.5b04091>
- He, M., Yan, Y., Pei, F., Wu, M., Gebreluel, T., Zou, S., & Wang, C. (2017). Improvement on lipid production by *Scenedesmus obliquus* triggered by low dose exposure to nanoparticles. *Scientific Reports*, 7(1), 1–12. <https://doi.org/10.1038/s41598-017-15667-0>
- Hemmati, A., Rashidi, H., Behradfar, K., & Kazemi, A. (2019). A comparative study of different mass transfer and liquid hold-up correlations in modeling CO<sub>2</sub> absorption with MEA. *Journal of Natural Gas Science and Engineering*, 62(December 2018), 92–100. <https://doi.org/10.1016/j.jngse.2018.12.004>
- Henning, C., Perreault, F., Oukarroum, A., Pedroso, S., Popovic, R., & Gerson, W. (2016a). Effect of chromium oxide ( III ) nanoparticles on the production of reactive oxygen species and photosystem II activity in the green alga *Chlamydomonas reinhardtii*. *Science of the Total Environment*, 565, 951–960. <https://doi.org/10.1016/j.scitotenv.2016.01.028>

- Henning, C., Perreault, F., Oukarroum, A., Pedroso, S., Popovic, R., & Gerson, W. (2016b). Effect of chromium oxide ( III ) nanoparticles on the production of reactive oxygen species and photosystem II activity in the green alga *Chlamydomonas reinhardtii*. *Science of the Total Environment*, 565, 951–960. <https://doi.org/10.1016/j.scitotenv.2016.01.028>
- Hernández-García, A., Velásquez-Orta, S. B., Novelo, E., Yáñez-Noguez, I., Monje-Ramírez, I., & Orta Ledesma, M. T. (2019). Wastewater-leachate treatment by microalgae: Biomass, carbohydrate and lipid production. *Ecotoxicology and Environmental Safety*, 174(March), 435–444. <https://doi.org/10.1016/j.ecoenv.2019.02.052>
- Hoecke, K. Van, Schamphelaere, K. A. C. De, Meeren, P. Van Der, Smagghe, G., & Janssen, C. R. (2011). Aggregation and ecotoxicity of CeO<sub>2</sub> nanoparticles in synthetic and natural waters with variable pH , organic matter concentration and ionic strength. *Environmental Pollution*, 159(4), 970–976. <https://doi.org/10.1016/j.envpol.2010.12.010>
- Hossain, N., Mahlia, T. M. I., & Saidur, R. (2019). Latest development in microalgae - biofuel production with nano - additives. *Biotechnology for Biofuels*, 1–16. <https://doi.org/10.1186/s13068-019-1465-0>
- Hu, J., Wang, J., Liu, S., Zhang, Z., Zhang, H., Cai, X., Pan, J., & Liu, J. (2018a). Effect of TiO<sub>2</sub> nanoparticle aggregation on marine microalgae *Isochrysis galbana*. *Journal of Environmental Sciences*, 66, 208–215. <https://doi.org/10.1016/J.JES.2017.05.026>
- Hu, J., Wang, J., Liu, S., Zhang, Z., Zhang, H., Cai, X., Pan, J., & Liu, J. (2018b). Effect of TiO<sub>2</sub> nanoparticle aggregation on marine microalgae *Isochrysis galbana*. *Journal of Environmental Sciences*, 66, 208–215. <https://doi.org/10.1016/J.JES.2017.05.026>
- Hu, Y. R., Wang, F., Wang, S. K., Liu, C. Z., & Guo, C. (2013). Efficient harvesting of marine microalgae *Nannochloropsis maritima* using magnetic nanoparticles. *Bioresource Technology*, 138, 387–390. <https://doi.org/10.1016/j.biortech.2013.04.016>
- Huang, C. H., & Tan, C. S. (2014). A review: CO<sub>2</sub> utilization. *Aerosol and Air Quality Research*, 14(2), 480–499. <https://doi.org/10.4209/aaqr.2013.10.0326>
- Huang, C. P., Cha, D. K., & Ismat, S. S. (2005). Progress report: short-term chronic toxicity of photocatalytic nanoparticles to bacteria, algae, and zooplankton. *EPA, 2005*, R831721.

- Hussain, F., Shah, S. Z., Ahmad, H., Abubshait, S. A., Abubshait, H. A., Laref, A., Manikandan, A., Kusuma, H. S., & Iqbal, M. (2021a). Microalgae an ecofriendly and sustainable wastewater treatment option: Biomass application in biofuel and bio-fertilizer production. A review. *Renewable and Sustainable Energy Reviews*, 137(August 2019), 110603. <https://doi.org/10.1016/j.rser.2020.110603>
- Hussain, F., Shah, S. Z., Ahmad, H., Abubshait, S. A., Abubshait, H. A., Laref, A., Manikandan, A., Kusuma, H. S., & Iqbal, M. (2021b). Microalgae an ecofriendly and sustainable wastewater treatment option: Biomass application in biofuel and bio-fertilizer production. A review. *Renewable and Sustainable Energy Reviews*, 137(August 2019), 110603. <https://doi.org/10.1016/j.rser.2020.110603>
- Iasimone, F., Panico, A., De Felice, V., Fantasma, F., Iorizzi, M., & Pirozzi, F. (2018). Effect of light intensity and nutrients supply on microalgae cultivated in urban wastewater: Biomass production, lipids accumulation and settleability characteristics. *Journal of Environmental Management*, 223, 1078–1085. <https://doi.org/10.1016/J.JENVMAN.2018.07.024>
- Ilves, V. G., Murzakaev, A. M., & Sokovnin, S. Y. (2018). On the interrelationship of porosity and structural defects in amorphous-crystalline nanopowders SiO<sub>2</sub>-doped Gd<sub>2</sub>O<sub>3</sub> with their magnetic and luminescent properties. *Microporous and Mesoporous Materials*, 271(May), 203–218. <https://doi.org/10.1016/j.micromeso.2018.05.044>
- Javed, F., Aslam, M., Rashid, N., Shamair, Z., Khan, A. L., Yasin, M., Fazal, T., Hafeez, A., Rehman, F., Rehman, M. S. U., Khan, Z., Iqbal, J., & Bazmi, A. A. (2019). Microalgae-based biofuels, resource recovery and wastewater treatment: A pathway towards sustainable biorefinery. *Fuel*, 255, 115826. <https://doi.org/10.1016/J.FUEL.2019.115826>
- Jeon, H. S., Park, S. E., Ahn, B., & Kim, Y. K. (2017). Enhancement of biodiesel production in *Chlorella vulgaris* cultivation using silica nanoparticles. *Biotechnology and Bioprocess Engineering*, 22(2), 136–141. <https://doi.org/10.1007/s12257-016-0657-8>
- Jeswani, H. K., Gujba, H., Brown, N. W., Roberts, E. P. L., & Azapagic, A. (2015). Removal of organic compounds from water: Life cycle environmental impacts and economic costs of the Arvia process compared to granulated activated carbon. *Journal of Cleaner Production*, 89, 203–213. <https://doi.org/10.1016/j.jclepro.2014.11.017>

- Ji, J., Long, Z., & Lin, D. (2011a). Toxicity of oxide nanoparticles to the green algae *Chlorella* sp. *Chemical Engineering Journal*, *170*(2–3), 525–530. <https://doi.org/10.1016/j.cej.2010.11.026>
- Ji, J., Long, Z., & Lin, D. (2011b). Toxicity of oxide nanoparticles to the green algae *Chlorella* sp. *Chemical Engineering Journal*, *170*(2–3), 525–530. <https://doi.org/10.1016/j.cej.2010.11.026>
- Jiang, Y., Pu, X., Zheng, D., Zhu, T., Wang, S., Deng, L., & Wang, W. (2018a). Cultivation of lipid-producing microalgae in struvite-precipitated liquid digestate for biodiesel production. *Biotechnology for Biofuels*, *11*(1), 1–9. <https://doi.org/10.1186/s13068-018-1102-3>
- Jiang, Y., Pu, X., Zheng, D., Zhu, T., Wang, S., Deng, L., & Wang, W. (2018b). Cultivation of lipid-producing microalgae in struvite-precipitated liquid digestate for biodiesel production. *Biotechnology for Biofuels*, *11*(1), 1–9. <https://doi.org/10.1186/s13068-018-1102-3>
- Johari, S. A., Sarkheil, M., Behzadi Tayemeh, M., & Veisi, S. (2018). Influence of salinity on the toxicity of silver nanoparticles (AgNPs) and silver nitrate (AgNO<sub>3</sub>) in halophilic microalgae, *Dunaliella salina*. *Chemosphere*, *209*, 156–162. <https://doi.org/10.1016/J.CHEMOSPHERE.2018.06.098>
- Kacheff, A., Fan, H., Wang, P., Oh, D. H., & Prouzet, E. (2014). Nano-coating of ceramic membranes for bubble-free injection of CO<sub>2</sub>. *Journal of CO<sub>2</sub> Utilization*, *6*, 12–16. <https://doi.org/10.1016/j.jcou.2014.02.003>
- Kadar, E., Rooks, P., Lakey, C., & White, D. A. (2012a). The effect of engineered iron nanoparticles on growth and metabolic status of marine microalgae cultures. *Science of the Total Environment*, *439*, 8–17. <https://doi.org/10.1016/j.scitotenv.2012.09.010>
- Kadar, E., Rooks, P., Lakey, C., & White, D. A. (2012b). The effect of engineered iron nanoparticles on growth and metabolic status of marine microalgae cultures. *Science of The Total Environment*, *439*, 8–17. <https://doi.org/10.1016/J.SCITOTENV.2012.09.010>
- Kadar, E., Rooks, P., Lakey, C., & White, D. A. (2012c). The effect of engineered iron nanoparticles on growth and metabolic status of marine microalgae cultures. *Science of The Total Environment*, *439*, 8–17. <https://doi.org/10.1016/J.SCITOTENV.2012.09.010>
- Kaliamurthi, S., Selvaraj, G., Cakmak, Z. E., Korkmaz, A. D., & Cakmak, T. (2019a). The relationship between *Chlorella* sp. and zinc oxide nanoparticles: Changes

- in biochemical, oxygen evolution, and lipid production ability. *Process Biochemistry*, 85, 43–50. <https://doi.org/10.1016/J.PROCBIO.2019.06.005>
- Kaliamurthi, S., Selvaraj, G., Cakmak, Z. E., Korkmaz, A. D., & Cakmak, T. (2019b). The relationship between *Chlorella* sp. and zinc oxide nanoparticles: Changes in biochemical, oxygen evolution, and lipid production ability. *Process Biochemistry*, 85, 43–50. <https://doi.org/10.1016/J.PROCBIO.2019.06.005>
- Kayani, Z. N., Arshad, S., Riaz, S., & Naseem, S. (2014). Synthesis of Iron Oxide Nanoparticles by Sol-Gel Technique and Their Characterization. *IEEE Transactions on Magnetics*, 50(8). <https://doi.org/10.1109/TMAG.2014.2313763>
- Khezerlou, A., Alizadeh-Sani, M., Azizi-Lalabadi, M., & Ehsani, A. (2018). Nanoparticles and their antimicrobial properties against pathogens including bacteria, fungi, parasites and viruses. *Microbial Pathogenesis*, 123(February), 505–526. <https://doi.org/10.1016/j.micpath.2018.08.008>
- Klaine, S. J., Alvarez, P. J. J., Batley, G. E., Fernandes, T. F., Handy, R. D., Lyon, D. Y., Mahendra, S., McLaughlin, M. J., & Lead, J. R. (2008). Nanomaterials in the environment: behavior, fate, bioavailability and effects. *Environmental Toxicology and Chemistry*, 27(9), 1825–1851. <https://doi.org/10.1897/08-090.1>
- Kluytmans, J. H. J., van Wachem, B. G. M., Kuster, B. F. M., & Schouten, J. C. (2003). Mass transfer in sparged and stirred reactors: Influence of carbon particles and electrolyte. *Chemical Engineering Science*, 58(20), 4719–4728. <https://doi.org/10.1016/j.ces.2003.05.004>
- Krishnan, V., Prakash, J. S., Manigandan, V., Venkatasubbu, G. D., Pugazhendhi, A., Brindhadevi, K., & Kalaivani, T. (2022). Synthesis of mesoporous SiO<sub>2</sub> nanoparticles and toxicity assessment in early life stages of zebrafish. *Microporous and Mesoporous Materials*, 330(July 2021), 111573. <https://doi.org/10.1016/j.micromeso.2021.111573>
- Kuai, J., & Zhang, H. (2019). Research on generation and polishing mechanisms of nano grain  $\alpha$ -Fe<sub>2</sub>O<sub>3</sub> in precision electrolytic in process dressing (ELID) grinding. *Procedia Manufacturing*, 37, 425–430. <https://doi.org/10.1016/j.promfg.2019.12.069>
- Kumar, R., Mangalapuri, R., Ahmadi, M. H., Vo, D. V. N., Solanki, R., & Kumar, P. (2020). The role of nanotechnology on post-combustion CO<sub>2</sub> absorption in process industries. *International Journal of Low-Carbon Technologies*, 15(3), 361–367. <https://doi.org/10.1093/IJLCT/CTAA002>

- Lau, A. K. S., Bilad, M. R., Nordin, N. A. H. M., Faungnawakij, K., Narkkun, T., Wang, D. K., Mahlia, T. M. I., & Jaafar, J. (2020a). Effect of membrane properties on tilted panel performance of microalgae biomass filtration for biofuel feedstock. *Renewable and Sustainable Energy Reviews*, *120*, 109666. <https://doi.org/10.1016/J.RSER.2019.109666>
- Lau, A. K. S., Bilad, M. R., Nordin, N. A. H. M., Faungnawakij, K., Narkkun, T., Wang, D. K., Mahlia, T. M. I., & Jaafar, J. (2020b). Effect of membrane properties on tilted panel performance of microalgae biomass filtration for biofuel feedstock. *Renewable and Sustainable Energy Reviews*, *120*, 109666. <https://doi.org/10.1016/J.RSER.2019.109666>
- Lei, C., Zhang, L., Yang, K., Zhu, L., & Lin, D. (2016a). Toxicity of iron-based nanoparticles to green algae : Effects of particle size , crystal phase , oxidation state and environmental aging \*. *Environmental Pollution*, *218*, 505–512. <https://doi.org/10.1016/j.envpol.2016.07.030>
- Lei, C., Zhang, L., Yang, K., Zhu, L., & Lin, D. (2016b). Toxicity of iron-based nanoparticles to green algae : Effects of particle size , crystal phase , oxidation state and environmental aging \*. *Environmental Pollution*, *218*, 505–512. <https://doi.org/10.1016/j.envpol.2016.07.030>
- Li, G., Zhang, J., Li, H., Hu, R., Yao, X., Liu, Y., Zhou, Y., & Lyu, T. (2020a). Towards high-quality biodiesel production from microalgae using original and anaerobically-digested livestock wastewater. *Chemosphere*, *xxxx*, 128578. <https://doi.org/10.1016/j.chemosphere.2020.128578>
- Li, G., Zhang, J., Li, H., Hu, R., Yao, X., Liu, Y., Zhou, Y., & Lyu, T. (2020b). Towards high-quality biodiesel production from microalgae using original and anaerobically-digested livestock wastewater. *Chemosphere*, *xxxx*, 128578. <https://doi.org/10.1016/j.chemosphere.2020.128578>
- Li, J., Shi, C., & Bao, A. (2021). Design of boron-doped mesoporous carbon materials for multifunctional applications: Dye adsorption and CO<sub>2</sub> capture. *Journal of Environmental Chemical Engineering*, *9*(3). <https://doi.org/10.1016/j.jece.2021.105250>
- Li, Q., Zhang, R., Wu, D., Huang, Y., Zhao, L., Wang, D., Gong, F., Li, L., Qiu, H., & Ma, G. (2016a). Cell-nanoparticle assembly fabricated for CO<sub>2</sub> capture and in situ carbon conversion. *Journal of CO<sub>2</sub> Utilization*, *13*, 17–23. <https://doi.org/10.1016/j.jcou.2015.11.004>
- Li, Q., Zhang, R., Wu, D., Huang, Y., Zhao, L., Wang, D., Gong, F., Li, L., Qiu, H., & Ma, G. (2016b). Cell-nanoparticle assembly fabricated for CO<sub>2</sub> capture and in

- situ carbon conversion. *Journal of CO<sub>2</sub> Utilization*, 13, 17–23.  
<https://doi.org/10.1016/j.jcou.2015.11.004>
- Liang, S. X. T., Wong, L. S., Dhanapal, A. C. T. A., & Djearmane, S. (2020). Toxicity of Metals and Metallic Nanoparticles on Nutritional Properties of Microalgae. *Water, Air, and Soil Pollution*, 231(2).  
<https://doi.org/10.1007/s11270-020-4413-5>
- Liao, J. jun, Gao, P. zhao, Xu, L., & Feng, J. (2018). A study of morphological properties of SiO<sub>2</sub> aerogels obtained at different temperatures. *Journal of Advanced Ceramics*, 7(4), 307–316. <https://doi.org/10.1007/s40145-018-0280-6>
- Lima, S., Villanova, V., Grisafi, F., Caputo, G., Brucato, A., & Scargiali, F. (2020a). Autochthonous microalgae grown in municipal wastewaters as a tool for effectively removing nitrogen and phosphorous. *Journal of Water Process Engineering*, 38(August), 101647. <https://doi.org/10.1016/j.jwpe.2020.101647>
- Lima, S., Villanova, V., Grisafi, F., Caputo, G., Brucato, A., & Scargiali, F. (2020b). Autochthonous microalgae grown in municipal wastewaters as a tool for effectively removing nitrogen and phosphorous. *Journal of Water Process Engineering*, 38(August), 101647. <https://doi.org/10.1016/j.jwpe.2020.101647>
- Ling, X., Guo, J., Liu, X., Zhang, X., Wang, N., Lu, Y., & Ng, I. S. (2015). Impact of carbon and nitrogen feeding strategy on high production of biomass and docosahexaenoic acid (DHA) by *Schizochytrium* sp. LU310. *Bioresource Technology*, 184, 139–147. <https://doi.org/10.1016/j.biortech.2014.09.130>
- Lu, D., Zhang, X. (Jackie), Liu, X., Zhang, L., & Hines, M. (2018). Sustainable microalgae cultivation by using anaerobic centrate and biogas from anaerobic digestion. *Algal Research*, 35(October 2017), 115–124.  
<https://doi.org/10.1016/j.algal.2018.08.028>
- Luo, Y., Le-Clech, P., & Henderson, R. K. (2020). Characterisation of microalgae-based monocultures and mixed cultures for biomass production and wastewater treatment. *Algal Research*, 49(February), 101963.  
<https://doi.org/10.1016/j.algal.2020.101963>
- Magalhães, I. B., Ferreira, J., de Siqueira Castro, J., Assis, L. R. de, & Calijuri, M. L. (2021). Technologies for improving microalgae biomass production coupled to effluent treatment: A life cycle approach. *Algal Research*, 57(April).  
<https://doi.org/10.1016/j.algal.2021.102346>

- Mahdy, A., Mendez, L., Ballesteros, M., & González-Fernández, C. (2015). Protease pretreated *Chlorella vulgaris* biomass bioconversion to methane via semi-continuous anaerobic digestion. *Fuel*, *158*, 35–41. <https://doi.org/10.1016/J.FUEL.2015.04.052>
- Manier, N., Bado-nilles, A., Delalain, P., Aguerre-chariol, O., & Pandard, P. (2013a). Ecotoxicity of non-aged and aged CeO<sub>2</sub> nanomaterials towards freshwater microalgae. *Environmental Pollution*, *180*, 63–70. <https://doi.org/10.1016/j.envpol.2013.04.040>
- Manier, N., Bado-nilles, A., Delalain, P., Aguerre-chariol, O., & Pandard, P. (2013b). Ecotoxicity of non-aged and aged CeO<sub>2</sub> nanomaterials towards freshwater microalgae. *Environmental Pollution*, *180*, 63–70. <https://doi.org/10.1016/j.envpol.2013.04.040>
- Manzo, S., Lucia, M., Rametta, G., Buono, S., & Di, G. (2013). Toxic effects of ZnO nanoparticles towards marine algae *Dunaliella tertiolecta*. *Science of the Total Environment*, *445–446*, 371–376. <https://doi.org/10.1016/j.scitotenv.2012.12.051>
- Marchello, A. E., Barreto, D. M., & Lombardi, A. T. (2018). Effects of Titanium Dioxide Nanoparticles in Different Metabolic Pathways in the Freshwater Microalga *Chlorella sorokiniana* (Trebouxiophyceae). *Water, Air, and Soil Pollution*, *229*(2). <https://doi.org/10.1007/s11270-018-3705-5>
- Marín, D., Carmona-Martínez, A. A., Blanco, S., Lebrero, R., & Muñoz, R. (2021). Innovative operational strategies in photosynthetic biogas upgrading in an outdoors pilot scale algal-bacterial photobioreactor. *Chemosphere*, *264*. <https://doi.org/10.1016/j.chemosphere.2020.128470>
- Marín, D., Carmona-Martínez, A. A., Lebrero, R., & Muñoz, R. (2020). Influence of the diffuser type and liquid-to-biogas ratio on biogas upgrading performance in an outdoor pilot scale high rate algal pond. *Fuel*, *275*(May), 117999. <https://doi.org/10.1016/j.fuel.2020.117999>
- Marín, D., Méndez, L., Suero, I., Díaz, I., Blanco, S., Fdz-Polanco, M., & Muñoz, R. (2022). Anaerobic Digestion of Food Waste Coupled with Biogas Upgrading in an Outdoors Algal-Bacterial Photobioreactor at Pilot Scale. *SSRN Electronic Journal*, *324*(March), 30–40. <https://doi.org/10.2139/ssrn.4057029>
- Marín, D., Ortíz, A., Díez-Montero, R., Uggetti, E., García, J., Lebrero, R., & Muñoz, R. (2019). Influence of liquid-to-biogas ratio and alkalinity on the biogas upgrading performance in a demo scale algal-bacterial photobioreactor.



- Bioresource Technology*, 280, 112–117.  
<https://doi.org/10.1016/J.BIORTECH.2019.02.029>
- Marín, D., Posadas, E., Cano, P., Pérez, V., Blanco, S., Lebrero, R., & Muñoz, R. (2018). Seasonal variation of biogas upgrading coupled with digestate treatment in an outdoors pilot scale algal-bacterial photobioreactor. *Bioresource Technology*, 263(February), 58–66.  
<https://doi.org/10.1016/j.biortech.2018.04.117>
- Marín, D., Posadas, E., Cano, P., Pérez, V., Lebrero, R., & Muñoz, R. (2018). Influence of the seasonal variation of environmental conditions on biogas upgrading in an outdoors pilot scale high rate algal pond. *Bioresource Technology*, 255(January), 354–358.  
<https://doi.org/10.1016/j.biortech.2018.01.136>
- Meier, L., Pérez, R., Azócar, L., Rivas, M., & Jeison, D. (2015). Photosynthetic CO<sub>2</sub> uptake by microalgae: An attractive tool for biogas upgrading. *Biomass and Bioenergy*, 73, 102–109. <https://doi.org/10.1016/J.BIOMBIOE.2014.10.032>
- Meier, L., Stará, D., Bartacek, J., & Jeison, D. (2018). Removal of H<sub>2</sub>S by a continuous microalgae-based photosynthetic biogas upgrading process. *Process Safety and Environmental Protection*, 119, 65–68.  
<https://doi.org/10.1016/J.PSEP.2018.07.014>
- Méndez, L., García, D., Perez, E., Blanco, S., & Munoz, R. (2022). Photosynthetic upgrading of biogas from anaerobic digestion of mixed sludge in an outdoors algal-bacterial photobioreactor at pilot scale. *Journal of Water Process Engineering*, 48(May). <https://doi.org/10.1016/j.jwpe.2022.102891>
- Miller, R. J., Lenihan, H. S., Muller, E. B., Tseng, N., Hanna, S. K., & Keller, A. A. (2010a). *Impacts of Metal Oxide Nanoparticles on Marine Phytoplankton*. 44(19), 7329–7334.
- Miller, R. J., Lenihan, H. S., Muller, E. B., Tseng, N., Hanna, S. K., & Keller, A. A. (2010b). *Impacts of Metal Oxide Nanoparticles on Marine Phytoplankton*. 44(19), 7329–7334.
- Miyawaki, B., Mariano, A. B., Vargas, J. V. C., Balmant, W., Defrancheschi, A. C., Corrêa, D. O., Santos, B., Selesu, N. F. H., Ordonez, J. C., & Kava, V. M. (2021). Microalgae derived biomass and bioenergy production enhancement through biogas purification and wastewater treatment. *Renewable Energy*, 163, 1153–1165. <https://doi.org/10.1016/j.renene.2020.09.045>

- Molinuevo-Salces, B., Mahdy, A., Ballesteros, M., & González-Fernández, C. (2016a). From piggery wastewater nutrients to biogas: Microalgae biomass revalorization through anaerobic digestion. *Renewable Energy*, *96*, 1103–1110. <https://doi.org/10.1016/j.renene.2016.01.090>
- Molinuevo-Salces, B., Mahdy, A., Ballesteros, M., & González-Fernández, C. (2016b). From piggery wastewater nutrients to biogas: Microalgae biomass revalorization through anaerobic digestion. *Renewable Energy*, *96*, 1103–1110. <https://doi.org/10.1016/j.renene.2016.01.090>
- Montingelli, M. E., Tedesco, S., & Olabi, A. G. (2015). Biogas production from algal biomass: A review. *Renewable and Sustainable Energy Reviews*, *43*, 961–972. <https://doi.org/10.1016/j.rser.2014.11.052>
- Mora-Godínez, S., Abril-Martínez, F., & Pacheco, A. (2020). Green synthesis of silver nanoparticles using microalgae acclimated to high CO<sub>2</sub>. *Materials Today: Proceedings*, *xxxx*. <https://doi.org/10.1016/j.matpr.2020.04.761>
- Morelli, E., Gabellieri, E., Bonomini, A., Tognotti, D., Grassi, G., & Corsi, I. (2018). TiO<sub>2</sub> nanoparticles in seawater: Aggregation and interactions with the green alga *Dunaliella tertiolecta*. *Ecotoxicology and Environmental Safety*, *148*(October 2017), 184–193. <https://doi.org/10.1016/j.ecoenv.2017.10.024>
- Moreno-Garrido, I., Pérez, S., & Blasco, J. (2015a). Toxicity of silver and gold nanoparticles on marine microalgae. *Marine Environmental Research*, *111*, 60–73. <https://doi.org/10.1016/J.MARENRES.2015.05.008>
- Moreno-Garrido, I., Pérez, S., & Blasco, J. (2015b). Toxicity of silver and gold nanoparticles on marine microalgae. *Marine Environmental Research*, *111*, 60–73. <https://doi.org/10.1016/J.MARENRES.2015.05.008>
- Moungmoon, T., Chaichana, C., Pumas, C., Pathom-aree, W., Ruangrit, K., & Pekkoh, J. (2020). Quantitative analysis of methane and glycolate production from microalgae using undiluted wastewater obtained from chicken-manure biogas digester. *Science of the Total Environment*, *714*, 136577. <https://doi.org/10.1016/j.scitotenv.2020.136577>
- Mulgund, A. (2022). Increasing lipid accumulation in microalgae through environmental manipulation, metabolic and genetic engineering: a review in the energy NEXUS framework. *Energy Nexus*, *5*(June 2021), 100054. <https://doi.org/10.1016/j.nexus.2022.100054>
- Mulu, E., Arimi, M. M. M., & Ramkat, R. C. (2021). A review of recent developments in application of low cost natural materials in purification and

- upgrade of biogas. *Renewable and Sustainable Energy Reviews*, 145(June 2020), 111081. <https://doi.org/10.1016/j.rser.2021.111081>
- Mulu, E., M'Arimi, M., Ramkat, R. c., & Kiprop, A. (2021). Biogas upgrade using modified natural clay. *Energy Conversion and Management: X*, 12, 100134. <https://doi.org/10.1016/j.ecmx.2021.100134>
- Munoz, M., Nieto-Sandoval, J., Álvarez-Torrellas, S., Sanz-Santos, E., Calderón, B., de Pedro, Z. M., Larriba, M., Fullana, A., García, J., & Casas, J. A. (2021). Carbon-encapsulated iron nanoparticles as reusable adsorbents for micropollutants removal from water. *Separation and Purification Technology*, 257(August 2020). <https://doi.org/10.1016/j.seppur.2020.117974>
- Navarro, E., Baun, A., Behra, R., Hartmann, N. B., Filser, J., Ai-Jun, M., Quigg, A., Santschi, P., & Sigg, L. (2008a). *Environmental behavior and ecotoxicity of engineered nanoparticles to algae , plants , and fungi*. 372–386. <https://doi.org/10.1007/s10646-008-0214-0>
- Navarro, E., Baun, A., Behra, R., Hartmann, N. B., Filser, J., Ai-Jun, M., Quigg, A., Santschi, P., & Sigg, L. (2008b). *Environmental behavior and ecotoxicity of engineered nanoparticles to algae , plants , and fungi*. 372–386. <https://doi.org/10.1007/s10646-008-0214-0>
- Ndiaye, M., Gadoin, E., & Gentric, C. (2018). CO<sub>2</sub> gas–liquid mass transfer and k<sub>La</sub> estimation: Numerical investigation in the context of airlift photobioreactor scale-up. *Chemical Engineering Research and Design*, 133(1998), 90–102. <https://doi.org/10.1016/j.cherd.2018.03.001>
- Nguyen, M. K., Moon, J.-Y., Bui, V. K. H., Oh, Y.-K., & Lee, Y.-C. (2019a). Recent advanced applications of nanomaterials in microalgae biorefinery. *Algal Research*, 41, 101522. <https://doi.org/10.1016/J.ALGAL.2019.101522>
- Nguyen, M. K., Moon, J.-Y., Bui, V. K. H., Oh, Y.-K., & Lee, Y.-C. (2019b). Recent advanced applications of nanomaterials in microalgae biorefinery. *Algal Research*, 41, 101522. <https://doi.org/10.1016/J.ALGAL.2019.101522>
- Nguyen, T. T. D., Nguyen, T. T., An Binh, Q., Bui, X. T., Ngo, H. H., Vo, H. N. P., Andrew Lin, K. Y., Vo, T. D. H., Guo, W., Lin, C., & Breider, F. (2020a). Co-culture of microalgae-activated sludge for wastewater treatment and biomass production: Exploring their role under different inoculation ratios. *Bioresource Technology*, 314(July), 123754. <https://doi.org/10.1016/j.biortech.2020.123754>

- Nguyen, T. T. D., Nguyen, T. T., An Binh, Q., Bui, X. T., Ngo, H. H., Vo, H. N. P., Andrew Lin, K. Y., Vo, T. D. H., Guo, W., Lin, C., & Breider, F. (2020b). Co-culture of microalgae-activated sludge for wastewater treatment and biomass production: Exploring their role under different inoculation ratios. *Bioresource Technology*, 314(July), 123754. <https://doi.org/10.1016/j.biortech.2020.123754>
- Nogueira, P. F. M., Nakabayashi, D., & Zucolotto, V. (2015). The effects of graphene oxide on green algae *Raphidocelis subcapitata*. *Aquatic Toxicology*, 166, 29–35. <https://doi.org/10.1016/j.aquatox.2015.07.001>
- Norouzi, A., & Nezamzadeh-Ejhieh, A. (2020).  $\alpha$ -Fe<sub>2</sub>O<sub>3</sub>/Cu<sub>2</sub>O heterostructure: Brief characterization and kinetic aspect of degradation of methylene blue. *Physica B: Condensed Matter*, 599(April). <https://doi.org/10.1016/j.physb.2020.412422>
- Oukarroum, A., & Popovic, R. (2012a). *Inhibitory effects of silver nanoparticles in two green algae, Chlorella vulgaris and Dunaliella tertiolecta*. 78, 80–85. <https://doi.org/10.1016/j.ecoenv.2011.11.012>
- Oukarroum, A., & Popovic, R. (2012b). *Inhibitory effects of silver nanoparticles in two green algae, Chlorella vulgaris and Dunaliella tertiolecta*. 78, 80–85. <https://doi.org/10.1016/j.ecoenv.2011.11.012>
- Pádrová, K., Lukavský, J., Nedbalová, L., Čejková, A., Cajthaml, T., Sigler, K., Vítová, M., & Řezanka, T. (2015). Trace concentrations of iron nanoparticles cause overproduction of biomass and lipids during cultivation of cyanobacteria and microalgae. *Journal of Applied Phycology*, 27(4), 1443–1451. <https://doi.org/10.1007/s10811-014-0477-1>
- Panahi, Y., Mellatyar, H., Farshbaf, M., Sabet, Z., Fattahi, T., & Akbarzadehe, A. (2018). Biotechnological applications of nanomaterials for air pollution and water/wastewater treatment. *Materials Today: Proceedings*, 5(7), 15550–15558. <https://doi.org/10.1016/j.matpr.2018.04.162>
- Paskuliakova, A., Tonry, S., & Touzet, N. (2016). Phycoremediation of landfill leachate with chlorophytes: Phosphate a limiting factor on ammonia nitrogen removal. *Water Research*, 99, 180–187. <https://doi.org/10.1016/j.watres.2016.04.029>
- Passos, F., Felix, L., Rocha, H., Pereira, J. de O., & de Aquino, S. (2016). Reuse of microalgae grown in full-scale wastewater treatment ponds: Thermochemical pretreatment and biogas production. *Bioresource Technology*, 209, 305–312. <https://doi.org/10.1016/j.biortech.2016.03.006>

- Passos, F., Hom-Diaz, A., Blaquez, P., Vicent, T., & Ferrer, I. (2016). Improving biogas production from microalgae by enzymatic pretreatment. *Bioresource Technology*, *199*, 347–351. <https://doi.org/10.1016/j.biortech.2015.08.084>
- Pedroso, S., Helena, R., Costa, R., Popovic, R., & Gerson, W. (2013a). *Evaluation of toxicity and oxidative stress induced by copper oxide nanoparticles in the green alga Chlamydomonas reinhardtii*. *143*, 431–440. <https://doi.org/10.1016/j.aquatox.2013.09.015>
- Pedroso, S., Helena, R., Costa, R., Popovic, R., & Gerson, W. (2013b). *Evaluation of toxicity and oxidative stress induced by copper oxide nanoparticles in the green alga Chlamydomonas reinhardtii*. *143*, 431–440. <https://doi.org/10.1016/j.aquatox.2013.09.015>
- Porto, B., Gonçalves, A. L., Esteves, A. F., de Souza, S. M. A. G. U., de Souza, A. A. U., Vilar, V. J. P., & Pires, J. C. M. (2020). Assessing the potential of microalgae for nutrients removal from a landfill leachate using an innovative tubular photobioreactor. *Chemical Engineering Journal*, *413*(October 2020). <https://doi.org/10.1016/j.cej.2020.127546>
- Posadas, E., Marín, D., Blanco, S., Lebrero, R., & Muñoz, R. (2017). Simultaneous biogas upgrading and centrate treatment in an outdoors pilot scale high rate algal pond. *Bioresource Technology*, *232*, 133–141. <https://doi.org/10.1016/j.biortech.2017.01.071>
- Posadas, E., Serejo, M. L., Blanco, S., Pérez, R., García-Encina, P. A., & Muñoz, R. (2015). Minimization of biomethane oxygen concentration during biogas upgrading in algal–bacterial photobioreactors. *Algal Research*, *12*, 221–229. <https://doi.org/10.1016/J.ALGAL.2015.09.002>
- Posadas, E., Szpak, D., Lombó, F., Domínguez, A., Díaz, I., Blanco, S., García-Encina, P. A., & Muñoz, R. (2016). Feasibility study of biogas upgrading coupled with nutrient removal from anaerobic effluents using microalgae-based processes. *Journal of Applied Phycology*, *28*(4), 2147–2157. <https://doi.org/10.1007/s10811-015-0758-3>
- Powell, C. D., Lounsbury, A. W., Fishman, Z. S., Coonrod, C. L., Gallagher, M. J., Villagran, D., Zimmerman, J. B., Pfefferle, L. D., & Wong, M. S. (2021). Nano-structural effects on Hematite ( $\alpha$ -Fe<sub>2</sub>O<sub>3</sub>) nanoparticle radiofrequency heating. *Nano Convergence*, *8*(1). <https://doi.org/10.1186/s40580-021-00258-7>
- Praveen, P., Guo, Y., Kang, H., Lefebvre, C., & Loh, K.-C. (2018). Enhancing microalgae cultivation in anaerobic digestate through nitrification. *Chemical*

- Engineering Journal*, 354, 905–912.  
<https://doi.org/10.1016/J.CEJ.2018.08.099>
- Qiu, Y., Frear, C., Chen, S., Ndegwa, P., Harrison, J., Yao, Y., & Ma, J. (2020). Accumulation of long-chain fatty acids from *Nannochloropsis salina* enhanced by breaking microalgae cell wall under alkaline digestion. *Renewable Energy*, 149, 691–700. <https://doi.org/10.1016/j.renene.2019.12.093>
- Rai, P. K., Kumar, V., Lee, S. S., Raza, N., Kim, K. H., Ok, Y. S., & Tsang, D. C. W. (2018). Nanoparticle-plant interaction: Implications in energy, environment, and agriculture. *Environment International*, 119(May), 1–19.  
<https://doi.org/10.1016/j.envint.2018.06.012>
- Raja, K., Mary Jacqueline, M., Jose, M., Verma, S., Prince, A. A. M., Ilangoan, K., Sethusankar, K., & Jerome Das, S. (2015). Sol-gel synthesis and characterization of  $\alpha$ -Fe<sub>2</sub>O<sub>3</sub> nanoparticles. *Superlattices and Microstructures*, 86, 306–312. <https://doi.org/10.1016/j.spmi.2015.07.044>
- Rana, M. S., Bhushan, S., Sudhakar, D. R., & Prajapati, S. K. (2020). Effect of iron oxide nanoparticles on growth and biofuel potential of *Chlorella* spp. *Algal Research*, 49(February), 101942. <https://doi.org/10.1016/j.algal.2020.101942>
- Rana, M. S., & Prajapati, S. K. (2021). Resolving the dilemma of iron bioavailability to microalgae for commercial sustenance. *Algal Research*, 59(July), 102458. <https://doi.org/10.1016/j.algal.2021.102458>
- Rao, B. N., Padmaraj, O., Kumar, P. R., Venkateswarlu, M., Madhusudhan Rao, V., & Satyanarayana, N. (2015). Synthesis of hematite  $\alpha$ -Fe<sub>2</sub>O<sub>3</sub> nanospheres for lithium ion battery applications. *AIP Conference Proceedings*, 1665, 17806–17812. <https://doi.org/10.1063/1.4917849>
- Rastogi, R. P., Madamwar, D., Nakamoto, H., & Incharoensakdi, A. (2020). Resilience and self-regulation processes of microalgae under UV radiation stress. *Journal of Photochemistry and Photobiology C: Photochemistry Reviews*, 43, 100322. <https://doi.org/10.1016/j.jphotochemrev.2019.100322>
- Ren, H.-Y., Dai, Y.-Q., Kong, F., Xing, D., Zhao, L., Ren, N.-Q., Ma, J., & Liu, B.-F. (2020). Enhanced microalgal growth and lipid accumulation by addition of different nanoparticles under xenon lamp illumination. *Bioresource Technology*, 297, 122409. <https://doi.org/10.1016/J.BIORTECH.2019.122409>
- Rocha, A. A., Wilde, C., Hu, Z., Nepotchatykh, O., Nazarenko, Y., & Ariya, P. A. (2017). Development of a hybrid photo-bioreactor and nanoparticle adsorbent system for the removal of CO<sub>2</sub>, and selected organic and metal co-pollutants.

- Journal of Environmental Sciences (China)*, 57, 41–53.  
<https://doi.org/10.1016/j.jes.2016.12.010>
- Rodero, M. del R., Carvajal, A., Arbib, Z., Lara, E., de Prada, C., Lebrero, R., & Muñoz, R. (2020). Performance evaluation of a control strategy for photosynthetic biogas upgrading in a semi-industrial scale photobioreactor. *Bioresource Technology*, 307(March), 123207.  
<https://doi.org/10.1016/j.biortech.2020.123207>
- Rodero, M. del R., Lebrero, R., Serrano, E., Lara, E., Arbib, Z., García-Encina, P. A., & Muñoz, R. (2019). Technology validation of photosynthetic biogas upgrading in a semi-industrial scale algal-bacterial photobioreactor. *Bioresource Technology*, 279(December 2018), 43–49.  
<https://doi.org/10.1016/j.biortech.2019.01.110>
- Rodero, M. del R., Severi, C. A., Rocher-Rivas, R., Quijano, G., & Muñoz, R. (2020). Long-term influence of high alkalinity on the performance of photosynthetic biogas upgrading. *Fuel*, 281(July), 118804.  
<https://doi.org/10.1016/j.fuel.2020.118804>
- Rodero, M. R., Ángeles, R., Marín, D., Díaz, I., Colzi, A., Posadas, E., Lebrero, R., & Muñoz, R. (2018). *Biogas Purification and Upgrading Technologies BT - Biogas: Fundamentals, Process, and Operation* (M. Tabatabaei & H. Ghanavati, Eds.; pp. 239–276). Springer International Publishing.  
[https://doi.org/10.1007/978-3-319-77335-3\\_10](https://doi.org/10.1007/978-3-319-77335-3_10)
- Romero, N., Visentini, F. F., Márquez, V. E., Santiago, L. G., Castro, G. R., & Gagnetten, A. M. (2020). Physiological and morphological responses of green microalgae *Chlorella vulgaris* to silver nanoparticles. *Environmental Research*, 189(April). <https://doi.org/10.1016/j.envres.2020.109857>
- Rosa, G. M. da, Moraes, L., Cardias, B. B., Souza, M. da R. A. Z. de, & Costa, J. A. V. (2015). Chemical absorption and CO<sub>2</sub> biofixation via the cultivation of *Spirulina* in semicontinuous mode with nutrient recycle. *Bioresource Technology*, 192, 321–327. <https://doi.org/10.1016/j.biortech.2015.05.020>
- Rosa, G. M. da, Morais, M. G. de, & Costa, J. A. V. (2018). Green alga cultivation with monoethanolamine: Evaluation of CO<sub>2</sub> fixation and macromolecule production. *Bioresource Technology*, 261(January), 206–212.  
<https://doi.org/10.1016/j.biortech.2018.04.007>
- Rudic, V., Cepoi, L., Rudi, L., Chiriac, T., Nicorici, A., Todosiciuc, A., & Gutsul, T. (2011). Synthesis of CdSe nanoparticles and their effect on the antioxidant activity of *Spirulina platensis* and *Porphyridium cruentum* cells. *ICNBME-*

2011: *International Conference on Nanotechnologies and Biomedical Engineering; German-Moldovan Workshop on Novel Nanomaterials for Electronic, Photonic and Biomedical Applications Proceedings*, 460.

- Sadiq, I. M., Dalai, S., Chandrasekaran, N., & Mukherjee, A. (2011a). Ecotoxicity study of titania (TiO<sub>2</sub>) NPs on two microalgae species: *Scenedesmus* sp. and *Chlorella* sp. *Ecotoxicology and Environmental Safety*, 74(5), 1180–1187. <https://doi.org/10.1016/j.ecoenv.2011.03.006>
- Sadiq, I. M., Dalai, S., Chandrasekaran, N., & Mukherjee, A. (2011b). Ecotoxicity study of titania (TiO<sub>2</sub>) NPs on two microalgae species: *Scenedesmus* sp. and *Chlorella* sp. *Ecotoxicology and Environmental Safety*, 74(5), 1180–1187. <https://doi.org/10.1016/j.ecoenv.2011.03.006>
- Sakthi Vignesh, N., Vimali, E., Sangeetha, R., Arumugam, M., Ashokkumar, B., Ganeshmoorthy, I., & Varalakshmi, P. (2020). Sustainable biofuel from microalgae: Application of lignocellulosic wastes and bio-iron nanoparticle for biodiesel production. *Fuel*, 278(June), 118326. <https://doi.org/10.1016/j.fuel.2020.118326>
- Sarma, S. J., Das, R. K., Brar, S. K., Le Bihan, Y., Buelna, G., Verma, M., & Soccol, C. R. (2014). Application of magnesium sulfate and its nanoparticles for enhanced lipid production by mixotrophic cultivation of algae using biodiesel waste. *Energy*, 78, 16–22. <https://doi.org/10.1016/J.ENERGY.2014.04.112>
- Sendra, M., Yeste, M. P., Gatica, J. M., Moreno-Garrido, I., & Blasco, J. (2017a). Direct and indirect effects of silver nanoparticles on freshwater and marine microalgae (*Chlamydomonas reinhardtii* and *Phaeodactylum tricorutum*). *Chemosphere*, 179, 279–289. <https://doi.org/10.1016/J.CHEMOSPHERE.2017.03.123>
- Sendra, M., Yeste, M. P., Gatica, J. M., Moreno-Garrido, I., & Blasco, J. (2017b). Direct and indirect effects of silver nanoparticles on freshwater and marine microalgae (*Chlamydomonas reinhardtii* and *Phaeodactylum tricorutum*). *Chemosphere*, 179, 279–289. <https://doi.org/10.1016/J.CHEMOSPHERE.2017.03.123>
- Shahid, A., Malik, S., Zhu, H., Xu, J., Nawaz, M. Z., Nawaz, S., Asraful Alam, M., & Mehmood, M. A. (2020a). Cultivating microalgae in wastewater for biomass production, pollutant removal, and atmospheric carbon mitigation; a review. *Science of the Total Environment*, 704, 135303. <https://doi.org/10.1016/j.scitotenv.2019.135303>



- Shahid, A., Malik, S., Zhu, H., Xu, J., Nawaz, M. Z., Nawaz, S., Asraful Alam, M., & Mehmood, M. A. (2020b). Cultivating microalgae in wastewater for biomass production, pollutant removal, and atmospheric carbon mitigation; a review. *Science of the Total Environment*, 704, 135303. <https://doi.org/10.1016/j.scitotenv.2019.135303>
- Shokri, A., & Fard, M. S. (2022). A critical review in Fenton-like approach for the removal of pollutants in the aqueous environment. *Environmental Challenges*, 7(January), 100534. <https://doi.org/10.1016/j.envc.2022.100534>
- Solórzano, L. (1969). Determination of ammonia in natural waters by the phenolhypochlorite method. *Limnology and Oceanography*, 14(5), 799–801.
- Sournia, A. (1978). Phytoplankton manual. In *Information sources in cartography*. [https://doi.org/10.5005/jp/books/13041\\_39](https://doi.org/10.5005/jp/books/13041_39)
- Su, Y. (2021). Revisiting carbon, nitrogen, and phosphorus metabolisms in microalgae for wastewater treatment. *Science of the Total Environment*, 762, 144590. <https://doi.org/10.1016/j.scitotenv.2020.144590>
- Suman, T. Y., Rajasree, S. R. R., & Kirubakaran, R. (2015a). Evaluation of zinc oxide nanoparticles toxicity on marine algae chlorella vulgaris through flow cytometric , cytotoxicity and oxidative stress analysis. *Ecotoxicology and Environmental Safety*, 113, 23–30. <https://doi.org/10.1016/j.ecoenv.2014.11.015>
- Suman, T. Y., Rajasree, S. R. R., & Kirubakaran, R. (2015b). Evaluation of zinc oxide nanoparticles toxicity on marine algae chlorella vulgaris through flow cytometric , cytotoxicity and oxidative stress analysis. *Ecotoxicology and Environmental Safety*, 113, 23–30. <https://doi.org/10.1016/j.ecoenv.2014.11.015>
- Sun, Y., Liao, Q., Huang, Y., Xia, A., Fu, Q., Zhu, X., & Zheng, Y. (2016). Integrating planar waveguides doped with light scattering nanoparticles into a flat-plate photobioreactor to improve light distribution and microalgae growth. *Bioresource Technology*, 220, 215–224. <https://doi.org/10.1016/J.BIORTECH.2016.08.063>
- Tan, X. B., Wan, X. P., Yang, L. Bin, Wang, X., Meng, J., Jiang, M. J., & Pi, H. J. (2021). Nutrients recycling and biomass production from Chlorella pyrenoidosa culture using anaerobic food processing wastewater in a pilot-scale tubular photobioreactor. *Chemosphere*, 270, 129459. <https://doi.org/10.1016/j.chemosphere.2020.129459>

- Terán Hilares, R., Garcia Bustos, K. A., Sanchez Vera, F. P., Colina Andrade, G. J., & Pacheco Tanaka, D. A. (2021). Acid precipitation followed by microalgae (*Chlorella vulgaris*) cultivation as a new approach for poultry slaughterhouse wastewater treatment. *Bioresource Technology*, 335(May).  
<https://doi.org/10.1016/j.biortech.2021.125284>
- Tighe-Neira, R., Carmora, E., Recio, G., Nunes-Nesi, A., Reyes-Diaz, M., Alberdi, M., Rengel, Z., & Inostroza-Blancheteau, C. (2018). Metallic nanoparticles influence the structure and function of the photosynthetic apparatus in plants. *Plant Physiology and Biochemistry*, 130(May), 408–417.  
<https://doi.org/10.1016/j.plaphy.2018.07.024>
- Toledo-Cervantes, A., Garduño Solórzano, G., Campos, J. E., Martínez-García, M., & Morales, M. (2018). Characterization of *Scenedesmus obtusiusculus* AT-UAM for high-energy molecules accumulation: deeper insight into biotechnological potential of strains of the same species. *Biotechnology Reports*, 17(November 2017), 16–23.  
<https://doi.org/10.1016/j.btre.2017.11.009>
- Toledo-Cervantes, A., Serejo, M. L., Blanco, S., Pérez, R., Lebrero, R., & Muñoz, R. (2016). Photosynthetic biogas upgrading to bio-methane: Boosting nutrient recovery via biomass productivity control. *Algal Research*, 17, 46–52.  
<https://doi.org/10.1016/J.ALGAL.2016.04.017>
- Tongprawhan, W., Srinuanpan, S., & Cheirsilp, B. (2014). Biocapture of CO<sub>2</sub> from biogas by oleaginous microalgae for improving methane content and simultaneously producing lipid. *Bioresource Technology*, 170, 90–99.  
<https://doi.org/10.1016/j.biortech.2014.07.094>
- Torkamani, S., Wani, S. N., Tang, Y. J., & Sureshkumar, R. (2010a). Plasmon-enhanced microalgal growth in miniphotobioreactors. *Applied Physics Letters*, 97(4), 1–4. <https://doi.org/10.1063/1.3467263>
- Torkamani, S., Wani, S. N., Tang, Y. J., & Sureshkumar, R. (2010b). Plasmon-enhanced microalgal growth in miniphotobioreactors. *Applied Physics Letters*, 97(4), 1–4. <https://doi.org/10.1063/1.3467263>
- Tseng, R. L., Wu, F. C., & Juang, R. S. (2010). Characteristics and applications of the Lagergren's first-order equation for adsorption kinetics. *Journal of the Taiwan Institute of Chemical Engineers*, 41(6), 661–669.  
<https://doi.org/10.1016/j.jtice.2010.01.014>
- Uggetti, E., García, J., Álvarez, J. A., & García-Galán, M. J. (2018). Start-up of a microalgae-based treatment system within the biorefinery concept: From

- wastewater to bioproducts. *Water Science and Technology*, 78(1), 114–124. <https://doi.org/10.2166/wst.2018.195>
- Van Wychen, S., & Laurens, L. M. L. (2016). Determination of Total Solids and Ash in Algal Biomass: Laboratory Analytical Procedure (LAP). *Technical Report NREL/TP-5100-60957 National Renewable Energy Laboratory (NREL)*, 303(December), 275–3000.
- Varaprasad, D., Raghavendra, P., Sudha, N. R., Sarma, L. S., Parveen, S. N., Chandana, P. S., Chandra, M. S., & Chandrasekhar, T. (2021). Bioethanol Production from Green Alga *Chlorococcum minutum* through Reduced Graphene Oxide-Supported Platinum-Ruthenium (Pt-Ru/RGO) Nanoparticles. *Bioenergy Research*. <https://doi.org/10.1007/s12155-021-10282-4>
- Vargas-Estrada, L., Hoyos, E. G., Sebastian, P. J., & Mu, R. (2022). Elucidating the role of nanoparticles on photosynthetic biogas upgrading : Influence of biogas type , nanoparticle concentration and light source. *Algal Research*, 68. <https://doi.org/10.1016/j.algal.2022.102899>
- Vargas-Estrada, L., Hoyos, E. G., Sebastian, P., & Munoz, R. (2023). Influence of Mesoporous Iron Based Nanoparticles on *Chlorella Sorokiniana* Metabolism During Photosynthetic Biogas Upgrading. *Fuel*, 333. <https://doi.org/10.2139/ssrn.4187585>
- Vargas-Estrada, L., Longoria, A., Arenas, E., Moreira, J., Okoye, P. U., Bustos-Terrones, Y., & Sebastian, P. J. (2021). A Review on Current Trends in Biogas Production from Microalgae Biomass and Microalgae Waste by Anaerobic Digestion and Co-digestion. *Bioenergy Research*. <https://doi.org/10.1007/s12155-021-10276-2>
- Vargas-Estrada, L., Longoria, A., Arias, D. M., Okoye, P. U., & Sebastian, P. J. (2020). Role of nanoparticles on microalgal cultivation : A review. *Fuel*, 280(March). <https://doi.org/10.1016/j.fuel.2020.118598>
- Vargas-Estrada, L., Longoria, A., Okoye, P. U., & Sebastian, P. J. (2021). Energy and nutrients recovery from wastewater cultivated microalgae: Assessment of the impact of wastewater dilution on biogas yield. *Bioresour Technol*, 341(June), 125755. <https://doi.org/10.1016/j.biortech.2021.125755>
- Vaz, B. da S., Alberto Vieira Costa, J., & Greque de Morais, M. (2020). Physical and biological fixation of CO<sub>2</sub> with polymeric nanofibers in outdoor cultivations of *Chlorella fusca* LEB 111. *International Journal of Biological Macromolecules*, 151, 1332–1339. <https://doi.org/10.1016/j.ijbiomac.2019.10.179>

- Vaz, B. da S., Costa, J. A. V., & Morais, M. G. de. (2019). Innovative nanofiber technology to improve carbon dioxide biofixation in microalgae cultivation. *Bioresource Technology*, 273(November 2018), 592–598. <https://doi.org/10.1016/j.biortech.2018.11.054>
- Vaz, B. da S., Mastrantonio, D. J. da S., Costa, J. A. V., & de Morais, M. G. (2019). Green alga cultivation with nanofibers as physical adsorbents of carbon dioxide: Evaluation of gas biofixation and macromolecule production. *Bioresource Technology*, 287(February). <https://doi.org/10.1016/j.biortech.2019.121406>
- Wang, C., Hong, F., Lu, Y., Li, X., & Liu, H. (2017). Improved biogas production and biodegradation of oilseed rape straw by using kitchen waste and duck droppings as co-substrates in two-phase anaerobic digestion. *PLoS ONE*, 12(8), 1–19. <https://doi.org/10.1371/journal.pone.0182361>
- Wang, D., Hu, J., Irons, D. R., & Wang, J. (2011). Synergistic toxic effect of nano-TiO<sub>2</sub> and As (V) on *Ceriodaphnia dubia*. *Science of The Total Environment*, 409, 1351–1356. <https://doi.org/10.1016/j.scitotenv.2010.12.024>
- Wang, F., Liu, T., Guan, W., Xu, L., Huo, S., Ma, A., Zhuang, G., & Terry, N. (2021). *Development of a Strategy for Enhancing the Biomass Growth and Lipid Accumulation of Chlorella sp . UJ-3 Using Magnetic Fe<sub>3</sub>O<sub>4</sub> Nanoparticles.*
- Wang, J., Li, H., Li, X., Cong, H., & Gao, X. (2021). An intensification of mass transfer process for gas-liquid counter-current flow in a novel microchannel with limited path for CO<sub>2</sub> capture. *Process Safety and Environmental Protection*, 149, 905–914. <https://doi.org/10.1016/j.psep.2021.03.046>
- Wang, L., Min, M., Li, Y., Chen, P., Chen, Y., Liu, Y., Wang, Y., & Ruan, R. (2010). Cultivation of green algae *Chlorella* sp. in different wastewaters from municipal wastewater treatment plant. *Applied Biochemistry and Biotechnology*, 162(4), 1174–1186. <https://doi.org/10.1007/s12010-009-8866-7>
- Wang, X., Duan, X., Chen, J., Fang, K., Feng, L., Yan, Y., & Zhou, Q. (2016). Enhancing anaerobic digestion of waste activated sludge by pretreatment: Effect of volatile to total solids. *Environmental Technology (United Kingdom)*, 37(12), 1520–1529. <https://doi.org/10.1080/09593330.2015.1120783>
- Xia, C., van Le, Q., Chinnathambi, A., Salmen, S. H., Alharbi, S. A., & Tola, S. (2021). Role of ZnO and Fe<sub>2</sub>O<sub>3</sub> nanoparticle on synthetic saline wastewater on growth, nutrient removal and lipid content of *Chlorella vulgaris* for sustainable

- production of biofuel. *Fuel*, 300(May), 120924.  
<https://doi.org/10.1016/j.fuel.2021.120924>
- Xu, J., Zhao, Y., Zhao, G., & Zhang, H. (2015). Nutrient removal and biogas upgrading by integrating freshwater algae cultivation with piggery anaerobic digestate liquid treatment. *Applied Microbiology and Biotechnology*, 99(15), 6493–6501. <https://doi.org/10.1007/s00253-015-6537-x>
- Yang, L., Su, Q., Si, B., Zhang, Y., Zhang, Y., Yang, H., & Zhou, X. (2022). Enhancing bioenergy production with carbon capture of microalgae by ultraviolet spectrum conversion via graphene oxide quantum dots. *Chemical Engineering Journal*, 429(September 2021), 132230.  
<https://doi.org/10.1016/j.cej.2021.132230>
- Yu, Z., Tetard, L., Zhai, L., & Thomas, J. (2015). Supercapacitor electrode materials: Nanostructures from 0 to 3 dimensions. *Energy and Environmental Science*, 8(3), 702–730. <https://doi.org/10.1039/c4ee03229b>
- Zeng, X., Danquah, M. K., Zhang, S., Zhang, X., Wu, M., Chen, X. D., Ng, I. S., Jing, K., & Lu, Y. (2012). Autotrophic cultivation of *Spirulina platensis* for CO<sub>2</sub> fixation and phycocyanin production. *Chemical Engineering Journal*, 183, 192–197. <https://doi.org/10.1016/j.cej.2011.12.062>
- Zhang, C., Wang, J., Tan, L., & Chen, X. (2016). Toxic effects of nano-ZnO on marine microalgae *Skeletonema costatum*: Attention to the accumulation of intracellular Zn. *Aquatic Toxicology*, 178, 158–164.  
<https://doi.org/https://doi.org/10.1016/j.aquatox.2016.07.020>
- Zhang, R., Zeng, L., Wang, F., Li, X., & Li, Z. (2022). Influence of pore volume and surface area on benzene adsorption capacity of activated carbons in indoor environments. *Building and Environment*, 216(March), 109011.  
<https://doi.org/10.1016/j.buildenv.2022.109011>
- Zhao, B., & Su, Y. (2014). Process effect of microalgal-carbon dioxide fixation and biomass production: A review. *Renewable and Sustainable Energy Reviews*, 31, 121–132. <https://doi.org/10.1016/j.rser.2013.11.054>
- Zhao, Y., Guo, G., Sun, S., Hu, C., & Liu, J. (2019). Co-pelletization of microalgae and fungi for efficient nutrient purification and biogas upgrading. *Bioresour Technol*, 289(June). <https://doi.org/10.1016/j.biortech.2019.121656>
- Zhou, H., Wang, X., Zhou, Y., Yao, H., & Ahmad, F. (2014a). Evaluation of the toxicity of ZnO nanoparticles to *Chlorella vulgaris* by use of the chiral

perturbation approach. *Anal Bioanal Chem*, 3689–3695.  
<https://doi.org/10.1007/s00216-014-7773-0>

Zhou, H., Wang, X., Zhou, Y., Yao, H., & Ahmad, F. (2014b). Evaluation of the toxicity of ZnO nanoparticles to *Chlorella vulgaris* by use of the chiral perturbation approach. *Anal Bioanal Chem*, 3689–3695.  
<https://doi.org/10.1007/s00216-014-7773-0>



# Appendix

**Fig. A1.** Elemental analysis of Fe<sub>2</sub>O<sub>3</sub> NPs.

Spectrum processin :

Peaks possibly omitte : 1.481, 1.739 keV

Processing option : All elements analyzed (Normalised)

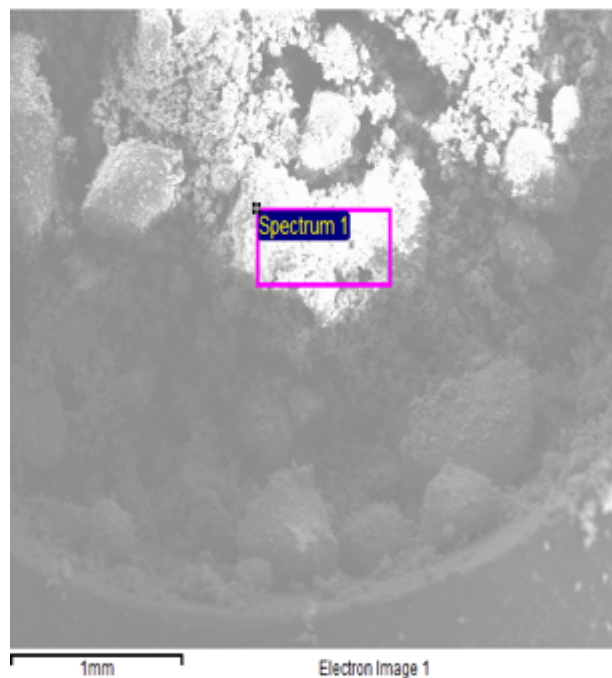
Number of iterations = 4

Standard:

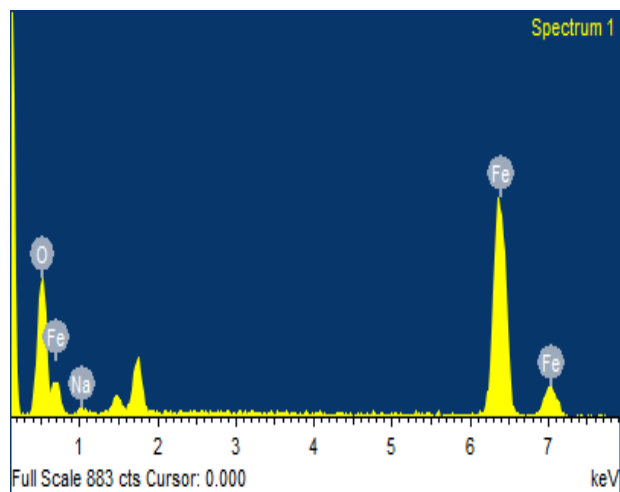
O SiO<sub>2</sub> 1-Jun-1999 12:00 AM

Na Albite 1-Jun-1999 12:00 AM

Fe Fe 1-Jun-1999 12:00 AM



Element	Weight%	Atomic%
O K	34.02	63.33
Na K	1.94	2.52
Fe L	64.04	34.16
Totals	100.00	



Comment: Hematite



**Fig. A2.** Elemental analysis of CALPECH NPs.

Spectrum processing:

Peaks possibly omitted: 1.484, 2.645 keV

Processing option: All elements analyzed  
(Normalized)

Number of iterations = 7

Standard:

C CaCO<sub>3</sub> 1-Jun-1999 12:00 AM

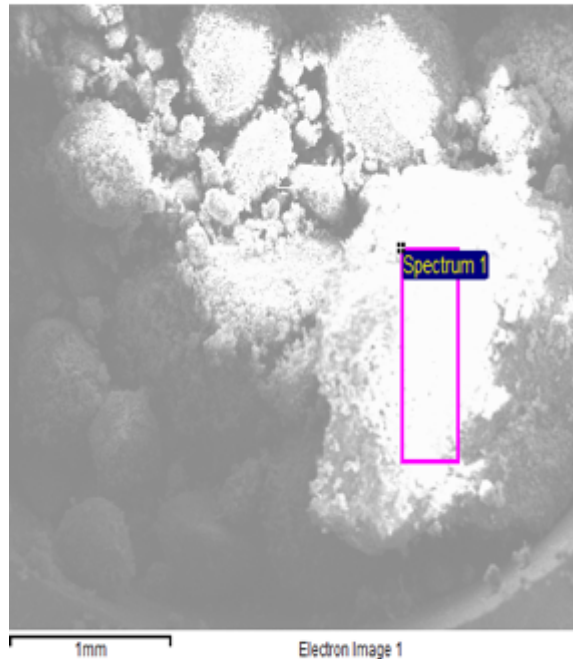
O SiO<sub>2</sub> 1-Jun-1999 12:00 AM

P GaP 1-Jun-1999 12:00 AM

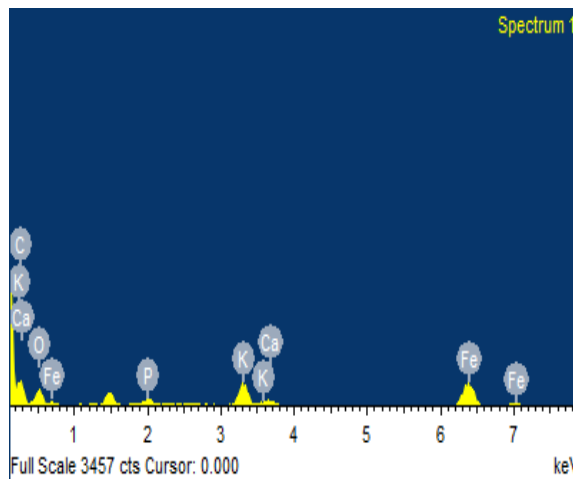
K MAD-10 Feldspar 1-Jun-1999 12:00 AM

Ca Wollastonite 1-Jun-1999 12:00 AM

Fe Fe 1-Jun-1999 12:00 AM



Element	Weight%	Atomic%
C K	76.38	85.06
O K	15.37	12.85
P K	0.21	0.09
K K	0.68	0.23
Ca K	0.10	0.03
Fe L	7.26	1.74
Totals	100.00	



Comment: CALPECH

**Fig. A3.** Elemental analysis of SMALLOPS NPs.

Spectrum processing:

Peak possibly omitted: 1.490 keV

Processing option: All elements analyzed (Normalised)

Number of iterations = 8

Standard:

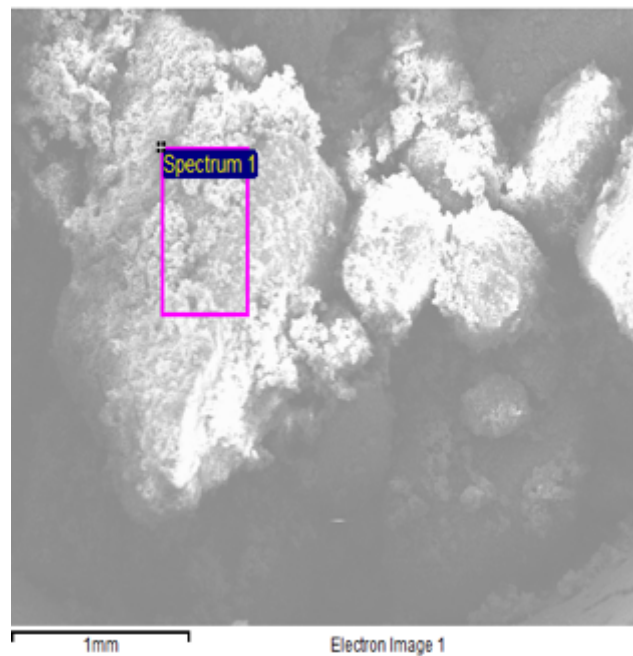
C CaCO<sub>3</sub> 1-Jun-1999 12:00 AMO SiO<sub>2</sub> 1-Jun-1999 12:00 AM

P GaP 1-Jun-1999 12:00 AM

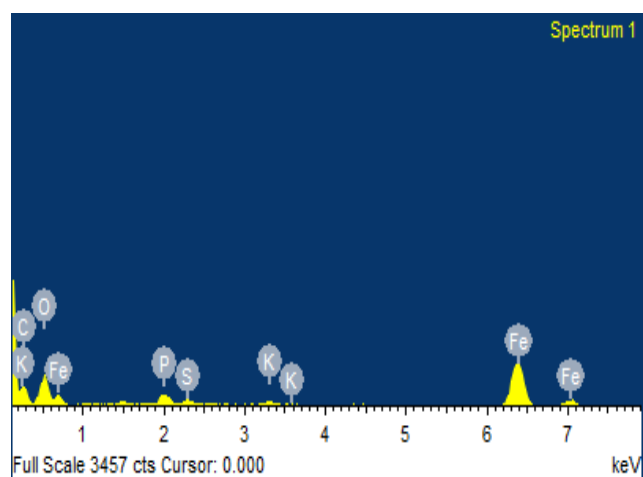
S FeS<sub>2</sub> 1-Jun-1999 12:00 AM

K MAD-10 Feldspar 1-Jun-1999 12:00 AM

Fe Fe 1-Jun-1999 12:00 AM



Element	Weight%	Atomic%
C K	39.44	58.32
O K	27.92	31.00
P K	0.78	0.45
S K	0.32	0.18
K K	0.17	0.08
Fe L	31.38	9.98
Totals	100.00	



Comment: Smallops

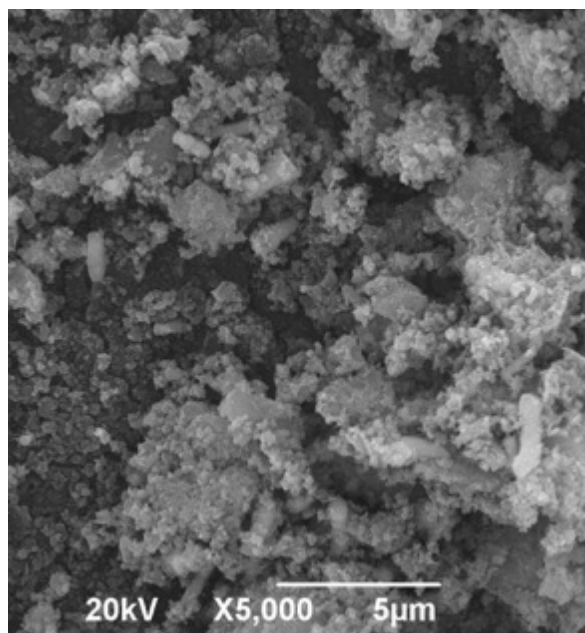


**Fig. A4.** SEM micrographs of CALPECH nanoparticles

**Table A1.** Influence of the type and concentration of nanoparticles on the initial and final IC concentrations of the batch assays as a function of the light source: visible light (white background) and visible light + UV light (grey background).

	<i>Fe<sub>2</sub>O<sub>3</sub></i>		<i>CALPECH</i>		<i>SMALLOPS</i>	
	<i>IC<sub>initial</sub></i>	<i>IC<sub>final</sub></i>	<i>IC<sub>initial</sub></i>	<i>IC<sub>final</sub></i>	<i>IC<sub>initial</sub></i>	<i>IC<sub>final</sub></i>
<b><i>Control</i></b>	1487 ± 76	1195 ± 29	1503 ± 23	1183 ± 15	1498 ± 21	1174 ± 21
<b><i>20 mg L<sup>-1</sup></i></b>	1483 ± 15	1204 ± 13	1522 ± 27	1057 ± 22	1478 ± 12	1133 ± 13
<b><i>40 mg L<sup>-1</sup></i></b>	1503 ± 25	1161 ± 40	1491 ± 34	984 ± 19	1489 ± 14	1019 ± 38
<b><i>70 mg L<sup>-1</sup></i></b>	1512 ± 39	1037 ± 41	1542 ± 39	933 ± 42	1498 ± 4	1008 ± 52
<b><i>Control</i></b>	1476 ± 13	1114 ± 11	1427 ± 20	935 ± 26	1416 ± 18	1123 ± 56
<b><i>20 mg L<sup>-1</sup></i></b>	1465 ± 25	1075 ± 22	1456 ± 17	870 ± 7	1418 ± 34	1045 ± 6
<b><i>40 mg L<sup>-1</sup></i></b>	1537 ± 94	1067 ± 35	1563 ± 22	787 ± 13	1428 ± 24	989 ± 9
<b><i>70 mg L<sup>-1</sup></i></b>	1511 ± 4	1102 ± 81	1483 ± 8	688 ± 14	1424 ± 10	962 ± 17

**Table A2.** Influence of the type and concentration of nanoparticles on the initial and final pH of the batch assays as a function of light source: visible light (white background) and visible light + UV light (grey background).

	<b><i>Fe<sub>2</sub>O<sub>3</sub></i></b>		<b><i>CALPECH</i></b>		<b><i>SMALLOPS</i></b>	
	<i>pH<sub>initial</sub></i>	<i>pH<sub>final</sub></i>	<i>pH<sub>initial</sub></i>	<i>pH<sub>final</sub></i>	<i>pH<sub>initial</sub></i>	<i>pH<sub>final</sub></i>
<b><i>Control</i></b>	7.87 ± 0.02	8.77 ± 0.06	7.75 ± 0.05	8.80 ± 0.04	7.80 ± 0.05	8.67 ± 0.03
<b><i>20 mg L<sup>-1</sup></i></b>	7.91 ± 0.08	8.76 ± 0.02	7.75 ± 0.08	9.08 ± 0.04	7.82 ± 0.05	8.80 ± 0.05
<b><i>40 mg L<sup>-1</sup></i></b>	7.78 ± 0.01	8.73 ± 0.05	7.75 ± 0.08	9.27 ± 0.11	7.78 ± 0.02	9.16 ± 0.10
<b><i>70 mg L<sup>-1</sup></i></b>	7.73 ± 0.03	9.17 ± 0.39	7.73 ± 0.01	9.42 ± 0.04	7.72 ± 0.02	9.12 ± 0.35
<b><i>Control</i></b>	7.85 ± 0.03	8.92 ± 0.03	7.80 ± 0.05	9.07 ± 0.04	7.80 ± 0.05	8.98 ± 0.11
<b><i>20 mg L<sup>-1</sup></i></b>	7.89 ± 0.02	9.04 ± 0.04	7.82 ± 0.05	9.33 ± 0.04	7.82 ± 0.05	9.16 ± 0.08
<b><i>40 mg L<sup>-1</sup></i></b>	7.83 ± 0.04	9.15 ± 0.10	7.78 ± 0.02	9.65 ± 0.11	7.78 ± 0.02	9.31 ± 0.05
<b><i>70 mg L<sup>-1</sup></i></b>	7.71 ± 0.03	9.04 ± 0.04	7.72 ± 0.02	9.94 ± 0.04	7.72 ± 0.02	9.43 ± 0.02